



Brunel
University
London

College of Health and Life Sciences
Department of Life Sciences
Division of Biosciences

**THE IDENTIFICATION OF CIRCULATING
TUMOUR CELLS IN PROSTATE CANCER
USING IMAGING FLOW CYTOMETRY**

Dr Hussein Nahidh M. S. Al Ali

February 2017

Declaration

I hereby declare that all the research presented in this thesis, including text, figures and tables, is my own work except where stated otherwise, and has not been submitted for any other degree.

A handwritten signature in black ink, appearing to read 'Hussein Al Ali', is written over several horizontal lines.

Hussein Al Ali

Abstract

The emergence of circulating tumour cells (CTCs) readily available in the blood, renewed hope of developing a tool that may serve as a surrogate biomarker for the identification of metastatic disease in cancer patients, in the form of a 'liquid biopsy' (i.e. peripheral blood sample instead of cancer tissue). Examination of CTCs has been attempted for a number of years and been limited by several factors including biological heterogeneity and the small number of CTCs present. Despite these limitations, there is increased evidence of the clinical utility of CTCs as diagnostic, prognostic and predictive markers in cancer patients.

In this study, I evaluated the possibility of detecting and distinguishing prostate CTCs from blood cells using the ImageStream^x, a novel device that uses multispectral imaging flow cytometry. In order to conduct this evaluation, PC3 prostate cancer cells were used to mimic CTCs in blood. To accurately define the sensitivity of imaging flow cytometry, immunological methods for CTC quantitation using the Epithelial Cell Adhesion Molecule (EpCAM), CD45 and Zonula Occludens Tight Junctions (ZO-1 TJ) antibodies were examined. Additionally, I have utilised the unique features of the ImageStream^x and examined its ability to distinguish CTCs from blood cells based on morphological and/or physical properties.

The immunostaining methods appeared to produce false negative identification of PC3 cells. However, when live PC3 cells pre-stained with a nucleic acid stain (DRAQ5) were analysed using solely physical and morphological parameters such as cell size, the results were a far more robust enumeration of the CTC population, thus increasing markedly the detection sensitivity. The live cell analysis approach was then validated using blood samples collected from metastatic castrate-resistant prostate cancer (CRPC) patients with an informed consent and ethical approval. CTC enumeration in these samples using the live cell analysis approach confirmed findings about the higher sensitivity of this procedure over immunological labelling of CTCs in imaging flow cytometry.

Publications

- **Al-Ali H N**, Chudasama D, Adam-Zahir S, Karteris E, Hall M; Parris CN. Identification of circulating tumour cells in prostate and ovarian cancers using imaging flow cytometry. **[Manuscript in preparation]**
- Parris CN, Adam-Zahir S, **Al-Ali H N**, Bourton EC, Plowman C, Plowman PN. Enhanced γ -H2AX DNA damage foci detection using multi-magnification and extended depth of field in imaging flow cytometry. *Journal of Cytometry, Part A*, 2015.

Acknowledgements

Firstly, I must thank God for the guidance to succeed in my work and allowing me the opportunities to achieve the pinnacle of my ability, especially during the challenging times in my PhD. My sincere gratitude goes to my supervisor Dr Christopher Parris, who I always considered a close friend. Thank you for helping me mature into the scientist I am today, from teaching me the basics of lab practises to your continuous encouragement throughout the past 3 years and even before I began my PhD. Special thanks go to the rest of my research group, Dr Sheba Adam-Zahir, Dr Rachel Lewis and Dr Emma Bourton as well as my second supervisor Dr Emmanouil Karteris for helping me with various needs during my degree.

My experience in the past few years would not have been the same had it not been to my colleagues in the department and my close friends, with whom I shared a very unforgettable time and helped influence my life greatly. A huge thank you to my friends Daniel, Elham, Javier, Joshua, Lorena, Luca, Marianne, Mursal, Nima, Omar, Phoebe, Samira and Savneet. I would like to also extend my gratitude to Mr Ayad Al-Bermani for his extensive support and advice on how to improve my work.

Lastly but by no means least, I would like to give a big thank you to my loving family. My mother and father: Sana and Nahidh, my two brothers Mohammed and Namir and my aunt Awatif. Words cannot describe how lucky I am to have your love and support and to know that you are always there by my side in happiness and grief.

This research and all my future work and successes are dedicated to my father, Nahidh M. Salih, my greatest supporter and the person I admire the most.

You are my inspiration in life and the one who always motivates me to be the best. I certainly would not be where I am today without you.

Thank you for everything.

TABLE OF CONTENTS

1.	Introduction	22
1.1	Cancer	22
1.1.1	Definition and origin	22
1.1.2	Cancer incidence worldwide	24
1.1.3	Principal risk factors	26
1.1.4	The Nature of Malignancy.....	28
1.1.5	Metastasis stages.....	29
1.1.6	Metastasis theories.....	33
1.1.7	Molecular mutations involved in metastasis	34
1.1.8	Cancer Types and Statistics.....	41
1.2	Prostate Cancer.....	44
1.2.1	Background and Epidemiology	44
1.2.2	History.....	46
1.2.3	Prostate cancer symptoms	48
1.2.4	Diagnosis	49
1.2.5	Treatment	52
1.3	Circulating tumour cells	56
1.3.1	Background and History.....	56
1.3.2	CTCs in prostate cancer.....	58
1.3.3	Methods of CTCs detection.....	60

1.4	Imaging flow cytometry	67
1.4.1	History and background	67
1.4.2	ImageStream ^x	70
1.5	AIM.....	73
2.	Materials and methods.....	75
2.1	Cell Maintenance	75
2.1.1	Cell culture	75
2.1.2	Cell trypsinisation.....	77
2.1.3	Cell Counting	78
2.1.4	Cell Freezing	80
2.1.5	<i>Mycoplasma</i> PCR for PC3 cell-line	81
2.2	Immunocytochemistry and live cell analysis	82
2.3	Sample acquisition and analysis using imaging flow cytometry	84
2.3.1	ImageStream ^x Mark II	84
2.3.2	INSPIRE®	86
2.3.3	Image Compensation	90
2.3.4	IDEAS®	92
2.4	Lymphocytes separation.....	96
2.5	Proof of principal (Mixing) experiment.....	97
2.6	Clinical samples preparation.....	98
3.	Identification of PC3 cells using the Epithelial Cell Adhesion Molecule	100
3.1	Introduction	100

3.2	Aim	102
3.3	Results.....	103
3.3.1	EpCAM antibody optimisation	103
3.3.2	PC3 cells staining with EpCAM antibody.....	105
3.3.3	GMO0893 staining with EpCAM antibody	108
3.3.4	PBL staining with EpCAM antibody.....	110
3.3.5	Mixing Experiment using EpCAM antibody.....	113
3.4	Discussion.....	117
4.	CD45 Antibody Staining for the Identification of PC3 cells.....	121
4.1	Introduction	121
4.2	Aim	124
4.3	Results.....	125
4.3.1	CD45 antibody optimisation	125
4.3.2	PC3 cells staining with CD45 antibody.....	127
4.3.3	GMO0893 staining with CD45 antibody	129
4.3.4	PBL staining with CD45 antibody	131
4.3.5	Mixing experiment using CD45 antibody.....	133
4.4	Discussion.....	137
5.	Identification of PC3 cells using Zonula Occludens-1 Tight Junctions Protein Antibody.....	140
5.1	Introduction	140
5.2	Aim	144
5.3	Results.....	145

5.3.1	ZO-1 TJ antibody optimisation	145
5.3.2	PC3 cells staining with ZO-1 TJ antibody.....	147
5.3.3	GMO0893 staining with ZO-1 TJ antibody	149
5.3.4	PBL staining with ZO-1 TJ antibody.....	152
5.3.5	Mixing experiment using ZO-1 TJ antibody.....	155
5.4	Discussion.....	159
6.	Live Cell Analysis for the Identification of PC3 cells.....	162
6.2	Introduction	162
6.3	Aim	165
6.4	Results.....	166
6.4.1	PC3 cell size range.....	166
6.4.2	GMO0893 cell size range	168
6.4.3	PBL cell size range	170
6.4.4	Mixing experiment using cell size comparison	172
6.4.5	Cellular morphology and structure comparison	176
6.4.6	Cell retrieval comparison	178
6.5	Discussion.....	180
7.	Identification of Circulating Tumour Cells in Prostate Cancer Patients.....	183
7.1	Introduction	183
7.2	Aim	185
7.3	Results.....	186
7.3.1	Identification of circulating tumour cells using EpCAM staining	186

7.3.2	Identification of circulating tumour cells using live cell analysis.....	190
7.3.3	Cellular morphology and structure comparison.....	193
7.3.4	Cell retrieval comparison.....	195
7.4	Discussion.....	196
8.	General discussion.....	199
8.1	Inclusive analysis of results.....	199
8.1.1	Identification of PC3 cells using Immunostaining methods.....	199
8.1.2	Identification of PC3 cells using live cell analysis.....	202
8.1.3	Clinical validation of CTC identification methods.....	203
8.2	Non-specific staining.....	204
8.3	Weaknesses and future work.....	207
	Bibliography.....	210

List of Figures

CHAPTER 1

FIGURE 1.1: CANCER INCIDENCE RATES WORLDWIDE.....	24
FIGURE 1.2: DISTRIBUTION OF DIFFERENT CANCER TYPES IN MALES AND FEMALES BASED ON HDI.....	25
FIGURE 1.3: THE DIFFERENT STAGES OF TUMOUR METASTASIS.....	29
FIGURE 1.4: GRAPHICAL REPRESENTATION OF HETERODIMERIC INTEGRINS.....	36
FIGURE 1.5: GRAPHICAL REPRESENTATION OF THE ACTIN MOTOR PROTEINS.....	37
FIGURE 1.6: EMT CONTRIBUTION TO TUMOUR PROGRESSION AND METASTASIS.....	38
FIGURE 1.7: GENDER DISTRIBUTION OF THE MOST COMMON CANCERS IN THE UK.....	41
FIGURE 1.8: AGE STANDARDISED SURVIVAL FOR SELECTED CANCERS IN ENGLAND AND WALES.....	43
FIGURE 1.9: MOST COMMON CANCERS IN MALES IN THE UK IN 2011.....	45
FIGURE 1.10: AVERAGE NUMBER OF PROSTATE CANCER CASES PER YEAR VS AGE AT DIAGNOSIS.....	46
FIGURE 1.11: GLEASON'S PATTERN SCALE.....	51
FIGURE 1.12: THE DIFFERENT APPROACHES OF CTC ENRICHMENT.....	60
FIGURE 1.13: EPISPOT ASSAY.....	64
FIGURE 1.14: CTC DETECTION APPROACHES.....	65

CHAPTER 2

FIGURE 2.1: COUNTING CELLS USING A CELL COUNTNESS.....	78
FIGURE 2.2: UTILISING THE USE OF EDF TECHNOLOGY IN THE IMAGESTREAM ^X	84
FIGURE 2.3: SAMPLE ACQUISITION USING INSPIRE [®]	86
FIGURE 2.4: INSPIRE [®] SAMPLE ACQUISITION CONTROL FEATURES.....	87
FIGURE 2.5: CAPTURED IMAGES OF CELLS USING THE IMAGESTREAM ^X	88
FIGURE 2.6: DISTRIBUTION OF CELLS BASED ON A VARIETY OF FEATURES USING INSPIRE [®]	89

FIGURE 2.7: A TYPICAL IMAGESTREAM ^X COMPENSATION MATRIX TABLE.....	90
FIGURE 2.8: COMPENSATED VS UNCOMPENSATED IMAGES OF PC3 CELLS.....	91
FIGURE 2.9: IDENTIFICATION OF SINGLE CELLS USING IDEAS [®]	92
FIGURE 2.10: IDENTIFICATION OF FOCUSED CELLS USING IDEAS [®]	93
FIGURE 2.11: IDENTIFICATION OF POSITIVELY STAINED CELLS USING IDEAS [®]	94
FIGURE 2.12: THE USE OF SCATTERPLOTS TO IDENTIFY EpCAM POSITIVE AND NEGATIVE PC3 CELLS.....	95

CHAPTER 3

FIGURE 3.1: THE VARIETY OF CAMs PRESENT ON EPITHELIAL CELLS.....	100
FIGURE 3.2: AN EXAMPLE OF EpCAM STAINING OF MCF-7 CELLS.....	101
FIGURE 3.3: EpCAM STAINING OF PC3 CELLS.....	105
FIGURE 3.4: DISTRIBUTION OF PC3 CELLS BASED ON THEIR EpCAM INTENSITY.....	106
FIGURE 3.5: EpCAM STAINING OF GMO0893 CELLS.....	108
FIGURE 3.6: DISTRIBUTION OF GMO0893 CELLS BASED ON THEIR EpCAM STAINING INTENSITY.....	109
FIGURE 3.7: EpCAM STAINING OF PBL CELLS.....	110
FIGURE 3.8: DISTRIBUTION OF PBL CELLS BASED ON THEIR EpCAM STAINING INTENSITY.....	111
FIGURE 3.9: EpCAM STAINING OF PC3 AND PBL CELLS.....	113
FIGURE 3.10: PC3 AND PBL CELLS DISTRIBUTION BASED ON THEIR EpCAM STAINING INTENSITY.....	115

CHAPTER 4

FIGURE 4.1: CD45 ANTIBODY STAINING OF LEUKOCYTES.....	122
FIGURE 4.2: CD45 STAINING OF PC3 CELLS.....	127
FIGURE 4.3: DISTRIBUTION OF PC3 CELLS BASED ON THEIR CD45 STAINING INTENSITY.....	128
FIGURE 4.4: CD45 STAINING OF GMO0893 CELLS.....	129

FIGURE 4.5: DISTRIBUTION OF GMO0893 CELLS BASED ON THEIR CD45 STAINING INTENSITY	130
FIGURE 4.6: CD45 STAINING OF PBL CELLS.....	131
FIGURE 4.7: DISTRIBUTION OF PBL CELLS BASED ON THEIR CD45 STAINING INTENSITY	132
FIGURE 4.8: CD45 STAINING OF PC3 AND PBL CELLS	133
FIGURE 4.9: DISTRIBUTION OF PC3 AND PBL CELL BASED ON THEIR CD45 STAINING INTENSITY	135

CHAPTER 5

FIGURE 5.1: THE PROTEIN COMPLEXES THAT EXIST WITHIN THE PARACELLULAR PATHWAY	141
FIGURE 5.2: ZO-1 TJ STAINING OF EPITHELIAL CELLS	142
FIGURE 5.3: ZO-1 TJ STAINING OF PC3 CELLS	147
FIGURE 5.4: DISTRIBUTION OF PC3 CELLS BASED ON THEIR ZO-1 TJ STAINING INTENSITY	148
FIGURE 5.5: ZO-1 TJ STAINING OF GMO0893 CELLS.....	149
FIGURE 5.6: DISTRIBUTION OF GMO0893 CELLS BASED ON THEIR ZO-1 TJ STAINING INTENSITY.....	150
FIGURE 5.7: ZO-1 TJ STAINING OF PBL CELLS.....	152
FIGURE 5.8: DISTRIBUTION OF PBL CELLS BASED ON THEIR ZO-1 TJ STAINING INTENSITY	153
FIGURE 5.9: ZO-1 TJ STAINING OF PC3 AND PBL CELLS	155
FIGURE 5.10: DISTRIBUTION OF PC3 AND PBL CELLS BASED ON ZO1 TJ STAINING INTENSITY	157

CHAPTER 6

FIGURE 6.1: VARIATION IN LYMPHOCYTES CELL SIZE.....	163
FIGURE 6.2: DISTRIBUTION OF PC3 CELLS BASED ON THEIR CELL SIZE	166
FIGURE 6.3: THE AVERAGE CELL SIZE RANGE FOR PC3 CELLS.....	167
FIGURE 6.4: DISTRIBUTION OF GMO0893 CELLS BASED ON THEIR CELL SIZE.....	168
FIGURE 6.5: THE AVERAGE CELL SIZE RANGE FOR GMO0893 CELLS	169
FIGURE 6.6: DISTRIBUTION OF PBL CELLS BASED ON THEIR CELL SIZE	170

FIGURE 6.7: THE AVERAGE CELL SIZE RANGE FOR PBL CELLS.....	171
FIGURE 6.8: COMPARISON BETWEEN PC3, GMO0893 AND PBL CELL SIZE RANGES	172
FIGURE 6.9: DISTRIBUTION OF PC3 AND PBL CELLS BASED ON THEIR CELL SIZE	174

CHAPTER 7

FIGURE 7.1: EPCAM STAINING OF CTCs AND WBCs IN PROSTATE CANCER PATIENTS.....	186
FIGURE 7.2: LACK OF EPCAM STAINING SPECIFICITY IN WBCs AND CTCs.....	187
FIGURE 7.3: DISTRIBUTION OF CTCs AND WBCs FROM Pt1 BASED ON THEIR EPCAM STAINING INTENSITY	188
FIGURE 7.4: DISTRIBUTION OF CTCs AND WBCs FROM Pt2 BASED ON THEIR EPCAM STAINING INTENSITY	189
FIGURE 7.5: LIVE CELL IMAGES OF CTCs AND WBCs IN PROSTATE CANCER SAMPLES	190
FIGURE 7.6: DISTRIBUTION OF CTCs AND WBCs FROM Pt1 BASED ON CELL SIZE.....	191
FIGURE 7.7: DISTRIBUTION OF CTCs AND WBCs FROM Pt2 BASED ON CELL SIZE.....	192

CHAPTER 8

FIGURE 8.1: MICROGRAPHS OF ISOLATED “DOUBLE POSITIVE” CELLS FROM PROSTATE CANCER PATIENTS USING THE HB-CHIP	204
---	-----

List of tables

CHAPTER 1

TABLE 1.1: COMMON CANCERS AND THEIR RISK FACTORS.....	27
TABLE 1.2: CANCER INCIDENCE AND DEATH RATES IN THE UK IN 2011 AND 2012	42
TABLE 1.3: FAMILY HISTORY AND PROSTATE CANCER	47
TABLE 1.4: PSA LEVELS AND RISK OF DEVELOPING PROSTATE CANCER	49
TABLE 1.5: CTC DETECTION METHODS	61
TABLE 1.6: STANDARD FLOW CYTOMETRY VS IMAGING FLOW CYTOMETRY	68

CHAPTER 2

TABLE 2.1: LIST OF CELL-LINES USED.....	76
TABLE 2.2: <i>MYCOPLASMA</i> PCR PROGRAM	81
TABLE 2.3: LIST OF THE THREE ANTIBODIES USED	83
TABLE 2.4: LIST OF FLUORESCENT ANTIBODIES THAT CAN BE USED WITH THE IMAGESTREAM ^x	85
TABLE 2.5: SERIAL DILUTION OF PC3 CELLS TO TEST CTC DETECTION SENSITIVITY.....	97

CHAPTER 3

TABLE 3.1: EpCAM STAINING OPTIMISATION FOR PC3 CELLS	103
TABLE 3.2: RETRIEVAL NUMBERS OF EpCAM POSITIVE CELLS.....	116

CHAPTER 4

TABLE 4.1: CD45 OPTIMISATION FOR GMO0893 CELLS	125
TABLE 4.2: RETRIEVAL NUMBERS OF CD45 NEGATIVE CELLS	136

CHAPTER 5

TABLE 5.1: ZO-1 TJ OPTIMISATION FOR PC3 CELLS	145
---	-----

TABLE 5.2: RETRIEVAL NUMBERS OF ZO-1 TJ POSITIVE CELLS.....	158
---	-----

CHAPTER 6

TABLE 6.1. APPROXIMATE RETRIEVAL NUMBERS OF LIVE PC3 CELLS.....	175
---	-----

TABLE 6.2: COMPARISON OF CELL MORPHOLOGY OBTAINED FROM THE FOUR CTC IDENTIFICATION METHODS USED	176
---	-----

TABLE 6.3: APPROXIMATE CTC RETRIEVAL NUMBER FROM THE FOUR METHODS EXAMINED	178
--	-----

CHAPTER 7

TABLE 7.1: EXAMPLES OF CTCs AND WBCs CAPTURED USING LIVE CELL ANALYSIS AND EPCAM STAINING	193
---	-----

TABLE 7.2: COMPARISON BETWEEN CELL RETRIEVAL FROM LIVE CELL ANALYSIS AND EPCAM STAINING	195
---	-----

Abbreviations

ADT – Androgen Deprivation Therapy

AF – Alexa Fluor

Apc – Adenomatous Polyposis Coli

APC – Antigen Presenting Cell

BF – Brightfield

CAM – Cell Adhesion Molecule

CD45 – Cluster of Differentiation 45

Ch – Channel

Cif – Compensated Image File

CK – Cytokeratin

CRPC – Castrate-Resistant Prostate Cancer

CTC – Circulating Tumour Cell

Daf – Data Analysis File

EBRT – External Beam Radiotherapy

EDF – Extended Depth of Field

EMT – Epithelial Mesenchymal Transition

EpCAM – Epithelial Cell Adhesion Molecule

FACS – Fluorescence-Activated Cell Sorting

FISH – Fluorescence *in-situ* Hybridisation

HDI – Human Development Index

IgG – Immunoglobulin G

ISET – Isolation by Size of Epithelial Tumour cells

KDa – Kilo Dalton

LSM – Lymphocyte Separation Medium

MHC – Major Histocompatibility Complex

Myo – Myosin

N/C – Nuclear Cytoplasmic Ratio

PBL – Peripheral Blood Lymphocyte

PBS – Phosphate Buffered Saline

PFA – Paraformaldehyde

PSA – Prostate Specific Antigen

Pt – Patient

Rif – Raw Image File

RPM – Revolution Per Minute

RT – Room temperature

RT-PCR – Real Time-Polymerase Chain Reaction

TCR – T-Cell Receptor

TJ – Tight Junctions

TURP – Transurethral Resection of the Prostate

ZO-1 TJ – Zonula Occludens-1 Tight Junctions

Chapter 1

Introduction

1. Introduction

1.1 Cancer

1.1.1 Definition and origin

Cancer is a collection of diseases in which a cell loses its normal reproduction function and begins multiplying without control, forming a tumour. This change is normally brought about when DNA damage takes place within cells (Hollstein et al., 1991). Cells have numerous mechanisms of detecting such damage and either repair it or induce programmed cellular death. This occurs either through autophagy, programmed necrosis or apoptosis (Ouyang et al., 2012). However, for a cell to become cancerous, six biological capabilities are thought to be required for such transformation. These capabilities comprise of cells maintaining proliferative signalling, being able to evade growth suppressors, resisting programmed cellular death, enabling immortality through continuous replication, the induction of angiogenesis and the activation of local invasion and metastasis. These changes are referred to as the six principal hallmarks of cancer (Hanahan and Weinberg, 2000). In the last decade, research advances have helped in recognising two new hallmarks, these include the process of reprogramming the energy metabolism as well as the ability to evade immune destruction (Hanahan and Weinberg, 2011).

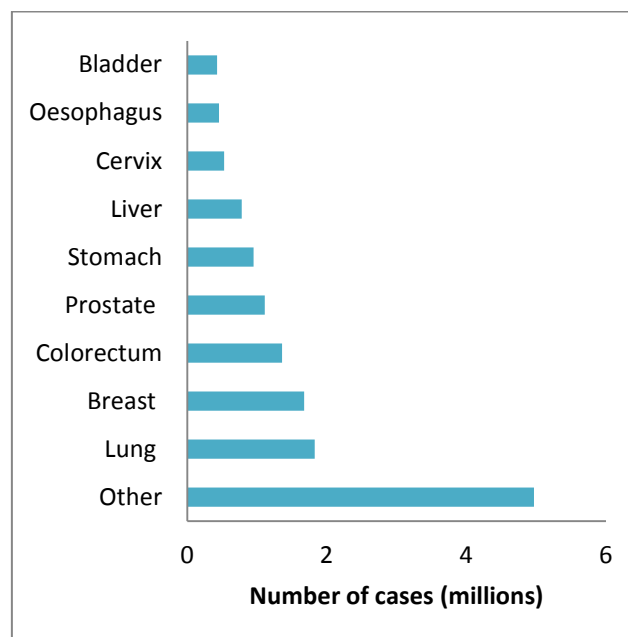
However, a recent study suggested that only a third of the variation in risk leading to cancer development in tissues is accredited to environmental factors or inheritance. It was proposed that the rest were simply due to an accumulation of random mutations in stem cells; in other words, “bad luck” (Tomasetti and Vogelstein, 2015). Conclusions made by that study were immediately met with heavy criticism for seemingly downplaying the essential role of an unhealthy life style in cancer development (Couzin-Frankel, 2015).

There are many types of cancer and they are usually named after the organs in which they are present or the tissue from which they originate. Tumours occur in two forms, benign and malignant. Benign tumours are formed in one location, self-limited and are normally encapsulated. They are localised to a particular region or organ and do not spread to other locations in the body. They are also known to generally have a better prognosis than malignant tumours. In comparison, malignant tumours very often invade surrounding tissues, while cancerous cells originating from these tumours are known to be able to travel in blood or in the lymphatic system to invade distant tissues, forming secondary tumours. This malignant nature of cancer is the single most challenging factor in the treatment of the majority of all cancers (Trosko, 2009).

1.1.2 Cancer incidence worldwide

In 2012, there were approximately 14 million new cases of cancer worldwide and more than 8 million cancer-related deaths, with the highest number of deaths occurring in lung cancer patients, resulting in 1.59 million deaths (Figure 1.1). These numbers are on the rise and are expected to rise by nearly 70% over the next 20 years. This increase is thought to be occurring as a result of various factors such as the emergence of sensitive diagnostic methods. Vast industrialisation and carcinogen exposure in developing countries might also have played a role in the rising numbers of cancer incidence and cancer-related deaths. Moreover, there are gender specific biases for certain types of cancer. For instance, the main cancers occurring amongst females are breast, stomach, cervix, lung and colorectum cancer. Whereas most cases of cancer in males are related to lung, stomach, liver and colorectum (de Martel et al., 2012).

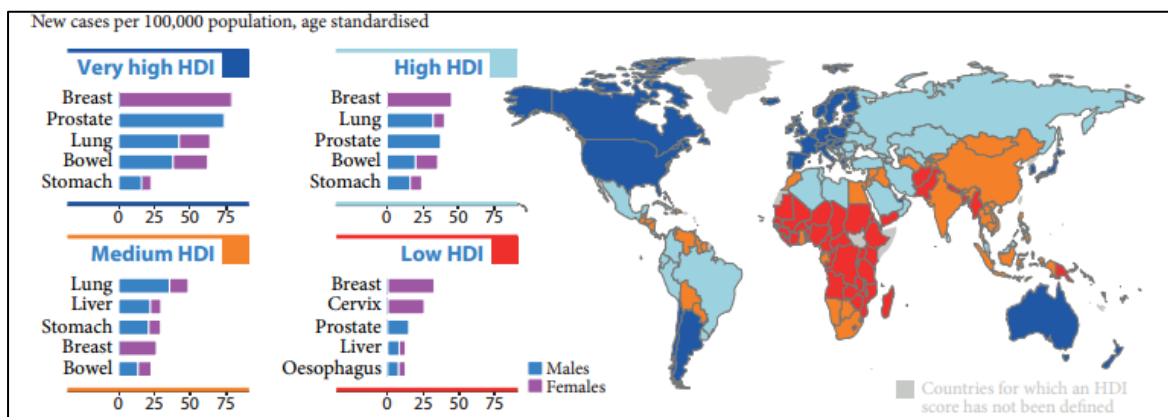
Figure 1.1: Cancer incidence rates worldwide.



The figure above shows the worldwide incidence rates of several cancers, such as lung, breast, colorectum and prostate cancers. The figure has been created using data set provided by CRUK (CRUK, 2012).

Cancer has also been found to be associated with the levels of human development index (HDI) in a particular region as demonstrated in Figure 1.2. Cancer numbers in low HDI countries were found to be much lower than those in high HDI regions. Breast cancer for instance was found to be prevalent in regions with very high HDI, but not as much with medium HDI countries, where it is replaced by higher incidence rate of Lung cancer. Lung cancer itself was in low numbers in low HDI countries compared to the rest, an effect that could have resulted from various environmental factors, such as the low industrialisation of low HDI regions (CRUK, 2012).

Figure 1.2: Distribution of different cancer types in males and females based on HDI.



The figure above shows the distribution of the different types of cancer between both genders and how the number of cancer cases vary from regions with high HDI to ones with low HDI (CRUK, 2012)

1.1.3 Principal risk factors

There are various risk factors associated with cancer and these differ from one cancer type to another. The fact remains however that age, tobacco use, alcohol intake, having an unhealthy diet and the lack of physical activity are the main environmental risk factors for most cancers worldwide (WHO, 2014). Table 1.1 on the following page shows the risk factors for different types of cancer. As can be seen, age is one factor that tops the list for most of the cancer types mentioned and the age-related risk in cancer is in fact attributed to the number of cellular divisions.

As mentioned earlier, a study by Tomasetti and Vogelstein revealed that about two thirds of cancer cases occur due to random mutations rather than due to risk factors associated with lifestyle differences of individuals (Tomasetti and Vogelstein, 2015). The study compared the number of lifetime stem cells divisions in a range of tissues with the life time cancer risk. As a result, it was found that random mutations were the main cause of cancer. Since its publication, the study received wide criticism, mainly from the International Agency for Research on Cancer (IARC), which argued that an unhealthy lifestyle remains a huge contributor to cancer incidence and that according to our current knowledge, nearly half of all existing cancer cases can be prevented in the first place.

In addition to age, other risk factors that are seen to be frequently associated with increased risk of cancer occurrence involve tobacco smoking and alcohol consumption. While some risk factors seem to be generally associated with several cancer types, others are more associated with certain types of cancer than others, such as exposure to radon gas and its link to lung cancer, or the increased risk of developing prostate cancer in men who have had a vasectomy (CRUK, 2014a).

Table 1.1: Common cancers and their risk factors

Cancer type	Risk factor
Lung	<ul style="list-style-type: none"> • Smoking • Air pollution • Exposure to radon gas • Exposure to chemicals • Family history • Lowered immunity
Breast	<ul style="list-style-type: none"> • Age • Family history • Alcohol • Smoking • Sex hormones • Ethnicity
Skin	<ul style="list-style-type: none"> • Age • Family history • Sun exposure • Skin conditions • Radiation exposure
Prostate	<ul style="list-style-type: none"> • Age • Ethnicity • Family history • Obesity • Height • Insulin like growth factor (IGF-1) • Vasectomy • Inflammation of the prostate
Ovarian	<ul style="list-style-type: none"> • Age • Family History (BRCA mutation) • History of breast cancer • Smoking • Infertility

The table above mentions some of the most common types of cancer for both males and females and outlines the major risk factors for each cancer type (CRUK, 2014a).

1.1.4 The Nature of Malignancy

Metastasis is the process in which cancerous cells detach from the primary tumour and travel to another anatomically distant location in the body forming a secondary tumour. Cancer cells can penetrate blood vessels and travel through the bloodstream or can invade lymphatic vessels and travel through lymph to various sites in the body (Klein, 2008). The invasive nature of cancerous cells is brought about by a number of biochemical and phenotypical factors that ultimately affect cell to cell adhesion, migration, cell polarity and cell motility as well as the upregulation of certain proteolytic enzymes, leading to metastasis (Leber and Efferth, 2009).

The process in which epithelial cells convert their phenotype into mesenchymal-like phenotype is referred to as the Epithelial Mesenchymal Transition (EMT) (Pecorino, 2012). The EMT is of a huge importance in the overall metastasis process and will be explained in detail on page 37 in this chapter.

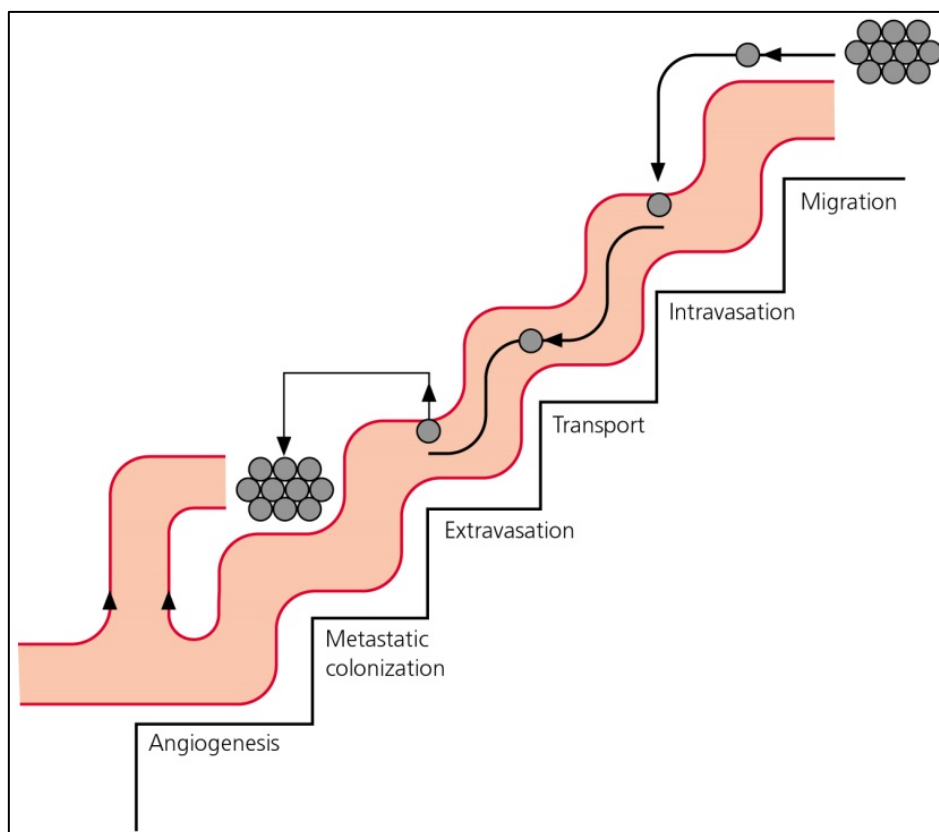
The propensity of tumour cells to invade and metastasise as cancerous cells is what makes cancer as a life-threatening disease and makes its treatment clinically challenging (Jiang et al., 2009). The process of invasion and metastasis is yet to be fully understood as it varies from one cancer to another. For instance, breast cancer very often metastasises to the lymph nodes, bones, lungs, liver and brain, forming secondary tumours there. While in the case of colon cancer, tumour cells were found to metastasise to the lymph nodes as well as the liver (Leber and Efferth, 2009).

1.1.5 Metastasis stages

The invasion-metastasis cascade is a series of events which brings about the formation of secondary tumours through the process of metastasis (Valastyan and Weinberg). The crucial steps that cancerous cells undertake during this cascade include invasion, intravasation, transport, extravasation and metastatic colonisation. Cancer cells often interact with normal cells in surrounding tissues and it is this interaction that can determine whether or not a cancerous cell will metastasise. In other words, metastasis is not only dependent on the cancerous cell being able to invade and travel in the body but also on the microenvironment where it resides (Pecorino, 2012).

The metastasis process is outlined in the figure below and subsequently explained in details.

Figure 1.3: The different stages of tumour metastasis



The figure above shows the different stages of metastasis. These include migration, intravasation, transport, extravasation and metastatic colonisation. The establishment of a secondary tumour is then followed by angiogenesis (Pecorino, 2012).

The details involved in each stage of tumour metastasis are mentioned below. While the molecular events associated with each stage, such as mutations that occur in cadherin and catenin, are discussed later in this chapter.

1.1.5.1 Detachment and migration

The process usually begins with the migration of cancer cells to subsequently begin local invasion of the nearby blood vessel tissue and is then followed by dissemination into the bloodstream or the lymphatic system. It is worth pointing out, however, that cancer invasion through blood circulation is considerably more frequent than that which takes place at the lymphatic lumina (Gupta and Massagué).

1.1.5.2 Intravasation

The intravasation process itself, appears to be influenced by a combination of molecular changes and the structural features of the blood vessels where the tumour resides, giving rise to cancer cells' invasion ability. This invasion is usually initiated by cancer cells migrating to a close blood vessel, which can either be found within the tumour itself or in close proximity (Reymond et al., 2013). Migration then takes place through the endothelial cells junctions or, in some cases, via transcellular movement through endothelial cells.

1.1.5.3 Transport

The process in which cancer cells are transported within blood is yet to be fully understood. However, as cancer cells are found to be relatively large in diameter with a range of 20-30 μm , it is thought the vast majority of these cells get trapped within minutes after the intravasation process is complete. This is likely to happen at various capillary beds, where the luminal diameter is around 8 μm in length. This relatively short circulation process could also explain how metastasis of cancer cells goes unalarmed very often (Valastyan and Weinberg). Another theory suggested that cancer cells are capable of specific attachment to particular tissues in the body. It is thought that tumour

cells have a fixed preference for a certain type of tissue which leads to their attachment within that region. An example of this was investigated in breast tumour cells expressing Metadherin, a highly expressed protein in breast cancers. These cells were found to have a prearranged preference of metastasising to the lungs (Brown and Ruoslahti).

1.1.5.4 Extravasation

The arrival and subsequent attachment of cancer cells at a distant organ may trigger the formation of an intraluminal growth, such that would continuously increase in size until it ruptures walls of nearby vessels. This allows the tumour cells to come in immediate contact with the tissue parenchyma. Alternatively, tumour cells may directly invade the new tissue via extravasation, a process that can be looked at as a contrary form to that of intravasation. This happens when these cells penetrate the endothelial cells layer as well as the pericyte layer, both of which separate vessel lumina and the stromal microenvironment (Al-Mehdi et al., 2000).

Migrated cancer cells often find it difficult to adapt to the new environment where they metastasise to, this is because the new microenvironment might be different from that of the primary tumour (Valastyan and Weinberg). In order for these cells to colonise within the new region, a “metastatic niche” must be created first (Psaila and Lyden, 2009). This is achieved when cancerous cells in the primary tumour release organ-specific fibronectin, up-regulating systemic signals that eventually alter the target microenvironment by making them more compatible sites for cancer cells prior to their arrival.

1.1.5.5 Metastatic colonisation and formation of secondary tumour

The metastatic colonisation leading to the growth of a new tumour, which concludes the metastasis process, is heavily dependent on two important factors, the identity of the primary tumour cells and the organ site at which the new tumour will grow (Valastyan and Weinberg). It should be noted that invasion-metastasis cascade is an extremely inefficient process, as many cancer cells fail in

completing the metastatic colonisation process. A study estimated that less than 0.01% of the cancer cells which have entered the blood circulation eventually result in the formation of macroscopic metastases (Chambers et al., 2002). The vast majority of cancer cells seem to suffer from attrition and slow destruction over a period that may span months even after surviving in their new foreign microenvironment.

1.1.6 Metastasis theories

There are several theories that describe how the process of metastasis occurs and try to explain the actions of cancerous cells as they migrate from one location to another, forming secondary tumours. One of these theories is the “Seed and Soil” theory (Qian and Teh, 2012). The theory was originally proposed in 1889 by Stephen Paget, an English surgeon. He proposed that the metastatic property of cancerous cells was not random, but rather due to some cancerous cells (the “seed”) having a unique attraction to environments that provide enhanced settings within specific organs (the “soil”) for them to grow (Ribatti et al., 2006). As previously mentioned, when tumour cells enter the blood circulation, they are disseminated wildly across the body. However, developed metastases can only be detected at the “soil” sites (Fidler, 2003).

This theory was backed by studies investigating organ selectivity to particular tumours, confirming enhanced survival rate of tumour cells in particular tissues but not in others. For example, melanoma cancer cells tested in mouse models showed capability of these cells to thrive in the *in situ* lungs as well as in implants of pulmonary and even ovarian tissues. The same could not be said about implanted renal tissues, where neoplastic lesions failed to develop (Hart and Fidler, 1980).

The past century saw discoveries of novel molecules that play key part with specific metastasis of a certain cancer with an organ. In addition, pathways leading to the occurrence of organ-specific metastasis have also been highlighted. All of which builds a strong identity to the “Seed and Soil” hypothesis (Fokas et al., 2007). Another theory suggested that tumour cells fusion with macrophages or other types of cells derived from the bone marrow would lead to metastasis (Pawelek and Chakraborty, 2008). Furthermore, metastases formation was also linked with cancer-transformed genes originating from the primary tumour and integrated in their identical form, with the help of a virus-vector function, into biologically potent recipient cells in other organs (Schischmanov, 2013).

1.1.7 Molecular mutations involved in metastasis

Cancer metastasis is believed to be largely influenced by cells adhesion molecules (CAM). Such molecules include cadherins, catenins, actin and integrin. Some molecular events are associated with these molecules and may contribute towards cells becoming cancerous. A perfect example of this would be the Wnt signalling pathway and its role in cancer. Molecular studies have confirmed that mutations occurring in this pathway might be responsible for approximately 90% of the cases of colorectal cancer (Sansom et al., 2004). Some of the essential CAM molecules and molecular events involved in tumorigenesis and metastasis are mentioned in this section:

1.1.7.1 Cadherin

Cadherins, which are transmembrane calcium-dependent glycol-proteins, play a big role in determining the metastatic property of a cancer cell (Takeichi, 1993). Cadherins mediate cell adhesion via coordination with catenins (through the cytoskeleton). Research in this area (Cavallaro et al., 2002) underlined that *in vitro* observations – carried out on a variety of tumour cell-lines – suggest a strong link between a “switch” in cadherins expression and tumour progression and metastasis. Furthermore, a change in cadherins’ expression has been associated with loss of epithelial morphology in the prostate, playing a key role in driving the invasiveness and metastasis of prostate cancer. Poor prostate cancer prognosis was also found to be linked with the loss of E-cadherin; however, further studies are required to study the link between cadherin switching and other cancer types (Tomita et al., 2000).

1.1.7.2 Catenin

Catenins are cytoplasmic proteins which bind to transcription factors and induce gene expression. Along with E-cadherin, they play a major role in mediating epithelial cell adhesion as well as intracellular signalling. There is a lot of evidence to suggest that mutation and/or loss of catenin expression very often drives forward tumour invasion and metastasis (Joo et al., 2002). It is of great

importance to understand the cadherin-catenin interaction as this might be the key to designing novel therapeutic approaches (Ramburan and Govender, 2002).

Additionally, the accumulation of β -catenin as a result of mutations is found to be present in more than 90% of all colorectal cancer patients (Giles et al., 2003). These mutations have an activating role on the canonical Wnt signalling pathway, which is a signal transduction pathway comprising of proteins that utilise cell surface receptors to transmit signals into cells. This activating effect is brought about by the loss of the Adenomatous Polyposis Coli (*Apc*) gene, which is a tumour-suppressor gene, leading to the stabilisation and accumulation of β -catenin in the nucleus, subsequently leading to the formation of tumour cells (Sansom et al., 2004). The loss of *Apc* itself also has a disturbing effect on the differentiation and proliferation of cells and is found to be linked with altering intestinal pathology and causing morbidity (Sansom et al., 2004, Logan and Nusse, 2004).

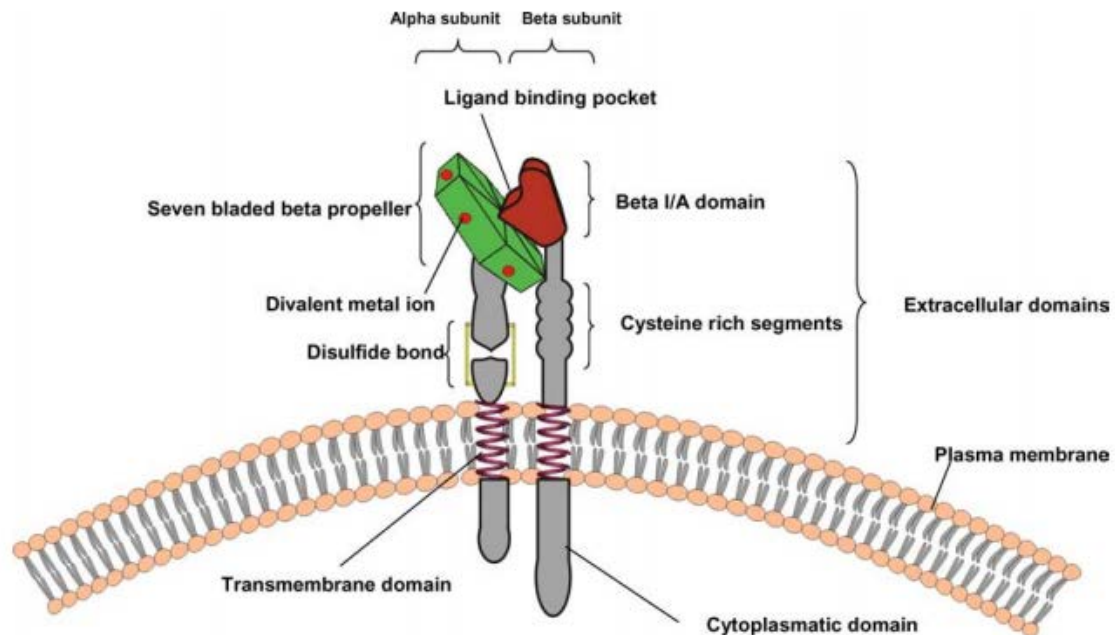
1.1.7.3 Integrin

The role of integrins is another significant factor that can determine the progression of cancer. Integrins form a family of heterodimeric cell surface receptors that is capable of detecting changes within cells as well as connecting the actin cytoskeleton to the extracellular matrix. Changes detected by integrins occur as a result of the extracellular matrix undergoing phenotypical degradation or deformation, as a result of a mechanical force (Seguin et al., 2015). Upon detection of such changes, integrins then activate a series of cellular responses that form a connection between the inside and the outside of the cell. These signals ultimately control cell survival, proliferation, migration, adhesion and differentiation (Desgrosellier and Cheresch, 2010).

Integrins comprise of a combination of alpha and beta subunits, forming at least 25 different receptors. Studies have shown that many of these integrins play a key role in tumour progression and invasiveness. One study investigated the effect of prostate cancer on bone microenvironment

and found that integrin-mediated interaction of prostate cancer cells was key in the development of bone metastasis (Keller and Brown, 2004).

Figure 1.4: Graphical representation of heterodimeric integrins



The figure above shows a graphical representation of the extracellular, transmembrane and cytoplasmic domains of heterodimeric integrins (Kuphal et al., 2005).

Integrins' role as invasiveness and metastasis regulators in prostate cancer was also confirmed by McCabe *et al* who demonstrated how integrin $\alpha\text{V}\beta\text{3}$ was mediating attachment to the bone microenvironment and, consequently, secondary tumour growth (McCabe et al., 2007). Additionally, integrins also play a vital role in tumour progression through increasing cellular matrix rigourousness, leading to increased microRNA expression, which in turn encourages tumour progression through integrin activation of β -catenin and MYC (Mouw et al., 2014).

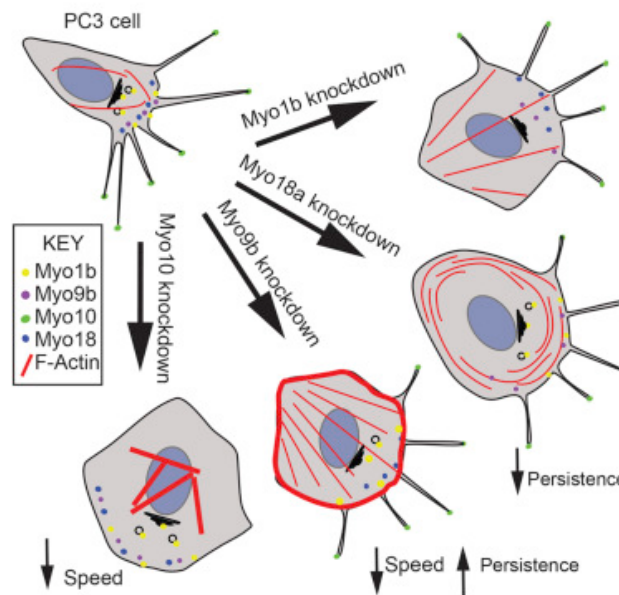
1.1.7.4 Actin

Actin is a globular protein that is found in abundance in the majority of eukaryotic cells and contributes more to protein-to-protein interactions than any other existing protein. Moreover, the actin cytoskeleton is also responsible for the machinery which leads to cell migration (Lodish H,

2000, Dominguez and Holmes, 2011). It is for these reasons that actin can be an influencing factor in determining the metastatic ability of cancerous cells as suggested in a study by Jiang *et al* (Jiang et al., 2009). Besides cellular motility, the actin cytoskeleton's proteins are also responsible for regulating cellular polarity, survival and the growth of normal cells as well as cancerous cells and their invasive ability (Stevenson et al., 2012).

Myosins (Myo), which are a diversely large family comprising of molecular motors, play a key role in cellular migration and motility by influencing actin organisation. The modulation of the expression of some myosin isoforms was found to have an upregulating effect on cells, driving them towards a more migratory phenotype (i.e. becoming metastatic) (Pulukuri et al., 2005).

Figure 1.5: Graphical representation of the actin motor proteins



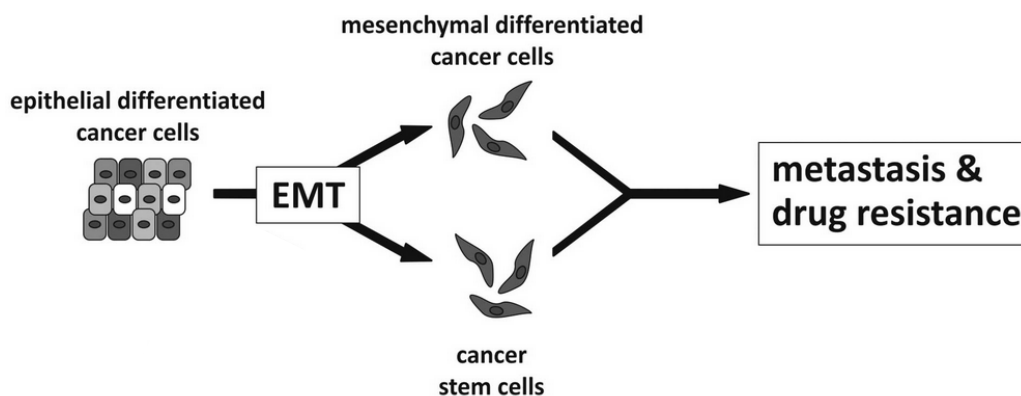
Actin motor proteins, such as Myo10, Myo9b and Myo1b and Myo18 (shown above), were linked with highly metastatic forms of prostate cancer as elevated expression levels of these proteins were observed in highly metastatic prostate cancer cell-lines, such as the PC3 cell-line (Makowska et al.). The figure shows how the knockdown of genes encoding for these proteins results in changes to cancer cells' morphology, migration and actin organisation.

1.1.7.5 Epithelial-mesenchymal transition (EMT)

It is fair to say that for a tumour to obtain the ability to invade surrounding tissues, the EMT mechanism – which includes the conversion of connected epithelial cells into mobile mesenchymal

cells – is of high importance (Pecorino, 2012). Despite its common occurrence during early embryogenesis, this transition shares many similarities with metastasis. For instance, EMT is known to be characterised by a loss of cell polarity as well as the upregulation of mesenchymal proteins (e.g. N-Cadherin) and the downregulation of epithelial markers (e.g. E-Cadherin). This was recently investigated in thorough details with relation to ovarian cancer (Davidson et al., 2015). The results showed frequent expression of the proteins analysed in cancer cells, including E-Cadherin and P-Cadherin. EMT occurs when signals from a tumour stroma – such as growth factors (e.g. HGF) – induce EMT in nearby tumour cells, triggering the activation of transcription factors such as Twist. These transcription factors in turn regulate sets of genes needed to activate EMT.

Figure 1.6: EMT contribution to tumour progression and metastasis



The EMT plays a key role in the cancer advancement and spread by initiating the metastasis process as well as enabling cancerous cells to withstand cancer treatment (Kiesslich, 2013).

In the context of metastatic invasion, EMT’s mechanisms may lead to the formation of circulating tumour cells that play a role in the creation of metastases in a distant body organ. EMT gives cells an enhanced migratory ability, tendency to invade as well as an elevated resistance capability to apoptosis, and its role does not end there (Kalluri and Weinberg). It is also found to hold the key to enhancing tumour cells with chemo and radiotherapy resistances (Barriere et al., 2015).

In 2008, a study revealed that the EMT also provides tumour cells with mammary stem cells' properties. Such properties include self-renewal and the ability to successfully colonise elsewhere in the body (Mani et al., 2008). EMT was used to generate mesenchymal-like cells while flow cytometry analysis revealed that most of these cells expressed a CD44^{high}/CD24^{low} pattern. This particular configuration of these two cell surface markers is directly associated with both, breast cancer stem cells and normal mammary epithelial stem cells.

At least four closely connected regulatory networks were found to be powering EMT. The activation of any of these networks would exert a relatively strong effect on the rest, leading to occurrence of EMT (Craene and Berx, 2013). Other studies also deduced that EMT plays a key role in converting normal epithelial cells to cancer stem cells. These in turn will acquire properties of normal stem cells that include self-renewal, invasiveness and colonisation ability. Such properties would indeed help these cells invade surrounding tissue and eventually reach the blood circulation, at which point they will be referred to as circulating tumour cells (Jolly et al., 2015).

Furthermore, cancer cells that become motile as a result of EMT usually come in two shapes and associated behaviour, mesenchymal and amoeboid (Huang et al., 2014). These cells are allowed to adopt functional behaviours that vary with phenotypical choices, external signals and genetic changes such as the ability to switch between the two mesenchymal and amoeboid shapes. An example of ovarian and prostate cancer cells that acquire and express numerous epithelial and mesenchymal markers highlights the link between the EMT phenotype and the increased aggressiveness of tumours (Strauss et al., 2009, Ruscetti et al., 2015).

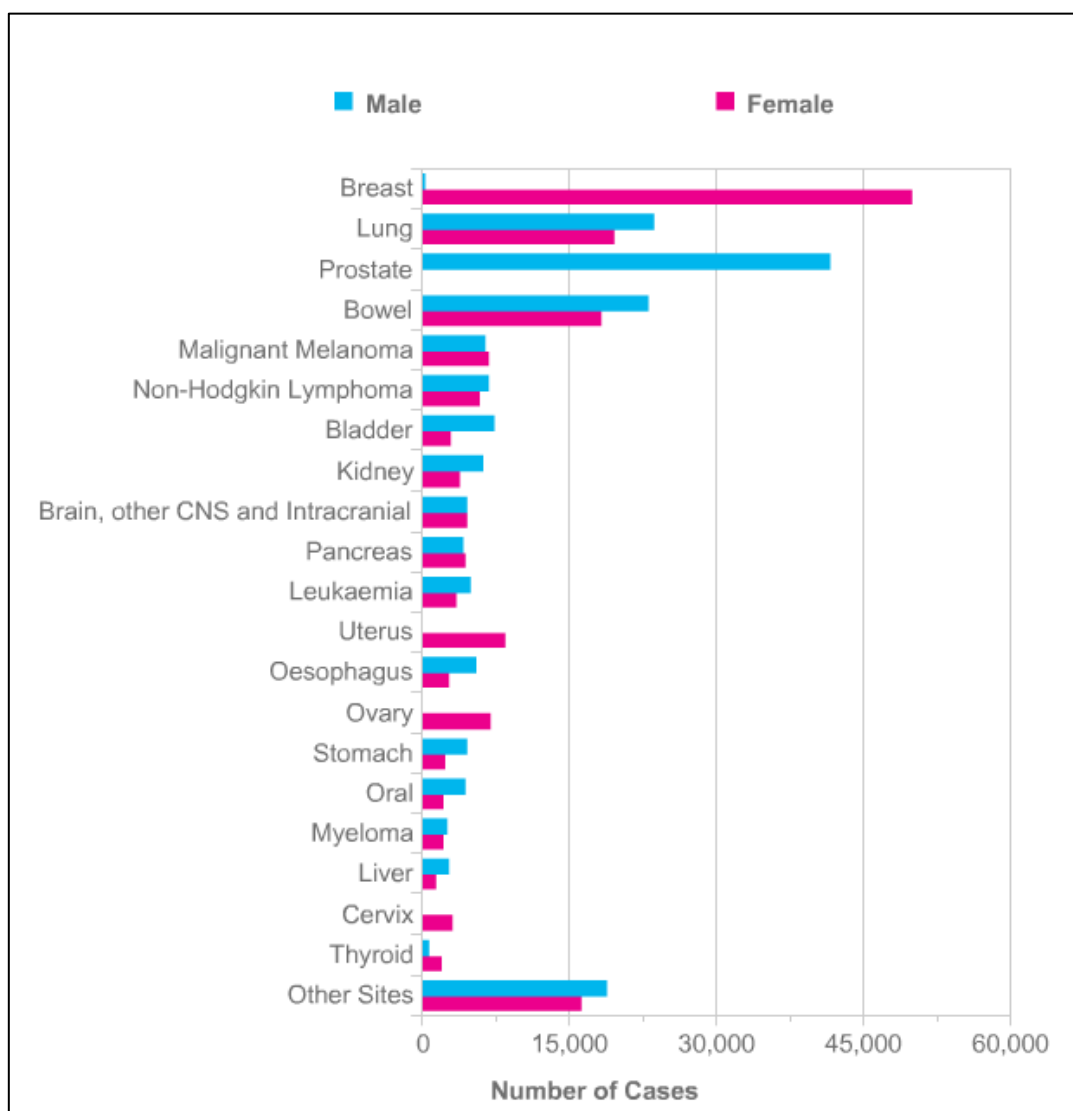
In comparison to cancer cells, normal cells are unable to undergo EMT and detach from their extracellular matrix due to anoikis. Anoikis is the mechanism in which cells are programmed to die if they were to detach from the extracellular matrix, preventing the colonisation of these cells to distant organs (Gilmore, 2005). Anoikis is resisted in cancer cells mainly due to two factors involving integrins and the tumour microenvironment. Mutations that occur in cancer cell's integrins have

several effects on these cells, including the ability to grow in different niches and the capacity to upregulate key enzymes involved in growth factor receptor signalling. The tumour microenvironment on the other hand aids in anoikis resistance via a number of ways, such as the modulation of matrix stiffness and increasing oxidative stress (Paoli et al., 2013).

1.1.8 Cancer Types and Statistics

As previously mentioned, certain types of cancers are more prevalent than others in certain regions and are also distributed differently, based on gender, age group and other factors. The figure below gives an account to the distribution of different cancer types based on gender in the UK. While the table on the following page provides figures of cancer incidence and deaths in the UK

Figure 1.7: Gender distribution of the most common cancers in the UK



The figure above shows the 20 most common cancers in the UK and the number of cases for each type between males and females (CRUK, 2014a).

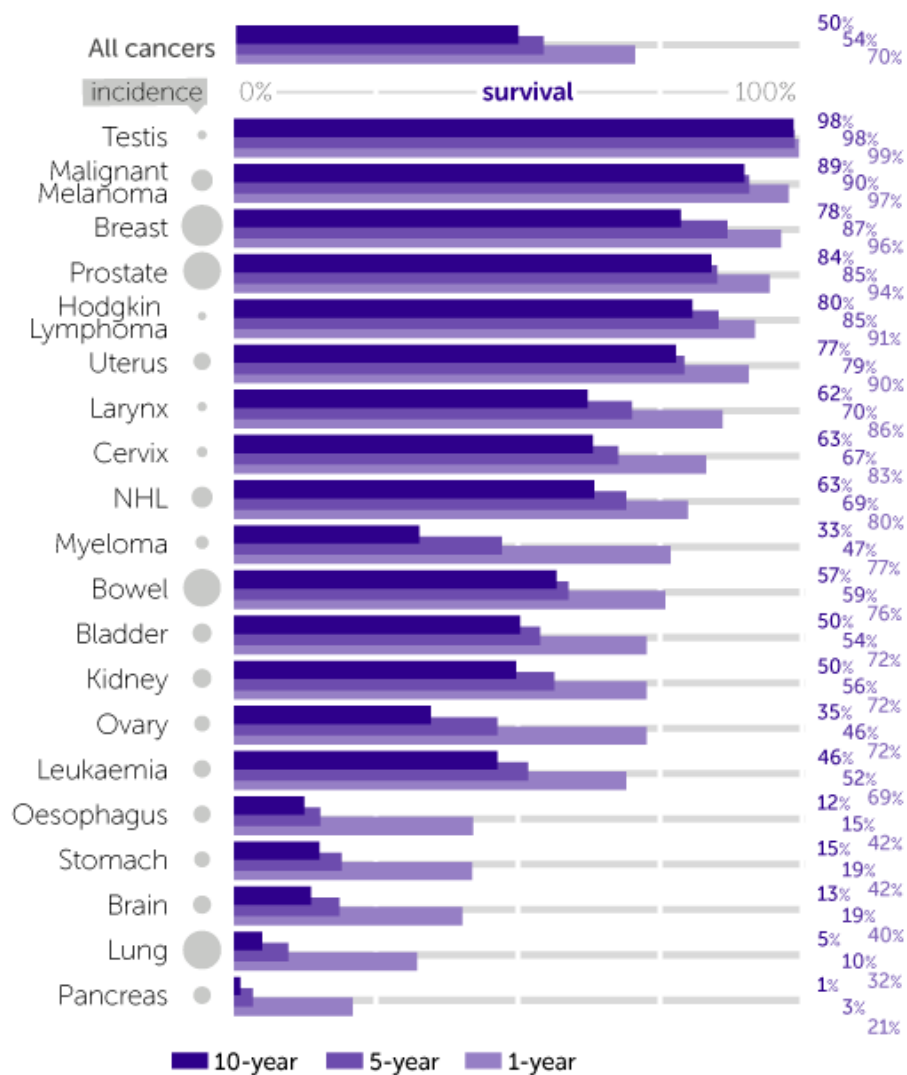
Table 1.2: Cancer incidence and death rates in the UK in 2011 and 2012

Cancer Statistics	Males	Females	Persons	Country	Year
Number of new cases per year	167,487	164,000	331,487	UK	2011
Incidence rate per 100,000 population	426.5	376.2	396.2		
Number of deaths per year	85,068	76,755	161,823	UK	2012
Mortality rate per 100,000 population	198.7	146.6	168.6		
One year survival rate	66.7%	74.1%	70.4%	England and Wales	2010-2011
Five-year net survival (predicted)	49.3%	59.2%	54.3%		
Ten-year net survival (predicted)	45.8%	53.7%	49.8%		

The table above shows cancer incidence and death rates in the UK in 2011 and 2012 as well as the survival rate and percentages between 2010 and 2011 (CRUK, 2014b).

Cancer survival in the UK has seen a tremendous improvement with recent statistical studies showing that in 2010-2011, about half of the adult cancer patients in England and Wales were predicted to survive 10 years or more with almost 46% of these being males and the rest being females (CRUK, 2014b).

Figure 1.8: Age standardised survival for selected cancers in England and Wales



The figure above shows age standardised one-, five- and ten-year survival for selected cancers in adults (aged between 15-99) in England and Wales (CRUK, 2014b).

As shown in Figure 1.8, survival varies greatly from one cancer type to another. The range extends from an excellent 98% ten-year age-standardised net survival for patients suffering from testicular cancer to a mere 1% for those with pancreatic cancer. Generally, cancer occurring in the testes, skin, prostate and in the blood, is usually associated with a very high survival rate (more than 80%). In contrast, survival rate for pancreatic, lung, brain and stomach cancers are at the lowest end of the range (less than 20%).

1.2 Prostate Cancer

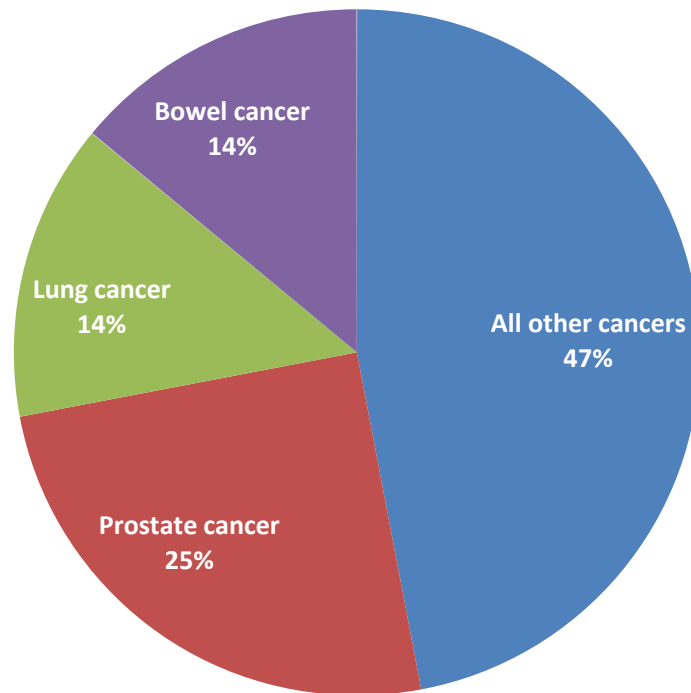
1.2.1 Background and Epidemiology

The Prostate gland is situated underneath the bladder and grows bigger as a male grows older. It is found to be surrounding the urethra and functions to produce semen. Some of the common illnesses that occur at this gland include prostate enlargement, prostatitis and prostate cancer (CRUK, 2014c).

Prostate cancer is an adenocarcinoma cancer that develops mostly in the epithelial glandular cells of the prostate in males (ACS, 2015). In the UK, prostate cancer is the most diagnosed cancer in men with more than 47,300 new cases every year (NHS, 2015a). It is found that one in six men, in the UK and the USA, will develop prostate cancer at some stage of their life time. Most cases, however, develop in elderly men and the tumour grows slowly as patients very often die with the cancer rather than as a result of it. Anatomically, prostate cancer is a type of cancer that is characterized by the development of a tumour in walnut-sized structure in the male reproductive system (Fall et al., 2009). It is known to be multifocal, as each tumour is present in a different location within the prostate (Bracarda et al., 2005).

Figure 1.9: Most common cancers in males in the UK in 2011

**Male incidence: 167,487 cases
UK, 2011**

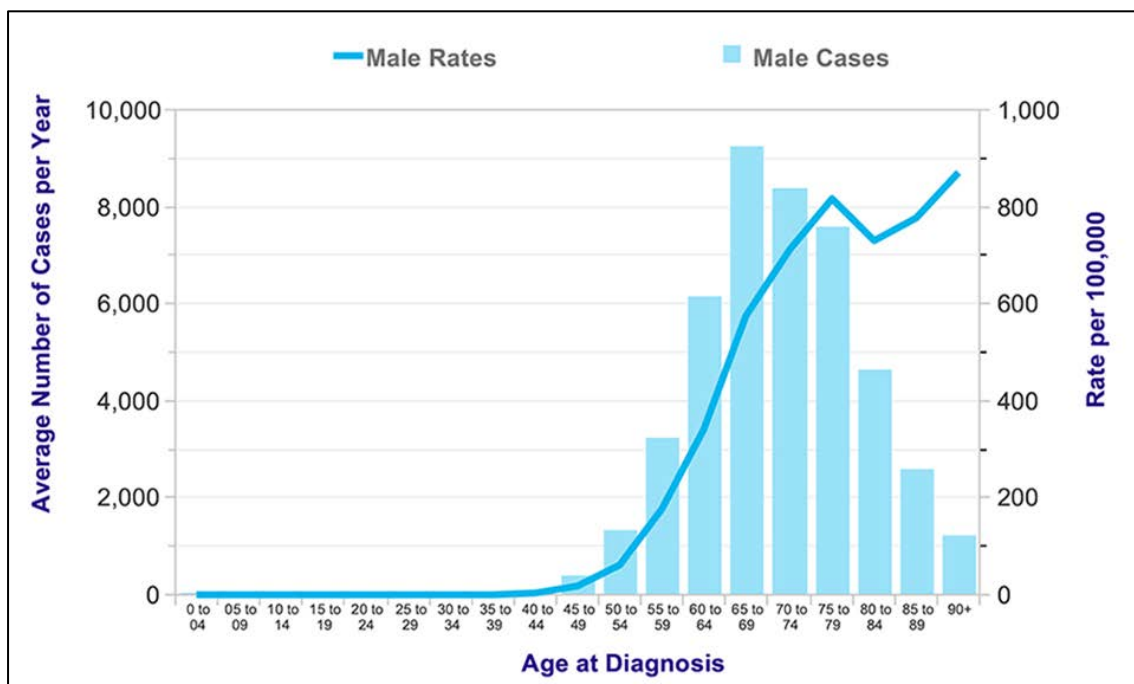


The figure above shows the most common cancers in males in the UK in 2011. Prostate cancer is the most common type with approximately 25% of the total number of cases (CRUK, 2014a). This figure was recreated using data from the original CRUK chart to create a clearer representation of cancer types' percentages.

1.2.2 History

The first case of prostate cancer was diagnosed in The London Hospital in 1853. Although the surgeon who first identified it histologically described it as a rare illness, prostate cancer incidence rate had been increasing since then (Denmeade and Isaacs, 2002). It was not clearly distinguished and was even regarded as another type of urinary obstruction until the early 1900s. Observation of prostate cancer incidence showed that a sharp increase in correlation with age, even more so than any other cancer type (Greenlee et al., 2001). Furthermore, an association with Western lifestyle has been suggested and backed by lower incidence rate in Asian populations in comparison to their Western counterpart. Those who migrated to Western countries also showed an increase in prostate cancer incidence rate, suggesting a possible environmental and/or dietary factor (Anand et al., 2008).

Figure 1.10: Average number of prostate cancer cases per year vs Age at diagnosis



The figure above shows the average number of new cases of prostate cancer per annum and the age-specific incidence rates for men in the UK between 2011 and 2013 (Burford et al., 2009).

The risk of prostate cancer is at a high with men above the age of 50 and that risk increases with age thereafter (Burford et al., 2009). The average age for a male to be diagnosed with prostate cancer is 65-69 and figures have also shown that family history is another major risk factor for the disease. Approximately 5-10% of all prostate cancers diagnosed are found to be linked with hereditary genetic mutations; Brunner *et al* demonstrated how family history is directly involved in increased risk of developing prostate cancer (Bruner et al., 2003).

Table 1.3: Family history and prostate cancer

Family history	Lifetime risk (%)
No history	8
Father with prostate cancer at ≥ 60 years	12
One brother affected ≥ 60 years	15
Father affected before 60 years	20
One brother affected before 60 years	25
Two male relatives with prostate cancer	30
Three or more affected male relatives	35-45

The table above shows the effect of prostate cancer family history on the lifetime risk of developing prostate cancer (Bruner et al., 2003).

Additionally, In 1941 Charles Brenton Huggins, who was an American physician specialising in prostate cancer, found that the metastatic form of prostate cancer responds well to androgen-ablation therapy (Huggins and Hodges, 2002). Huggins' discovery led to a whole new approach in combatting the disease and, even today, androgen ablation remains the most commonly suitable prostate cancer treatment (Denmeade and Isaacs, 2002).

1.2.3 Prostate cancer symptoms

It is very uncommon for prostate cancer to show any symptoms until the tumour is effectively large enough to create pressure on the urethra that the patient can feel (NHS, 2015b). Such pressure on the urethra can have various implications, such as feeling the need to rush to the toilet and urinate more frequently than usual, a difficulty in starting to urinate (urinary hesitancy), weak flow of urine, taking a long time to urinate and even when finished, the patient might get the feeling that their bladder has not been fully emptied.

Although such symptoms do not always mean the patient has developed prostate cancer, it remains of great importance that the patient should visit a doctor and get checked when one or many of these symptoms are experienced. Other symptoms can be experienced and may indicate that the cancer had spread to other organs in the body. Such include testicular pain, loss of appetite accompanied with unexplained weight loss as well as bone and back pain. In addition, gross haematuria had also been observed in prostate cancer patients. A study revealed that its aetiology could depend on the primary treatment of the cancer (Gofrit et al., 2013). It suggested that if radical surgery is not the primary treatment for a prostate cancer patient then haematuria is mostly caused by the cancer itself.

1.2.4 Diagnosis

1.2.4.1 Prostate-specific antigen

Prostate-specific antigen (PSA) is a glycoprotein synthesised as a proenzyme by the secretory cells lining the prostate glands. It is then secreted into the lumen where the propeptide is removed to convert it from proPSA to active PSA. The deactivation of PSA then occurs via the action of proteolysis to generate inactive PSA. Small amounts of inactive PSA then enter the blood circulation and travels in the blood in an unbound form as free PSA (Adhyam and Gupta, 2012). In healthy individuals, the levels of free PSA are higher than that of prostate cancer patients. Prostate cancer is instead associated with higher levels of complexed PSA (Bjork et al., 1996).

PSA is widely used as a prostate cancer biomarker with elevation indicating a high chance of developing the disease. Serum PSA measurement is possibly the most commonly used prostate cancer clinical test. It has contributed to an immense improvement in cancer detection in patients over the past 20 years (Hernández and Thompson, 2004).

Table 1.4: PSA levels and risk of developing prostate cancer

PSA Level (ng/mL)	Risk of prostate cancer (%)
0 – 0.5	6.6
0.6 – 1	10.1
1.1 – 2	17.0
2.1 – 3	23.9
3.1 – 4	26.9

The table above shows the correlation between the PSA levels in the blood and the risk of developing prostate cancer (Heidenreich et al., 2014b). As can be observed, the higher the PSA levels in the blood, the higher the risk of developing prostate cancer.

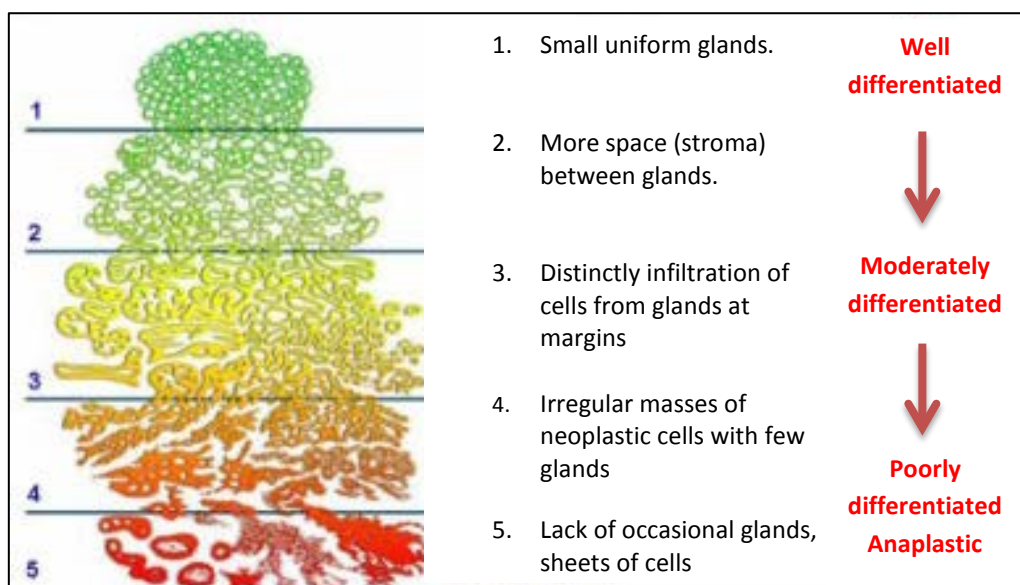
Annual PSA screenings have been generally advised, especially for elderly men (Polascik et al., 1999) and men with PSA levels of >4 ng/mL who would then undergo prostate biopsy following a repeat

abnormal PSA test (Erol et al., 2014). In spite of its satisfactory sensitivity, PSA screening reliability remains limited due to its inadequate specificity (Thompson et al., 2004). Recent studies had shown that PSA screening might not be very beneficial and, in some cases, men with a PSA level lower than 4ng/mL developed prostate cancer while other men with higher PSA levels did not (Lilja et al., 2008, Etzioni, 2013, Hayes and Barry, 2014). It is worth mentioning that PSA levels can fluctuate and are influenced by a range of factors which are not necessarily related to prostate cancer. Such factors include prostatitis and benign prostatic hyperplasia. In addition to these factors, PSA elevation also occurs when the prostate is manipulated in instances of ejaculation, urinary retention and prostate biopsy. As a result, patients undertaking PSA testing, must refrain from having a sexual intercourse for 1 or 2 days prior to the test (Zorn, 2016).

1.2.4.2 Gleason score

Knowing the stage of cancer in a patient is very important in determining the treatment. One way of doing that is by looking at how differentiated the cells are following a biopsy. If the cells are well differentiated then the cancer is at a least advanced stage than if the cells were poorly differentiated. Observing cells' differentiation is carried out using a microscope and the cells are then given a 'Gleason score'. The score range is from 3 to 5, with 3 being well differentiated and 5 being poorly differentiated. A doctor would look at many samples from a patient and then takes the two most common grades and adds them. If the two most common grades for a patient are 3 and 4 then the Gleason score for that patient is 7. The Gleason score can give an idea of the cancer's differentiation, but it cannot be relied upon to make clear-cut decisions about cancer progression and treatment (CRUK, 2014c).

Figure 1.11: Gleason's Pattern Scale



The figure above describes the Gleason grading system, showing its usefulness in predicting cancer risk through classifying how differentiated cancerous cells are (Middlesexhospital.org, 2016).

1.2.5 Treatment

Treatment for prostate cancer differs from one patient to another, vitally depending on the severity of the disease and how far the cancer has spread. For example, patients with stage I prostate cancer (e.g. T1, N0, M0, Gleason score of 6 or less, PSA less than 10) may be treated in one or more of the following ways:

1.2.5.1 Radical prostatectomy

This method is used to remove the patient's entire prostate as well as the tumour that lies within it. It represents an ideal treatment solution for men with localised prostate cancer and might even be considered for prostate tumours that have invaded adjacent tissues – depending on how far these tumours have spread. The operation requires the patient to be physically fit as complications might occur in vulnerable individuals during or even after the treatment. Radical prostatectomy might not be suitable for patients who are over 70 or suffering from heart problems. It is also advisable to avoid this treatment for patients who are overweight (Heidenreich et al., 2014b).

1.2.5.2 External-beam radiation therapy (EBRT) and Brachytherapy

Both of these are radiotherapy approaches that are used to treat early stage prostate cancer. Accurate calculations are carried out to locate the right angle for aiming the radiation beams straight at the tumour, in a process known as the 'simulation'. Brachytherapy, however, is very similar to the interstitial radiation therapy in using relatively small radioactive pellets, placed directly into the prostate. Imaging techniques, such as CT scans or MRI, might be used to provide guidance in implanting these pellets (Babaian et al., 2008).

1.2.5.3 Transurethral resection of the prostate (TURP)

TURP is an approach which aims at relieving the symptoms of prostate cancer rather than curing it and it has been used in early stage prostate cancer as well as the cancer's advanced stages. The inner part of the prostate is removed, while the skin itself is not damaged as an instrument called the resectoscope is used. The resectoscope is inserted through the tip of the penis and into the

urethra until it reaches the enlarged prostate. Once in range, an electric voltage is used to heat the wire and vaporise the tissue. Sometimes a laser is used to burn through the tumour tissue in the prostate using the same method (Rassweiler et al., 2006).

1.2.5.4 Interstitial implantation of radioisotopes

The use of interstitial radioisotopes implanted adjacent to or directly into the tumour provides an efficient tool to deliver radioactive doses to the tumour without harming the surrounding normal tissue. This method could be used as a temporary or as a permanent solution to early stage prostate cancer and the delivery method varies from needles to catheters. This kind of implantation may also include administering an unsealed radioactive source that the body is able to metabolise over a period of time (Janetschek, 2008).

1.2.5.5 Watchful waiting

Watchful waiting or active surveillance might be ideal following treatment and is carried out to observe the development of prostate cancer that is not accompanied by any symptoms or causing any immediate health problems. Furthermore, as it is often the case, most prostate tumours are slow growing and potentially might not require treatment during the patient's lifespan, watchful waiting might be an optimal strategy to deal with this type of tumours. Should an unexpected rapid growth of the tumour take place, then immediate treatment options will be considered to manage the tumour (Loeb et al., 2013). Watchful waiting in cases of prostate cancer includes digital rectal examination, regular PSA testing, transrectal needle biopsies and transrectal ultrasound (NCI, 2014).

On the other hand, patients with a more advanced stage of prostate cancer (e.g. T4, N1, M1, Gleason >8, PSA >20) may require more aggressive approaches, such as:

1.2.5.6 Chemotherapy

Until 2004, the treatment for patients with advanced prostate cancer was limited to the use of androgen deprivation therapy (ADT) in an attempt to slow down the progression of the disease. The

recording of two positive cases at phase III trials of docetaxel presented a huge step forward in the treatment of advanced prostate cancer (Petrylak et al., 2004, Tannock et al., 2004). In addition to docetaxel, research advances have paved way for more chemotherapeutic drugs, such as TAX 327 and SWOG 99-16, to be used in the treatment of prostate cancer. However, with the side effects of chemotherapy, more attention is now given to the detection and treatment of prostate cancer before it becomes castration-resistant as patients with early treatment were found to be healthier than those treated with castration-resistant forms of the cancer (Davda et al., 2016).

1.2.5.7 Immunotherapy

Advanced and recurrent forms of prostate cancers are often treated with immunotherapeutic techniques such as Provenge®. Such systems rely on the enhancement of the body's own immune system to target cancerous cells (Thara et al., 2011). This stimulation of the immune system is focused mainly on the immune checkpoint inhibitors and presents oncologists with a less toxic approach when compared with chemotherapy and a more efficient and optimisable way in which the immune system can be stimulated (Gulley and Madan, 2016). An example of an immunotherapeutic vaccine is sipuleucel-T, targeting the prostatic acid phosphatase. The method relies on the use of the patient's immune cells that have been previously extracted from circulation and processed *ex vivo*, before being injected back into the patient's circulation (Kantoff et al., 2010).

1.2.5.8 Hormone therapy

Hormone therapy alone does not cure prostate cancer; instead it aims to slow down its progression by preventing testosterone from reaching the prostate (Heidenreich et al., 2014a). This is achieved via a variety of ways, including the use of implants to inhibit the production of testosterone by the testicles, orchidectomy (surgical removal of one of the testicles or both) or through drugs that inhibit the production of testosterone (Nguyen and Pastuszak, 2016, Heidenreich et al., 2014a). Despite evidence supporting the role of hormone therapy in relieving prostate cancer symptoms in advanced

stage patients, some argued it may also lead to the deterioration in the quality of life in these patients (Alibhai et al., 2006).

1.3 Circulating tumour cells

1.3.1 Background and History

Circulating tumour cells (CTCs) are cells which shed from the primary tumour in which they originate and migrate away from that site, travelling in blood or lymph circulation and attaching to another distant location forming a secondary tumour (Millner et al., 2013). The link between CTCs and metastasis was first examined by Thomas Ashworth, an Australian physician, in 1869 (Krebs et al., 2010). He reported microscopic observations of cancer cells in a sample of blood from a patient with metastatic cancer. He then went on to compare the morphology these cancerous cells with ones from different cancer lesions in that patient and stated that “if they (CTCs) came from an existing cancer structure, they must have passed through the greater part of the circulatory system to have arrived at the internal saphena vein of the sound leg” (Ashworth, 1869).

His findings have paved way for thousands of studies in the years that followed, which focused on using these cells as possible biomarkers for detecting metastasis. However, despite all the work that has been carried out in the past 140 years, the CellSearch[®] remains the only method to have undergone rigorous testing and succeeded in becoming an FDA-approved method for detecting CTCs in the US (Miller et al., 2010). However, even in the case of CellSearch[®], the system requires specific high end equipment to perform the test and is limited a few types of cancers, clearly indicating that more work in the CTC-detection field remains a necessity.

Although metastasis in malignant tumours is believed to be a result of CTCs entering blood circulation and migrating to distant sites where they form secondary tumours, full confirmation of this has been challenged by their rarity (one CTC per 100 million blood cells) in peripheral circulation. Enumeration and identification of CTCs in the blood can provide us with a much greater understanding of the biology of cancer metastasis as well as help us find novel therapeutic targets for cancer treatment (Paterlini-Brechot and Benali, 2007). CTCs can also be used to monitor the

effectiveness of treatment and identify cancers that have relapsed. Early metastasis detection might be a very vital tool that CTCs can aid in, but their use is not limited there. Successful cancer treatment can lead to complete remission of the tumour, however, in some cases cancer relapses occur. It is of great importance to be able to detect CTCs before and after a patient is treated in order to evaluate the success of the treatment. As a result, CTCs might indeed be crucial as a biomarker in a point-of-care test that would evaluate a patient's health status and assist in making accurate therapeutic decisions (Franken et al., 2012).

Because of their low numbers in the blood, most CTC detection techniques rely heavily on enrichment methods to separate CTCs from the rest of the sample to help detect and identify them (Millner et al., 2013). CTC enrichment techniques aim at condensing the number of CTCs within a sample and separate them from unwanted hematopoietic cells. This is usually carried out by separating cells based on their size, density, migratory properties and protein expression.

It is also believed that many CTCs evade the immune system and detection via their interaction with platelets in blood circulation after the intravasation process is complete (Lou et al., 2015). Platelets may play a role in protecting CTCs from host cells attacks, shear stress inflicted upon migrating cells as well as apoptosis. Additionally, CTC surface-coating with platelets may provide the perfect barrier to prevent the accurate labelling of these cells with epithelial-specific immunological markers (Storkus and Dawson, 1991, Nierodzik et al., 1995, Lou et al., 2015).

CTCs rarity also makes detecting them both expensive and time consuming (Heitzer et al., 2013, Nagrath et al., 2007a). These difficulties along with their unique molecular characteristics makes isolating CTCs from blood very difficult and therefore limits their use as potential biomarkers for cancer research and therapy development (Hou et al., 2013). Additionally, many CTC diagnostic techniques do not take into account different heterogeneous phenotypes of CTCs. Not to mention their incapability of capturing functionally viable CTCs, which may aid in predicting the site at which metastasis would take place and thus tailoring personalised treatment (Millner et al., 2013).

1.3.2 CTCs in prostate cancer

CTCs have previously been linked with metastasis in the prostate and their enumeration was found to be potentially useful as a prognostic molecular marker for prostate cancer (Thalgott et al., 2013). Most studies, have focused solely on certain patient groups (such as ones that have recently been treated) and may need to cover a wide range of patients. However, advanced methods have improved the detection of CTCs in early stages of prostate cancer (Danila et al., 2011, Friedlander and Fong, 2014). Aside from informing physicians of the metastatic properties of a cancer within a patient, CTCs can also provide a molecular profile of the tumour to help predict the patient's sensitivity or resistance to treatment.

Knowing the molecular profile of the tumour plays a big part in developing a personalised treatment for cancer patients, thus increasing their chances of survival. The focus is now on developing a very sensitive assay that is capable of detecting even the smallest amounts of CTCs in the blood as their rarity makes detecting them even more valuable than using other diagnostic techniques, such as the PSA test. This is also confirmed by a study which stated that CTCs' enumeration in castrate-resistant prostate cancer (CRPC) was indeed a very useful prognostic method which can aid in redirecting and optimising therapy (Goldkorn et al., 2014).

Prostate cancer is directly associated with metastases in the bone and lymph and this is thought to be a hugely contributing factor in morbidity-associated deaths through skeletal related events such as spinal cord compression (Saylor et al., 2011). Numerous studies have confirmed the presence of CTCs in CRPC; perhaps the most notable one was the CellSearch[®] assay study which enrolled 276 patients with progressive CRPC (de Bono et al., 2008). The study carried out tests before treatment and on a monthly basis afterwards. Patients were said to have an unfavourable CTC count if 5 or more CTCs were detected in 7.5mL of their blood or a favourable count if less than 5 CTCs were observed. Categorising patients in this way was previously used in similar studies that looked at CTC detection in breast cancer (Miyamoto et al., 2014).

Numerous studies have been conducted to investigate the possibility of molecular characterization of CTCs in prostate cancer. In 2009, a study by Attard *et al* concluded that CTCs obtained from prostate cancer patients showed chromosomal translocation which resulted in TMRSS2-EGR gene fusion in about 30-70% of the therapy-naive cases examined (Attard et al., 2009). The study used real time-polymerase chain reaction (RT-PCR) as well as fluorescence *in situ* hybridization (FISH) to confirm the 100% concordance in EGR gene status between primary tumour biopsies and CTCs.

Another study reported the fusion of the same gene in RNAs extracted from CTCs in metastatic prostate cancer patients (Stott et al., 2010b). The study made use of PSA to stain cells believed to be CTCs in men with the localised and metastatic forms of the tumour. 8 out of 19 patients with the localised tumour that were yet to receive treatment tested positive for CTCs with a range of 38 to 222 CTCs per millilitre of blood. Whereas 23 patients out of 36 tested, who had the malignant form of the disease, showed CTCs presence at a range of 14 to 5000 per millilitre of blood. *TMRSS2-EGR* fusion was detectable in 45% of the patients with malignant prostate tumours.

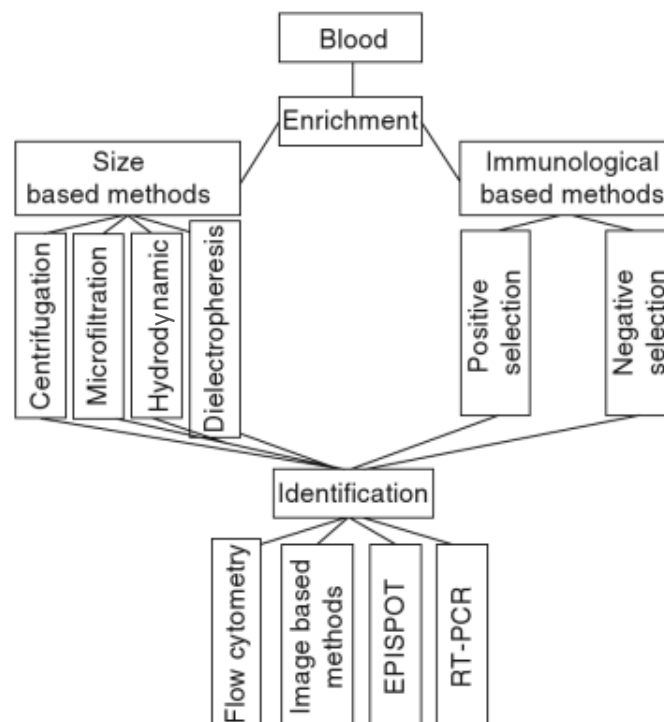
Whether it is to be used for early metastasis detection or for disease management, the use of CTCs as biomarkers in prostate cancer still requires more work. Limitations have been identified in methods mentioned earlier and other ones that used imaging modalities and bones biopsies. New CTC detection methods showed great sensitivity and improved isolation methods of CTCs that target cells' surface receptors or cells that are undergoing EMT (Miyamoto et al., 2014). However, extensive validation remains a requirement before any of these techniques can be approved for clinical use.

1.3.3 Methods of CTCs detection

In prostate cancer, CTCs can be found and identified as possible biomarkers for the different stages of the disease with a variety of methods, including CellSearch® System, CAM Assay, CTC-chip microchip, Epispot assay, Ikoniscope® imaging system and others (Thalgott et al., 2013). Macroscale CTCs isolation or enrichment are used in CTCs detection and include:

- Density gradient centrifugation
- Red blood cell (RBC) lysis, to extract mononuclear cells
- Physical filtration, using commercial filter pores (Isolation by size of epithelial tumour cells (ISET))
- Immunomagnetic separation

Figure 1.12: The different approaches of CTC enrichment



Above is an illustration of the approaches used in CTC enrichment and identification which include kinetic (physical) and immunological methods (Barh, 2014)

Table 1.5: CTC detection methods

Approach	Source/volume	Detection
CellSearch® system	Blood/ 7.5 mL	Positive marker: CK Negative marker: CD45 Nucleus: DAPI
CTC-chip microchip	Blood/0.9 mL	Positive marker: CK Negative marker: CD45 Nucleus: DAPI
EPISPOT assay	Blood, bone marrow/10 mL	Secretion of proteins:CK19, MUC1, Cath-D (breast); CK19 (colon); PSA (prostate); TG (thyroid)
ACIS®Ariol® Automated scanning of chromogenic immunostainings	Bone marrow/blood	Positive markers: CK Negative control: MOPC-21 Nucleus: hemalaun
CAM Assay	Blood, 3 mL	Positive marker: CK 4,5,6,8, 10,13, and 18 Negative marker: CD45
Ikoniscope® imaging system	Blood/1 mL	Positive markers: EpCAM, CK7/8 PSA (prostate only) FISH: chromosomes 7 and 8 Nucleus: DAPI

The table above shows a summary of principal methods used in CTC detection, with the CellSearch® system being the only FDA approved method listed here (Riethdorf, 2010).

1.3.3.1 CellSearch® System

The CellSearch® technology is used to detect, identify and count CTCs in a blood sample. The data gathered by the CellSearch® system would then help physicians make informed decisions on choosing the best course of treatment for cancer patients (Armakolas et al., 2010). The system had previously been tried and tested in metastatic breast, prostate and colorectal cancer and the manufacturing company claims that the system can also give a good estimation of the progression-free survival as well as the overall survival of patients. CellSearch® is often used in conjunction with other detection methods and tests to enhance the accuracy of the diagnosis.

The system requires 7.5mL of blood for each analysis and is comprised of two vital steps. Initially it enriches epithelial cells via the selection of epithelial cell adhesion molecule (EpCAM) positive cells. This is done by mixing peripheral blood samples with iron particles coated with EpCAM to confer magnetic properties within all epithelial cells present. The identification of epithelial carcinoma cells then follows and is achieved via double staining with cytokeratin (CK) and CD45 antibodies while using DAPI to visualise the cells' nuclei. Anti-CK antibodies are used to identify epithelial cells whereas anti-CD45 antibodies would inform the user which cells are lymphocytes and should be disregarded from further analysis. Automated digital fluorescence microscopy is the final step where the CTCs population can be viewed and assessed (Barh, 2014).

Studies have confirmed that using a combination of diagnostic methods (including CellSearch®) provides significantly more reliable prognostic information in comparison to using serum PSA alone, especially in cases of metastatic CRPC (Helo et al., 2009). The CellSearch® system is used in more than 17 countries and remains the only FDA-approved test used for CTCs detection in some cancers.

1.3.3.2 CTC-chip microchip

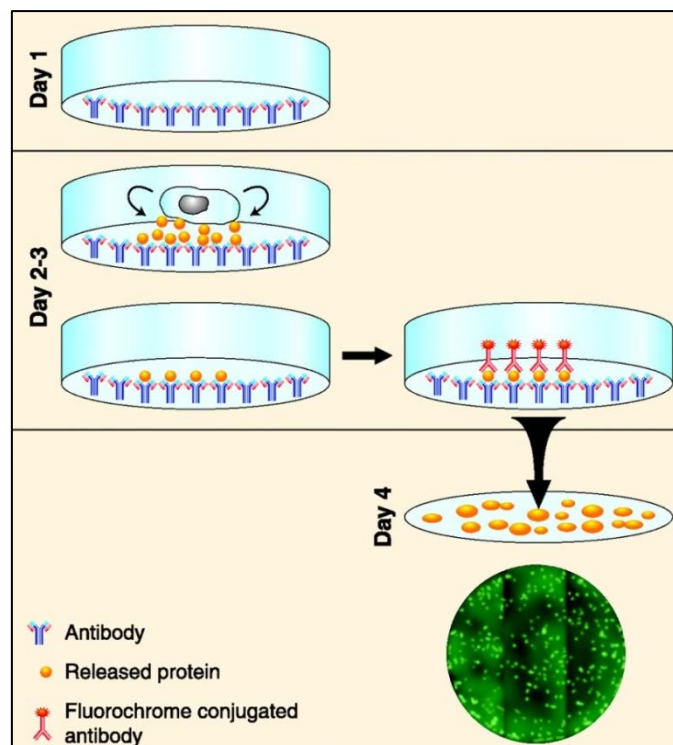
CTC-chip is a microfluidic device which allows for the isolation and enumeration CTCs from peripheral whole blood samples (Nadal et al., 2013). Originally developed by a team of investigators from the Massachusetts General Hospital, CTC-chip helps in the selective separation of viable CTCs via the interaction of the targeted CTCs with EpCAM-coated microposts. All of which is achieved under carefully controlled laminar flow conditions. The method had worked well when tested on patients with metastatic lung, prostate, pancreatic, breast and colon cancers with a success rate of 99% of the cases (115 case out of 116) (Nagrath et al., 2007b).

CTC-chip has a purity of about 50% and was able to detect a range of CTCs in the samples trialled, ranging from 5 CTC/mL of blood in some samples to 1281 CTC/mL in others. For prostate cancer patients, CTCs were isolated in all of the cases (7 patients in total) despite the patients being in the early stage of the disease. In addition, CTC-Chip was also tested to see its efficiency in monitoring patient's response to anti-cancer treatment. The changes in CTCs numbers showed a reasonable correlation with the clinical course of the disease.

1.3.3.3 Epithelial ImmunoSPOT (EPISPOT) Assay

The EPISPOT assay has a vital advantage over other CTC detection methods in that it allows for the detection of viable epithelial secreting cells only. This detection is performed after CD45⁺ cell depletion and with the use of protein markers such as MUC1 and CK19 (Nadal et al., 2013). This is achieved as dying cells do not secrete the usual amounts of these proteins and thus the assay will not regard them as epithelial cancerous cells (Alix-Panabieres et al., 2005). Despite the correlation between the increased detection of CK19 mRNA transcripts in a blood sample and bad survival outcomes in early stage breast cancer patients with oestrogen receptor-negative tumour (Ignatiadis et al., 2007), further research and validation are required to prove that EPISPOT is in fact a reliable tool for CTCs detection. The assay general steps are explained in Figure 1.13 below.

Figure 1.13: EPISPOT assay

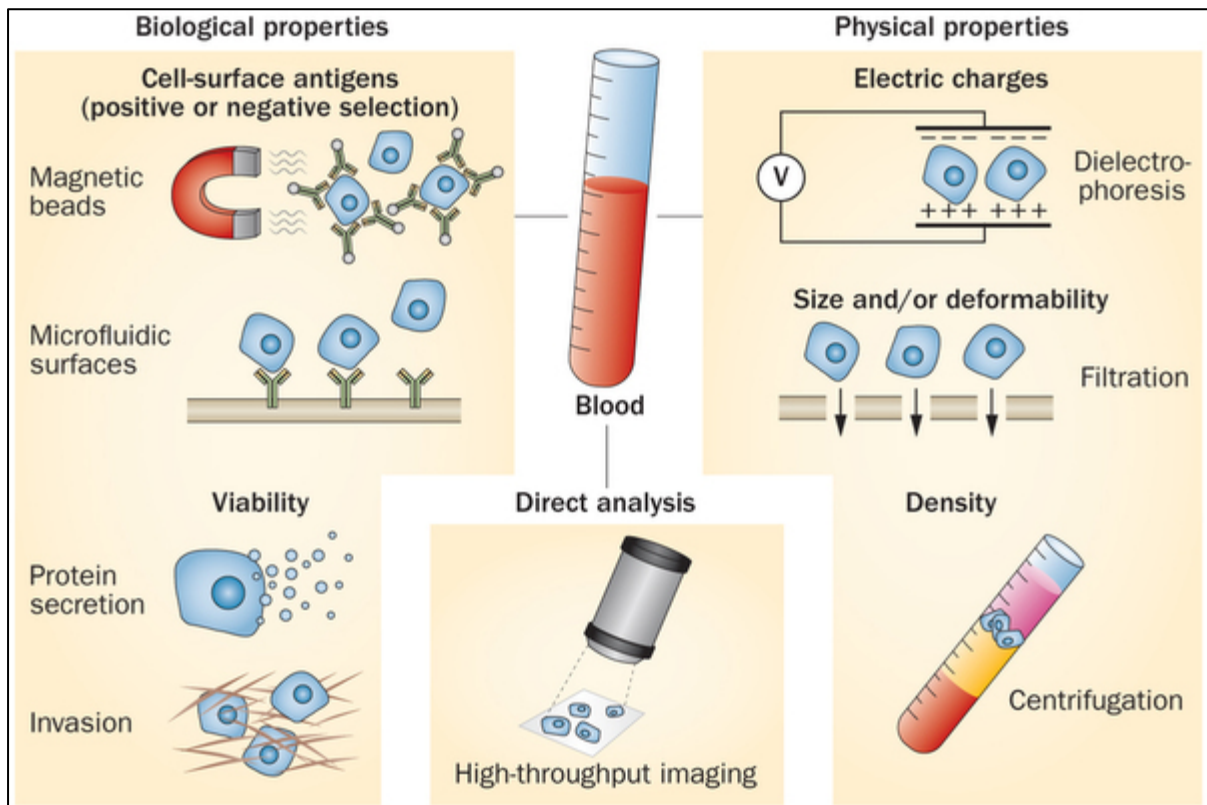


The figure above briefly describes the key events taking place during the EPISPOT assay. Initially, the membranes of the EPISPOT plates are coated with a specific antibody as shown in day 1. During the next two days, cells are seeded in each well and cultured for 48 hours. The immunocapture of the released proteins takes place at this stage during the incubation period and is achieved via the immobilised antibody at the bottom of the well. After washing the plates to remove the cells, the presence of the released protein is revealed using a fluorochrome-conjugated antibody. Finally, on the 4th day, the fluorescent immunospots are counted; one immunospot represents one protein-releasing viable cell (Alix-Panabières et al., 2008).

1.3.3.4 Other methods

Other CTCs detection methods vary in the approach taken to isolate and enumerate CTCs but most systems use enrichment methods that rely on the biological and physical properties of cells captured as shown in Figure 1.14 below (Miyamoto et al., 2014).

Figure 1.14: CTC detection approaches



Above is an illustration showing variation of methods used in the detection of CTCs. Some methods rely on the use of biological properties such as cell surface antigens. By doing so, these antigens are targeted with immunofluorescent antibodies to identify and isolate them in what is known as positive or negative selection. Some biological methods rely on the depletion of cells and detecting cellular viability. Other techniques involve the use of advanced imaging technique for direct analysis. Whereas another approach is to examine the physical properties of cells, such as the electric charges or cellular density (Miyamoto et al., 2014).

Automated Cellular Imaging System (ACIS®) and Ariol® system are also used for the enumeration of CTCs. Ariol® is an automated system that is used for image capture and analysis and is capable of combining multiple fluorescent and brightfield images of the same cell at the same time. The system

had previously been tested in cases of metastatic breast cancer (Deng et al., 2008) and was found to have higher sensitivity, accuracy and reproducibility than the CellSearch® system mentioned earlier.

Another method of detection is the Ikoniscope® Imaging System which relies on the use of Ikoniscope® robotic microscope. The company describes its product as self-handling and can do automated scanning, eliminating in the process many of the factors that cause human error in testing. The company also claims that the device can provide real-time image capture and analysis of up to 2 million cells on a single slide. Spiking experiments involving samples taken from prostate, colorectal and ovarian cancer patients were carried out and analysed with Ikoniscope® microscope (Ntouroupi et al., 2008). Results showed that less than one epithelial cell per one millilitre of blood can be detected. However, despite being unable to detect CTCs in only 2 out of the 25 colorectal cancer patients tested on, the method was deemed relatively simple, rapid and useful for clear-cut identification of CTCs for possible cancer screening and monitoring purposes.

Other antibody-based capture assays for CTCs detection include Magsweeper (EpCAM-based), GILUPI cell collector, Adna Test and IsoFlux. Physical characteristic-based assays include ISET®, Dean Flow Fractionation and Dielectrophoretic field-flow fractionation. There are also other CAM assays, High-throughput fluorescent scanning and DEPArray (Krebs et al., 2014).

1.4 Imaging flow cytometry

1.4.1 History and background

In 1968, Wolfgang Gödhe from the University of Münster in Germany developed the first fluorescence-based flow cytometry device, the ICP 11. The technology used by the ICP11, was named pulse cytophotometry and was then changed to flow cytometry 10 years later (BeckmanCoulter, 2015). The term rapidly became popular and many devices soon emerged such as Cytofluorograph, PAS 8000, ICP 22, Epics and the first Fluorescence-Activated Cell Sorter (FACS).

In the past 10 years, imaging flow cytometry emerged as a powerful tool used for cell capture and analysis. There were few challenges, however, that have been long associated with the imaging of cells in flow. Such include acquiring sufficient fluorescence sensitivity, the production of high spatial resolution imagery, combining fluorescence imagery with other imaging modes and the ability to image all of the cells in flow (Basiji et al., 2007).

Advanced imaging flow cytometers (such as Amnis ImageStream^x) combine the powers of microscopy and flow cytometry to help scientists detect, capture images and analyse thousands of heterogeneous cells in flow in seconds. The cell capture and analysis is done in real time and graphs can be produced to compare cell parameters, staining intensity and other criteria (Barteneva et al., 2012). Imaging flow cytometers are commercially available nowadays from Amnis Incorporated (Merck Millipore) and are involved in a wide range of research involving the detection and analysis of tumour cells in different cancer types as well as various cell-lines in other diseases (van Beers et al., 2014, Hui et al., 2014). Imaging flow cytometry methods also aid in the detection of changes within cells themselves. Such changes include DNA damage and nuclear alterations.

When compared with normal flow cytometry, the imaging aspect of this technology allows for the detection of chromosomal signalling, antigen localization and other events that take place within the

cell as demonstrated by Grimwade *et al* in the study that explored the use of an imaging flow cytometer in the diagnostic assessment of acute leukaemia (Grimwade et al., 2017). The technique showed a major advantage in its ability to visualise certain cells of interest as well as the localising the cellular compartment in which an antigen is expressed. Full comparison between standard and imaging flow cytometry is summarised in the table below.

Table 1.6: Standard flow cytometry vs imaging flow cytometry

	Standard flow cytometry	Imaging flow cytometry
Visualise cell morphology	No	Yes
Analyse differences in cell size and shape	No	Yes
Immunophenotype cells based on antigen expression detected with fluorescent antibodies	Yes	Yes
Assess multiple fluorescent parameters simultaneously	Yes	Yes
Determine cellular location of antigen expression, i.e. cytoplasmic versus nuclear	No	Yes
Determine the pattern of antigen expression, i.e. diffuse versus punctate	No	Yes
Ability to perform all tests required in leukaemia diagnosis in one analysis, as defined by WHO Classification , i.e. morphology, phenotype and chromosomal analysis	No	Yes
Multiparametric analysis of small volume (<100µl) or low cell number	Limited	Yes
Return any residual sample after you have finished acquiring	Yes	Yes
Automated data analysis software available	Yes	Yes
Ability to use software to create “masks” to calculate similarity or co-localisation of expression	No	Yes
High throughput analysis, i.e. >100 cells per second	Yes	Yes
In Vitro Diagnosis (IVD) compliant	Yes	Pending

Above is a comparison between imaging flow cytometry and standard flow cytometry (Grimwade et al., 2017)

Another study utilised the use of this technology in studying the biology and different pathologies of erythrocytes (Samsel and McCoy Jr, 2015). It praised how easily the process of enucleation in mammalian erythrocyte maturation was detected but warned that the use of such technique has its limits too. For example, cells are required to be in suspension in order for them to be examined

rather than having them on a slide or adhered to a plate. There is also the concern that adherent cells might be damaged when they are trypsinised and removed prior to being analysed; such damage may come in the shape of affecting cell surface receptors.

Imaging flow cytometry also showed a great potential in the analysis of primary megakaryocytes isolated from murine bone marrow in order to study the decreased platelet production by these cells following bone marrow injury, which could ultimately lead to thrombocytopenia (Niswander et al., 2014a). All in all, both studies as well as many others concluded that the use of such technology would indeed provide us with a highly sophisticated insight in a less time-consuming manner than traditional methods.

1.4.2 ImageStream^X

The ImageStream^X is one of the commercially available imaging flow cytometers that combines microscopy with flow cytometry. Enhanced with the powerful analysis software IDEAS[®], the ImageStream^X is capable of producing 60,000 images of 10,000 cells in approximately 30 seconds. IDEAS[®] is useful in the analysis of captured images of cells as it compares cellular morphology, fluorescent signal strength, signal locations and other cellular features. The software provides 40 quantitative features per image, allowing for approximately 250 features to be analysed per cell (Basiji et al., 2007). The results based on these features are displayed on scatterplots or histograms, giving an accurate count of each population gated in each analysis.

The instrument's mother company, Millipore, recently released the Amnis ImageStream^X Mark II with multiple magnification powers (20×, 40× and 60× objective), twin excitation lasers – with a maximum of 12 channels for image acquisition – and the Extended Depth of Field (EDF) feature using multilayer stacking to allow the capture of whole cells in flow (Headland et al., 2014).

Even prior to the injection of these new features, numerous works had been published with the help of the imaging tools provided by the ImageStream^X. Such publications include the study of primary megakaryocytes and their involvement in thrombocytopenia (Niswander et al., 2014b), an investigation into the possibility of using extracellular matrix domain formation as an indicator of chondrocyte dedifferentiation and hypertrophy (Wu et al., 2014) as well as research into CTCs detection and metastasis (Lopez-Riquelme et al., 2013).

Furthermore, a recent study explored how the use of the ImageStream^X can benefit scientists in the detection and characterisation of CTCs in different types of cancer (Dent et al., 2016). It utilised the cancer cells' expression of a range of biomarkers such as EpCAM and CK. CTCs were detected in patients with oesophageal, hepatocellular, thyroid and ovarian cancers. The authors showed that the method they developed may be piloted for other cancer types and has the advantage in reduced

cell damage when handling cancer cells with cell recoveries greater than 50%. The relatively fast speed at which the test was performed was highlighted, as well as the lack of reliance on a single expression of a biomarker by cancer cells.

Unenriched samples could also be analysed, but in comparison with enriched samples, they would be vastly time consuming. A 5mL unenriched sample would require about 15 hours to be fully analysed for the presence of CTCs, whereas it would take 1 hour 40 minutes to analyse an enriched sample. Additionally, the recovery of cells was also compared between enriched and unenriched samples. Enrichment led to CTC losses which accounted for about 38.1%, and there were also losses of about 6.7% which occurred during image collection. However, unlike CellSearch® which positively selects cells that are EpCAM positive only, cell recovery was increased with the use of EasySep® magnetic separation kit. This is because many cancerous cells undergo EMT and as a result, they are likely to lose EpCAM expression or have it changed during the cell cycle (Hyun et al., 2016).

CTCs detection using the ImageStream^X system was recently tested against the CellSearch® system in pancreatic cancer (Lopez-Riquelme et al., 2013). The study used PANC-1 pancreatic cancer cells in cells spiking experiment with healthy peripheral blood cells. It was claimed that the enumeration of these cells was lower using the ImageStream^X platform than it was using CellSearch®. Despite using the same biomarkers for CTC detection in both systems, the enrichment methods used – which as previously explained, accounts for a considerable cell loss – differed for each system, rendering the results of that study questionable.

Our research group recently explored the benefits of using the ImageStream^X system and how it surpassed older methods used (Parris et al., 2015b). We demonstrated that the detection of γ -H2AX DNA damage foci can be further enhanced when using the new ImageStream^X Mark II featuring the multi-magnification of 20 \times , 40 \times , and 60 \times as well the EDF focus stacking module. This was achieved by imaging and quantifying γ -H2AX foci in human cells with normal and defective DNA double-strand break repair capacity.

Our study showed that using the new 60× magnification and EDF helped to accurately detect 40-50% more foci in cell nuclei. Thus, the use of these new features may be utilised in diagnostic tests developed to predict the response of cancer patients to clinical radiotherapy or for the detection of CTCs. This work comes as a follow up to what has been previously published by our group about the use of imaging flow cytometry as a novel and robust technique for the estimation and quantification of γ -H2AX in cells (Bourton et al., 2012).

1.5 AIM

The aim of my study is develop and validate a reliable diagnostic method that is capable of identifying CTCs in blood samples using Amnis ImageStream^X Mark II. Initially, PC3 prostate cancer cells were used (mimicking the role of CTCs) in samples containing peripheral blood lymphocytes (PBLs). A comparison between a number of immunological and physical methods will be conducted to deduce the most specific and sensitive approach for the identification of CTCs.

The attainment of a precise CTC detection method will be followed by a validation test using clinical samples obtained from different metastatic CRPC patients. Defining the sensitivity of the test will give a clue as to how effective it can be in the early detection of CTCs in prostate cancer patients, determining the metastatic properties of prostate tumours and, possibly, utilising its use as point-of-care system in monitoring cancer patients before and after treatment.

In this research, I will be thoroughly investigating a number of biomarkers and their staining intensity and localisation such as the Epithelial Cell Adhesion Molecule (EpCAM), Zonula Occludens-1 Tight Junctions (ZO-1 TJ) protein antibody and the leukocyte-specific marker, CD45 antibody. Moreover, the physical characteristics of CTCs and leukocytes will be examined using a range of comparison features provided by the analysis software, IDEAS[®], such as cell size and aspect ratio.

Chapter 2

Materials and Methods

2. Materials and methods

2.1 Cell Maintenance

2.1.1 Cell culture

PC3 cells derived from a primary epithelial prostate cancer were used and regularly maintained in Hams F-12 medium containing 10% foetal calf serum, 100 units/mL penicillin–streptomycin (Biosera, Sussex, UK) and 2 mM L-glutamine. Cells were grown in T75 flasks at a temperature of 37°C and a humidified atmosphere of 5% CO₂ in air. PC3 cells were sub-cultured in a Heraeus Class II Laminar Flow hood for no more than 10 times and not beyond 60 passages.

Peripheral blood lymphocytes (PBL) were obtained from various healthy individuals with full ethical approval and with informed consent and kept in liquid nitrogen until use. When required for an experiment, vials containing PBL were thawed in a water bath at 37°C, washed with RPMI-1640 medium (Biosera, Sussex, UK) containing 10% foetal calf serum, 100 units/mL penicillin–streptomycin and 2mM L-glutamine, and then grown in PB-MAX (Thermo Scientific™, Leicestershire, UK) medium in T25 flasks for approximately two days prior to use. PBL are also maintained at a temperature of 37° C and a CO₂ level of 5%. GMO0893 cells were maintained in RPMI-1640 medium containing 10% foetal calf serum, 100 units/mL penicillin–streptomycin and 2 mM L-glutamine and sub-cultured in a similar way to PC3 cells.

The PC3 cell-line (human prostate cancer cells) is used to mimic the role of CTCs in blood with similar characteristics to prostatic small cell carcinoma (Tai et al., 2011), whereas the PBLs – which were taken from different healthy individuals – and the GMO0893 cell-line played the role of blood cells in the body. The sources for the three types of cells used are mentioned in Table 2.1.

Table 2.1: List of cell-lines used

Cell-line	Supplier	Medium	Growth conditions
PC3	Kind gift from Professor Robert Newbold, Brunel University	Ham's F12	Incubation at 37°C in a humidified atmosphere of 5% CO ₂ in air
GMO0893	Coriell Institute, New Jersey, USA	RPMI 1640	Incubation at 37°C in a humidified atmosphere of 5% CO ₂ in air
PBL	Multiple donors	PB-MAX	Incubation at 37°C in a humidified atmosphere of 5% CO ₂ in air

Above is a table listing the cell-lines used, their suppliers, their media and growth conditions.

2.1.2 Cell trypsinisation

The PC3 cells were grown as monolayers in T75 cell culture flasks (Tai et al., 2011), the Hams F12 medium the cells grew in was initially removed using a glass Pasteur pipette. Cells were then washed with 10mL of phosphate-buffered saline (PBS) (Scientific Laboratory Supplies Ltd., Loughborough, UK). The PBS was then aspirated and 1.5 mL of Trypsin-EDTA (SLS) was added to each flask and incubated at 37°C for 5 minutes.

Flasks were then examined under the microscope to ensure that most cells have detached from the flask. The cells were then resuspended in 10mL of Hams F12 medium and either transferred into multiple new flasks to grow or placed into a 15mL falcon tube and used in an experiment.

2.1.3 Cell Counting

Prior to using any cell-line for culture or in an experiment, cells in each flask were counted using one of two methods, a glass haemocytometer or the Cell Countess device (Invitrogen, Life Technologies, Paisley, UK). To count the cells, Trypsin was first used to detach them from the flask if they were adherent as previously explained. After recovering the cells in 10mL growth medium, a 10 μ l sample was taken from the cell suspension and added to another 10 μ l of Trypan Blue dye in an Eppendorf tube. This was performed to distinguish between live and dead cells when counting. Trypan blue is an extensively used dye for staining and identifying dead cells. The dye is negatively charged and would only interact with cells with damaged membranes, Figure 2.1 below demonstrates the steps taken to count cells using Trypan Blue and a Cell Countess (Tran et al., 2011).

Figure 2.1: Counting cells using a Cell Countess



The figure shows the steps of staining dead cells with Trypan Blue and how the number of viable cells is counted using a Cell Countess device (Invitrogen, Life Technologies, Paisley, UK). The graphics in steps A and C are taken from the Nanoentek website (Nanoentek, 2015).

According to the manufacturer's instructions, the Cell Countess is limited to a certain cell concentration to ensure accurate counting, with a minimum of 1×10^4 cells/mL and a maximum of 1×10^7 cells/mL. In cases of low cell numbers, cells were reseeded in 20mL of medium and back into their T75 flasks and returned in the incubator where they are left to grow and while being periodically observed. In rare occasions, cell numbers were found to exceed the range beyond which

the Countess accuracy would no longer be reliable. For these experiments, a Neubauer haemocytometer was used and the samples were stained with the Trypan Blue dye and then loaded onto the slide. Cell counting was carried out at 20× magnification using an Olympus CK2 microscope.

2.1.4 Cell Freezing

Cells were used over a restricted range of 10 passages, thus frozen cell stocks were produced for future use. To freeze cells for future use in experiments, a freezing solution was made comprising of 10% DiMethyl Sulfoxide (Sigma-Aldrich), 10% foetal calf serum and 80% medium containing penicillin/streptomycin and L-glutamine.

As described before, cells were grown in T75 flasks until they reach a confluency of about 90%. They were then trypsinised (in the case of adherent PC3 cells) and recovered with 10mL of growth medium and moved into a 15mL falcon tube (Sarstedt). After centrifugation for 5 minutes at 1500 rotation per minute (rpm), the medium was aspirated and 1mL of the freezing solution was added to cells. These were then transferred into cryo-vials (Sarstedt) and placed in a cell freezing container (Nalgene, Sigma-Aldrich). These containers were used to ensure that the samples stored reached at least -80°C temperature before storing them in liquid nitrogen dewars.

Freezing containers comprise a foam insert that is soaked in isopropanol, a solution which allows for a slow freezing rate of cells at about 1°C/minute. The freezing containers were then left in the -80°C freezer for at least 24 hours before transferring the samples into the liquid nitrogen dewars.

2.1.5 *Mycoplasma* PCR for PC3 cell-line

The Mycosensor PCR Assay Kit (Agilent Technologies™) was used to verify the existence of mycoplasma in the PC3 cell-line. The primer mix is capable of detecting *mycoplasma* infections in cell cultures in a procedure that lasts 3 and half hours using 100µl of cell culture supernatant (Agilent, 2016). The test showed no presence of *mycoplasma* in the PC3 cell-line that was used.

One hundred microliters of the Hams F-12 medium in which PC3 cells were growing was used to determine the presence of mycoplasma in the culture. This amount was then transferred into an Eppendorf tube and heated to 95°C for 5 minutes using a heat block. The medium was then centrifuged for about 30 seconds at a speed of 14k rpm at room temperature. 10µl of Strataclean (non-flammable slurry of proprietary hydroxylated silica particles) was added to the sample and mixed by gentle agitation, ensuring that resin had combined with the medium. Centrifugation followed for 1 minute at a speed of 13k rpm and then 5µl was transferred into a 0.25mL PCR tube containing 45µl of the required PCR mastermix. The mastermix consisted of 13.5µl nuclease free water, 25µl 2x reaction mix, 2µl primer mix and 4µl internal control template.

The 0.25mL PCR tube containing PC3 medium was then placed into the thermal cycler with 10 µl of the final product being later used in a 1% agarose gel. Below is a table outlining the conditions used in the thermal cycler:

Table 2.2: *Mycoplasma* PCR program

Steps	Temperature	Duration	Cycles
Denaturation	94°C	30 seconds	1
Denaturation	94°C	30 seconds	35
Annealing	55°C	1 minute	35
Elongation	72°C	1 minute	35
Extension	72°C	10 minutes	1

Above is the table outlining the conditions used in the thermal cycler for the *Mycoplasma* PCR program.

2.2 Immunocytochemistry and live cell analysis

In this research, two types of experiments were conducted. A set of experiments used cells that were fixed before mixing them with another cell-line to reconstruct presence of CTCs in the blood. These cells were then stained with a number of biomarkers such as EpCAM, ZO1 TJ and CD45 antibodies to detect CTCs based on the immunological staining of cells in the test samples. The other set of experiments used cells that were live in order to measure and compare the physical and morphological properties of these cells.

To fix these cell-lines, PC3 cells were first washed with 10mL of PBS and detached from the flask by trypsinisation in 1.5mL in Trypsin-EDTA. They were then fixed in 1mL of 3.7% Paraformaldehyde (PFA) for approximately 5 minutes on ice. GMO0893 and PBL cells were washed with PBS and fixed in a similar way to PC3 cells but without adding Trypsin to these cells.

Following fixation, cells they were then washed with PBS to rehydrate them. They were then centrifuged at 2000rpm for 3 minutes and blocked with 1mL block buffer containing 5% rabbit serum (or goat serum when using CD45 antibody) (Thermo Scientific, Leicestershire, UK) and 95% PBS and left to rotate on a spinning wheel (Bibby Scientific, Staffordshire, UK) for 1 hour at a speed of 20 rpm at room temperature. Cells were then washed with 1mL PBS and the primary antibody (diluted in blocking buffer) was added before incubating them at 4°C overnight. Table 2.3 on the following page outlines the antibodies used, their source and dilution.

After 24 hours of incubation, the cells were then centrifuged at 2000rpm for 3 minutes before being washed with 1mL of PBS and incubated with 1µl of the secondary rabbit anti-mouse (or goat anti-rabbit, in the case of CD45 antibody) IgG Alexafluor 488 conjugated antibody diluted at 1:1000 in blocking buffer (Invitrogen Scientific, Paisley, Scotland, UK) on the rotating wheel at a speed of 25rpm for 1 hour at room temperature while covered from light. 100µl of Accumax (Global Cell Solutions Inc., Charlottesville, VA, USA) was added to samples and incubated at 4°C overnight. 1µl of

the nuclear stain DRAQ5 (Biostatus, Hitchin, Herts, UK.) was added to the samples and left to stand for 15 minutes prior to ImageStream^x image capture.

Table 2.3: List of the three antibodies used

Antibody	Source	Dilution (in blocking buffer)
EpCAM	IgG mouse monoclonal antibody (ABCAM, Cambridge, UK. Clone number: HEA125)	200µl (Prediluted)
CD45	IgG rabbit monoclonal antibody (ABCAM, Cambridge, UK. Clone number: EP322Y)	1:1000
ZO-1 TJ	IgG mouse monoclonal antibody (ABCAM, Cambridge, UK. Clone number: mAbcam 61357)	1:200

The table above shows the different antibodies used to detect PC3 cells, GMO0893 or PBL cells. The source and dilution of each antibody are also mentioned.

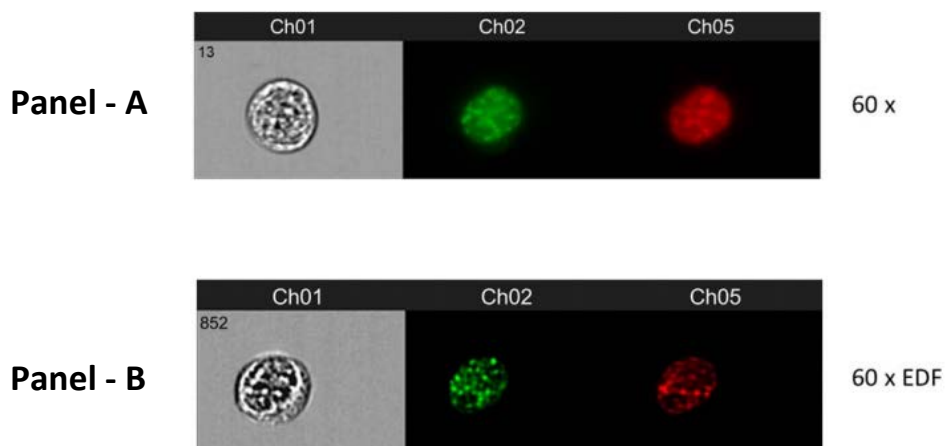
Cells used in live cell analysis were prepared in a similar procedure to the one used in the immunostaining method with the exception of fixing, blocking and staining of cells with primary and secondary antibodies. Following the transfer of cells from flasks to Eppendorf tubes, they were resuspended in 100µl of Accumax and stored for approximately 20 minutes at 4°C. 1µl of the nuclear stain DRAQ5 was then added to the samples and were left to stand for 15 minutes prior to ImageStream^x image capture.

2.3 Sample acquisition and analysis using imaging flow cytometry

2.3.1 ImageStream^X Mark II

The ImageStream^X Mark II (Amnis Inc., Seattle, Washington), as previously described, is a flow cytometer with microscopic capabilities. It is capable of capturing thousands of images of cells in flow on twelve different channels simultaneously. The Mark II is an upgrade on the previous version and possesses unique features such as multi-magnifications (20×, 40× and 60×) as well as the extended depth of field (EDFTM) technology. EDFTM makes use of Wavefront Coding technology which combines the use of specialised optics and a special imaging processing algorithms, allowing for all information about a captured cell to be grouped onto a single focal plane using focus stacking (Parris et al., 2015a). This allows for an in-depth imaging of cellular morphology without losing the sensitivity of fluorescence staining (Millipore, 2016).

Figure 2.2: Utilising the use of EDF technology in the ImageStream^X



The figure above shows two panels to compare the difference between normal cell imaging and EDF-enabled imaging. Both images are captured at 60×; however, Panel - B shows more detailed features (Parris et al., 2015a).

The device is also capable of capturing images on different optical channels using a range of lasers, of which the 800nm will be used to capture brightfield (BF) images, the 488nm for Alexa Fluor (AF)

and 642nm for DRAQ5. Below is a table which describes the uses of these lasers and the fluorochromes used in this study.

Table 2.4: List of fluorescent antibodies that can be used with the ImageStream^x

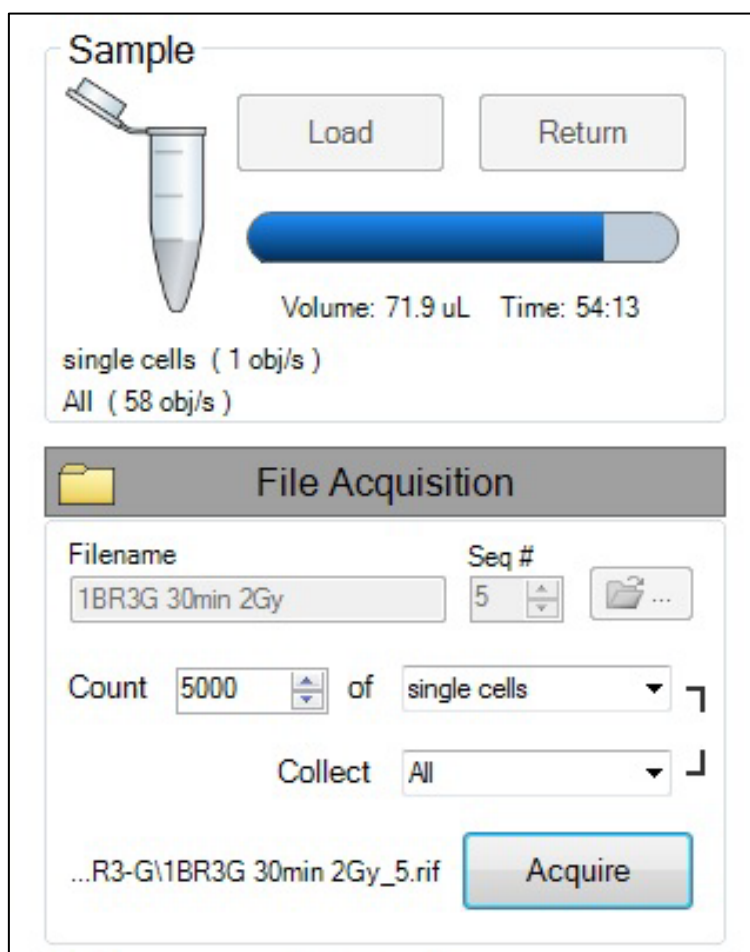
Laser	275nm	405nm	488nm	561nm	592nm	642nm
Example Dyes	DAPI Hoechst 33258 Alexa Fluor 405 Marina Blue Pacific Blue Cascade Blue LIVE/DEAD Violet DyLight 405 eFluor 450 Spectrum Aqua DyeCycle Violet Alexa Fluor 430 Pacific Orange Cascade Yellow Lucifer Yellow Qdot 525 Qdot 434 Qdot 565 Qdot 585 Qdot 605 Qdot 625 eFluor 605 Qdot 705 eFluor 650 Qdot 800	CFP DAPI Hoechst 33258 Alexa Fluor 405 Marina Blue Pacific Blue Cascade Blue LIVE/DEAD Violet DyLight 405 eFluor 450 Spectrum Aqua DyeCycle Violet Alexa Fluor 430 Pacific Orange Cascade Yellow Lucifer Yellow Qdot 525 Qdot 434 Qdot 565 Qdot 585 Qdot 605 Qdot 625 eFluor 605 Qdot 705 eFluor 650 Qdot 800	FITC GFP YFP Acridine Orange Alexa Fluor 488 Alexa Fluor 500 Alexa Fluor 514 SYTO Spectrum Green LysoTracker Green DyeCycle Green Calcium Green-1 MitoTracker Green DyLight 488 DsRed Dil Cy3 R-phycoerythrin OFP 7-AAD PE-Texas Red (ECD) PE-Alexa Fluor 610 Propidium Iodide PerCP PerCP-Cy5.5 PE-Alexa Fluor 647 PE-Alexa Fluor 680 PE-Cy5 PE-Cy5.5 DRAQ5 PE-Cy7 PE-Alexa Fluor 750	DsRed Dil Cy3 R-phycoerythrin OFP Alexa Fluor 546 Alexa Fluor 555 DyLight 549 Calcium Orange PE-Texas Red (ECD) PE-Alexa Fluor 610 Propidium Iodide Spectrum Orange MitoTracker Red LysoTracker Red RFP mCherry Alexa Fluor 568 Alexa Fluor 593 Alexa Fluor 610 DyLight 594 Texas Red PE-Alexa Fluor 647 PE-Alexa Fluor 680 PE-Cy5 PE-Cy5.5 DRAQ5 Nile Blue PE-Cy7 PE-Alexa Fluor 750	mCherry Alexa Fluor 568 Alexa Fluor 594 Alexa Fluor 610 DyLight 592 Texas Red Spectrum Red Calcium Crimson Nile Blue APC APC-Cy5.5 DyLight 649 MitoTracker Deep Red APC-Cy7 APC-Alexa Fluor 750 APC-eFluor780	Nile Blue APC APC-Cy5.5 DyLight 649 MitoTracker Deep Red Alexa Fluor 647 Alexa Fluor 660 Alexa Fluor 680 DRAQ5 Cy5 Cy5.5 APC-Cy7 APC-Alexa Fluor 750 APC-eFluor780 DyLight 750

The table above shows different fluorescent antibodies that can be used with the ImageStream^x (Millipore, 2016). The highlighted fluorochromes are the ones that were used in this research.

2.3.2 INSPIRE®

Samples containing no less than 20µl were prepared for ImageStream^X analysis and cells were gently resuspended to break cell clumps before each run on the ImageStream^X. The option “Load” was used to load the sample into the machine while “Acquire” was used to examine the sample and capture single cells in real time using a premade INSPIRE® template.

Figure 2.3: Sample acquisition using INSPIRE®

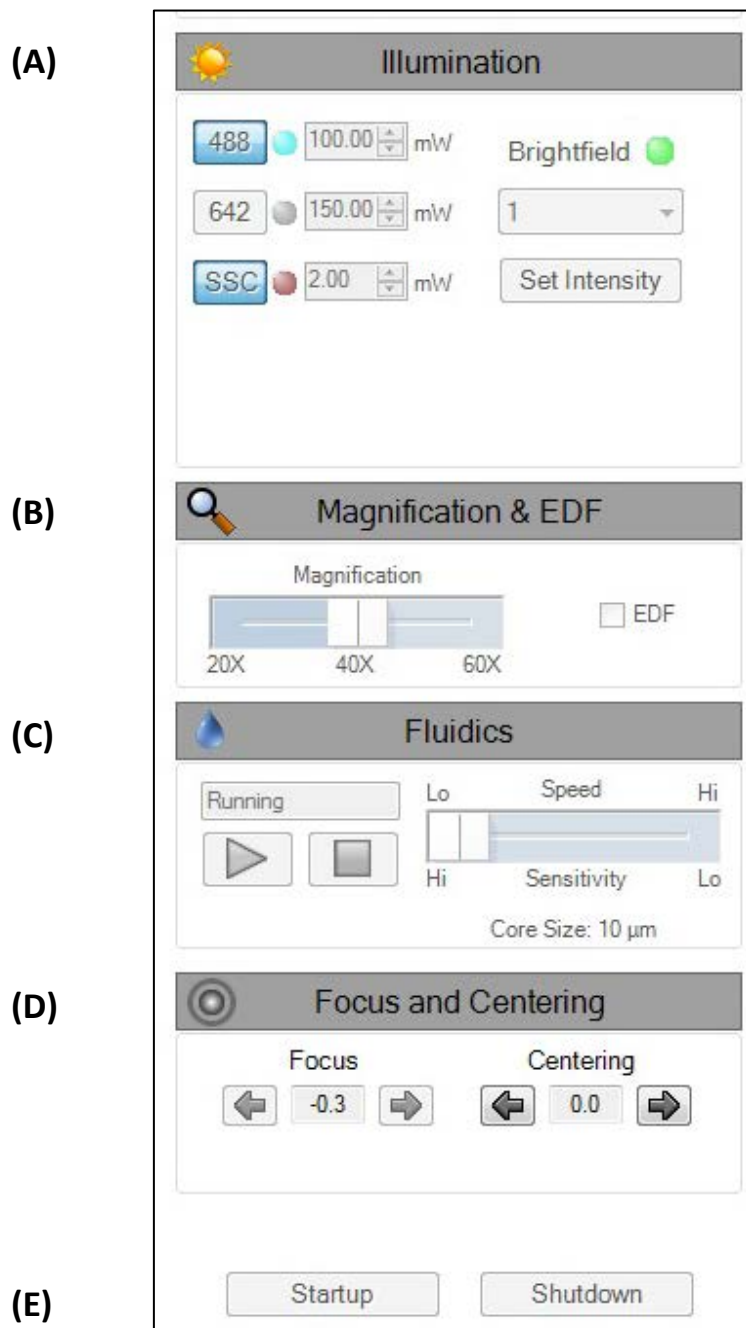


The figure above shows the sample acquisition function buttons as currently used in the ImageStream^X Mark II. The ‘Load’ button was used upon placement of the sample inside the machine to inform the device that the sample is ready to be examined. The ‘Return’ button on the other hand is used upon the completion of sample acquisition. Acquisition information that can be provided by the user includes the sample name, sequence number, number of cells required to be captured and the population of (gated) cells to collect images from. The remaining sample volume is demonstrated by the blue bar with the exact volume figure displayed directly underneath the bar. The acquire function button was used to begin the capture process and the creation of .rif files.

The number of cells captured from one sample may differ to others. In some experiments there was a shortage of cells available for examination (e.g. when cells were lost in washes or when there were

not many cells to begin with). The 488 excitation laser power was set to 100mW, while the side scatter was set to 2mW as shown in Figure 2.4.

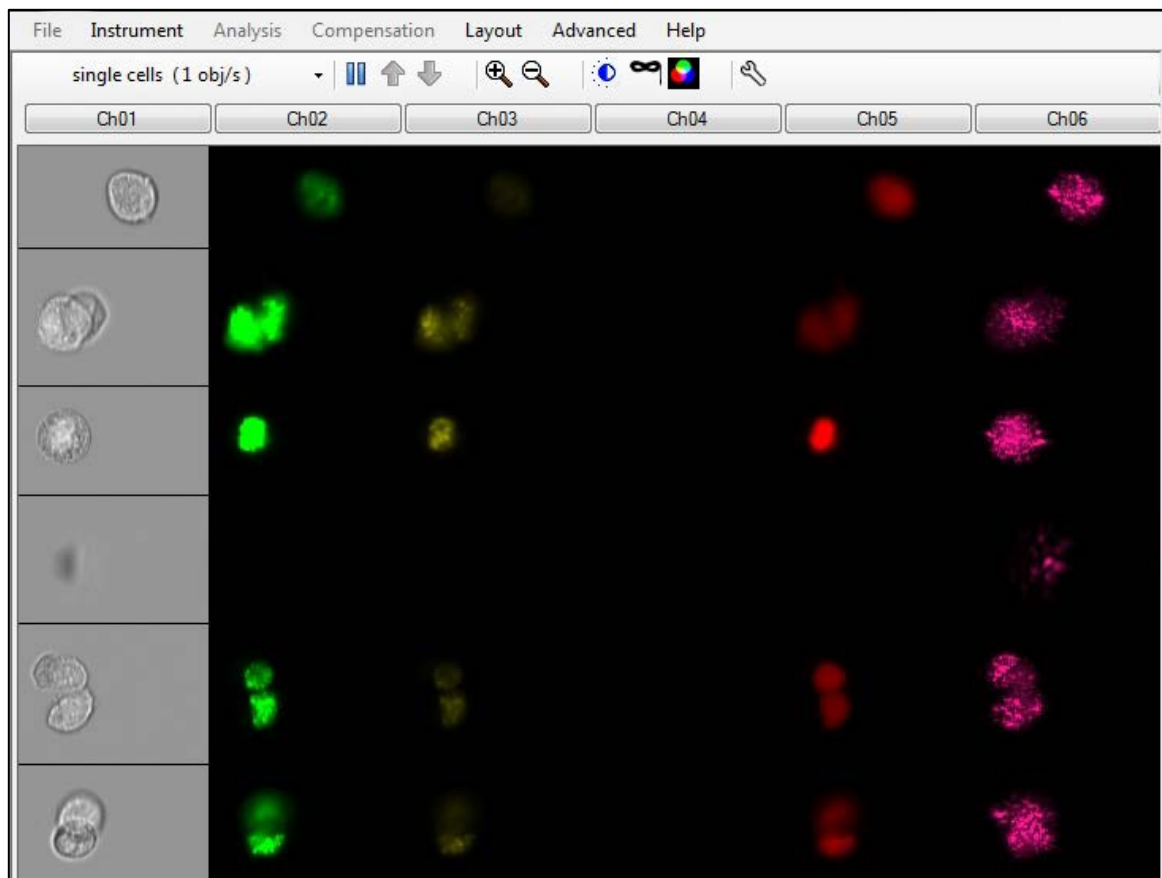
Figure 2.4: INSPIRE® sample acquisition control features



The figure above shows various INSPIRE® settings such as illumination, magnification and fluidics which can be modified prior to capturing cells from a sample. (A) The laser power is set to 100mW but can be changed depending on the intensity of staining. (B) The ImageStream^X Mark II also allows for a 60× objective which proved very useful, especially in the most diluted samples. In addition there is also the option of extended depth of field (EDF) which helps in projecting all structures and probes for an increased focus and better image clarity. (C) Fluidics control provided a balance between speed of cell capture and the sensitivity of the device. (D) The Focus and Centering was automatically controlled by the device, however, at times it required adjustment to obtain the optimal results. (E) The Startup and Shutdown functions are used to initiate the ImageStream^X and to shut it down along with the acquisition computer.

Cell classifiers were then set to a minimum cell size of 50 and a maximum cell size of 900. This was set on Ch01 when collecting cell images from normal samples, on Ch02 for the capture of AF 488 intensity from the AF compensation tube and on Ch05 for the DRAQ5 compensation tube. Furthermore, compensation settings must be applied before loading the compensation tubes.

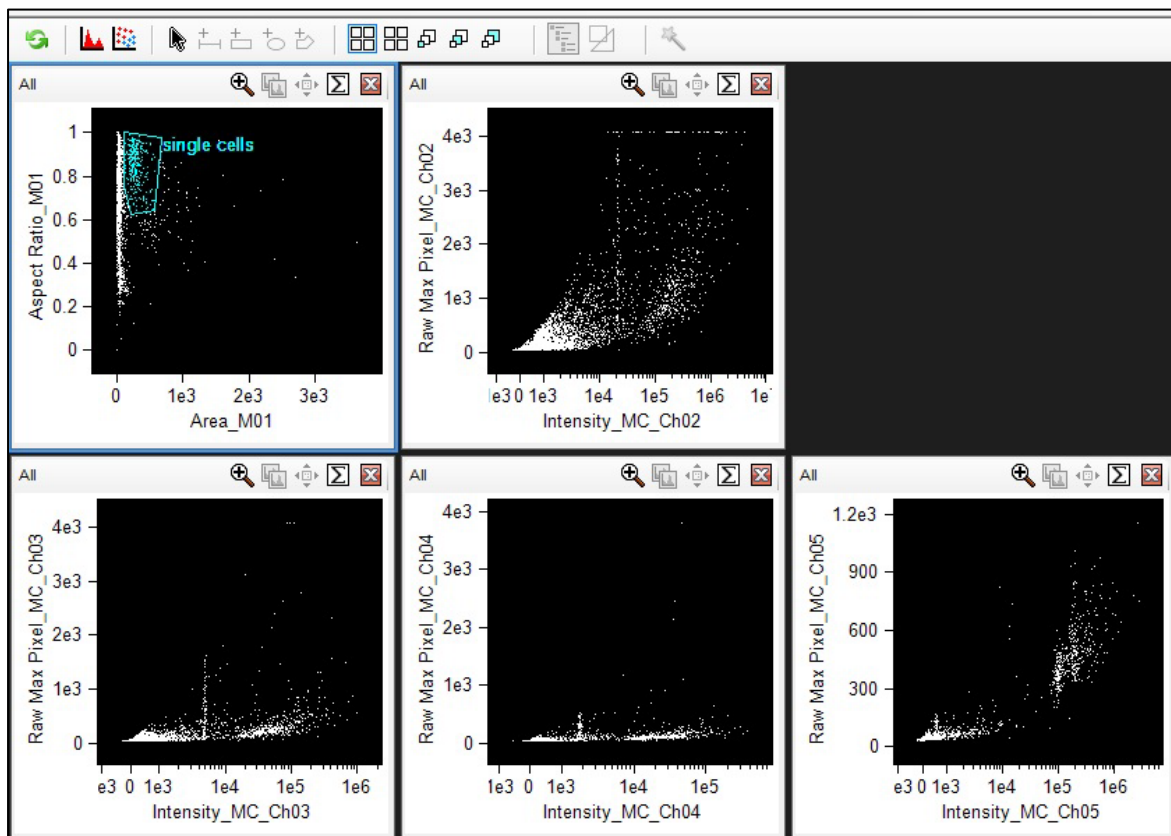
Figure 2.5: Captured images of cells using the ImageStream^X



The INSPIRE[®] software was used to display and capture cells from the ImageStream^X. Images of cells are displayed on six different channels as shown above. Channel 1 (Ch01) represents brightfield images of cells captured, channel 2 (Ch02) displays primary antibody staining of these cells, while channel 5 (Ch05) shows the nuclear staining with DRAQ5 antibody. The toolbar above the six channels shows a range of modification tools including ones that could be utilised to adjust properties of images captured, such as brightness and contrast.

The option Acquire was then used to capture images of the cells, the process usually takes no more than 3 minutes. A raw image file (.Rif) was saved onto the computer and then used for analysis via the IDEAS[®] analysis software. When data collection from one sample was complete, the sample was returned via the option “Return” before loading the next sample.

Figure 2.6: Distribution of cells based on a variety of features using INSPIRE®



Different graphs are created by the capture software, INSPIRE®, to select the regions from where images of cells will be captured, with each white dot in these graphs representing an object (e.g. cell, cluster of cells, debris). The graphs also show real-time numbers of cells (displayed as white dots) and in which region they fall with regards to each feature displayed (e.g. area, intensity of antibody on channel 2, etc.). Selected regions such as the one displayed in blue (Single cells) allow for selective capture of cells within these gates only.

Once work with the machine is complete, the option “Shutdown” was then used to sterilise the ImageStream^x prior to shutting it down. This includes physically emptying the waste tank and filling up any empty reagent bottles within the machine.

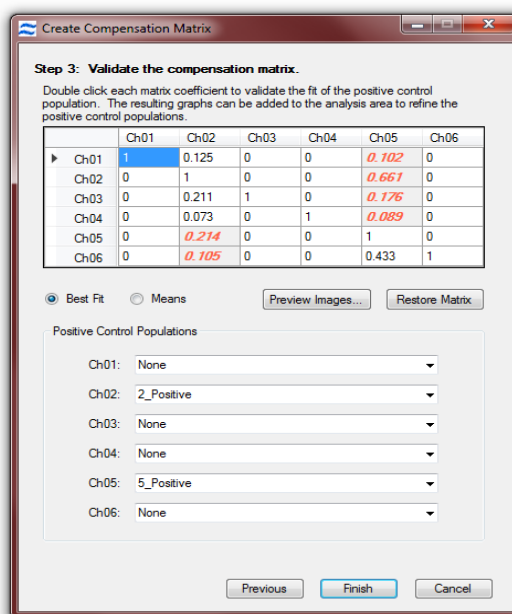
2.3.3 Image Compensation

In every experiment in which two different fluorescent labels were used (such as EpCAM [488nm] and DRAQ5 [648nm]), image compensation was carried out. This was done to measure the intensity of fluorescence, relying only on a single source of illumination and the reason behind that is to eliminate the fluorescence leaked into adjacent channels.

Image compensation is performed with a single source of illumination (the 488nm laser). A compensation matrix was generated using the Wizard tool in the image capture software INSPIRE®.

The process is made easier than the older models in which the two different compensation files were used in the analysis software IDEAS® to generate a coefficients table where light captured from images was placed on the corresponding channel (e.g. Ch05 for DRAQ5) on a pixel by pixel basis. These coefficients represent the leakage of a certain fluorochrome into adjacent channels and would require to be normalized to 1.

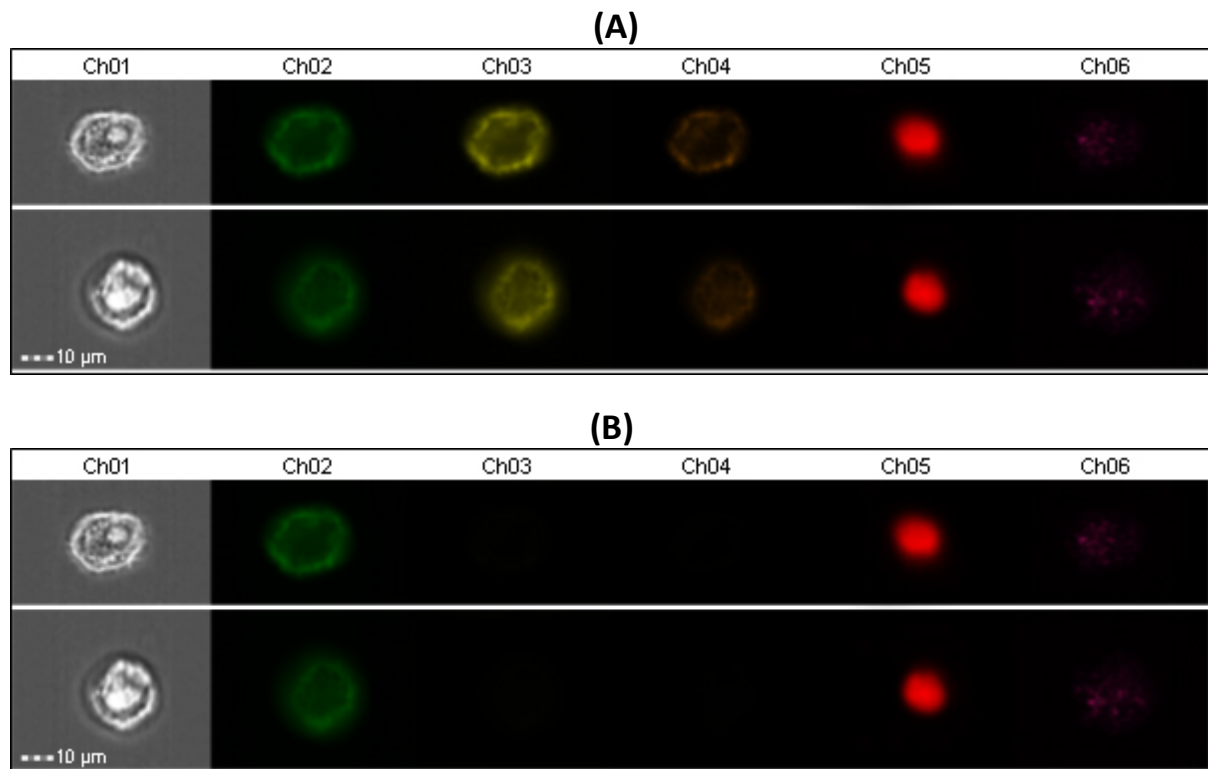
Figure 2.7: A typical ImageStream^x compensation matrix table



The figure above shows an example of a compensation matrix table created by the analysis software IDEAS® prior to analysing the sample. Values shown in this table represent coefficient figures of leakage into adjacent channels. The coefficient of leakage decreases as it becomes distant from the principal channel indicated with a 1 value. The values used in this research were adjusted to have a margin of error that is less than 0.001.

Image compensation helps in representing the true intensity of certain fluorescent lights for each image and will therefore lead to an accurate data capture and analysis. The method which generates a compensation matrix using IDEAS® has been previously explained by our research group (Parris et al., 2015a).

Figure 2.8: Compensated vs uncompensated images of PC3 cells

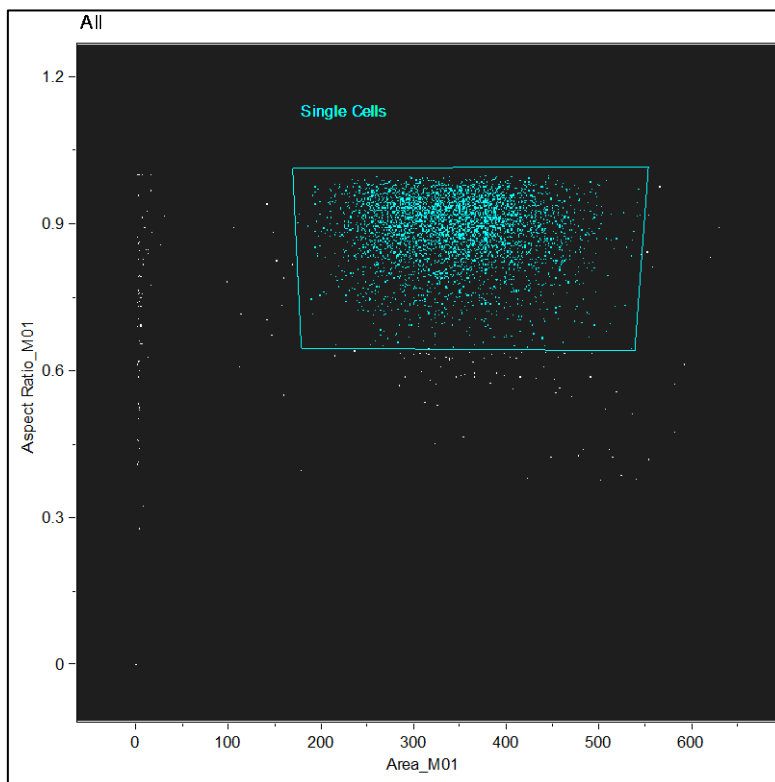


(A) Shows examples of uncompensated images of PC3 cells captured in this research using the ImageStream^X. Channel 2 shows EpcAM staining, while fluorochrome leaks can be seen on adjacent channels (e.g. Ch03). Using the Image Compensation tool in the IDEAS® allows for the correction of this leakage. **(B)** shows the exact same PC3 cells displayed in (A), only now they were compensated and the fluorochrome leakage in channels 3 and 4 has been rectified.

2.3.4 IDEAS®

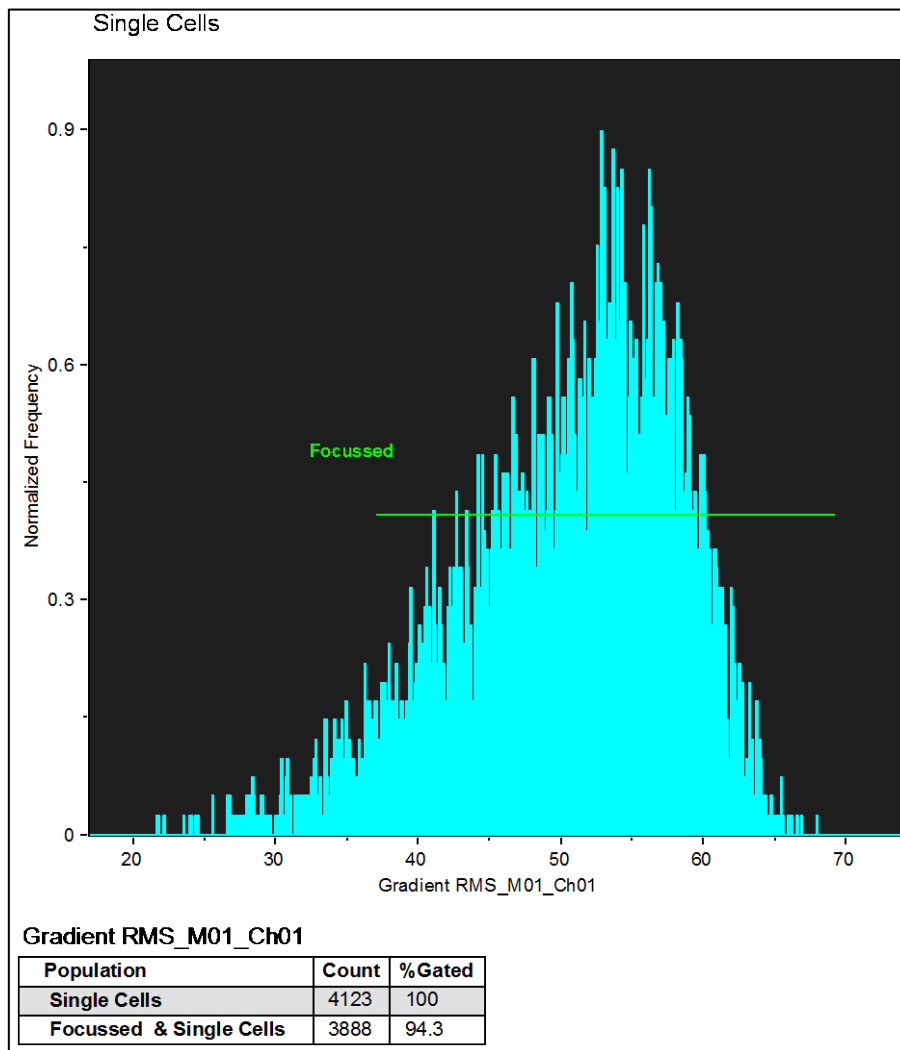
The IDEAS® software is used to analyse samples captured with the ImageStream^X, forming data analysis files (.Daf). The software firstly views all of the captured objects (cells, debris, etc.) and allows the user to gate a section of them (based on manual examination of these objects) and tag them as single viable cells, the analysis can then proceed using only single cells. It is worth mentioning that the INSPIRE® capture software allows for single cells to be isolated and exclusively collected; however, careful examination of collected cells is important, this is done to exclude small clusters of cells that might have been accidentally included in the original capture. The next step is to narrow the analysis only to focused cells which have a clear cell structure and morphology.

Figure 2.9: Identification of single cells using IDEAS®



The Y-axis shows the distribution of the cells in terms of their aspect ratio while the X-axis shows their distribution in terms of size. Each one of the blue dots represents one captured object (e.g. cell, debris, cell clusters). The “_M01” at the end of the axis’ name refers to the channel it applies to. The software automatically generates statistics about the captured data such as the number of cells, mean and more and these statistics are displayed in a table below the graph. Careful examination of these dots or cells was then followed by gating single cells to exclusively analyse them.

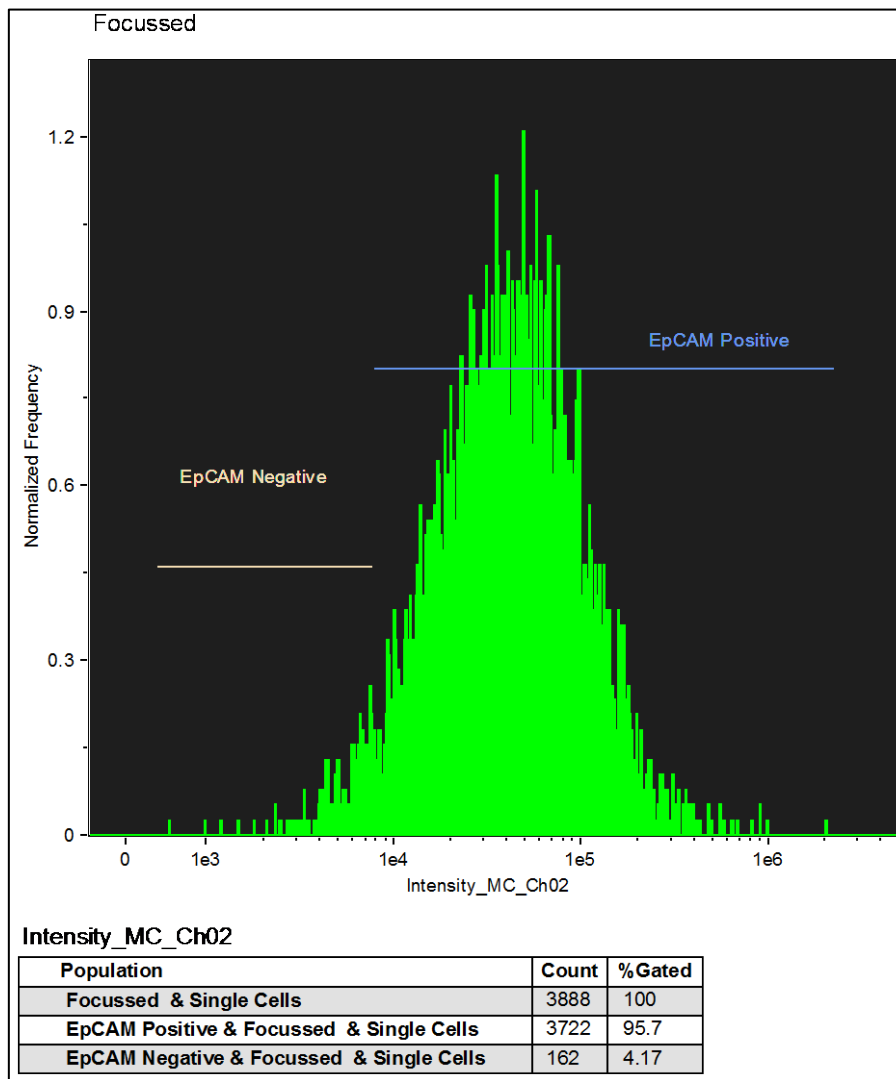
Figure 2.10: Identification of focused cells using IDEAS®



A graph was then created from the single cells that were gated to identify the clearly focused cells and exclude any blurred cells from further analysis. On the X-axis, a gradient of cells based on image focus is used, while the Y-axis represented the normalised frequency. Following examination, a line gate was created (in green) separating single focused cells from blurred unclear cells. The table below the graph is automatically generated by the analysis software after a number of cells in that graph are gated. This is done to show the number and percentage of cells included in that range.

Choosing from the focused cells only, the software was used to create a gradient based on the intensity of EpCAM staining in the PC3 cells (Figure 2.11). When the graph was created in the IDEAS® software, different sections of it were examined to decide points at which cells would be classified as positively stained. When created, statistics regarding percentages of each section of the graph as well as cell numbers can be obtained. This gives us precise numbers in terms of how well the cells stained for each dilution of the antibody used.

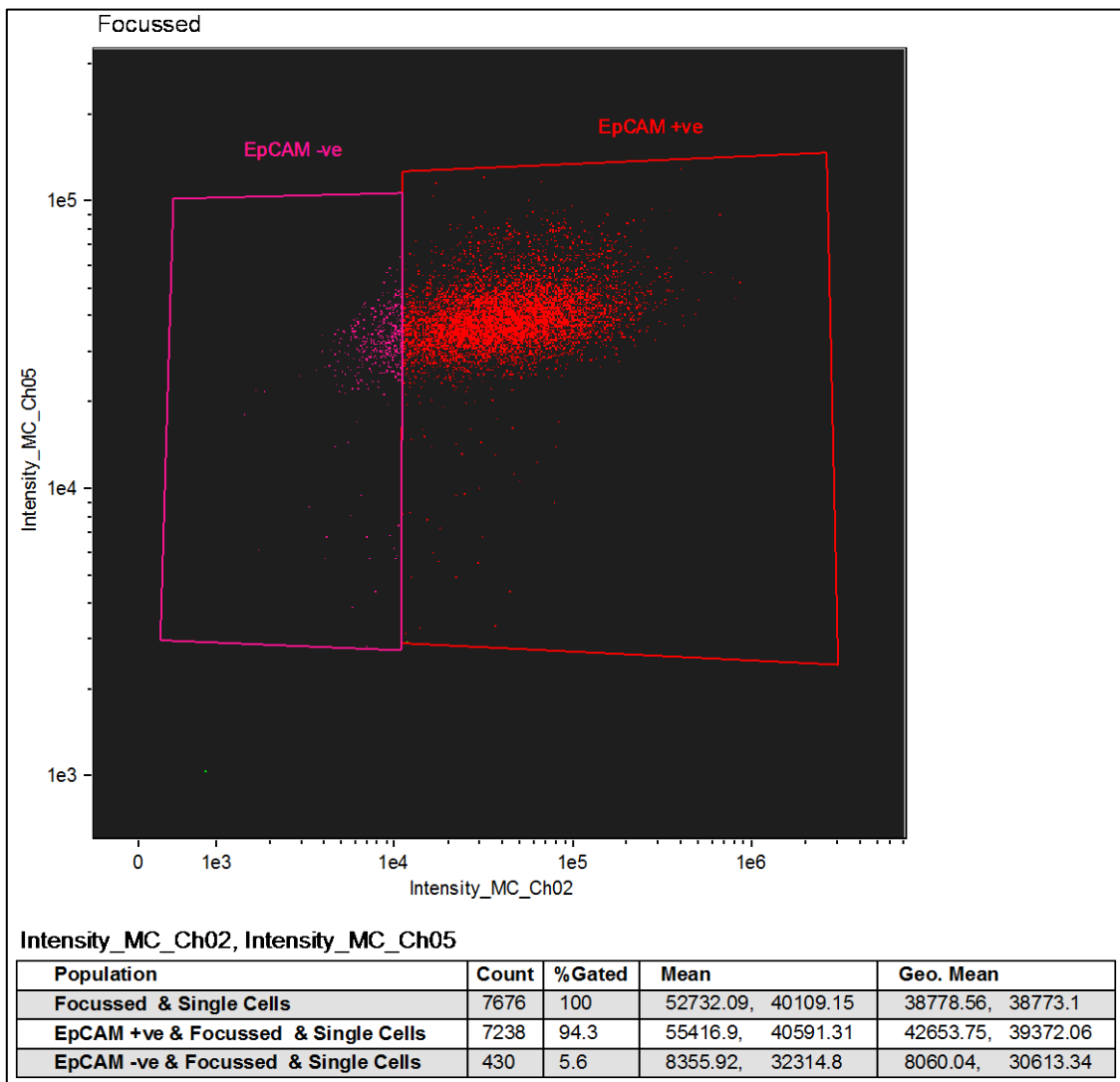
Figure 2.11: Identification of positively stained cells using IDEAS®



The histogram above was used to identify focused EpCAM-positive and negative cells. The figure shows normalised frequency on the Y-axis against antibody staining intensity (captured on channel 2) on the X-axis. A region-selecting tool was used to obtain a cell count for cells that were stained with EpCAM. These were determined after examining various regions and then gating them with the line tool.

Figure 2.12 compared the intensity of the primary antibody staining on the X-axis against the intensity of DRAQ5 staining on the Y-axis. This graph gave a better representation of each cell within the EpCAM positive and negative regions and I was able to view each cell's morphology, primary antibody cell staining as well as its nuclear staining.

Figure 2.12: The use of scatterplots to identify EpCAM positive and negative PC3 cells



A scatterplot created to help in identifying and gating focused EpCAM positive and negative PC3 cells, each dot represents a captured cell. After manual examination of various cells, the population of cells that was EpCAM positive was gated and separated from the population that was EpCAM negative as can be seen in the red and purple boxes in the figure above.

2.4 Lymphocyte separation

The isolation of peripheral blood lymphocytes from whole blood was achieved using lymphocyte separation medium (LSM[®]) (SLS, Nottingham) in a method explained by the solution manufacturer. The LSM was mixed thoroughly by inverting it few times. 3mL of LSM was then transferred to a 15mL tube. 2mL of defibrinated blood was then diluted by mixing it with 2mL of RPMI medium (1:1). It was then layered carefully in a way that the blood was positioned right above the 3mL separation medium at room temperature, creating a sharp blood-LSM interface.

Centrifugation of the tube then took place at 400 x g at room temperature for 15-30 minutes. This was done in order to deposit erythrocytes and polymorphonuclear leukocytes to the bottom of the tube, while drawing mononuclear lymphocytes to a level above the LSM. The top layer, containing clear plasma, was then aspirated to within 2-3mm above the lymphocytes layer, which itself was then transferred to a new tube along with approximately half of the LSM layer below it.

An equal volume of buffered balanced salt solution was added to the tube and centrifuged at room temperature for 10 minutes at a speed of 200 x g. This speed was chosen to deposit the cells to the bottom of the tube without causing cellular damage. The cells were then washed with buffered balanced salt solution and resuspended in PB-MAX to be used immediately or frozen in liquid nitrogen in a method previously explained. The reason for washing cells is to remove LSM from the sample, as well as reducing the percentage of platelets (MPBiomedicals, 2016).

2.5 Proof of principle (mixing) experiment

To test the sensitivity of the CTC identification method used and to evaluate which analysis feature would be most suitable to distinguish CTCs from other blood cells, a series of serial dilution experiments were conducted. PC3 cells were diluted and mixed with PBLs as shown in the table below before being examined using the ImageStream^X. This was also done to compare cell retrieval numbers when immunological approaches were used to when the live cell analysis approach is undertaken.

Table 2.5: Serial dilution of PC3 cells to test CTC detection sensitivity

Tube number	Total PC3 cells spiked in 1mL	Total number of PBLs in 1mL
1	3,000,000	3,000,000
2	300,000	3,000,000
3	30,000	3,000,000
4	3000	3,000,000
5	300	3,000,000
6	30	3,000,000

An outline is given above of how samples were spiked with different dilutions of PC3 cells to test the sensitivity of the ImageStream^X using immunological and physical approaches.

The spiking step was carried out after both cell-lines were counted using the Countess and calculations were made of the volume required for each sample. Care was taken when mixing both cell-lines and very often dilutions were made instead of relying on using pipettes to deliver minute volumes for test tubes 4, 5 and 6, ensuring the number of cells in these tubes were very accurate. The proof of principal experiment was also carried out using fixed cells in a three days experiment and live cell analysis within one day to test which approach provided better PC3 cell retention.

2.6 Clinical sample preparation

Whole blood samples were collected from two metastatic castrate-resistant prostate cancer (CRPC) patients with informed consent and NHS ethical approval. The samples were initially collected in EDTA tubes and inverted several times. 7mL of red blood cell (RBC) lysis buffer was added to each sample in a falcon tube and inverted several times prior to 10 minutes incubation on ice. The samples were then centrifuged for 10 minutes at a speed of 2500rpm at room temperature. The supernatant was removed from each sample and an additional 3mL of RBC lysis buffer was used to resuspend the cells pellet.

The samples were then centrifuged again at 2500rpm for 10 minutes at room temperature to create RBC-free pellets of cells. Following the centrifugation of samples, the supernatant in each sample was carefully aspirated and the cells were then immediately used for live cell analysis or fixed with 3.7% PFA, blocked with a blocking buffer and stained with primary and secondary antibodies as explained in the immunocytochemistry and live cell analysis methodology on page 82.

Chapter 3

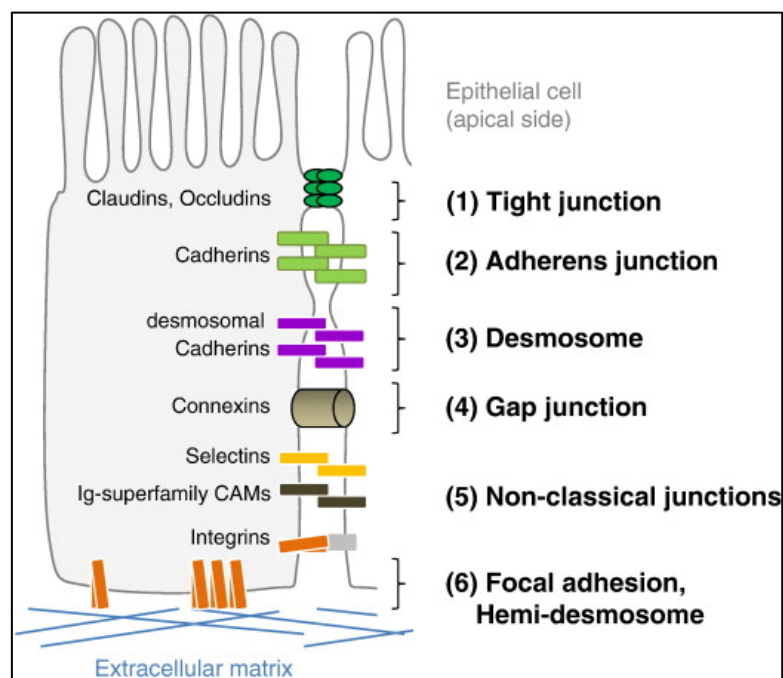
Identification of PC3 cells using the Epithelial Cell Adhesion Molecule

3. Identification of PC3 cells using the Epithelial Cell Adhesion Molecule

3.1 Introduction

Epithelial cell adhesion molecule (EpCAM) is a glycoprotein expressed in epithelia and in the majority of carcinomas, prompting interest in utilising its use as a possible biomarker for cancer detection (Litvinov et al., 1994). In a study that investigated 3360 cases of primary colon, lung, prostate and stomach tumours, EpCAM was found to be overexpressed in 94.1% of them (Went et al., 2006). The epithelial tissue lines all external and internal surfaces in multicellular organisms, providing a well-governed barrier of molecular exchange with the extracellular milieu. Epithelial tissue is made up of two main types; simple epithelium and stratified epithelium and features an abundance of cell adhesion molecules (CAMs) (Schnell et al., 2013).

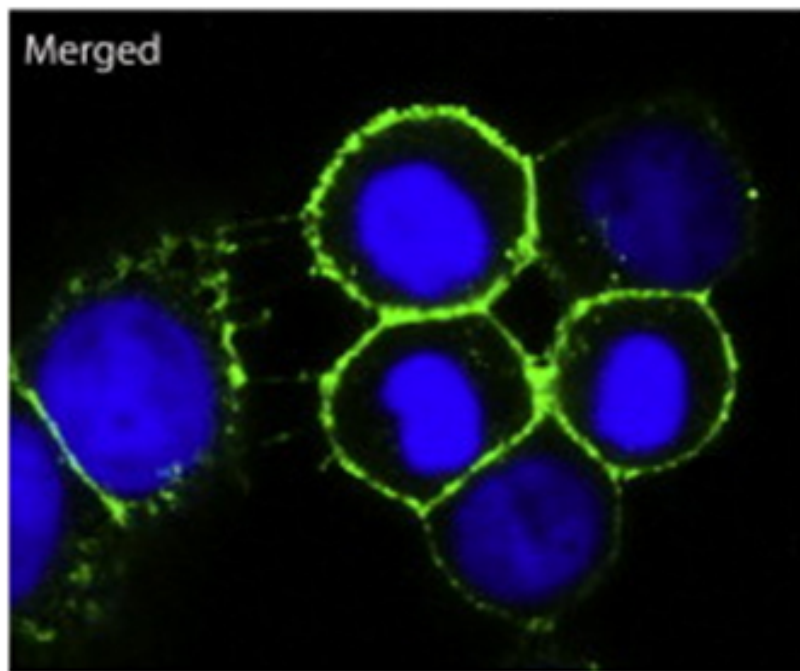
Figure 3.1: The variety of CAMs present on epithelial cells



The variety of CAMs that exist in epithelial tissue and play a vital role in upholding epithelial cellular adhesion. Mutations in these CAMs may also give rise to diseases like cancer (Schnell et al., 2013).

Many diseases affect the integrity of the epithelial layers. These include pathogenic infections, autoimmune diseases and cancer. EpCAM is a cell adhesion protein and was identified as a tumour antigen in the 1970s when functional screens were carried out to identify possible tumour-specific cell surface antigens that can be used as cancer biomarkers (Herlyn et al., 1979).

Figure 3.2: An example of EpCAM staining of MCF-7 cells



The figure above shows a modified diagram by Gadalla *et al* of anti-EpCAM antibody staining (green) in dividing MCF-7 cells. The blue stain represents nuclear staining with DAPI (Gadalla et al., 2013).

The EpCAM antibody has a molecular mass of approximately 40 kDa with variable levels of expression. However, there is a usually lower expression in normal epithelia in comparison to carcinoma cells (Trzpis et al., 2007). With regards to prostate cancer, EpCAM is found to be expressed at high levels in most of its metastatic cell-lines and in metastatic forms of prostate cancer compared to non-metastatic primary cell-lines and tissue samples. Interestingly, the EpCAM marker may be a useful indicator of chemotherapeutic efficacy and expression of EpCAM is found to be suppressed during cytotoxic chemotherapy induction in the EMT (Ni et al., 2013a, Massoner et al., 2014).

3.2 Aim

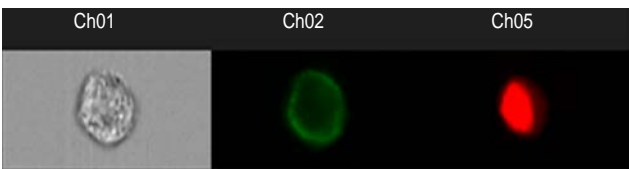
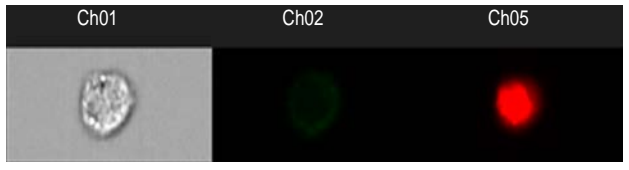
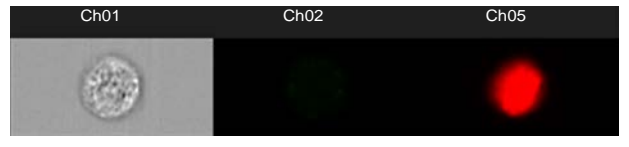
1. The identification of PC3 cells by exploiting the EpCAM epithelial marker using immunocytochemical techniques
2. Determination of the efficacy of EpCAM staining for the identification of PC3 cells within a mixture of PBL cells
3. Determination of the sensitivity of EpCAM identification of PC3 cells by spiking PBL samples with dilutions of PC3 cells
4. Determination of the specificity of CTC identification using EpCAM antibody
5. To determine the effect of these methods on cell morphology and localisation of fluorescent staining.

3.3 Results

3.3.1 EpCAM antibody optimisation

Prior to using EpCAM for the identification of PC3 epithelial cells, it was serially diluted in an extensive series of optimisation tests to determine the best dilution at which the majority of epithelial (PC3) cells were visibly stained. Three test tubes were used, each with a different dilution, as shown in the table below.

Table 3.1: EpCAM staining optimisation for PC3 cells

EpCAM dilution	Percentage of stained cells	Example of a stained cell
Tube 1 (1/1)	95.8%	
Tube 2 (1/5)	60.4%	
Tube 3 (1/10)	20.1%	

The table above shows brightfield images of PC3 cells (Ch01), EpCAM staining of these cells (Ch02) and nuclear staining with DRAQ5 (Ch05). In tube 1, the dilution was kept the same as the recommended volume and 200µl of the prediluted EpCAM antibody was used. In tube 2, 40µl of the EpCAM antibody was diluted by adding it to 160µl of the blocking buffer. Whereas in tube 3, the dilution was doubled as only 20µl of EpCAM was added to 180µl blocking buffer.

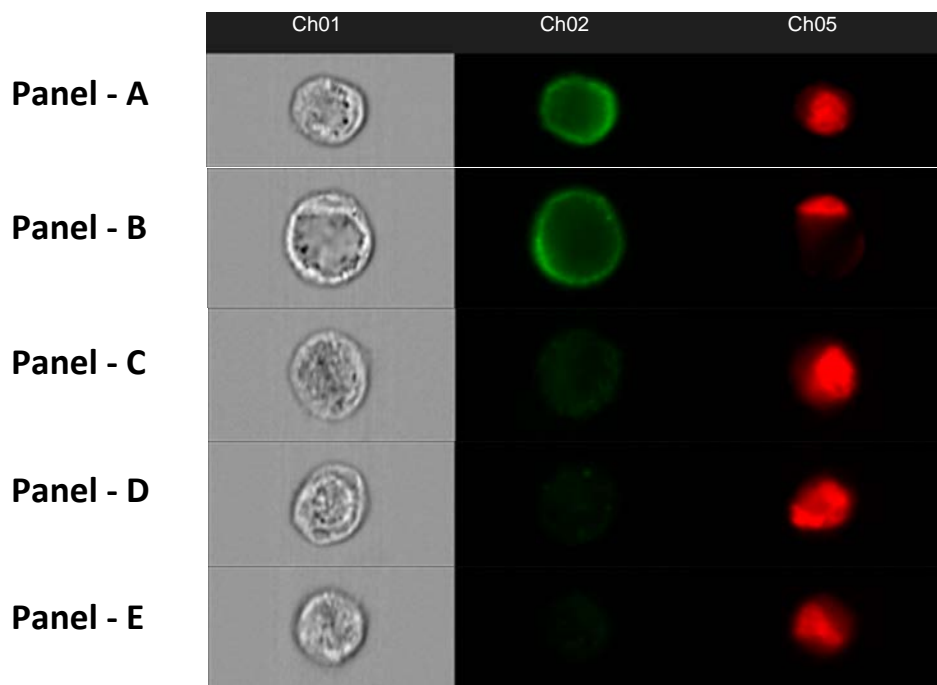
This data demonstrated that the clarity of EpCAM staining was optimal when the recommended prediluted antibody was used to stain the cells. There was visible staining in tube 2 (1/5 dilution), some cells were clearly stained but the vast majority showed lower EpCAM intensity in comparison to PC3 cells in Tube 1. Cells in tube 3 on the other hand showed little or no EpCAM staining (1/50 dilution). These experiments were repeated several times using various amounts of EpCAM. The

optimal dilution was found to be the original in which the antibody is provided, with the amount of antibody added to each sample recommended to be no less than 200 μ l. The optimisation experiments and observations indicated that the 200 μ l of the prediluted EpCAM antibody was optimal and was used in all further EpCAM staining experiments.

3.3.2 PC3 cells staining with EpCAM antibody

Various optimisation strategies were conducted to confirm the optimal staining conditions for the labelling of PC3 cells with the EpCAM antibody. Parameters that were examined were the antibody incubation time, fixation method and fixation time. Different batches of the EpCAM antibody were also examined to test the efficacy and specificity of each batch in labelling PC3 cells. The anti-EpCAM antibody batch that showed clear membrane staining in most PC3 cells captured was the HEA125 EpCAM antibody (ABCAM, Cambridge).

Figure 3.3: EpCAM staining of PC3 cells

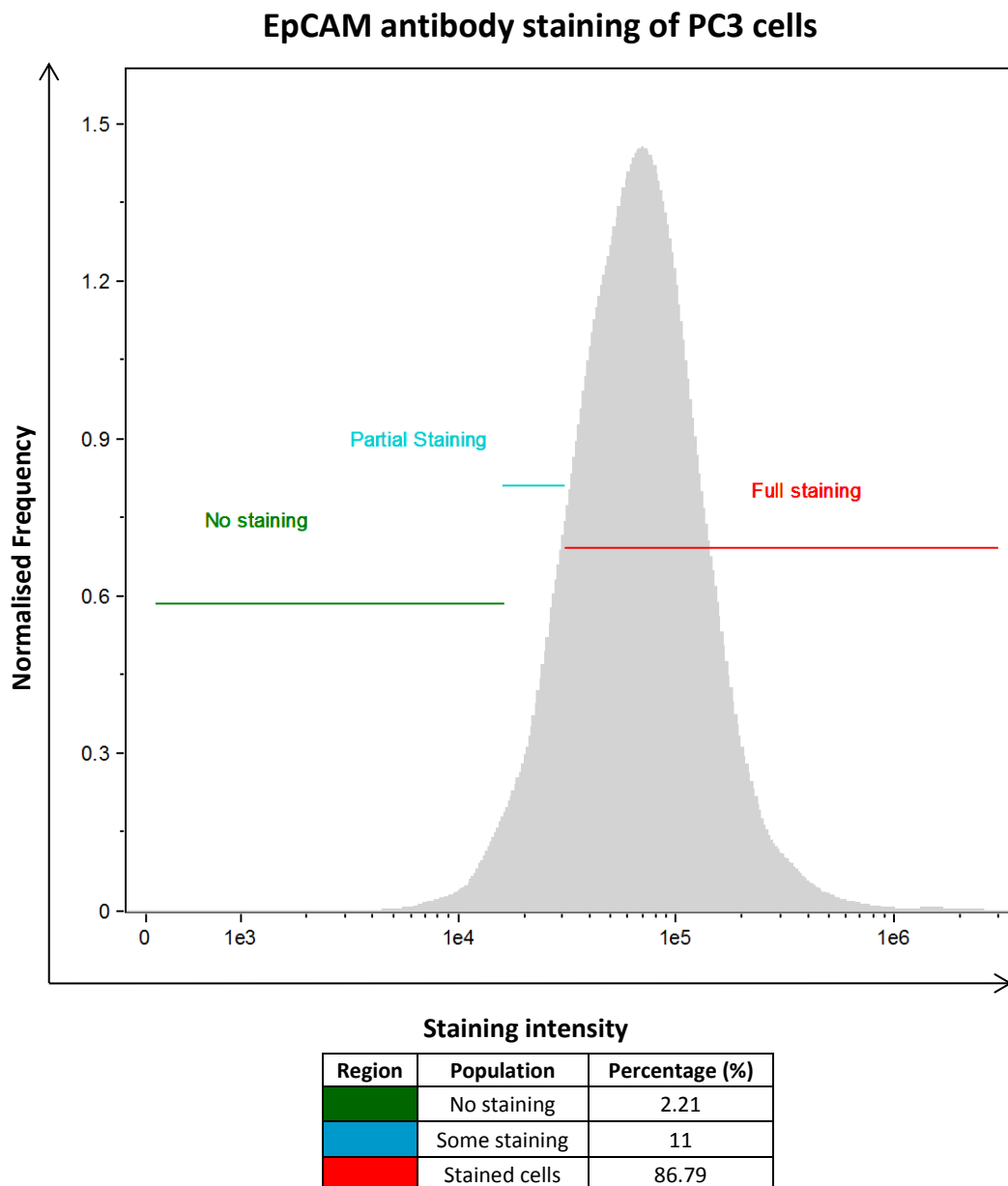


Samples shown in the figure above demonstrate different patterns of staining of PC3 cells with the EpCAM antibody. The first column, titled brightfield shows brightfield images of cells captured at 40× on Ch01. The second column shows EpCAM antibody staining in green on Ch02. DRAQ5 nuclear staining is displayed in red in the third column, titled Ch05.

The majority of PC3 cells in all experiments showed an optimal level of staining. There was, however, a small percentage in each PC3 population in which the intensity of EpCAM staining was barely detectable or non-existent even when the optimised method was used. Examples of such cells are shown in Figure 3.3 on panels C, D and E. The intensity of staining was less than that of A and B and

in some cases, panel C for example, staining of the cytoplasm of cells was observed. The percentage of cells that showed weak but detectable staining was approximately 11% of the entire PC3 population captured. There were also few PC3 cells (2.21%) that did not stain with EpCAM, such as the ones shown in panels D and E.

Figure 3.4: Distribution of PC3 cells based on their EpCAM intensity



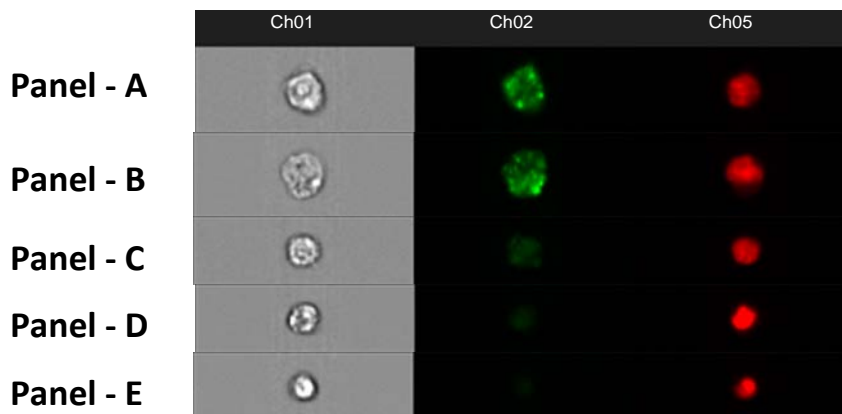
The figure above shows the normalised frequency of PC3 cells (Y axis) against the intensity of EpCAM antibody in these cells (X axis). Cells on the left (marked in green) were cells that showed no staining at all or a very minute antibody intensity that would also be obtained without using any antibodies. The blue region in the middle categorises cells with higher intensity of EpCAM antibody, but not high enough to be classified as EpCAM-positive cells. Cells on the right (within the red region) were EpCAM-positive cells. The table below the graph displays the exact percentages of PC3 cells within these three regions.

Some of the PC3 cells that were partially stained or not stained at all presented a less intact structural morphology than cells with optimal staining. This observation prompted a hypothesis that perhaps alterations to the structural integrity of these cells were brought about by the numerous and rigorous steps required in sample preparation before cells are examined with the ImageStream^x. However, prolonged examination of several PC3 samples stained with EpCAM revealed many more cells that expressed no EpCAM staining, yet possessed morphology that was similar, if not better than that of EpCAM positive cells. This indicated that the poor morphology and cell structure in EpCAM-negative cells might not be the only reason behind the lack of staining and that this acquisition of false-negative PC3 cells might be linked to non-specific abnormalities observed in immunostaining experiments where biomarkers such as EpCAM antibody were used (Punnoose et al., 2010).

3.3.3 GMO0893 staining with EpCAM antibody

The use of GMO0893 lymphoblastoid cells in an immunological experiment involving the EpCAM antibody was done to test if this cell-line will show negative staining behaviour as expected of non-epithelial cell-lines. The figure below shows examples of various types of EpCAM staining patterns observed in a GMO0893 sample.

Figure 3.5: EpCAM staining of GMO0893 cells

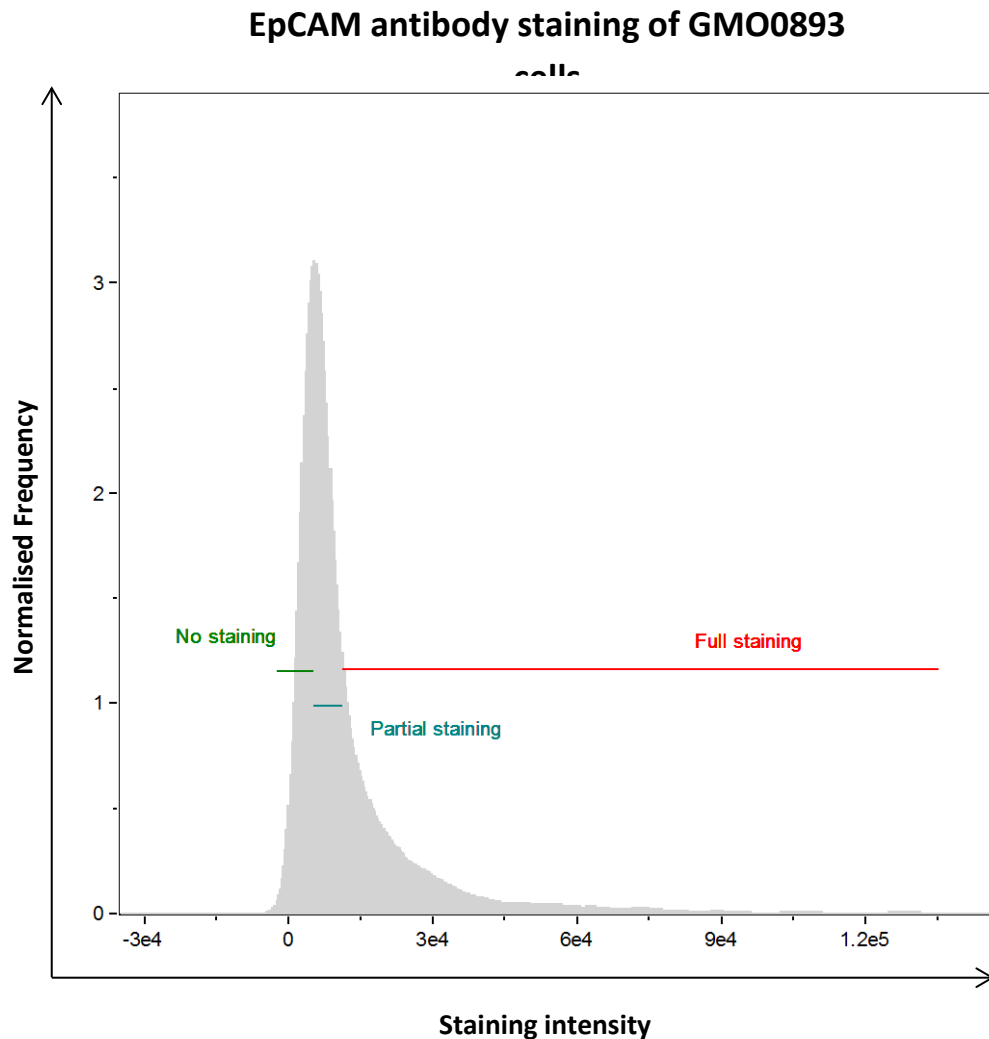


Samples shown in the figure above demonstrate different patterns of staining of GMO0893 cells with the EpCAM antibody. The first column, titled Ch01 shows brightfield images of cells captured at 40× on channel 1. The second column (Ch02) shows EpCAM antibody staining in green colour. DRAQ5 nuclear stain is displayed in red on the third column (Ch05). Panel A and B are examples of EpCAM-positive cells, while panel E is an example of a GMO0893 cells that was not stained with the antibody. Panels C and D show variable levels of weak staining with EpCAM.

Approximately 30% of the cells in the sample were EpCAM positive, a strong indication that non-specific staining with EpCAM is predominant in the GMO0893 cells. The structure of cells examined was generally in poor status compared to the two other cell-lines used. Nevertheless, only the staining for cells with robust shape and morphology was taken into account when the analysis of EpCAM non-specific staining was conducted.

Perhaps the more interesting fact was the higher percentage of partially stained cells compared to other cell-lines. Approximately 39.1% of the cells displayed a weak level of EpCAM intensity, similar to that demonstrated in Figure 3.5 panel – C above.

Figure 3.6: Distribution of GMO0893 cells based on their EpCAM staining intensity



Region	Population	Percentage (%)
	No staining	30.6
	Some staining	39.1
	Stained cells	30.3

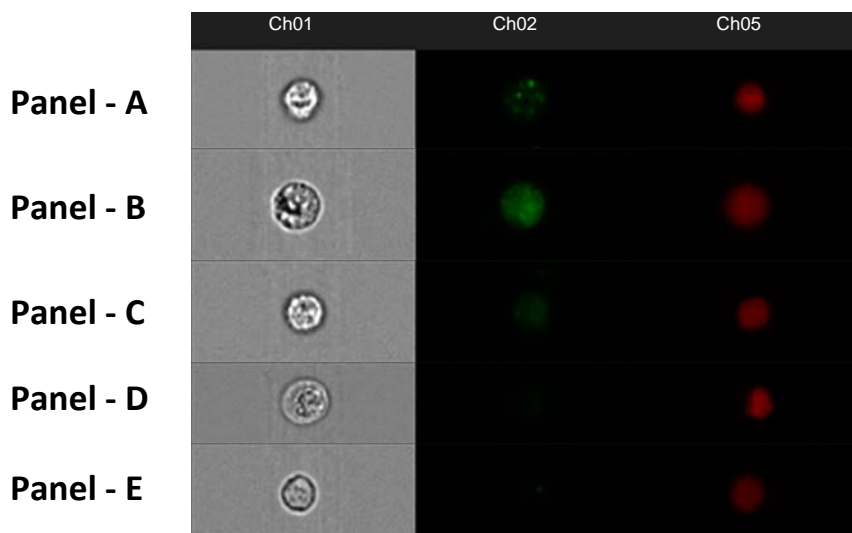
The figure above shows the normalised frequency of GMO0893 cells (Y axis) against the intensity of EpCAM antibody in these cells (X axis). Cells on the left (marked in green) were cells that showed no staining at all or a very minute antibody intensity that would even be obtained without using any antibodies. The blue region in the middle categorises cells with higher intensity of EpCAM antibody, but not high enough to be classified as EpCAM-positive cells. Cells on the right (within the red region) were EpCAM-positive cells. The table below the graph displays the exact percentages of GMO0893 cells within these three regions.

The pattern of EpCAM staining in GMO0893 cells differs from that of PC3 cells in that it was not peripheral (restricted to the membrane) in any of the cells. This could be an indication that the staining observed in GMO0893 cells is not caused by antibody-antigen binding but rather by the loss of structure in these cells.

3.3.4 PBL staining with EpCAM antibody

The failure of GMO0893 cells to maintain a prototypical and optimal morphology and structure prompted the need for an alternative substitute for these cells. Peripheral blood lymphocytes (PBLs) from historical stock of frozen cells from normal individuals (collected with ethical approval and informed consent) provided just that and were compared in every step of this research to GMO0893 cells in their ability to limit nonspecific staining and maintain optimal morphology and structure. In this chapter they were stained with the same prediluted form of EpCAM used on PC3 and GMO0893 cells and the results were as follows:

Figure 3.7: EpCAM staining of PBL cells

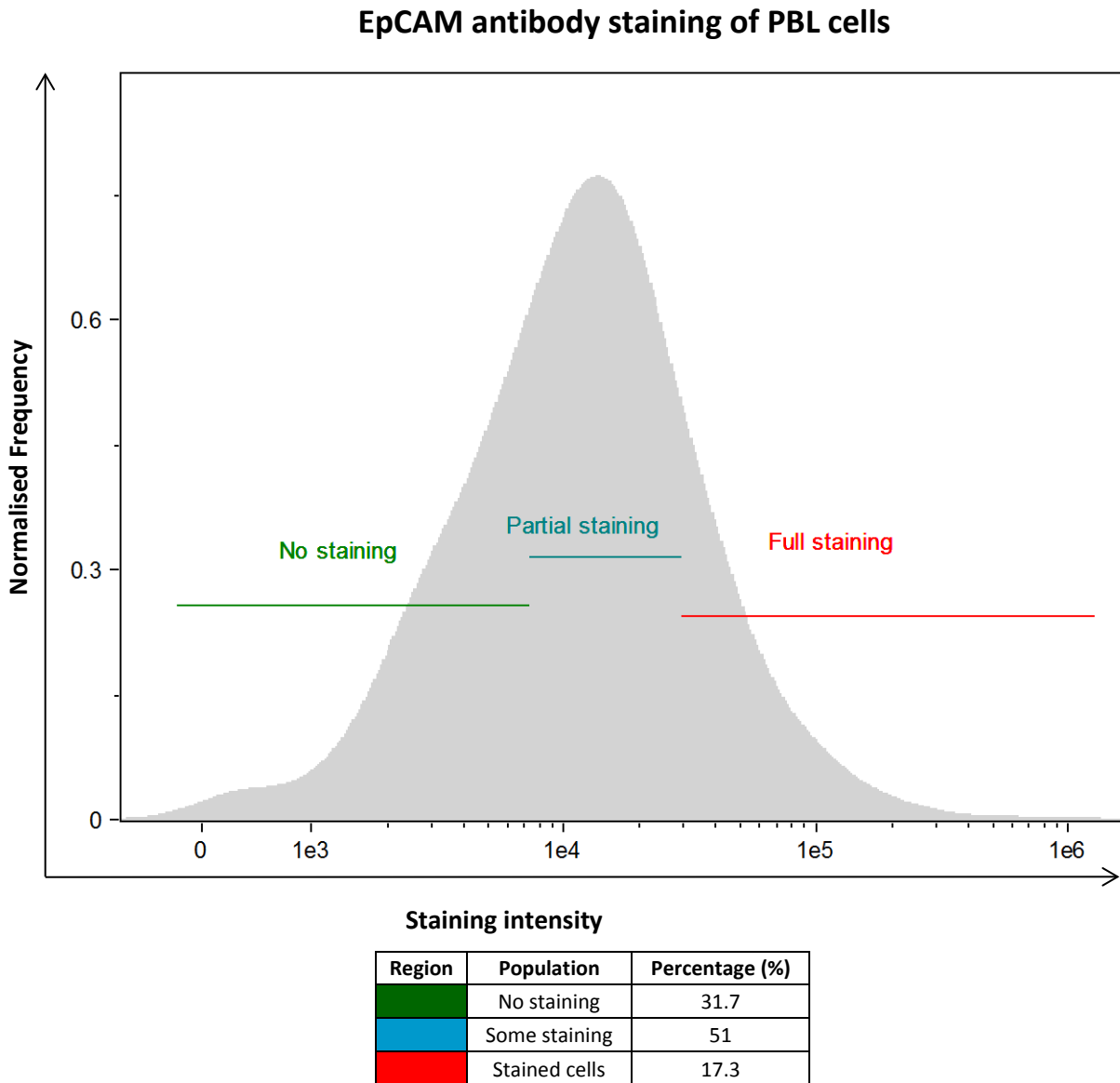


Examples shown in the figure above demonstrate different patterns of staining of PBL cells with the EpCAM antibody. The first column, titled Ch01 shows images of cells captured at 40 \times . The second column (Ch02) shows EpCAM antibody staining in green colour. DRAQ5 nuclear stain is displayed in red on the third column (Ch05). Panel A and B are examples of EpCAM-positive cells with variable levels and patterns of staining, while panels D and E are EpCAM-negative cells. Panel C is an example of a partially or weakly stained PBL cell.

As can be seen in the figure above, the staining with EpCAM was apparent in a number of PBL cells (17.3%). However, the total percentage of cells that were partially stained or not stained at all represented 82.7% of the entire PBL population. A percentage that is higher than that of the GMO0893 cells that were partially or not stained (69.7%). However, the disadvantage in using PBL

cells was that more than half (51%) of the PBL cells were partially stained such as shown in the example in Panel – C of Figure 3.7.

Figure 3.8: Distribution of PBL cells based on their EpCAM staining intensity



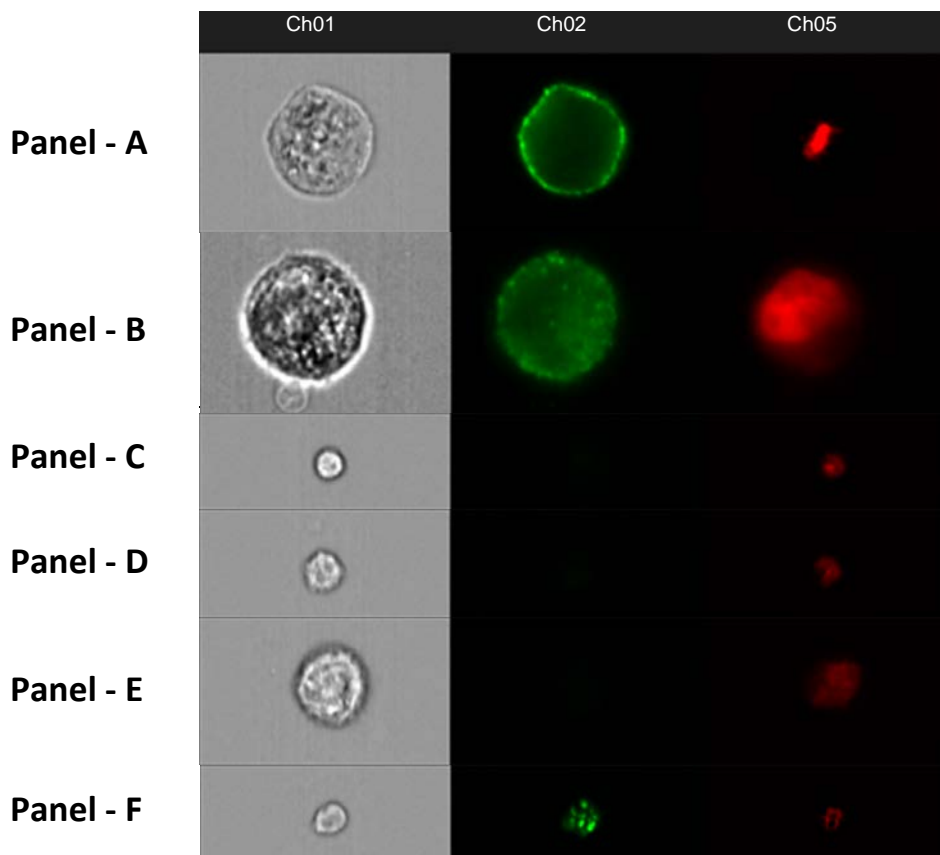
The figure above demonstrates the distribution of PBL based on the intensity of EpCAM antibody in these cells. Cells on the left (marked in green) were cells that showed no staining at all or a very minute EpCAM intensity that would otherwise be observed even without using any antibodies. The blue region in the middle represents cells with higher intensity of EpCAM, but not high enough to be classified as EpCAM-positive cells. Cells on the right (within the red region) were EpCAM-positive cells. The table below the graph shows exact percentages of the cells within each one of the three regions mentioned.

Single focused cells, which were derived as described in the materials and methods chapter by using the gating and regions tools, were divided based on their level of EpCAM staining as shown in Figure 3.8. Cells with little or no staining can be found on the left of the graph (green region) while those with a visually detectable level of staining are positioned on the right of the intensity plot graph (red region).

3.3.5 Mixing Experiment using EpCAM antibody

Based on a comparison of results in the two previous sections of this chapter, examining staining behaviours of GMO0893 and PBL cells, it was unequivocal that PBL cells were to be used in mixing experiments which reconstruct the presence of CTCs in the blood of prostate cancer patients by spiking PBL samples with different dilutions of PC3 cells. The experiment aims at verifying the sensitivity of EpCAM marker in labelling and isolating PC3 cells using the ImageStream^x. All samples contained a constant number of PBL cells and varying dilutions of PC3 cells as explained in the proof of principal (mixing) experiment section of the materials and method chapter of this research. Examples of images captured of both cell-lines are given below:

Figure 3.9: EpCAM staining of PC3 and PBL cells



The figure above shows a gallery of images captured from a sample containing both PC3 and PBL cells. Ch01 column shows the brightfield images of cells captured, Ch02 column shows staining patterns with the EpCAM antibody in green, while the Ch05 column shows nuclear staining with the DRAQ5 antibody. Panels A and B show examples of PC3 cells that were EpCAM-positive, while Panels C and D shows examples of PBL cells that were EpCAM-negative. Panel E shows an

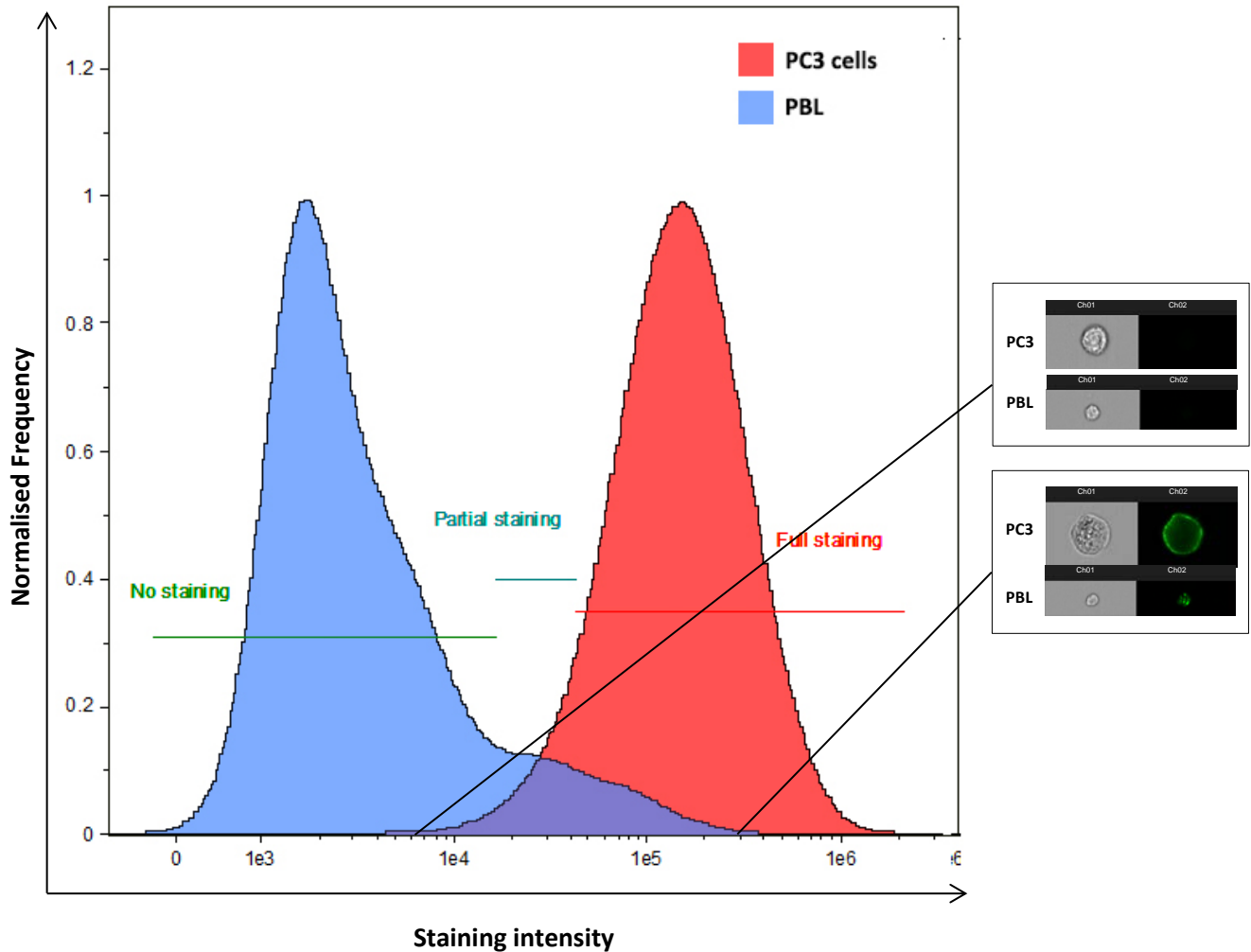
example of PC3 cells that was EpCAM-negative (false negative) and Panel F demonstrates how some PBL cells can be found to be EpCAM-positive (false positive).

Images captured of both cell-lines revealed that the majority of PC3 cells (94.4%) were EpCAM-positive and that the vast majority of PBL cells (89.13%) were EpCAM-negative as demonstrated in Figure 3.10 on the following page. Examination of EpCAM-positive PC3 cells revealed that some PC3 cells had peripheral EpCAM staining confined to the membrane region of these cells (Figure 3.9, Panel – A), while others expressed high intensity of EpCAM staining on the membrane of the cells as well as the cytoplasm (Panel – B), an indication of an increased permeabilisation of some of these PC3 cells. More importantly, however, a small percentage of the PC3 population (5.6%) was found to have weak or no EpCAM staining. Although this percentage may be relatively small, the number of PC3 false-negative cells that it represents (966 cells) is higher than can be ignored.

On the other hand, careful examination of the PBL region also revealed that there was a small percentage of PBL cells that were stained with EpCAM as shown in panel F of the same figure. The staining patterns of PBL cells were different from PC3 cells in that there was no staining confinement to the periphery of these cells but rather high intensity patches distributed irregularly within the cells. Despite this clear difference in staining, EpCAM false-positive PBL cells were seen to overlap in parts of the intensity graph in Figure 3.10 with PC3 cells due to the high intensity of staining in these cells. Several repetitions of this experiment yielded varying numbers of false positive and negative PC3 and PBL cells, but all of them confirmed the persistence of EpCAM lack of specificity.

Figure 3.10: PC3 and PBL cells distribution based on their EpCAM staining intensity

EpCAM antibody staining of PC3 and PBL cells



PC3 cells			PBL cells		
Region	Population	Percentage (%)	Region	Population	Percentage (%)
No staining	0.55	0.55	No staining	89.13	89.13
Partial staining	5.05	5.05	Partial staining	5.97	5.97
Full staining	94.4	94.4	Full staining	4.9	4.9

The figure above shows the distribution of PC3 and PBL cells from the same sample. The X axis shows the intensity of the EpCAM antibody staining, while the Y axis represents the normalised frequency for both cell-lines. Different staining intensities are categorised on three different sections and the overlapping region between the two cell-lines – where intensity of staining was similar – is highlighted in a purple. The table below the graph shows exact percentages for cells that were fully stained (red section), partially stained (blue section) and ones that did not stain (green section) for both cell-lines.

When EpCAM was used to measure cell retrieval of PC3 cells, the numbers were much lower than the original used. The percentage of cell retrieved might have varied, but the number of cells was in decline as the number of PC3 cells used decreased. The numbers presented in Table 3.2 do not give a precise account for the actual number of PC3 cells captured but of the cells that fall within the EpCAM positive region on the scatterplot as some of these cells were later identified as PBLs when individually examined. Additionally, there were PC3 cells that were not accounted for as they did not express a high EpCAM staining to be considered amongst the PC3 population. Furthermore, there were also cells that lost their structural integrity and had a relatively bad morphology and structure accompanied with a high EpCAM intensity; these were also counted as PC3 cells by the analysis software.

Table 3.2: Retrieval numbers of EpCAM positive cells

Total PC3 cells spiked into 1mL	Approximate retrieval of EpCAM stained cells
3,000,000	24.98% (749,540)
300,000	0.66% (1973)
30,000	2.27% (680)
3000	15.97% (479)
300	7% (21)
30	16% (5)

The table above shows the number of PC3 cells counted and spiked in each of the test tubes and the number of PC3 cells retrieved following examination with the ImageStream^x. The percentage of cells acquired fluctuated from one tube to another, but the number of cells was in constant decline. These numbers do not represent the actual number of PC3 cells retained but the number of cells that lie within the PC3 region on the scatterplot based on their EpCAM intensity. Upon manual examination of some of these cells, it was found that some PBL cells were identified amongst cells attributed to the PC3 population.

3.4 Discussion

In this study, imaging flow cytometry was used to investigate the identification of CTC cells by exploiting the EpCAM epithelial marker using immunocytochemical techniques. It also explored the specificity and sensitivity of PC3 identification using the EpCAM antibody. Staining localisation and general structural and morphological properties of cells were also observed. The method used was originally optimised to ensure that PC3 cells would stain with EpCAM, an epithelial-specific marker. PC3 cells were used to mimic CTCs in cancer patients, whereas GMO0893 cells and PBLs were used as blood cells. The use of GMO0893 cells was limited to simply testing if EpCAM would stain these cells and whether they can withstand the sample preparation steps, comprising of several washes. These cells displayed poor morphology upon examination and it was decided that they would not be further used to optimise a protocol to detect CTCs in blood using EpCAM. EpCAM was tested with each cell-line separately and a proof-of-principal experiment was then conducted where samples containing PBLs were spiked with dilutions of PC3 cells. The aim was test the efficacy of EpCAM in specifically targeting PC3 cells and distinguishing them from other cells in a given sample.

A number of EpCAM dilutions were initially tested to establish the most efficient amount of the antibody required to stain PC3 cells. It was found that 200µl of the pre-diluted form in which the antibody was provided was sufficient to stain the majority of cells in a given sample. There was, however, the problem of having a percentage of the PC3 population that would stain inadequately or not stain at all. Increasing the amount of antibody used or its concentration did not help solve this issue, which remained persistent even when the experiment was repeated several times with a variety of fixation methods and timing as well as other protocol modifications that were applied.

In the case of GMO0893 cells, EpCAM staining was prevalent throughout these cells with more than 30% of them found to be EpCAM-positive. These cells are lymphoblastoid cells and are not expected to stain with an epithelial marker such as EpCAM. The fact that the majority of them did, may provide an insight of a vital weakness in the functionality of this antibody. In addition to failing in

obtaining specific staining, images of GMO0893 cells revealed poor morphology, which can be attributed to the prolonged protocol and its rigorous washing steps. Following careful observation of captured images, it became clear that the nonspecific staining of these cells can also be attributed to the loss of cellular integrity throughout the sample preparation steps. This was also evident for other antibody staining methods tested on this cell-line, which will be demonstrated in the next few chapters.

When PBLs were used, an identical problem of nonspecific staining was recurring. More than 17% of a sample containing PBLs was positively stained for EpCAM, even though they should not have. However, unlike their GMO0893 counterparts, PBLs maintained a good morphology throughout the experiment. The EpCAM staining patterns observed differed from those obtained in the other two cell-lines. EpCAM staining did not cover the entire cell like it did with the GMO0893 cells, nor did it stain the periphery of these cells, as in the case of PC3 cells. EpCAM was observed in localised regions across PBLs in an irregular pattern. Despite the relatively small area these regions covered, the intensity of antibody staining in them was equivalent if not higher than that of some PC3 cells. As a result, many of these cells were falsely categorised as PC3 cells based on their EpCAM staining intensity when an EpCAM staining-intensity graph was created.

The proof of principle (mixing) experiment was the core aim of this study, as it would examine whether or not this immunological method would provide accurate results in the identification of CTCs in real cancer patients. To implement it, samples containing identical amounts of PBLs were spiked with dilutions of PC3 cells. This was done to test if the assay developed can identify PC3 cells based upon their staining patterns and intensity of EpCAM antibody as well as validating the sensitivity of this test. Six Eppendorf tubes were used with the highest retrieval being 24.98% for the tube containing 3×10^6 PC3 cells. The percentage then fluctuated from one sample to another, with the most diluted sample having a retrieval percentage of approximately 16% (5 cells out of 30). However, cells that were retrieved based on their EpCAM staining were not easily confirmed as PC3

cells due to the relatively poor morphology and structure of cells which may have also incorrectly contributed to their positive staining. As described before, some PBLs showed similar EpCAM staining patterns to PC3 cells and were often found in overlapping regions together when histograms were created from the data captured. Low EpCAM staining in some epithelial cells has previously been reported as a weakness of this antibody in a number of studies (Punnoose et al., 2010, Millner et al., 2013).

Another issue that needed to be addressed was the severe loss of PBL and PC3 cells during the sample preparation steps. The retrieval rate of cells in general was relatively low and can be explained by the excessively long procedure in which the cells were prepared prior to ImageStream^x examination. This poor recovery of cells was indeed a major setback as it meant that many PC3 cells that could have been detected by the device were lost before they could get to the image capture stage. This raised few doubts on whether the current assay is capable of preserving cell numbers and maintaining a good morphology for the cells.

The use of EpCAM as a sole marker for PC3 cells also became unconvincing following a series of consistent incidents in which a number of PC3 cells showed no patterns of EpCAM staining. On the other hand, some GMO0893 and PBLs showed high levels of EpCAM intensity. Although the staining patterns are generally different from one cell-line to another when examined individually, the creation of scatterplots became tricky as these cell-lines overlapped.

Chapter 4

CD45 antibody staining for the Identification of PC3 cells

4. CD45 Antibody Staining for the Identification of PC3 cells

4.1 Introduction

In the previous chapter I investigated the use of the EpCAM epithelial marker for the identification of prostate epithelial (PC3) cells within a mixture of peripheral blood lymphocytes (PBLs). It was demonstrated that the EpCAM antibody was a promiscuous marker where non-epithelial cells were positively stained. This made the accurate enumeration of PC3 cells very challenging. As a result, the use of an antibody that was specific to haematopoietic cells was considered. The aim was to target GMO0893 and PBL cells and then to enumerate the CD45-negative cells (PC3 cells).

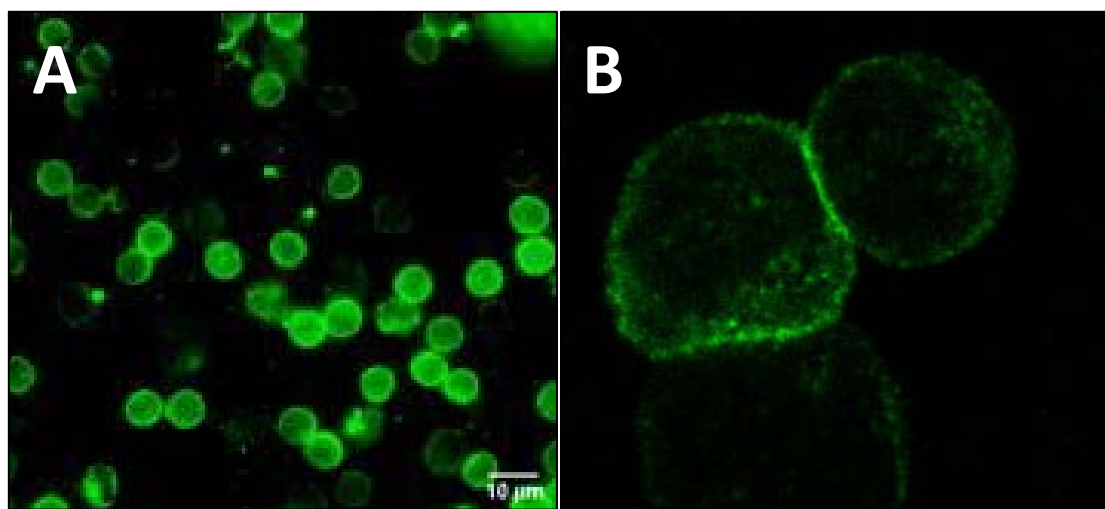
The CD45 antigen (lymphocyte common antigen) is a glycoprotein found to be expressed exclusively in all hematopoietic cells with the exception of mature erythrocytes. It is also known as the human common leukocyte antigen and has a molecular weight of approximately 200kDA (Nakano et al., 1990). Furthermore, CD45 plays vital roles in the immune system as the prototypic member of transmembrane receptor-like protein tyrosine phosphatases (RPTPs). Essentially, CD45 is required for the development process of T and B cells as well as the antigen-induced activation of these cells (Nam et al., 2005).

T cell activation often takes place when a foreign antigen is presented as short peptides by an antigen presenting cell (APC) such as macrophages, dendritic cells, Langerhans cells and B-lymphocytes. T cells may also be activated by a process that can be achieved via other class I or class II major histocompatibility complexes (MHC) (Malissen and Schmitt-Verhulst, 1993). Recognition of these molecules by T cells follows, leading to the activation of the T cell receptor (TCR), resulting in a cascade of events comprising of intracellular responses that consequently lead to T cells differentiation (Perlmutter et al., 1993). Besides TCR, a number of other T cell surface molecules were also found to be essential for T cell activation.

Previous studies found that co-receptor molecules such as CD4 and CD8 were expressed on different T cell subsets. These molecules were found to have a key role in initiating or stabilizing the T cell-APC interaction. Furthermore, these studies also suggested that CD45 molecules expression on T cells is vital for an effective activation of T cells (Ledbetter et al., 1993, Altin and Sloan, 1997).

CD45 has been previously used to distinguish PBL cells in various types of metastatic cancer cells from blood cells in patient samples (Figure 4.1).

Figure 4.1: CD45 antibody staining of leukocytes



The figure above shows two images of cells stained with CD45 antibody. Image A shows an example of white blood cells peripherally stained with CD45 antibody (Chen et al., 2016). Image B shows similar but clearer image of CD45 staining. However, the cells in (B) are Jurkat cells, an immortalised cell-line of human T lymphocyte cells (ABCAM, 2016).

An example of that are enrichment methods utilising anti-CD45 monoclonal antibodies in combination with FISH to deplete haematopoietic WBCs from patient samples, leaving behind a more concentrated sample of CTCs (Ning et al., 2014).

Additionally, FACS has also been used for the sensitive detection of CTCs via labelling leukocytes with anti-CD45 antibody. FACS is a flow cytometry technique that can sort or isolate a mixture of heterogeneous cells based on the fluorescent characteristics or the light scattering of cells. Using this method, CD45 negative cells (potential CTCs) were isolated and examined using immunostaining with CK18 and conventional cytology. The study used samples containing cells isolated from patients

with advanced localised gastric cancer and found that this technique might be useful in detecting and isolating CTCs (Baran et al., 1998). Despite all the studies conducted about the biology and function of CD45, there are still many aspects of it that remain unclear. Studies of CD45 variations between different human individuals might hold the key to a better understanding of this molecule (Holmes, 2006).

In this chapter, the CD45 antibody was used to stain lymphoblastoid cells and PBLs before testing its sensitivity in identifying PC3 cells via the negative selection of CD45 positive cells. Therefore I attempted to distinguish PC3 cells from a population of Epstein Barr transformed B-lymphocyte cells as a proof principle of the utility of using CD45 immunostaining and imaging flow cytometry to distinguish CTC cells from non-CTC cells.

4.2 Aim

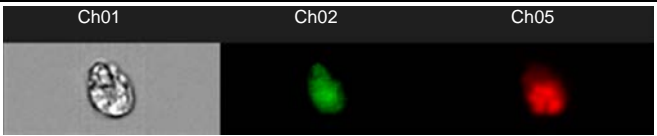
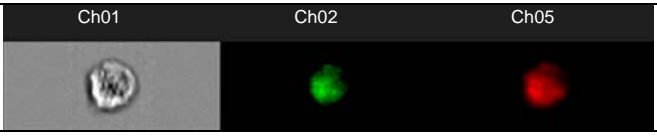
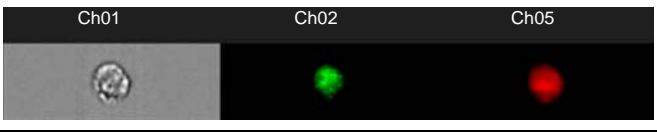
- To identify PC3 cells by negative selection of cells stained with CD45 antibody through an immunocytochemical technique and imaging flow cytometry
- To determine the efficacy of CD45 antibody staining in distinguishing PC3 cells spiked in a sample containing PBL cells
- To determine the sensitivity of CD45 staining in the identification of CTCs through the staining of PBL cells spiked with PC3 cells
- To determine the specificity of PC3 identification using CD45 antibody
- To investigate the effects of the CD45 staining approach on the morphology and structure of the cells used, as well as on the localisation of fluorescent staining

4.3 Results

4.3.1 CD45 antibody optimisation

Prior to staining cells with the CD45 antibody, optimisation tests similar to those conducted for the use of EpCAM were undertaken. It was vital to determine the best dilution of the antibody required to specifically stain all the non-epithelial cells within the sample, subsequently minimising the use of reagents and the cost of procedure. As previously explained, these tests were aimed at using a number of antibody dilutions, mixed with blocking buffer and then observing the percentage of cells – in this study GMO0893 – that were visibly stained. GMO0893 cells are lymphoblastoid cells that were expected to stain with CD45 antibody and were initially used to optimise the dilution of this antibody prior using it on other cell-lines. The method of staining with CD45 antibody is similar to that of EpCAM antibody staining described in the materials and method chapter.

Table 4.1: CD45 optimisation for GMO0893 cells

Dilution	Percentage of cells stained	Example of a stained cell
1/15	36.4%	
1/100	35.2%	
1/200	35.1%	

The table above shows the dilutions of the CD45 antibody that were used to stain GMO0893 cells. The 2nd column displays the percentage of GMO0893 cells that were positively stained with CD45 out of the total number of cells collected in the sample. In the 3rd column, examples of stained cells are given, showing brightfield images of GMO0893 cells on Ch01, Ch02 shows the intensity and pattern of the CD45 antibody staining while Ch05 shows DRAQ5 nuclear stain in red.

The use of CD45 dilutions did not yield expected results as all dilutions used showed very similar percentages of cells staining as well as similar staining regions within the cells. The percentage of

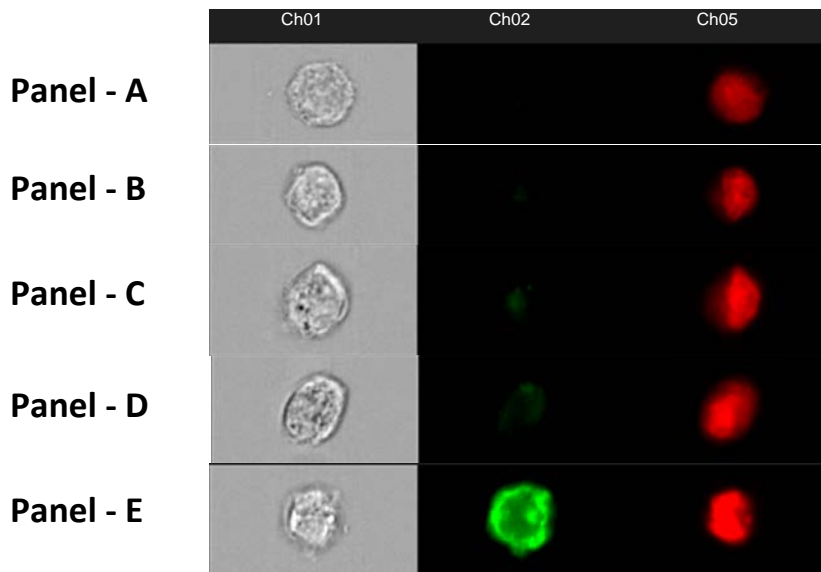
cells stained remained lower than anticipated even when the empirically determined optimal dilution of the antibody was used (1/15). It is worth pointing out that the morphology of the GMO0893 cells was relatively poor in all samples and might be a contributing reason as to why many cells did not express a high intensity of CD45 staining.

4.3.2 PC3 cells staining with CD45 antibody

Classified as epithelial cells, PC3 cells were not expected to be stained with the CD45 antibody.

However, they were subject to an experiment that would verify this and test whether non-specific staining would occur or not.

Figure 4.2: CD45 staining of PC3 cells

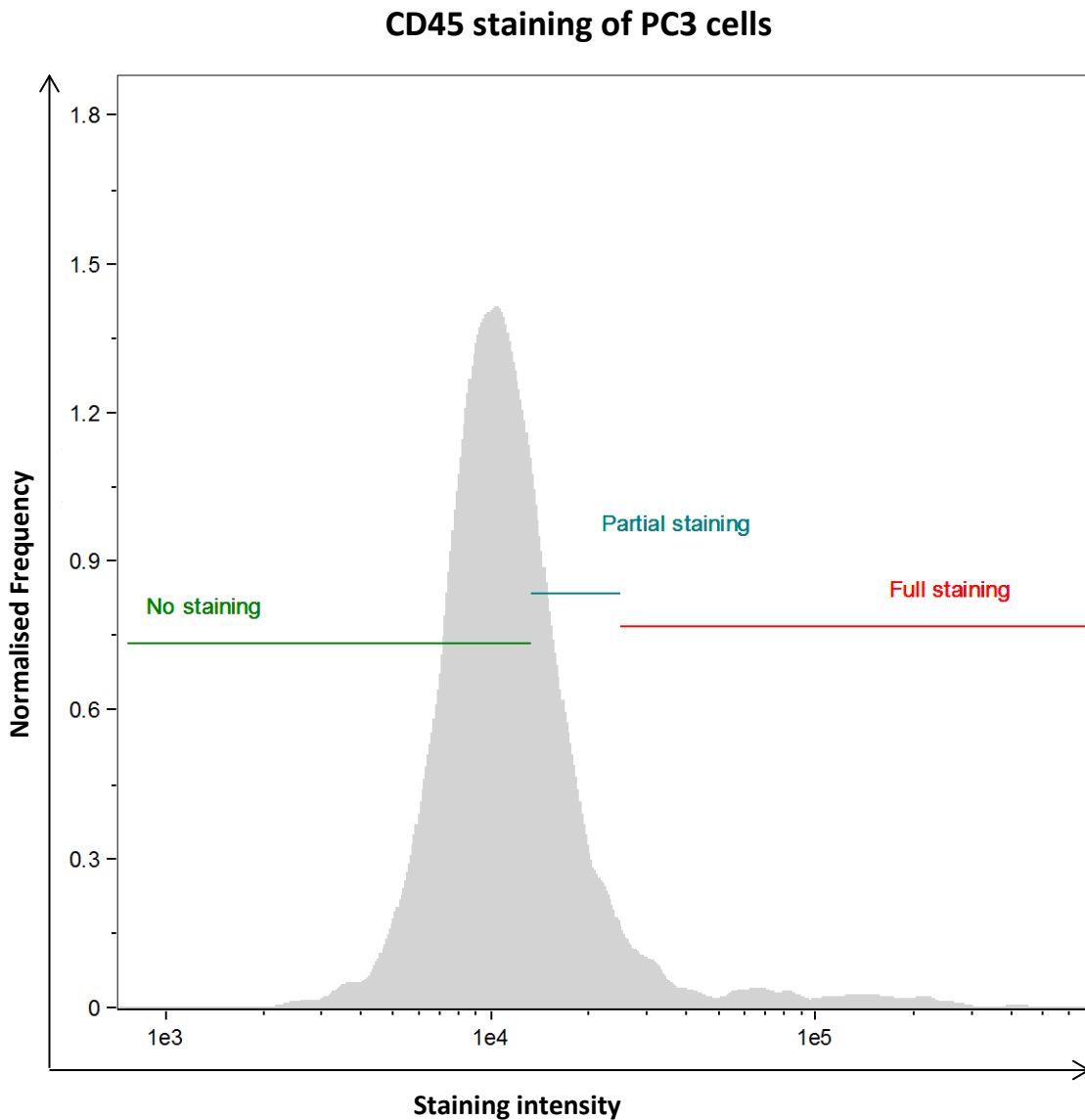


Samples shown in the figure above demonstrate different patterns of staining of PC3 cells with the CD45 antibody. The first column, titled Ch01 shows brightfield images of cells captured at 40x. The second column (Ch02) shows CD45 antibody staining in green. DRAQ5 nuclear staining is displayed in red in the third column titled Ch05.

The morphology and structure of these cells was optimal for most of the cells captured, although some cells did show loss of structure which could have resulted in the high levels of CD45 non-specific staining observed in some cells. Panels-A and B show examples of PC3 cells that showed no CD45 staining; these cells accounted for approximately 69.9% of the total population of PC3 cells in that sample. Panels-C and D show examples of cells that might initially appear as CD45 negative; however, the presence of small but high-intensity patches of CD45 within these cells forces the software to classify them as CD45 positive cells. The total number of these cells accounted for 23.3% of the PC3 cells in that sample. Lastly, there were cells that expressed non-specific staining with the CD45 antibody at an elevated and clear intensity. An example of these cells is demonstrated in

Panel-E; these cells accounted for approximately 6.8% of the entire sample. Figure 4.3 below shows the distribution of these three intensities of CD45 staining.

Figure 4.3: Distribution of PC3 cells based on their CD45 staining intensity



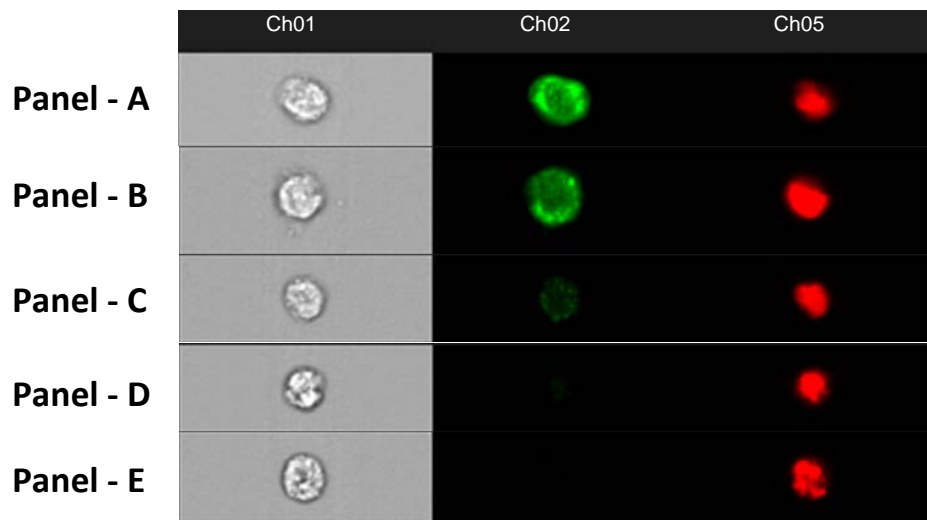
Region	Population	Percentage (%)
	No staining	69.9
	Partial staining	23.3
	Full staining	6.8

The figure above shows normalised frequency of PC3 cells (Y axis) against the intensity of CD45 antibody in these cells (X axis). Cells on the left (marked in green) were cells that showed no staining at all or a very minute CD45 intensity that would otherwise be observed even without using any antibodies. The blue region in the middle highlights cells with higher intensity of CD45, but not high enough to be classified as CD45 positive cells. Cells on the right (within the red region) were CD45 positive cells.

4.3.3 GMO0893 staining with CD45 antibody

GMO0893 cells are lymphoblastoid cells that are expected to be captured by the ImageStream^X as CD45 positive cells. This experiment was conducted to test the percentage of GMO0893 cells that would stain with the marker in what is essentially a similar experiment to the one testing the efficacy of different dilutions of CD45 in staining GMO0893 cells.

Figure 4.4: CD45 staining of GMO0893 cells

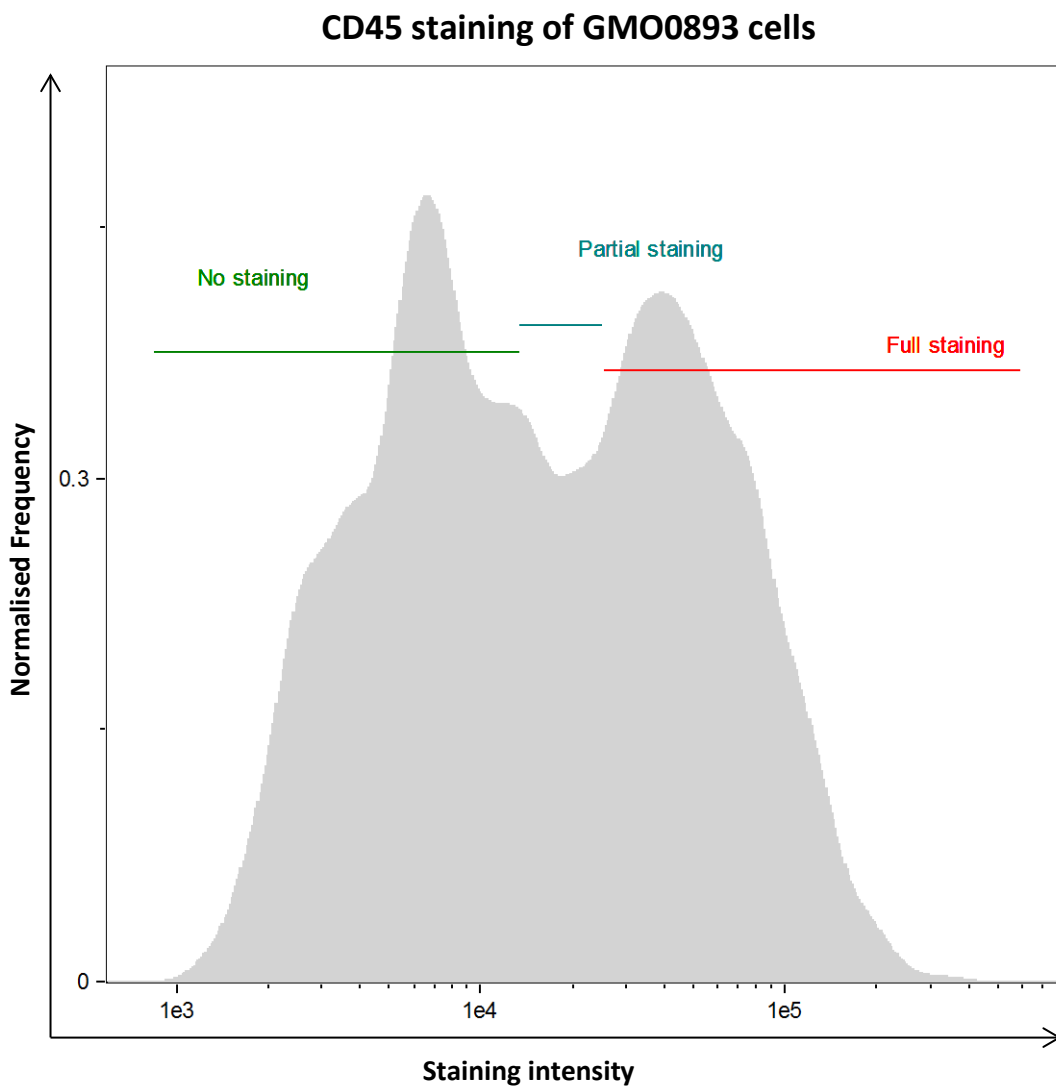


Samples shown in the figure above demonstrate different patterns of staining of GMO0893 cells with the CD45 antibody. The first column, titled Ch01 shows brightfield images of GMO0893 cells captured at 40 \times . The second column shows CD45 antibody staining in green colour on Ch02. DRAQ5 nuclear stain is displayed in red on the third column on Ch05. Panels A and B are examples of CD45 positive cells, while panels D and E are cells that were not stained with the antibody. Panel C shows an example of a partially/weakly stained cell.

Figure 4.4 above demonstrated that GMO0893 cells have similar staining patterns to the ones observed before in Figure 4.1 in the introduction of this chapter. There were, however, cells that showed higher CD45 staining intensity in their cytoplasm and the percentage of stained cells was found to be 39.9%, an increase on what was previously recorded for this cell-line with the same dilution of the antibody (35.1% positively stained GMO0893 cells), examples of such staining is shown in panels-A and B. It is worth noting that the morphology of these cells as well as the cell in panel-C, which was only partially stained, was not satisfactory like that of panel-E. A vast number of cells (46.3% of the entire GMO0893 population captured) did not show any forms of CD45 staining, examples of these cells are those shown in Panels-D and E. The remaining 13.8% of the cells in the

sample were partially stained (e.g. panel-C). These cells showed slight levels of staining with a lower intensity than the fully stained cells. They were also characterised with a morphology and structure that is less robust than that of the negatively stained cells. The distribution of these cells within the sample are demonstrated in the figure below, which shows the varying intensities of CD45 staining recorded for cells in this experiment.

Figure 4.5: Distribution of GMO0893 cells based on their CD45 staining intensity



Region	Population	Percentage (%)
	No staining	46.3
	Some staining	13.8
	Stained cells	39.9

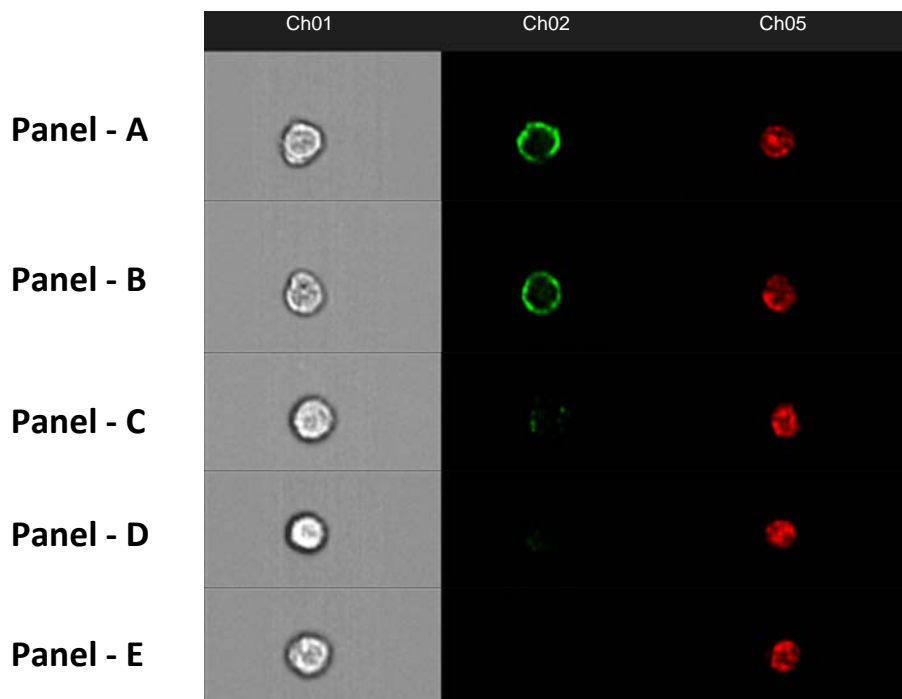
The figure above shows the distribution of GMO0893 cells based on the intensity of CD45 antibody in these cells. Cells on the left (marked in green) were cells that showed no staining at all or a very minute CD45 intensity that would otherwise be observed even without using any antibodies. The blue region in the middle highlights cells with higher intensity of CD45, but not high enough to be classified as CD45 positive cells. Cells on the right (within the red region) were CD45 positive cells.

4.3.4 PBL staining with CD45 antibody

The procurement of less than 40% CD45 positive GMO0893 cells raised concerns as to whether this cell-line is to be used to examine the sensitivity of using the CD45 biomarker in identifying PC3 cells. PBL cells had previously produced improved morphology and better antibody specificity when EpCAM was used; therefore they were stained with the CD45 antibody separately to examine the patterns and percentage of positive staining and compare it to the GMO0893 cells.

Images of PBL cells stained with the CD45 antibody are shown in Figure 4.6 below.

Figure 4.6: CD45 staining of PBL cells

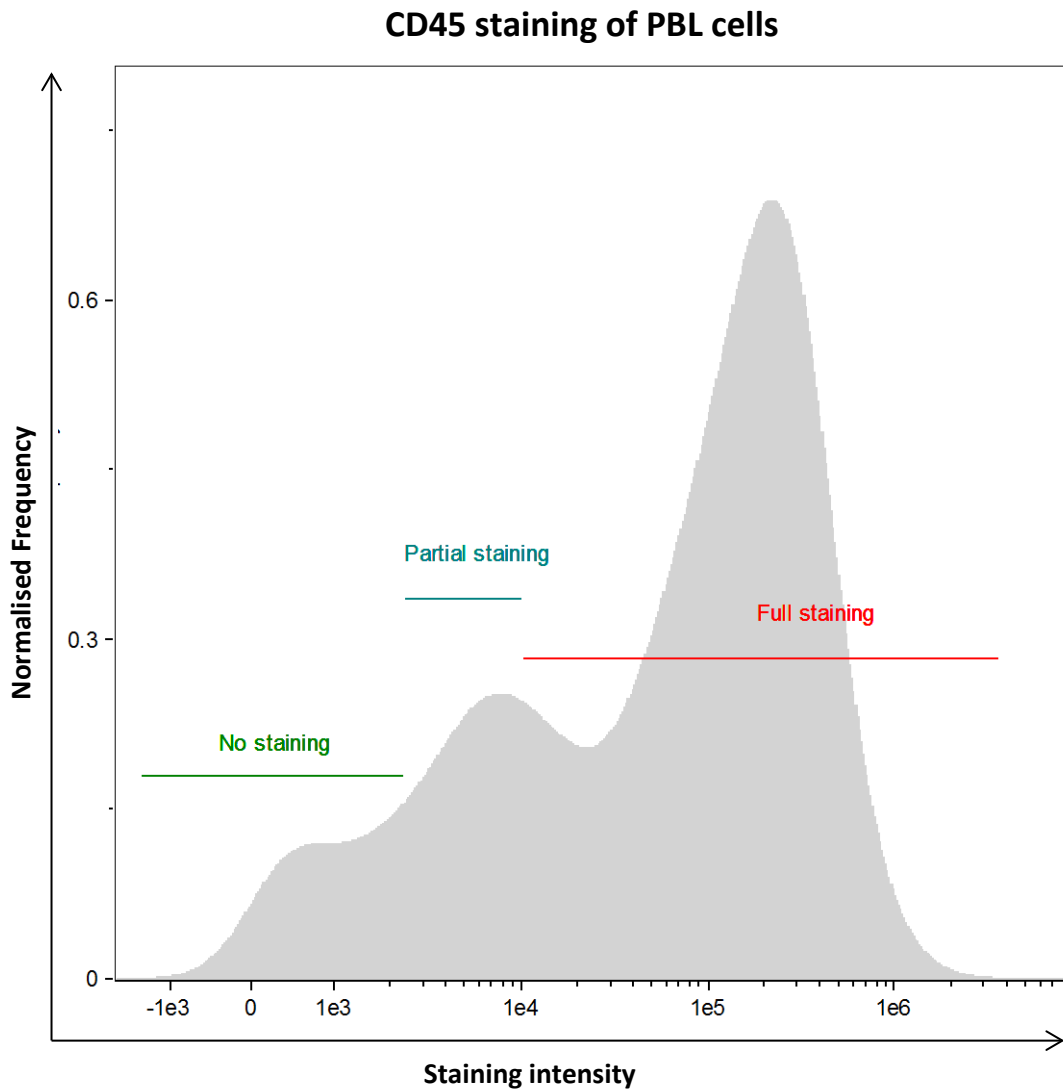


Samples shown in the figure above demonstrate different patterns of staining of PBL cells with the CD45 antibody. The first column, titled Ch01 shows images of cells captured at 60x. The second column shows CD45 antibody staining in green colour on Ch02. DRAQ5 nuclear stain is displayed in red on the third column on Ch05. Panels-A and B are examples of CD45 positive cells, while panel C is an example of a cell that was partially/weakly stained with the antibody. Panels-D and E are examples of CD45 negative PBL cells.

As can be observed in the figure above, the expected staining configuration of CD45 was acquired in many CD45 cells. In fact, 75.5% of the PBL cells were stained positive with CD45 antibody, a vast improvement on the 39.9% obtained with the GMO0893 cell-line. The levels of CD45 staining

intensity varied in PBL cells, with some (e.g. Panel C) showing weak or partial staining in their periphery. Some PBL cells showed no CD45 staining, and these accounted for approximately 10.3% of the entire sample. Despite acquiring a number of PBL cells with no CD45 staining present, the use of PBL cells was preferred to the GMO0893 cells when the sensitivity test was conducted.

Figure 4.7: Distribution of PBL cells based on their CD45 staining intensity



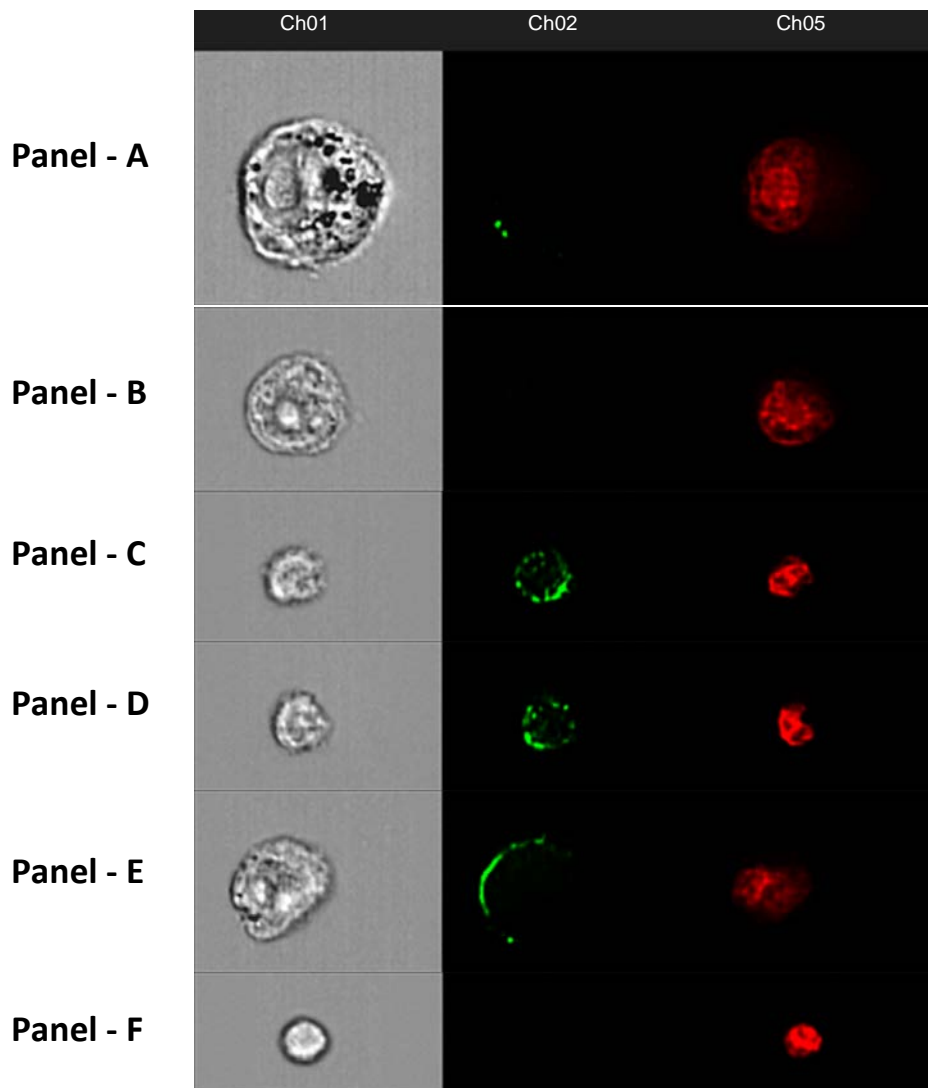
Region	Population	Percentage (%)
	No staining	10.3
	Some staining	14.2
	Stained cells	75.5

The figure above demonstrates the distribution of PBL based on the intensity of CD45 antibody in these cells. Cells on the left (marked in green) were cells that showed no staining at all or a very minute CD45 intensity of similar level to that of background staining. The blue region in the middle represents cells with higher intensity of CD45 antibody, but not high enough to be classified as CD45-positive cells. Cells on the right (within the red region) were CD45 positive cells. The table below the graph shows exact percentages of the cells within each one of the three regions mentioned.

4.3.5 Mixing experiment using CD45 antibody

Samples containing PBL cells were spiked with dilutions of PC3 cells to test the sensitivity of CD45 antibody in identifying non epithelial cells. Figure 4.8 below shows examples of positively and negatively stained PC3 and PBL cells, as well as cells false negative and positive cells for both populations of cells.

Figure 4.8: CD45 staining of PC3 and PBL cells



The figure above shows a gallery of images captured from a sample containing both PC3 and PBL cells. The Ch01 column shows the brightfield images of cells captured at 60 \times , Ch02 column shows staining patterns with the CD45 antibody in green, while the Ch05 column shows nuclear staining with the DRAQ5 antibody. Panels-A and B show examples of PC3 cells that were CD45 negative, while Panels-C and D shows examples of PBL cells that were CD45 positive. Panel-E shows an example of PC3 cells that was CD45 positive (false positive staining) and Panel-F demonstrates a PBL cell that was CD45 negative (false negative cell).

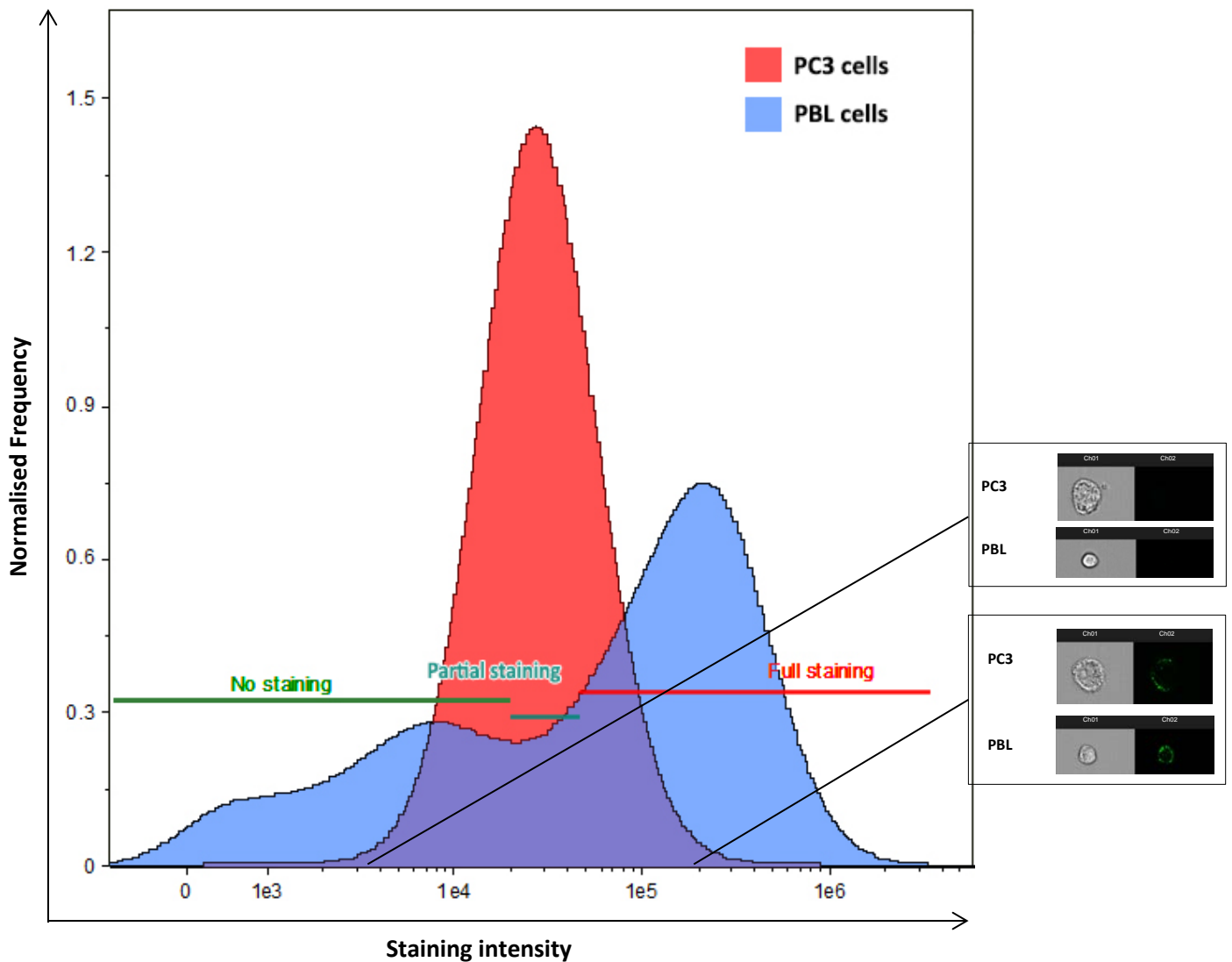
As shown by images taken of both cell-lines in the sample, the majority (83.8%) of the PC3 cells showed weak or no CD45 staining as would be expected since CD45 is a haematopoietic marker. Examples of similar cells are shown in panels-A and B of the figure above. However, the rest of the PC3 cells were found to exhibit a high CD45 staining intensity. The PC3 cells that showed high staining intensity were found to have poorer morphology than those that did not. Comparison of brightfield images of panels-A and B with that of panel E in Figure 4.8 provides evidence that PC3 cells with different staining intensity had contrasting morphologies.

On the other hand, 62.27% of the PBL population in that sample were found to be stained positive for CD45 antibody (Panels C and D, Figure 4.8). The existence of false negative cells was present too with more than 30% of the PBL cells showing no CD45 staining (e.g. Panel F). There were also cells that were partially stained, accounting for approximately 6.83% of the entire PBL population. Distribution of staining characteristics of both cell-lines is presented in Figure 4.9 which also highlights the existence of an overlapping region (purple section) between the two cell-lines, in which the staining intensity is very similar, making it difficult to distinguish PC3 cells from PBL cells based on their CD45 staining intensity.

Furthermore, it is worth noting that the CD45 staining observed in PC3 cells was different to that of the PBL cells. In some PC3 cells, CD45 highly stained regions were distributed randomly across these cells, forming fluorescent dots. The existence of several small areas with high CD45 intensities in some PC3 cells deceived the analysis software into categorising these cells in the same region as PBL cells on the CD45 intensity graph. Careful examination of several cells from both populations, however, demonstrated the massive difference in the patterns of CD45 staining between the two cell-lines.

Figure 4.9: Distribution of PC3 and PBL cell based on their CD45 staining intensity

CD45 staining of PC3 and PBL cells



PC3 cells			PBL cells		
Region	Population	Percentage	Region	Population	Percentage
	No staining	22.3		No staining	30.9
	Partial staining	61.5		Partial staining	6.83
	Full staining	16.2		Full staining	62.27

The figure above shows the distribution of PC3 and PBL cells imaged from the same sample. The X axis shows the intensity of the CD45 staining, while the Y axis represents the normalised frequency. Different staining intensities are categorised on three different sections and the overlapping region between the two cell-lines – where intensity of staining was parallel – is coloured in purple. The table below the graph shows exact percentages for cells that were fully stained, partially stained and ones that did not stain for both cell-lines.

The isolation of CD45 negative cells was done for samples serially diluted with PC3 cells. The numbers in the table below might be inaccurate due to the nonspecific CD45 staining observed, but they represent an improvement on the number of PC3 cells identified through the positive selection of EpCAM stained cells.

Table 4.2: Retrieval numbers of CD45 negative cells

Total PC3 cells spiked into 1mL	Approximate retrieval of CD45 negative cells
3,000,000	5.8% (174,107)
300,000	2.19% (6579)
30,000	7.01% (2105)
3000	1.8% (54)
300	8.76% (26)
30	33.33% (10)

The table above shows the number of PC3 cells counted and spiked in each of the test tubes and the number of PC3 cells retrieved following examination with the ImageStream^x. The percentage of cells acquired fluctuated from one tube to another, but the number of cells was in constant decline. These numbers do not represent the actual number of PC3 cells retained but the number of cells that lie within the PC3 region on the histogram based on their CD45 staining intensity. Upon manual examination of some of these cells, it was found that some PBL cells were identified amongst cells attributed to the PC3 population

4.4 Discussion

Imaging flow cytometry was used in this study to investigate the possibility of using the CD45 antibody to distinguish epithelial (PC3) cells from haematopoietic cell derivatives (In this case the B-lymphoblastoid cell-line derived from a normal individual – GMO0893 as well as PBLs) by negative selection. The CD45 antibody was used to target the GMO0893 and PBL cells. GMO0893 and PBL cells were expected to be identified as CD45-positive, whereas PC3 cells – which are epithelial cells – were not expected to stain with this antibody. The specificity of the CD45 antibody was tested as follows

1. By staining of GMO0893 cells,
2. Staining PBLs,
3. Spiking PC3 cells in samples containing PBL cells and staining these samples with the CD45 antibody.

The number of false positives and negatives would give a clear indication of how specific the antibody is. The sensitivity of the antibody was also tested by diluting the number of PC3 cells in PBL samples and identifying the CD45-negative cells. Initially, the dilution of the CD45 antibody was optimised so that most of the PBL and GMO0893 cells would be identified by the ImageStream^x as CD45-positive. The initial recommended dilution of 1/15 was used, as well as 1/100 and 1/200. The percentage of CD45 positive GMO0893 cells for these three dilutions was similar, and the 1/200 dilution was used thereafter.

Most of the sample containing PC3 cells showed no CD45 antibody staining (69.9%). However, with the more than 6% of the cells being CD45-positive, the non-specificity of the CD45 antibody was becoming apparent. This was further confirmed when a sample containing GMO0893 cells were also partially stained with the same antibody. This time, only 39.9% of the sample was CD45-positive at

an optimal level, and more than 46% of the cells showing no CD45 staining at all. PBL cells were used instead of GMO0893 cells for the proof of principal experiment as more PBL cells (75.1%) were found to be CD45 positive than GMO0893 cells (39.9%). Using PBL cells for the sensitivity test (spiking them with PC3 cells) was investigated to test the sensitivity of this approach in identifying PC3 cells through negative selection of stained cells.

It is worth mentioning that a relatively poor morphology was observed for the cell-lines used and most of the cells' structure did not appear intact for most cells. Perhaps this lack of a comprehensive cellular structure could have contributed to PC3 cells exhibiting nonspecific CD45 staining. Patterns of false positive PC3 cells and false negative PBL cells were evident throughout the results. The difference when the cell-lines are mixed is that more PC3 cells were stained positively with the antibody (6.2% separately and 16.2% when mixed) and less PBL cells were detected as CD45-positive than when spiked with PC3 cells (75.1% separately and 62.27% when spiked with PC3 cells). The overlapping region (in Figure 4.9) in which both, PC3 and PBL cells, showed similar staining intensities and patterns was relatively large, due to the prevalence of nonspecific CD45 staining. The presence of this overlap presented a huge disadvantage in distinguishing cells based their CD45 staining intensity.

Additionally, the inadequate morphology of both cell-lines – possibly caused by the numerous sample preparation steps, such as cells fixing – did not help in discriminating between both populations of cells. It remains possible that some PBL cells might have lost their cellular structure and expanded in size, making them closer in appearance to PC3 cells than the usual PBLs. This loss of structure may have also contributed to the absence of staining in some PBL cells. Despite the fact that many PC3 cells did not stain with the CD45 antibody and that the majority of PBL cells were observed to be fully stained, the isolation of PC3 cells based on CD45 staining might not be the most accurate method in imaging flow cytometry.

Chapter 5

Identification of PC3 cells using Zonula Occludens-1 Tight Junction Protein Antibody

5. Identification of PC3 cells using Zonula Occludens-1 Tight Junction Protein Antibody

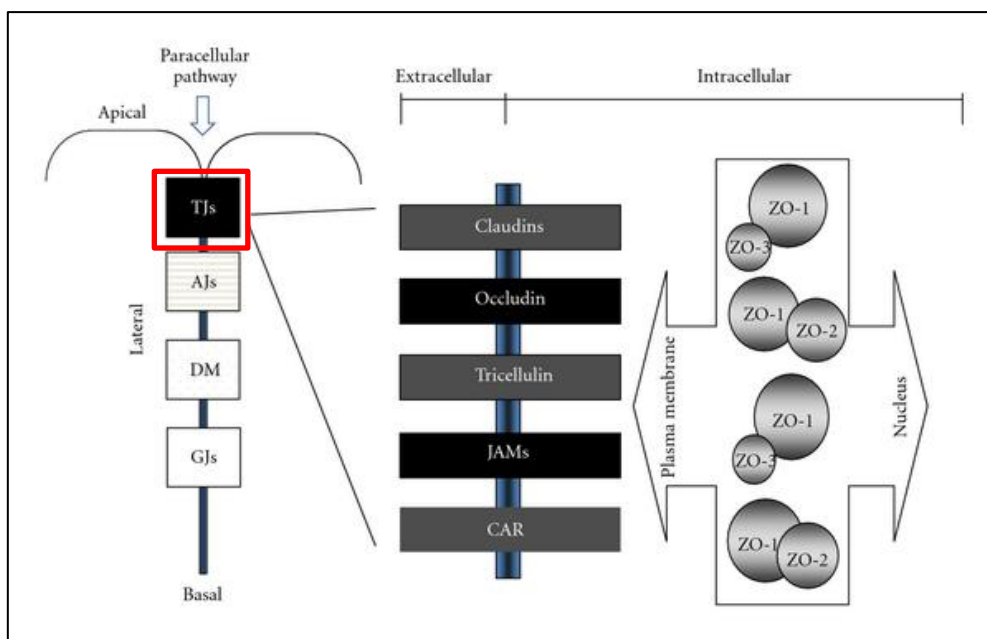
5.1 Introduction

Following the approach previously taken in this research in which PC3 cells were targeted with an epithelial-specific marker, an alternative was also tested targeting PC3 cells in the form of Zonula Occludens-1 tight junction (ZO-1 TJ) protein antibody. This approach was investigated as a possible alternative due to the lack of specificity of EpCAM antibody. The interaction between adjacent epithelial cells and between epithelial cells and their extracellular matrix is mediated by special protein complexes that are also responsible for cells' adhesion such as tight junctions (TJ). These junctions are located at the lateral membrane of epithelia and play a key role as barriers, regulating the diffusion of ions and molecules through the paracellular pathway (between cells) in accordance to their size and charge (Balda and Matter, 2016).

TJ comprise of a very complex set of transmembrane proteins that are found to function as signalling centres controlling epithelial processes such as proliferation, polarisation and differentiation. The mechanisms in which TJ control such processes, however, remain poorly understood (Zihni et al., 2014). There are at least 40 different proteins at the TJ, some of which are transmembrane ones that are divided into three domain proteins groups: Occludin, MarvelD2 and MarvelD3 (González-Mariscal et al., 2003). Others proteins are intracellular plaque proteins which provide a structural support platform between transmembrane proteins and the actin skeleton. An example of such structure-supporting intracellular proteins is ZO-1, which additionally has a gene expression regulatory role that contributes to epithelial cellular proliferation through various signalling pathways (Balda et al., 2003).

ZO-1 was the first identified as a TJ-associated protein and has a molecular mass of about 220kDA. Some suggested a possible link between this protein and the development of cancer. For example, one study investigated the role of ZO-1 in the formation of gap junctions' plaques as well as the creation of intracellular coupling (Hervé et al., 2014). Cancer is thought to be associated with cell-to-cell communication malfunction as a multitude of tumours were observed to have gap junction defects (Cronier et al., 2009); potentially linking ZO-1 to cancer development and metastasis.

Figure 5.1: The protein complexes that exist within the paracellular pathway



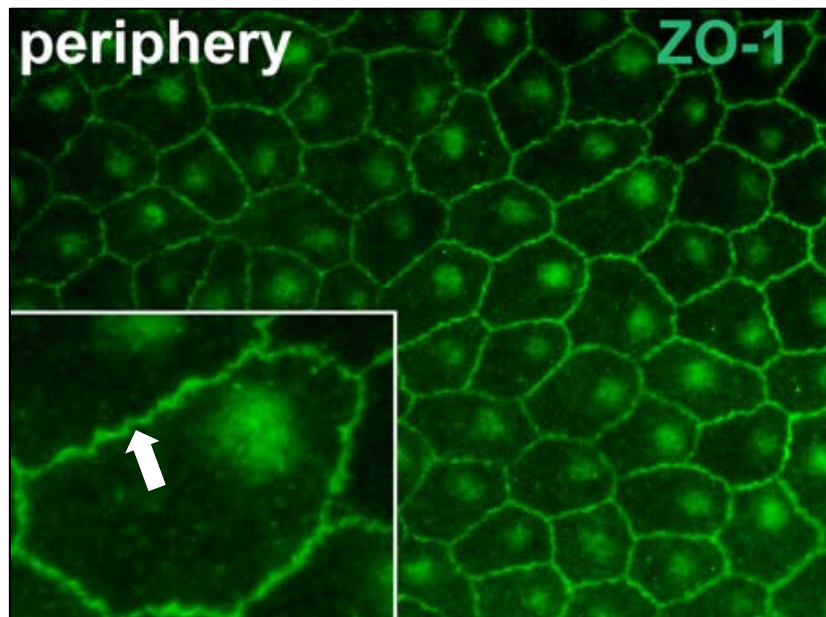
The figure above shows the paracellular pathway between cells comprising of several protein complexes, such as TJ (in red outline). TJ consist of several transmembrane proteins such as caludins and occludin that interact directly with ZO proteins. ZO proteins are also found to be associated with several peripheral junctional proteins, creating a complex intracellular network (Bauer et al., 2010). More direct interactions occur between these proteins and actin filaments, highlighting their crucial function as crosslink mediators between TJ strands and the cytoskeleton (Fanning et al., 1998).

Previous work in this area already presented clear links between TJ and cancer metastasis (Martin, 2014), and some studies even demonstrated ZO-1 involvement in intracellular signalling and gene expression with one study particularly highlighting the urgent need for an intensive investigation of similar proteins (Bauer et al., 2010). There has also been strong evidence to suggest that the ZO-1 protein is associated with several regulatory molecules such as growth factors, subsequently regulating the cell cycle. Moreover, while thorough work is still required to confirm it, it was

hypothesised that these proteins might also play a role in virus-induced cancers and hold the key to a better understanding of such diseases (Javier, 2008).

Some studies have utilised the ZO-1 TJ antibody to label epithelial cells and distinguish them from other types of cells that do not possess TJ (Zahabi et al., 2012, Leung et al., 2012). These studies confirmed the high expression of ZO-1 in epithelial cells and gave an insight into its role in several cellular events such as membrane fusion and cell detachment. Others have used this marker to detect expression levels of ZO-1 in non-small cell lung cancer (NSCLC) (Ni et al., 2013b). The study by Ni *et al* concluded that high expression levels of ZO-1 can be interpreted as a good prognostic outcome in cases of NSCLC.

Figure 5.2: ZO-1 TJ staining of epithelial cells



The figure above shows an immunofluorescence image demonstrating ZO-1 TJ protein antibody staining of murine peripheral retinal pigmented epithelium cells. The green stain on the outer layer (pointed at) of cells indicate the localisation of TJ in these cells (Kokkinopoulos et al., 2011).

In this study ZO-1 TJ antibody was used to stain the epithelial PC3 cells in a similar way to the EpCAM antibody. PC3 cells were cultured in flasks and required to be trypsinised before they were used in experiments. In order for Trypsin to achieve cell detachment, tight junctions between epithelial cells were processed and dissolved first (Vilen et al., 2012). Meaning that, unlike studies that examined TJ

staining patterns in conventional microscopy, flow cytometry staining of these junctions might be different and disrupting. ZO-1 TJ was also tested on control samples containing GMO0893 cells or PBL cells only, before testing its sensitivity in the proof of principle experiment.

5.2 Aim

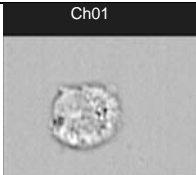
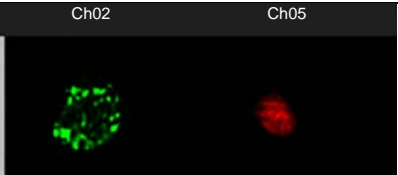
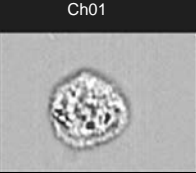
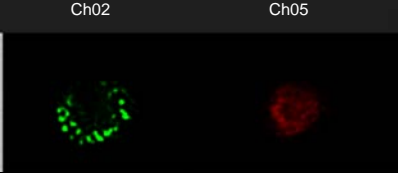
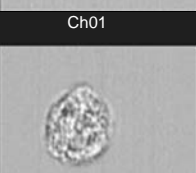
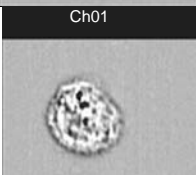
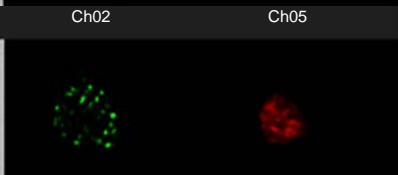
- To identify PC3 cells by the positive selection of cells stained with ZO-1 TJ antibody through an immunocytochemical technique
- To determine the efficacy of ZO-1 TJ antibody staining in distinguishing PC3 cells spiked in a sample containing PBL cells
- To determine the specificity of ZO-1 TJ antibody staining in the possible identification of CTCs through the staining of PC3
- To observe and categorise different ZO-1 TJ staining patterns for PC3, GMO0893 and PBL cells
- To determine the sensitivity of ZO-1 TJ staining in the identification of PC3 cells by spiking PBL samples with dilutions of PC3 cells
- To investigate the effects of the ZO-1 TJ staining method on the morphology, shape and structure of the cells used, as well as on the localisation of fluorescent staining

5.3 Results

5.3.1 ZO-1 TJ antibody optimisation

Optimisation of the ZO-1 TJ antibody was conducted prior to using it for staining the three cell-lines (PC3, GMO0893 and PBL cells) in a very similar way to the way EpCAM and CD45 antibodies were optimised. The initial step was to establish which dilution of the antibody would adequately stain most of the PC3 cells. The dilution of the antibody recommended by the supplier was 1/50; however, additional titres of the antibody were also tested to determine the efficacy and specificity of staining as shown in the table below.

Table 5.1: ZO-1 TJ optimisation for PC3 cells

Dilution	Percentage of cells stained	Example of a stained cell		
		Ch01	Ch02	Ch05
1/50	81.4			
1/100	76.5			
1/150	86			
1/200	89.4			
1/500	94.7			

The table above shows the dilutions of the ZO-1 TJ antibody in the first column. The 2nd column contains the percentages of PC3 cells that were positively stained with ZO-1 TJ antibody out of the total number of cells collected in the sample. The 3rd column shows examples of stained cells, including brightfield images of PC3 cells on Ch01, the intensity of ZO-1 TJ staining on Ch02 in green and nuclear staining of these cells using DRAQ5 on Ch05.

The staining patterns for all dilutions were different than those observed when EpCAM and CD45 antibodies were used. Instead of a continuous membrane staining like that of the EpCAM, the ZO-1 TJ antibody was staining small separate sites within PC3 cells. Some of these sites were located within the cells while others were observed at the cell's periphery.

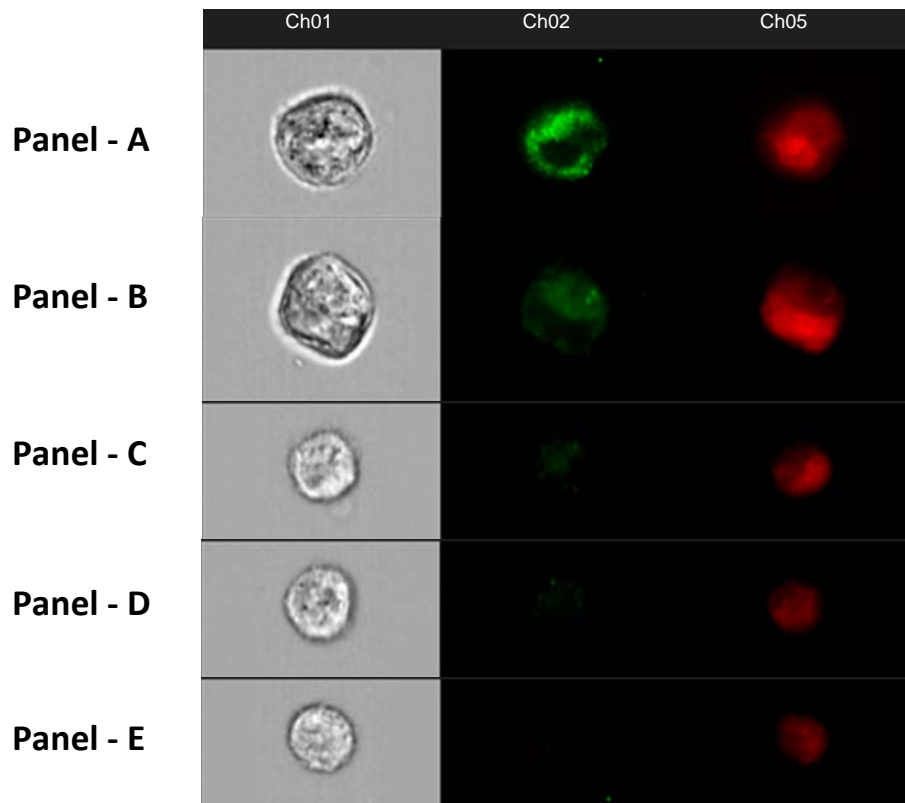
The ZO-1 TJ antibody, as explained previously in the introduction of this chapter, targets the tight junctions on the membrane of the epithelial cells. Hence why, it is vital to observe the various effects inflicted on these complexes by different reagents used in the optimisation process. For example, Trypsin-EDTA is used to dissociate the adherent PC3 cells from flasks in order to collect them for experimental use. This dissociation process is achieved by dissolving the CAM molecules (such as TJ) between the cells and the flask as well as those between cells themselves. Once dissolved, complexes such as TJ are expected to be seen displaced within the cell or even outside it. Which may explain the why ZO-1 TJ staining was observed in sites where these complexes reside within cells rather than at cell periphery. It might also provide evidence for the elevated levels of background staining intensity, when compared to staining using other markers, such as EpCAM.

The 1/50 dilution demonstrated high intensity staining of PC3 cells that was, for a number of cells, far too excessive causing these cells to appear completely concealed by the antibody on Ch02. Reducing the concentration of the antibody certainly resulted in a clearer staining of cells, with the percentage of stained cells reaching elevated levels when the 1/500 dilution was used (94.7% ZO-1 TJ-positive PC3 cells). As a result, the 1/500 dilution became the standard dilution of this antibody that was used for the immunostaining of PC3, GMO0893 and PBL cells. It was also used in the proof of principle experiment to test the sensitivity of this marker in identifying PC3 cells.

5.3.2 PC3 cells staining with ZO-1 TJ antibody

As the only epithelial cell-line used in this research, PC3 cells were expected to be stained with the ZO-1 TJ antibody. The figure below shows different types of staining observed when a sample containing PC3 cells was stained with the ZO-1 TJ antibody.

Figure 5.3: ZO-1 TJ staining of PC3 cells

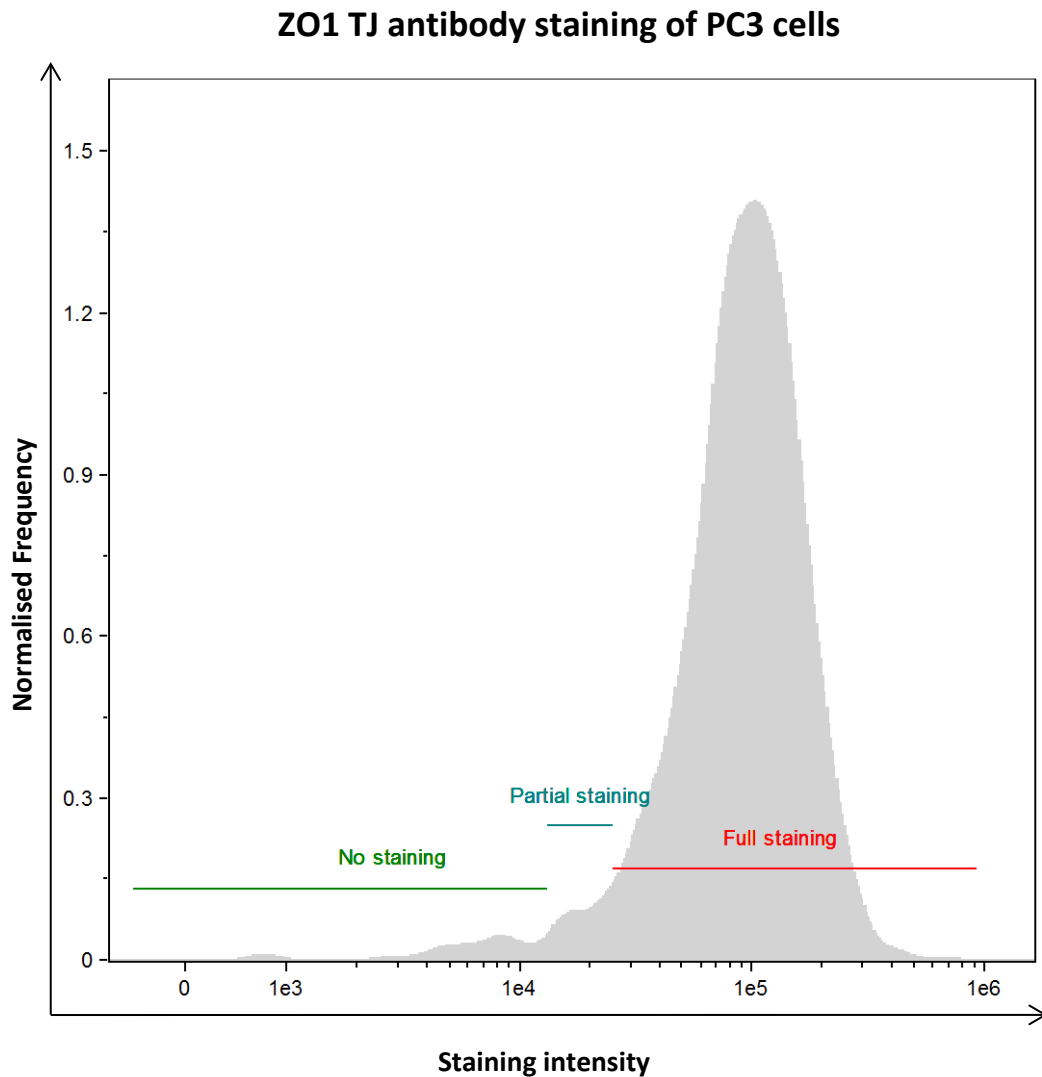


Samples shown in the figure above demonstrate different patterns of staining of PC3 cells with the ZO-1 TJ antibody. The first column, titled Ch01 shows brightfield images of cells captured at 40× magnification. The second column shows ZO-1 TJ antibody staining in green on Ch02. DRAQ5 nuclear staining is displayed in red in the third column, titled Ch05.

Figure 5.3 demonstrates how different cells showed different intensity levels of ZO-1 TJ staining. The vast majority (95.76%) of PC3 cells, however, showed high and clearly visible staining patterns such as the ones displayed by cells in panels-A and B. A very low number of PC3 cells (1.94%) showed a slight staining intensity, such as these shown in panels-C and D. The number PC3 cells that were not stained at all with the ZO-1 TJ antibody was also low (2.3%). Cells which showed a clearly visible ZO-1 TJ staining, regardless of the localisation of that staining, were classified as ZO-1 TJ-positive cells. It is

worth mentioning that the percentage of PC3 cells that were ZO-1 TJ-positive was higher than that of the EpCAM-positive PC3 cells. The distribution of PC3 cells in this experiment, with regards to level of staining intensity of the ZO-1 TJ, is represented with the histogram in Figure 5.4 below.

Figure 5.4: Distribution of PC3 cells based on their ZO-1 TJ staining intensity



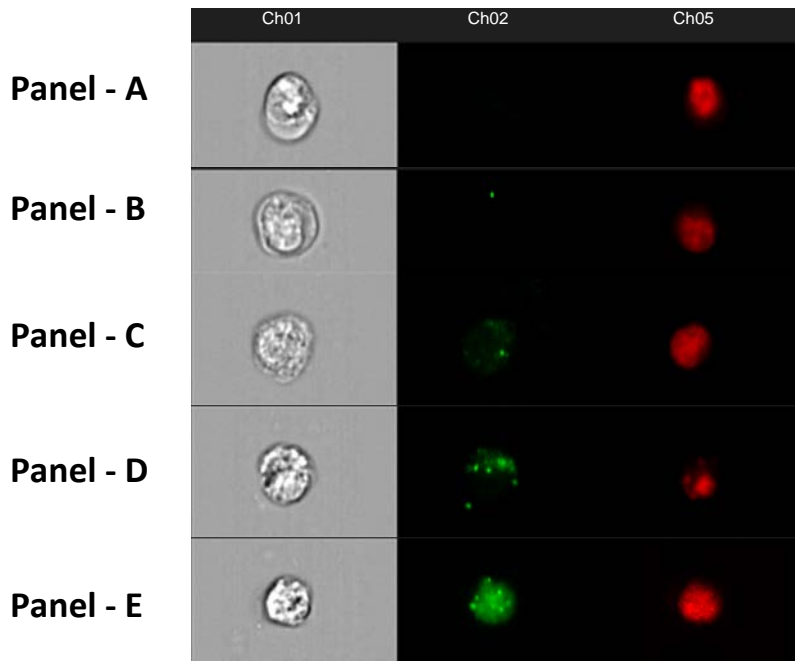
Region	Population	Percentage (%)
	No staining	2.3
	Some staining	1.94
	Stained cells	95.76

The figure above shows the normalised frequency of PC3 cells (Y axis) against the intensity of ZO-1 TJ antibody in these cells (X axis). Cells on the left (marked in green) were cells that showed no staining at all or a very minute antibody intensity that would even be obtained without using any antibodies. The blue region in the middle categorises cells with higher intensity of ZO-1 TJ antibody, but not high enough to be classified as ZO-1 TJ-positive cells. Cells on the right (within the red region) were ZO-1 TJ-positive cells. The table below the graph displays the exact percentages of PC3 cells within these three regions.

5.3.3 GMO0893 staining with ZO-1 TJ antibody

As lymphoblastoid cells, GMO0893 cells were not expected to show ZO-1 TJ staining, mainly because these cells do not possess TJ like epithelial cells do. A sample containing GMO0893 cells was stained with ZO-1 TJ antibody to verify this and the results can be seen in Figure 5.5 below.

Figure 5.5: ZO-1 TJ staining of GMO0893 cells

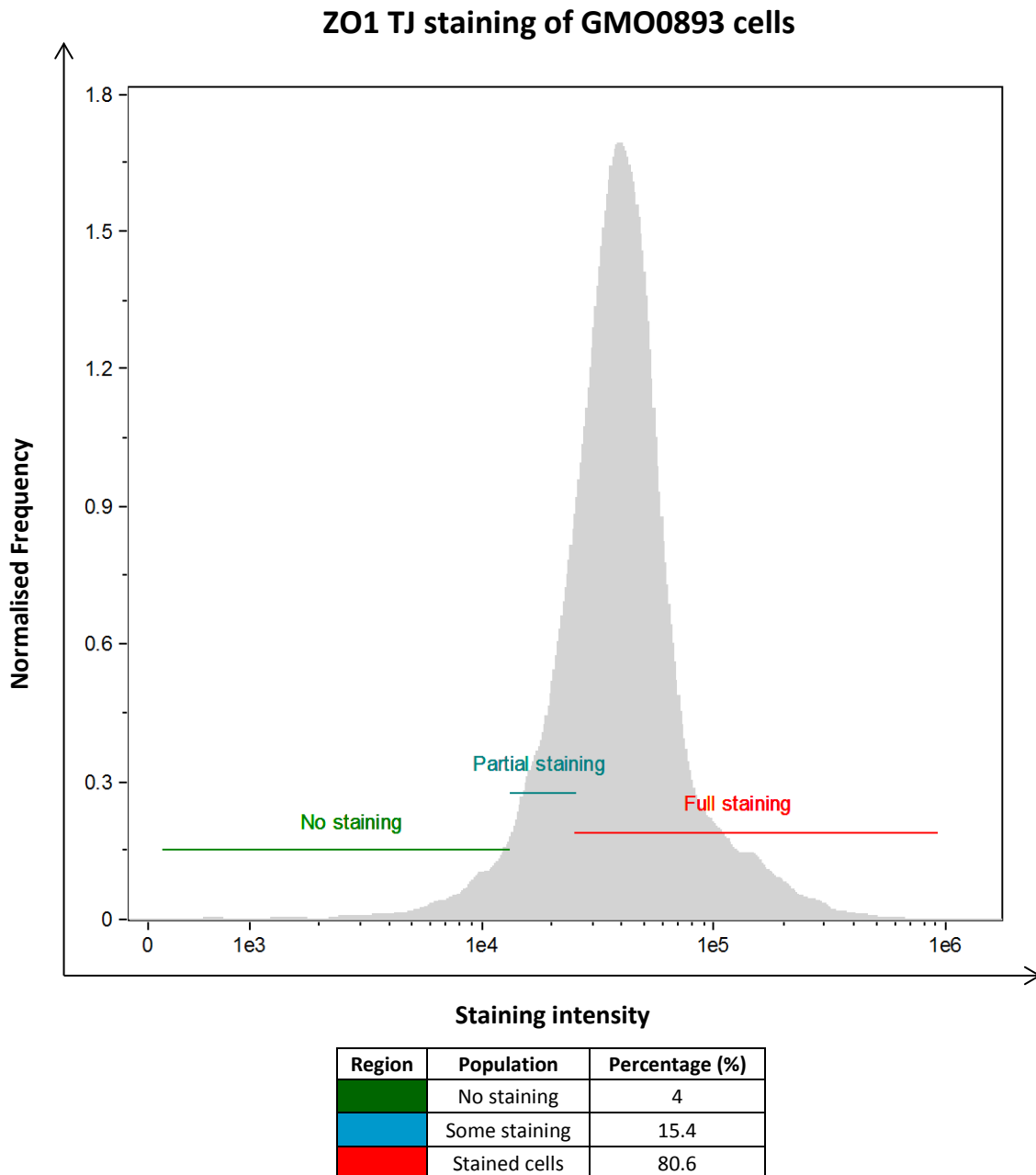


Samples shown in the figure above demonstrate different patterns of staining of GMO0893 cells with the ZO-1 TJ antibody. The first column, titled Ch01 shows brightfield images of cells captured at 40x. The second column shows ZO-1 TJ antibody staining in green colour on Ch02. DRAQ5 nuclear stain is displayed in red on the third column on Ch05. Panels-A and B are examples of ZO-1 TJ-negative cells, while panels D and E are GMO0893 cells that were stained with the antibody. Panel-C shows an example of a partially or weakly stained GMO0893 cell.

Images of different GMO0893 cells displayed in the figure above show a relatively poor morphology compared to prior experiments. It was expected that these cells would not stain with an epithelial marker such as ZO-1 TJ antibody, but this was true for only 4% of the GMO0893 cells in that sample. Panels-A and B show examples of GMO0893 cells that were ZO-1 TJ-negative. Cells that showed partial ZO-1 TJ staining (e.g. Panel-C) accounted for 15.4% of the cells in that sample. The vast majority of cells in that sample were ZO-1 TJ positive (80.6%), panels-D and E are perfect examples of these cells. Obtaining a high number of false positive cells is quite unusual, especially when

considering the fact that these cells do not possess TJ to allow them to be stained with this antibody. Some of the patterns of ZO-1 TJ staining in these cells were similar to those observed in PC3 cells. GMO0893 cells were arranged in order of their staining intensity with ZO-1 TJ and are shown in a histogram in Figure 5.6 below.

Figure 5.6: Distribution of GMO0893 cells based on their ZO-1 TJ staining intensity



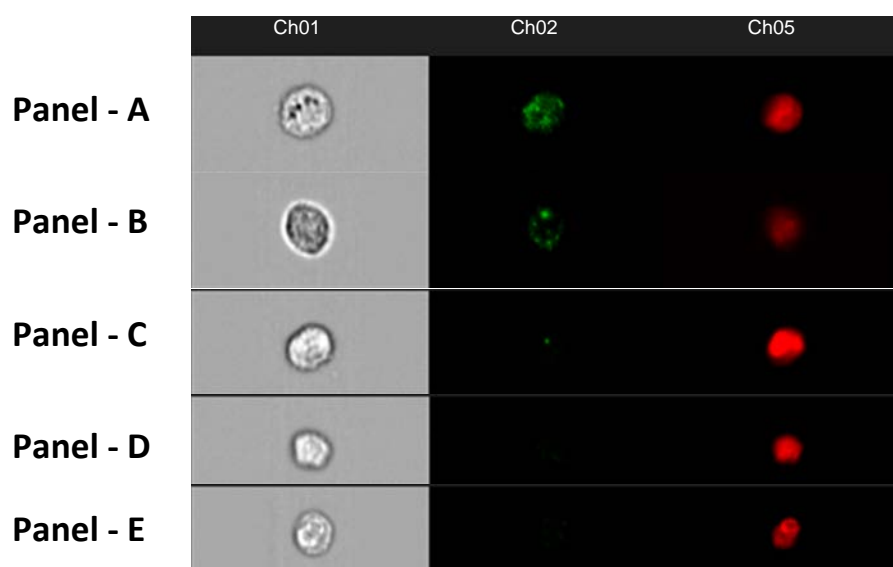
The figure above shows the distribution of GMO0893 cells based on the intensity of ZO-1 TJ antibody in these cells. Cells on the left (marked in green) were cells that showed no staining at all or a very minute ZO-1 TJ intensity that would otherwise be observed even without using any antibodies. The blue region in the middle represents cells with higher

intensity of ZO-1 TJ antibody, but not high enough to be classified as ZO-1 TJ-positive cells. Cells on the right (within the red region) were ZO-1 TJ-positive cells. The table below the graph shows exact percentages of the cells within each one of the three regions mentioned.

5.3.4 PBL staining with ZO-1 TJ antibody

Blood lymphocytes do not possess any TJ and are not expected to be stained with the ZO-1 TJ antibody. This experiment was conducted to confirm the level of ZO-1 TJ staining in PBL and compare it to that PC3 cells and GMO0893 cells. The results are shown by images in Figure 5.7 and the graph and table in Figure 5.8.

Figure 5.7: ZO-1 TJ staining of PBL cells

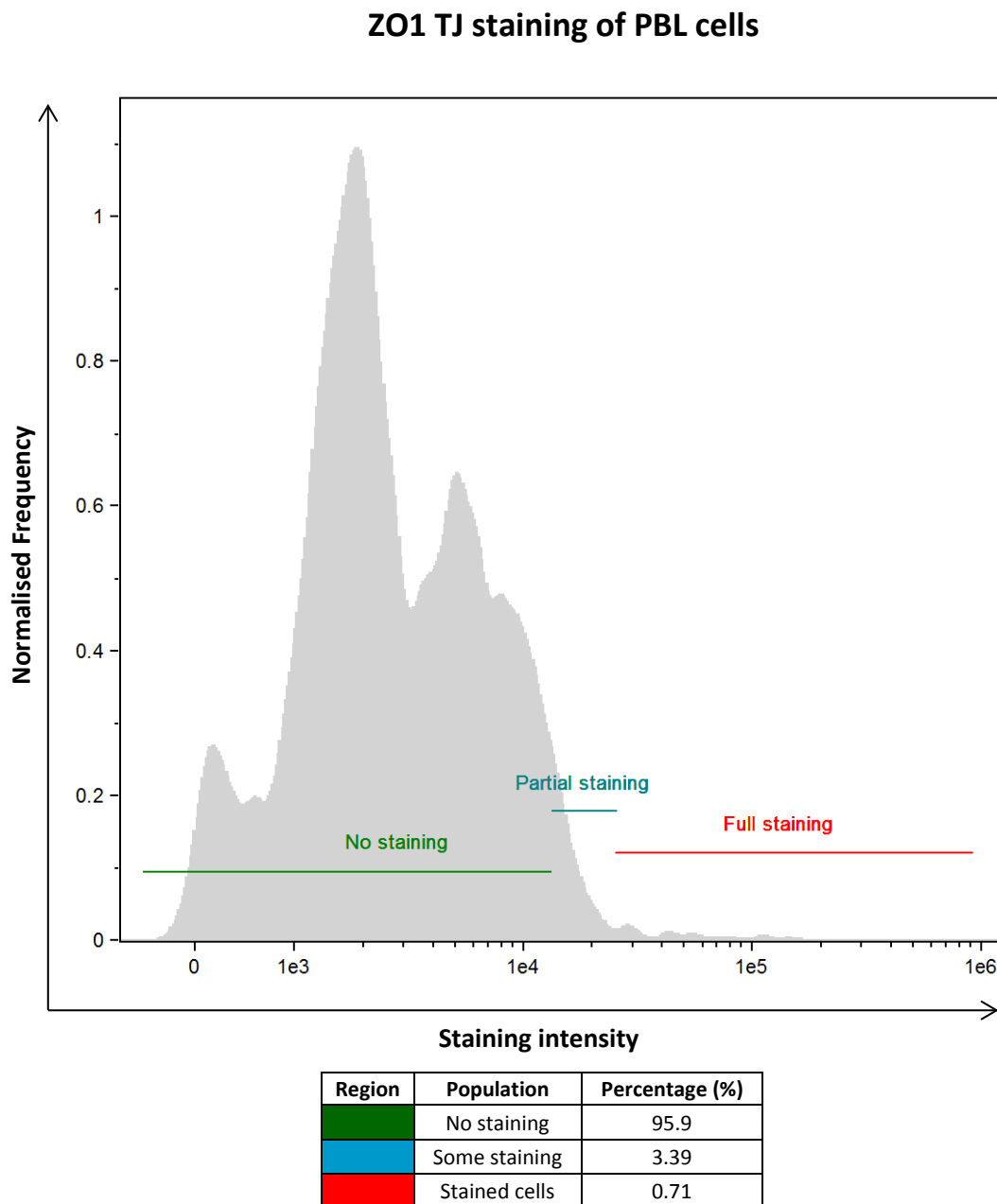


Examples shown in the figure above demonstrate different patterns of staining of PBL cells with the ZO-1 TJ antibody. The first column, titled Ch01 shows brightfield images of cells captured at 40x. The second column shows ZO-1 TJ antibody staining in green colour on Ch02. DRAQ5 nuclear stain is displayed in red on the third column in Ch05. Panel A and B are examples of ZO-1 TJ-positive cells, while panels D and E are ZO-1 TJ-negative cells. Panel C shows an example of a partially or weakly stained PBL cell.

PBL expressed lower level of ZO-1 TJ staining compared to that of PC3 cells and the false-positive GMO0893 cells. In fact, only 0.71% of the PBL cells in the sample were ZO-1 TJ-positive (e.g. Panel A and B). 3.39% of the cells showed very weak/partial staining (Panel - C) while the rest (95.9%) did not stain at all, such as cells in panels-D and E. It is also worth noting that the ZO-1 TJ positive cells were larger than the ZO-1 TJ-negative ones and displayed poorer morphology, which may explain the non-specific staining observed in these few cells. Overall, the morphology of most PBL was optimal and presented an improvement on what has been previously achieved with the GMO0893 cell-line. The

staining patterns that were observed in the positive cells had lower intensity than their GMO0893 counterparts. However, these staining patterns resembled some of the staining seen in the previous experiment where GMO0893 cells were used. The graph and table in Figure 5.8 below demonstrate the low number of false positive staining in PBL cells.

Figure 5.8: Distribution of PBL cells based on their ZO-1 TJ staining intensity



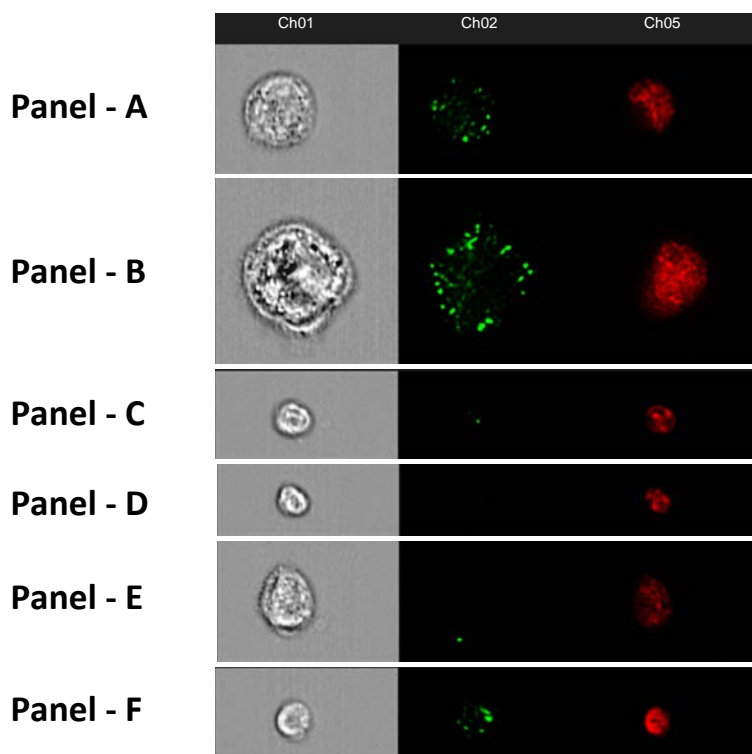
The figure above demonstrates the distribution of PBL based on the intensity of ZO-1 TJ antibody in these cells. Cells on the left (marked in green) were cells that showed no staining at all or a very minute ZO-1 TJ intensity that would otherwise be observed even without using any antibodies. The blue region in the middle represents cells with higher

intensity of ZO-1 TJ antibody, but not high enough to be classified as ZO-1 TJ-positive cells. Cells on the right (within the red region) were ZO-1 TJ-positive cells. The table below the graph shows exact percentages of the cells within each one of the three regions mentioned.

5.3.5 Mixing experiment using ZO-1 TJ antibody

Samples containing PBL cells were spiked with dilutions of PC3 cells as previously explained in the second chapter of this research. This was done to test the sensitivity of the ZO-1 TJ antibody in identifying PC3 cells found in a sample comprising of PBL cells. Figure 5.9 below shows examples of the cells found in that sample following careful observation.

Figure 5.9: ZO-1 TJ staining of PC3 and PBL cells



The figure above shows a gallery of images captured at 60 \times from a sample containing both PC3 and PBL cells. Ch01 column shows the brightfield images of cells captured, Ch02 column shows staining patterns with the ZO-1 TJ antibody in green, while the Ch05 column shows nuclear staining with the DRAQ5 antibody. Panels-A and B show examples of PC3 cells that were ZO-1 TJ-positive, while Panels-C and D shows examples of PBL cells that were ZO-1 TJ-negative. Panel-E shows an example of PC3 cells that was ZO-1-TJ-negative (false negative) and Panel-F demonstrates an example of a PBL cell that was ZO-1 TJ-positive (false positive).

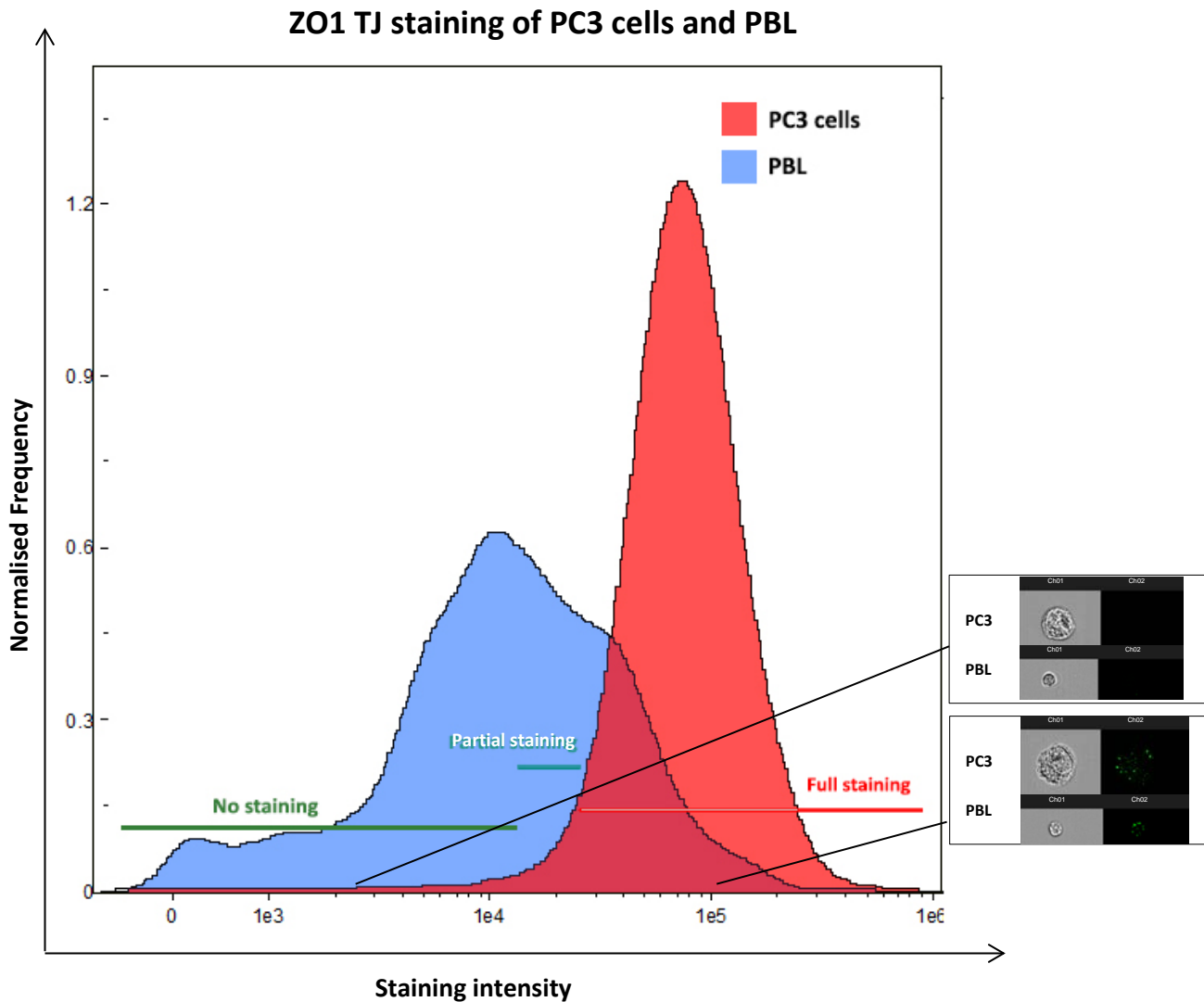
The PC3 cells showed similar forms of staining to the ones observed previously when ZO-1 TJ antibody was used. The displacement of TJ was present and clear around the cells, mostly near the membrane of these cells. The vast majority of PC3 cells were ZO-1 TJ-positive, accounting for 96.12%. A small percentage of PC3 cells was partially stained (2.36%) while only 1.52% of the PC3

population was not stained at all. In comparison, the majority of PBL were ZO-1 TJ negative (53.25%), but this was a vastly lower percentage than the one previously obtained from a sample containing PBL cells only. 20.45% of the PBL population showed partial staining, while 26.3% of the PBLs were fully stained with the epithelial marker.

This abnormal change in the percentage of ZO-1 TJ positive PBL cells when spiked with PC3s is perhaps attributed to the effect of PC3 cells spiked, as these cells possess dissolved TJ complexes within them and within the PBS solution in which they resided. The existence of dissolved TJ molecules in samples containing PC3 and PBL cells might be the main reason for obtaining this high false-positive percentage of PBL cells. PC3 cells on the other hand maintained a very low percentage of false-negative cells. However, the large overlapping region caused by the high number of false-positive PBL cells made it difficult to distinguish between the two cell-lines based on ZO-1 TJ staining. This staining overlap is demonstrated in the Figure 5.10 on the next page.

Additionally, Table 5.2 shows PC3 retention numbers for each of the samples in which PC3 cells were spiked. The table demonstrates the sensitivity of using ZO-1 TJ antibody staining in identifying and isolating PC3 cells spiked in sample containing PBL cells.

Figure 5.10: Distribution of PC3 and PBL cells based on ZO1 TJ staining intensity



PC3 cells			PBL cells		
Region	Population	Percentage (%)	Region	Population	Percentage (%)
No staining	1.52	1.52	No staining	53.25	53.25
Partial staining	2.36	2.36	Partial staining	20.45	20.45
Full staining	96.12	96.12	Full staining	26.3	26.3

The figure above shows the distribution of PC3 and PBL cells within from the same sample. The X axis shows the intensity of the ZO1 TJ antibody staining, while the Y axis represents the normalised frequency for both cell-lines. Different staining intensities are categorised on three different sections and the overlapping region between the two cell lines – where intensity of staining was parallel – is highlighted in a dark red colour between the two populations of cells. The table below the graph shows exact percentages for cells that were fully stained (red section), partially stained (blue section) and ones that did not stain (green section) for both cell lines.

Table 5.2: Retrieval numbers of ZO-1 TJ positive cells

Total cells spiked in to 1mL	Approximate retrieval Tight Junctions stained cells
3,000,000	20.68% (620,503)
300,000	3.4% (10,202)
30,000	4.22% (1267)
3000	11.9% (357)
300	13% (39)
30	66.67% (20)

The table above shows the numbers of PC3 cells counted and spiked in each of the test tubes and the number of PC3 cells retrieved following examination with the ImageStream^x. The percentage of PC3 cells acquired fluctuated from one dilution to another, but the number of cells was in constant decline. These numbers do not represent the actual number of PC3 cells retained but the number of cells that lie within the PC3 region on the scatterplot based on their ZO-1 TJ antibody intensity. Upon careful examination of some of these cells, it was found that some PBL cells were identified amongst these cells and attributed to the PC3 population. Other PC3 cells were simply burst cells that were identified as viable and ZO-1 TJ-positive PC3 cells.

5.4 Discussion

The ZO-1 TJ antibody staining was chosen as a final immunological method to be tested in identifying PC3 cells. With the failure of EpCAM and CD45 antibodies in establishing an accurate PC3 identification method, the use of the ZO-1 TJ antibody was then considered to enhance PC3 detection specificity and sensitivity using the ImageStream^x.

Following a similar antibody optimisation protocols that were previously applied to the first two antibodies used, it was decided that a 1/500 dilution of the ZO-1 TJ antibody would sufficiently stain most the PC3 cells in the sample. Table 5.1 demonstrated how the sample stained with a 1/500 dilution of the ZO-1 TJ antibody provided almost 95% ZO-1 TJ positive PC3 cells, compared to only 81.4% in the sample where a 1/50 dilution of the antibody was used. It was apparent from early experiments that the existence of TJ within PC3 cells rather than on the membrane might have been due to the effect of Trypsin-EDTA used to dissociate PC3 cells from the flasks.

The experiments that followed in this research focused on staining each cell-line individually with the antibody before spiking PC3 cells in samples containing PBL cells in what would be a reconstruction of the proof of principle experiment. Most of the PC3 cells – much like when the antibody dilution was optimised – were ZO-1 TJ-positive. In fact, only 2.3% of these cells did not show any ZO-1 TJ antibody staining. The GMO0893 cells on the other hand were characterised with a relatively poor morphology and the vast majority of them (80.6%) were found to be ZO-1 TJ-positive. In contrast, there was only a small percentage (0.71%) of ZO-1 TJ-positive cells when PBL cells were stained with the antibody. The results of these experiments meant, in theory at least, that mixing PC3 cells with PBL might be the most sensitive immunological tool obtained in this research in discriminating PC3 cells from PBLs.

The mixing experiment delivered unforeseen results to what was originally anticipated, with approximately 26.3% of the PBL cells being ZO-1 TJ-positive. There was also a small population

(1.52%) of the PC3 cells that were observed to be false negative. The overlap between PC3 cells and PBL (as shown in Figure 5.9) meant that, just like its predecessors, the ZO-1 TJ antibody might not be the ideal tool to isolate PC3 cells using imaging flow cytometry.

The morphology of the cells was perceived to be an improvement on what was previously obtained when the CD45 antibody was used. Although, few exceptions in which cells looked overly enlarged/expanded and had completely lost their structural integrity were also evident. The existence of TJ within cells could be due to the effect caused by Trypsin-EDTA which was used to dissociate PC3 cells from their flasks. Trypsin-EDTA helps in dislodging cells by dissolving the cell-to-cell adhesion molecules, such as TJ, however, the presence of positively stained areas within PBL cells may be due to an increased permeabilisation of these cells.

Perhaps a better approach would be to avoid using Trypsin-EDTA in the sample preparation protocol; however, this may prove difficult as cultured PC3 cells must first be dissociated from their flasks before being used. To overcome this problem, blood samples from cancer patients containing CTCs may need to be considered, as these cells would have their membrane and its CAM molecules intact and possibly undamaged.

Table 5.2 showed the PC3 cell retention numbers for the mixing experiment. The percentage of PC3 cell retained was remarkable, especially for the most diluted sample, in which only 30 PC3 cells were spiked. 20 of the cells were identified to be ZO-1 TJ-positive; however, upon close examination of these cells, it became very apparent that many of them were simply damaged cells or large debris that were identified as PC3 cells due to their high staining intensity. This flaw, as well as the existence of false positive and negative cells when PC3 cells were mixed with PBL, meant that the use of ZO-1 TJ antibody might not be an ideal approach in detecting and isolating PC3 cells in imaging flow cytometry.

Chapter 6

Live Cell Analysis for the Identification of PC3 cells

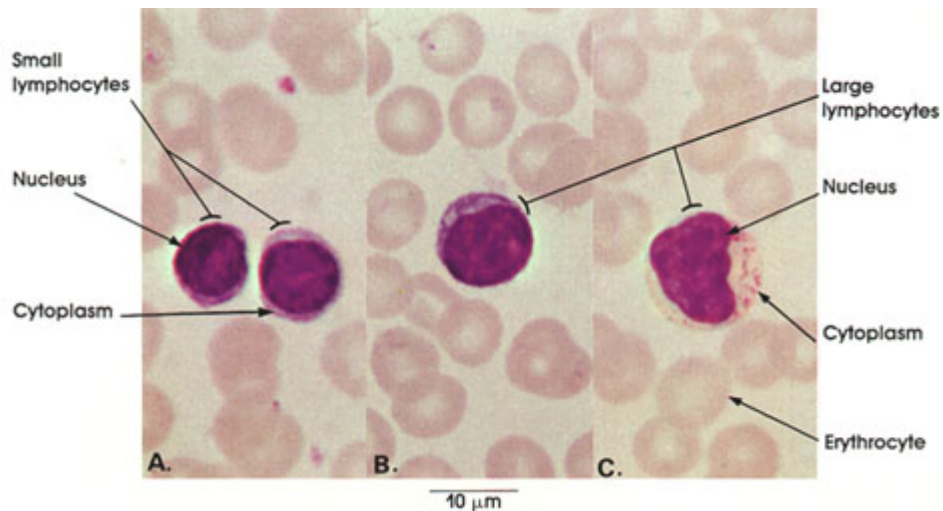
6. Live Cell Analysis for the Identification of PC3 cells

6.2 Introduction

It has long been known that the number of cells is what makes an individual smaller or larger than another rather than the size of the cells within that individual (Wilson, 1925, Conlon and Raff, 1999). Cell size is relatively constant throughout the life cycle of the individual and they differ from one type of cells to another (Ginzberg et al., 2015). The mechanisms involved in determining a specific cell size remain ambiguous (Lloyd, 2013); however, the consistency at which types of cells fall within specific cell size ranges has made it a potential area to exploit differences between different cells for identification purposes.

The focus in this research was revolved around prostate cancer epithelial cells and how they differ from lymphocytes and other blood cells. Peripheral blood consists of RBC, WBC and platelets (Mohammadi et al., 2014). Lymphocytes are the second most common WBC, making up around 20-50% of the total number of WBC in humans (Peckham, 2003). In a normal adult, the average number of lymphocytes fluctuates between 5000 and 9000 cell per mm^3 of blood. However, these numbers may be higher or lower than that range when influenced by diseases (Bergman et al., 2016). Most lymphocytes are small in size, and are only slightly larger than red blood cells with a diameter length of approximately 6-9 μm . The rest (accounting for 10% of the total number of lymphocytes in the blood) are larger in size and range between 10-14 μm in diameter (Bergman et al., 2016, Peckham, 2003).

Figure 6.1: Variation in lymphocytes cell size



Examples of two types of lymphocyte cells are shown in the figure above. The two cells shown in (A) represent small lymphocytes (6-9 μm) and are the majority of lymphocytes in the body. The other two cells (B and C) are large lymphocytes (10-14 μm) and form around 10% of the entire lymphocyte population. Both sets of cells possess the same morphological structure comprising of a nucleus and cytoplasm (Bergman et al., 2016).

The other cells investigated in this research were prostate cancer cells and even though the origin of these cells was thought to be from prostate epithelial basal cells only (Goldstein et al., 2010), recent work by Park *et al* confirmed that prostate cancer can originate from both, the primary human basal and the luminal epithelial cells (Park et al., 2016). Prostate epithelial cells are classified as epithelial cells which are larger than lymphocytes and, once cancerous, the size of these cells is prone to change. The reason behind this change is attributed to a number of factors, such as various gene mutations. For example, mutations that occur in the PTEN gene, which is a tumour suppressor gene that negatively regulates cell survival and its mutation is associated with poor prognosis for prostate cancer patients (Deocampo et al., 2003), lead to variation in cell size based on the expression levels of this gene in cells (Backman et al., 2002).

Cell size alterations were observed *in vitro* in my research and were mostly noticed in previous experiments when cells were prepared in varying approaches during method optimisation. There has also been *in vivo* evidence to suggest that external signals might have an effect on the size of cells. A perfect example of this was explained by Edgar *et al* when they examined the effects of low

nutrient levels during the development of flies and how it leads to 15% reduction in their size compared to normal flies (Edgar, 2006). Upon reaching maturation, cells were found to reach a state of growth balance, possibly resulting from having a defined growth pathway signalling. This balanced state results in a no net change in the cell volume or mass (Koivusalo et al., 2009).

In line with what has been observed in my research about morphological changes in the cell-lines used, it is worth mentioning that in studies that have examined the use prostate cancer cells or cell-lines, there have been reports of “dramatic” changes to the size and shape of these cells. Such changes might be brought about as a result of treating these cells with Trypsin or other sample processing reagents such as those used in CellSearch® system (Park et al., 2014). In fact, one major concern identified by Park *et al* was how the CellSearch® sample preparation protocol leads to cell shrinkage, resulting in smaller, elongated cells.

Other approaches that observed morphological properties of cells relied on the use convenient microscopy. Cross-sectional microscopy images might be of higher clarity than flow cytometry but there are few challenges that present bias into the way cell sizes are estimated in this way. For example, larger cells examined with microscopy have a higher chance of being caught by the slice than those of smaller size. Additionally, it was found that the radius of a cross-sectional cell is smaller than that of the actual cell radius where the centre of the cell investigated is not at the centre of the slide (Lenz et al., 2016).

In this research, another approach which was considered was to distinguish cell-lines based on their physical and morphological properties. Therefore, the morphology of live PC3, GMO0893 and PBL cells were examined using imaging flow cytometry. Morphological aspects such as cell area and aspect ratio were considered in the analysis of samples from both cell-lines. The accuracy of results obtained in this study was compared to that where immunological methods (such as EpCAM and CD45 staining) were used to discriminate different cell types (PC3, GMO0893 and PBL cells).

6.3 Aim

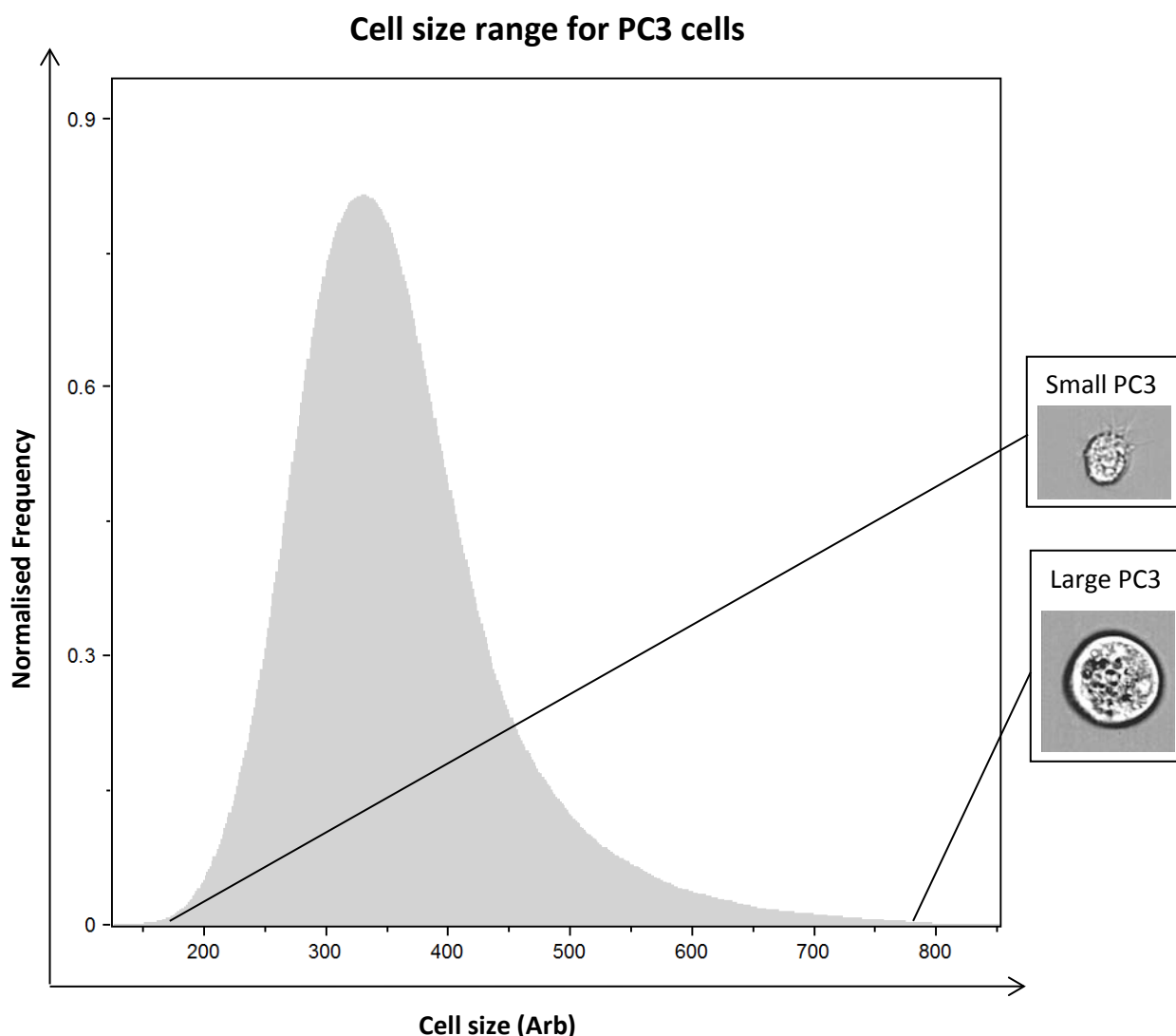
- To establish a cell size range for PC3, GMO0893 and PBL cells
- To identify PC3 cells and distinguish them from GMO0893 cells and PBL based on the morphological and physical properties of these cells
- To determine the efficacy live cell analysis in identifying PC3 cells spiked in samples containing PBL cells
- To compare the sensitivity of cell size analysis with the previously tested immunological approaches
- To observe and compare the morphology and cell structure of PC3, GMO0893 and PBL cells and compare it with that of immunological methods
- To determine the sensitivity of live cell analysis and compare it with previous methods used
- To compare the cells retention between the live cell analysis method and the three immunocytochemical approaches previously explored.

6.4 Results

6.4.1 PC3 cell size range

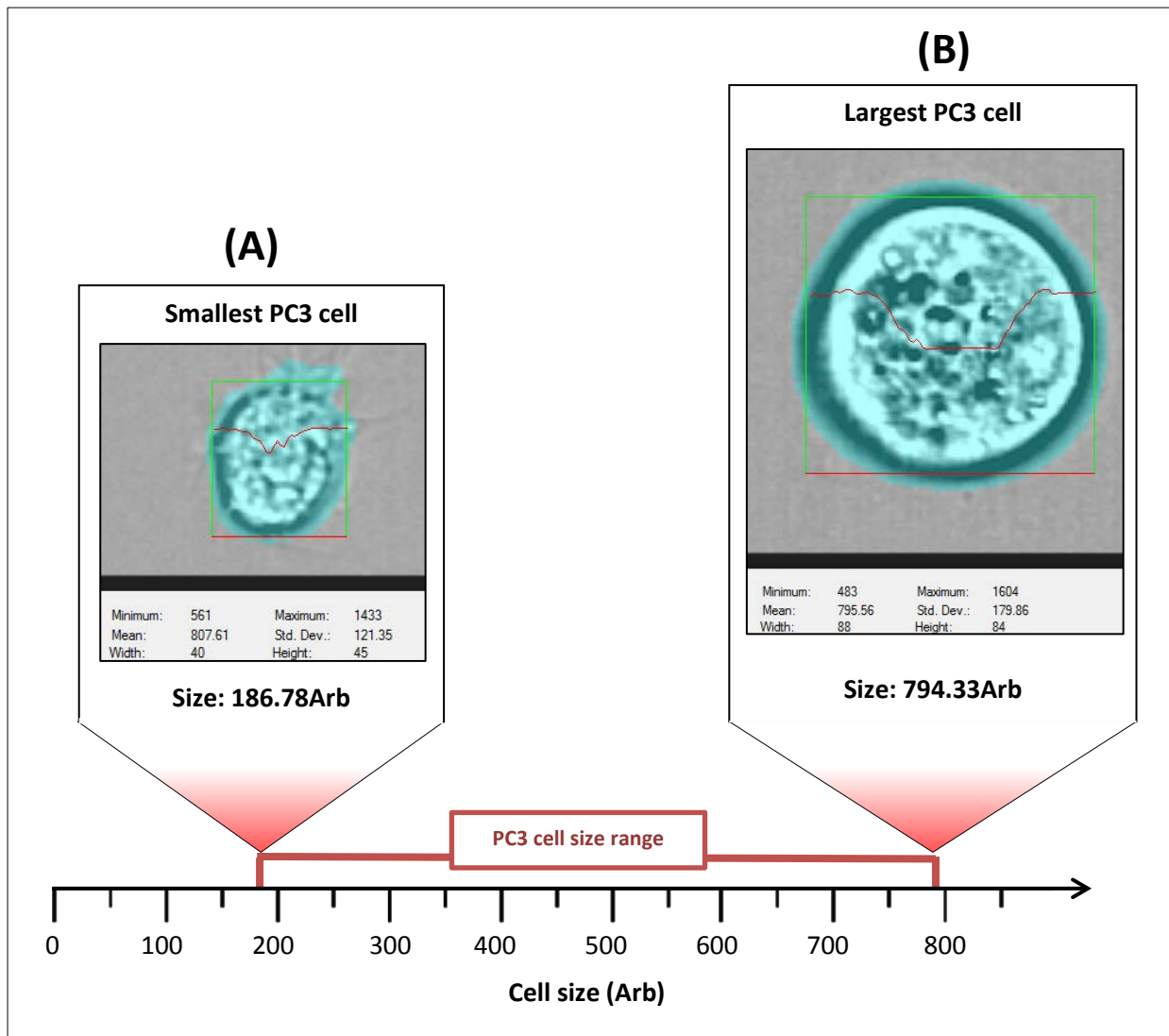
PC3 cells were trypsinised with Trypsin-EDTA and washed with PBS. They were then resuspended in Accumax and stained with DRAQ5 antibody prior to examination with the ImageStream^x. The distribution of PC3 cells based on their cell size is demonstrated in Figure 6.2 below.

Figure 6.2: Distribution of PC3 cells based on their cell size



The figure above shows the difference in size between PC3 cells captured using the ImageStream^x. Cell size is represented in arbitrary units (Arb) on the X-axis, while the Y-axis represents normalised frequency. Examples of small and large PC3 cells are shown through brightfield images of cells captured at both ends of the graph, demonstrating that within the same PC3 sample, cells may considerably vary in size. Most PC3 cells, however, appear to be within the size range of 250-550Arb. Images shown in this figure are captured at 60 \times plus EDF image acquisition.

Figure 6.3: The average cell size range for PC3 cells



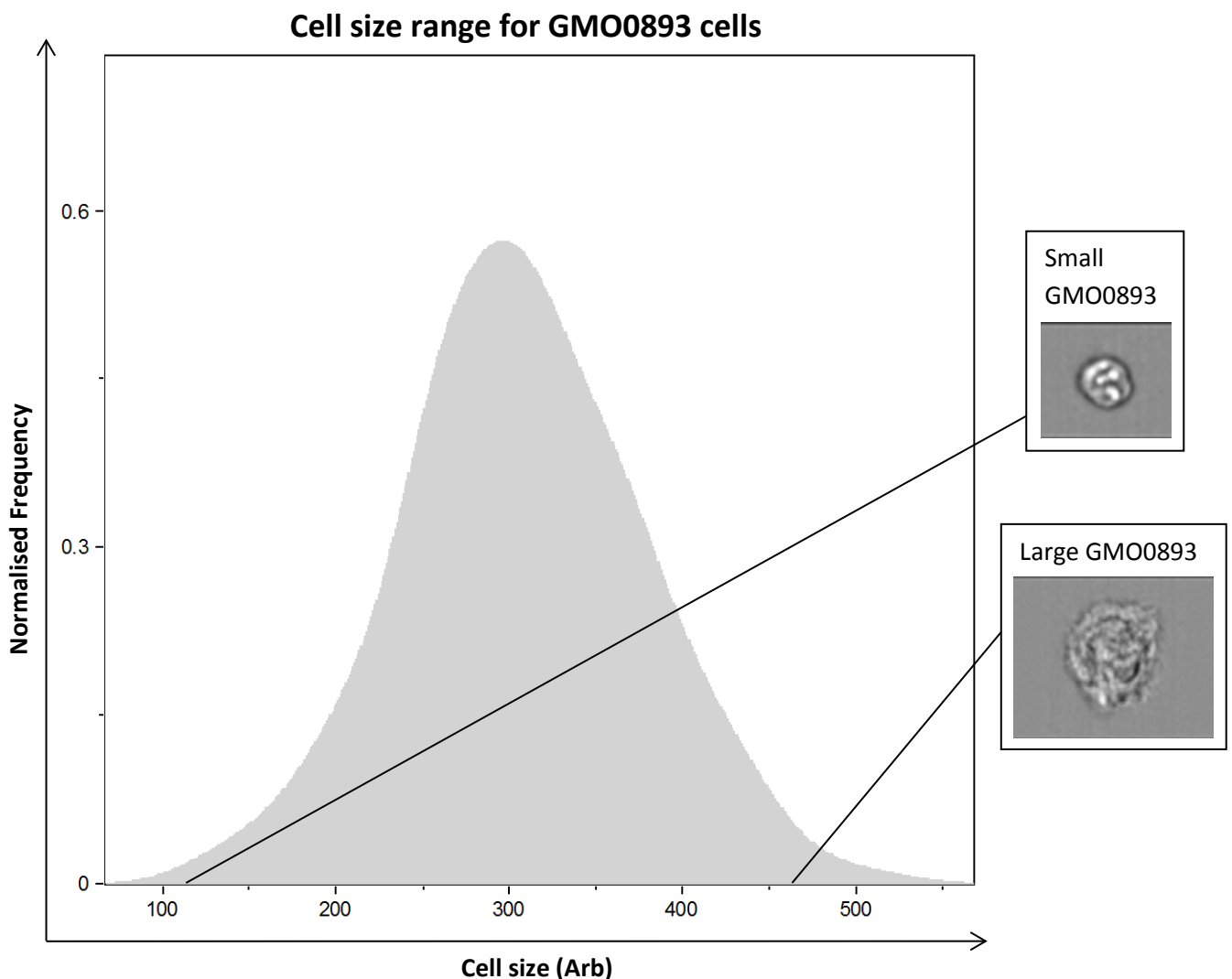
The figure above shows the average cell size scale and outlines the region of it where PC3 cells are located. The PC3 cell size range is coloured red and expands from 186.78Arb to 794.33Arb. Cell A is the smallest cell detected, whereas cell B is the largest PC3 cell observed in these samples. Detailed analysis and structure figures are given below each cell. Both brightfield images are highlighted with a blue mask as the software measured variable statistics for both cells and calculated their size. Images shown in this figure are captured at 60× plus EDF image acquisition.

Careful analysis and observation of the captured PC3 cells outlined an accurate range for this cell-line. Cells that had a relatively poor morphology as well as clusters of cells were rejected and not included in the final cell area measurement. Overall, the morphology of cells collected in this study was far superior to that of the immunostaining approaches previously used. The cell count and sample processing time were also faster than immunostaining methods.

6.4.2 GMO0893 cell size range

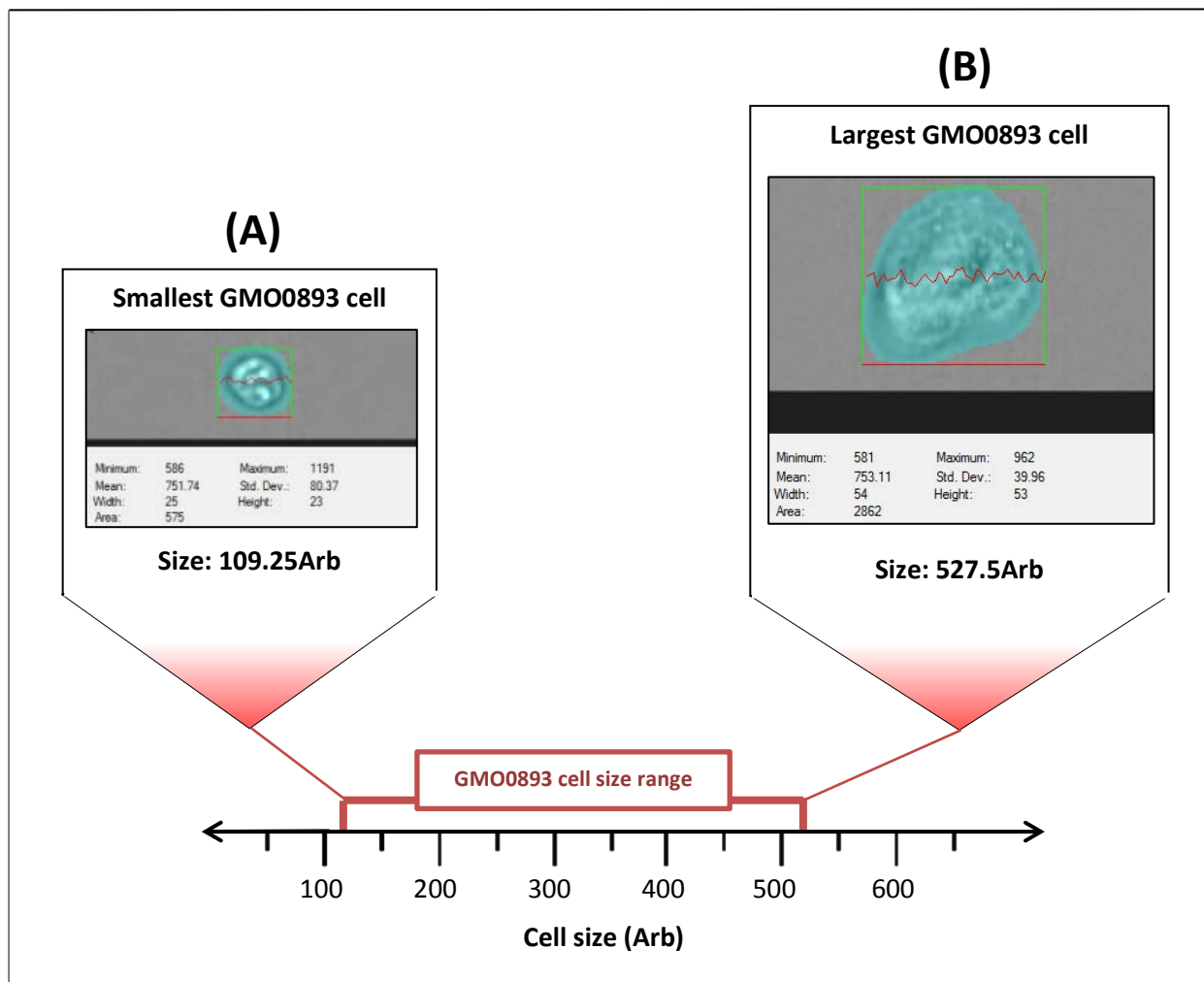
The GMO0893 cell-line has been associated with a dubious morphology that was more undistinguishable than the other two cell-lines, even before this study was conducted. Therefore, this the perfect test to verify whether the inadequate morphology of these cells was caused by the prolonged procedure of staining them or was due to the cell-line itself. Figure 6.4 below, shows the range of cells captured and examples of small and large GMO0893 cells.

Figure 6.4: Distribution of GMO0893 cells based on their cell size



The figure above shows the difference in size between GMO0893 cells captured using the ImageStream^x. Cell size is represented in arbitrary units (Arb) on the X-axis, while the Y-axis represents normalised frequency. Examples of small and large GMO0893 cells are shown through brightfield images of cells captured of cells at both ends of the graph, demonstrating that within the same GMO0893 sample, cells vary significantly in size. Most GMO0893 cells, however, appear to be within the size range of 200-400Arb. Images shown in this figure are captured at 60x plus EDF image acquisition.

Figure 6.5: The average cell size range for GMO0893 cells



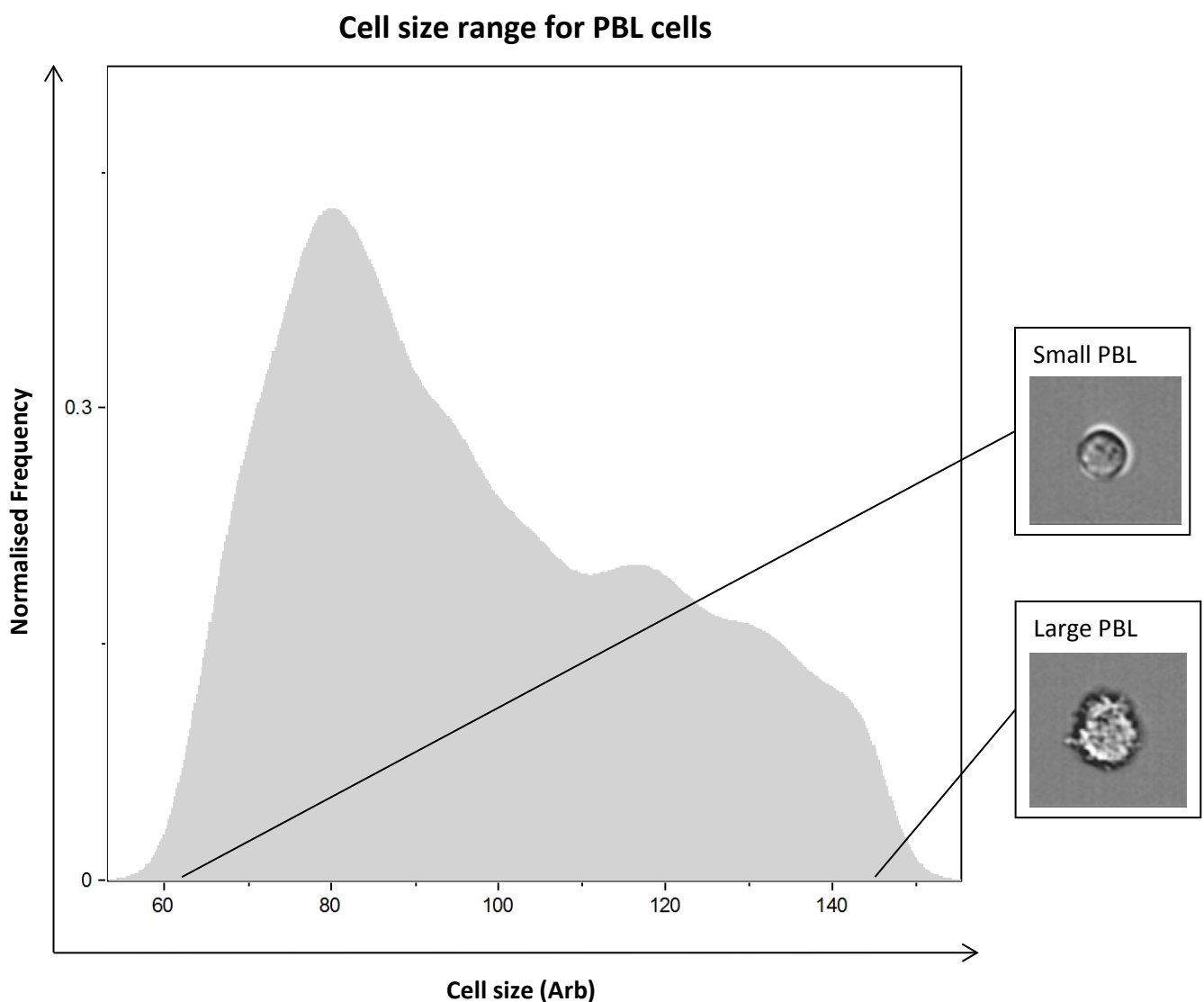
The figure above shows the cell size scale and outlines the region of it where GMO0893 cells are located. The GMO0893 cell size range is coloured red and expands from 109.25Arb to 527.5Arb. Cell A is the smallest cell detected in all samples containing GMO0893 cells that were tested. Whereas cell B is the largest GMO0893 cell observed. Detailed analysis and structure figures are given below both cells. Both brightfield images are highlighted with a blue mask as the software measured variable statistics for each cell and calculated their size. Images shown in this figure are captured at 60x plus EDF image acquisition.

The range recorded for the GMO0893 cell-line varied greatly and exceeded what was originally hypothesised. Most cells seem to have enlarged and it is unclear whether this resulted from the centrifugation process or the cell resuspension steps. Moreover, the size range of GMO0893 cells overlaps greatly with that of PC3 cells, rendering the cell-line useless for size and morphology comparison. This observation of GMO0893 cells' poor morphology was also evident in repeat experiments, indicating that previous immunostaining results obtained with this cell-line might not be credible.

6.4.3 PBL cell size range

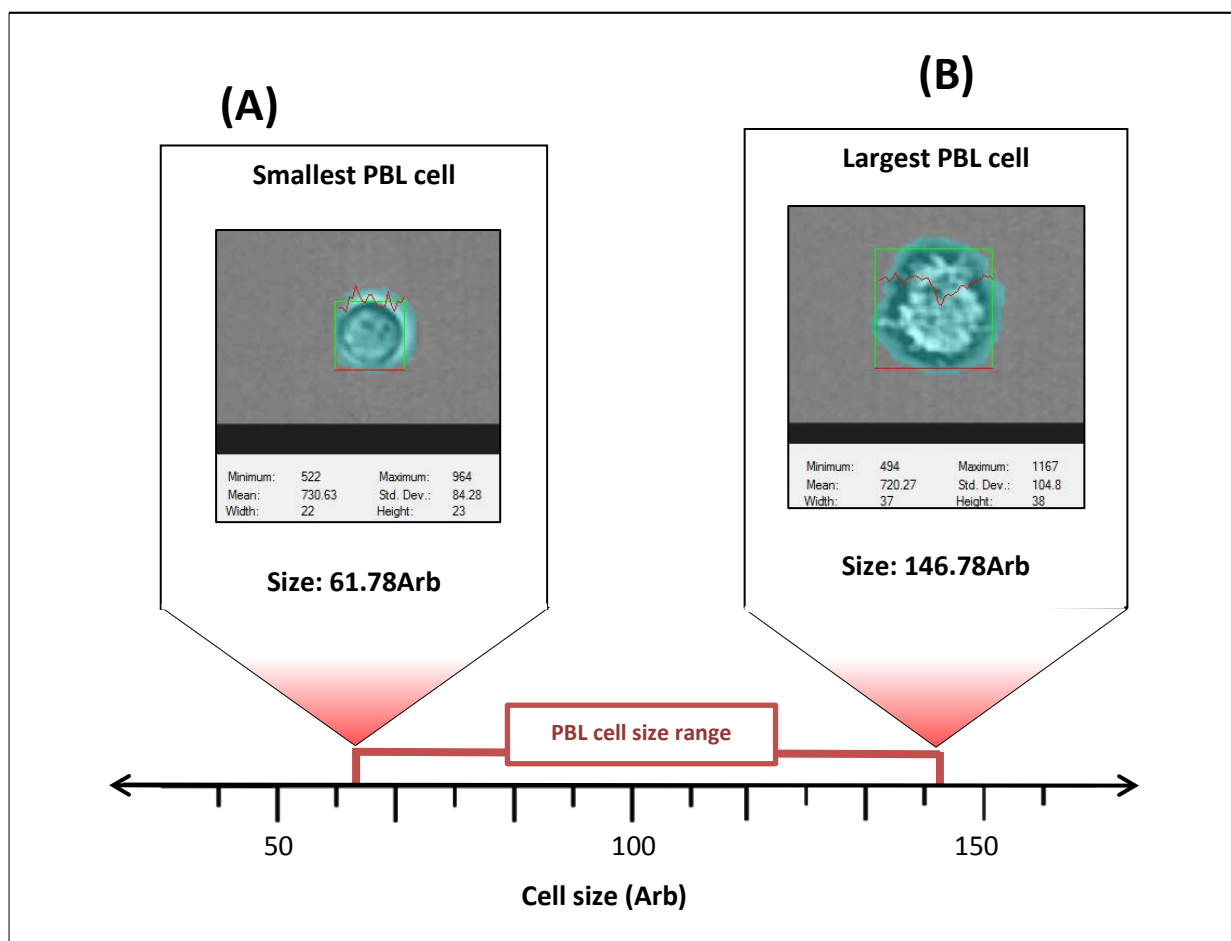
As the GMO0893 cell-line maintained a size range that greatly overlapped with that of the PC3 cell-line, the use of PBL for morphological comparison became essential. In previous experiments, PBL have maintained an optimal shape and structure throughout varying immunological tests. Samples containing millions of PBL cells were observed with the ImageStream^x and Figure 6.6 below shows the distribution of these cells based on their size.

Figure 6.6: Distribution of PBL cells based on their cell size



The figure above shows the difference in size between PBL cells captured using the ImageStream^x. Cell size is represented in arbitrary units (Arb) on the X-axis, while the Y-axis represents normalised frequency. Examples of small and large PBL cells are shown through brightfield images of cells captured at both ends of the graph, demonstrating that within the same PBL sample, cells may vary in size, but only slightly. Most PBL cells appeared to be within the size range of 70-130Arb. Images shown in this figure are captured at 60× plus EDF image acquisition.

Figure 6.7: The average cell size range for PBL cells



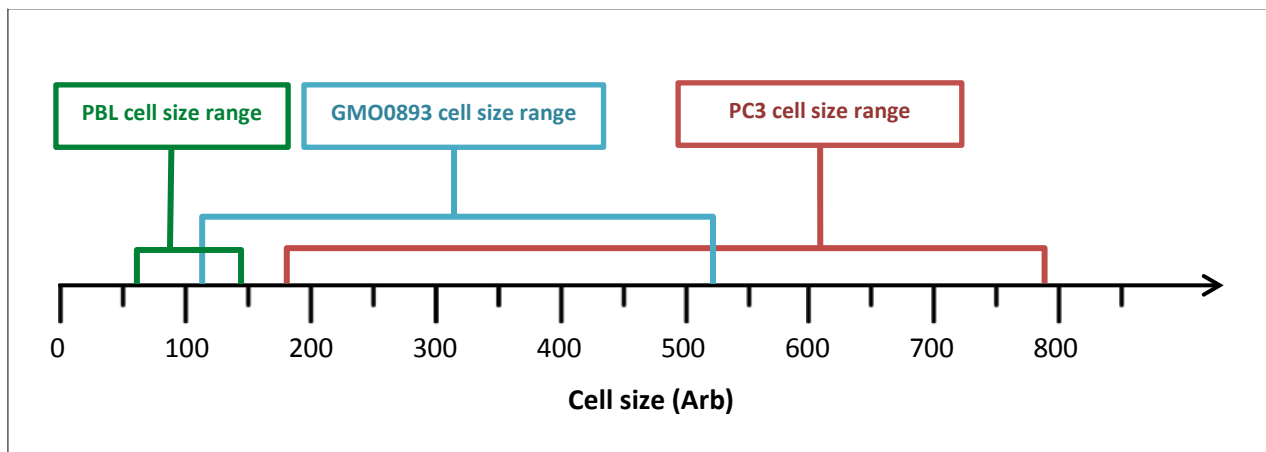
The figure above shows the cell size scale and outlines the region of it where PBL cells are located. The PBL cell size range is coloured red and expands from 61.78Arb to 146.78Arb. Cell A is the smallest cell detected in all samples containing PBL cells that were tested. Whereas cell B is the largest PBL cell observed. Detailed analysis and structure figures are given below both cells. Both brightfield images are highlighted with a blue mask as the software measured variable statistics for each cell and calculated their size. Images shown in this figure are captured at 60x plus EDF image acquisition.

Unlike the GMO0893 cell-line, the size range of PBL cells was not overlapping with that of the PC3 cells. In fact, the largest PBL captured was approximately 40Arb smaller than the smallest PC3 cell. The overall morphology and cell structure of PBL was exceptional, excluding few cells that were also larger than average PBL size, such as cell B in Figure 6.7 above. The consistency of PBL cells in maintaining a preserved structure meant that they were the ideal choice to be used in combination with PC3 cells to test the sensitivity of this approach.

6.4.4 Mixing experiment using cell size comparison

As mentioned in the previous cell size range tests, PC3 cells were used in combination with PBL cells to conduct the sensitivity test. Opting against using the GMO0893 cell-line in this experiment was due to the abnormally large cells obtained when it was previously used. The size range provided by the GMO0893 cell-line overlaps greatly with that of the PC3, making it difficult to distinguish between them. Figure 6.8 below demonstrate the problem with using the GMO0893 cell-line in the identification of PC3 cells based on cellular size. The advantage of using PBL cells must also be noted in that their consistency in maintaining a relatively small size makes them a perfect tool to test the sensitivity of this approach.

Figure 6.8: Comparison between PC3, GMO0893 and PBL cell size ranges



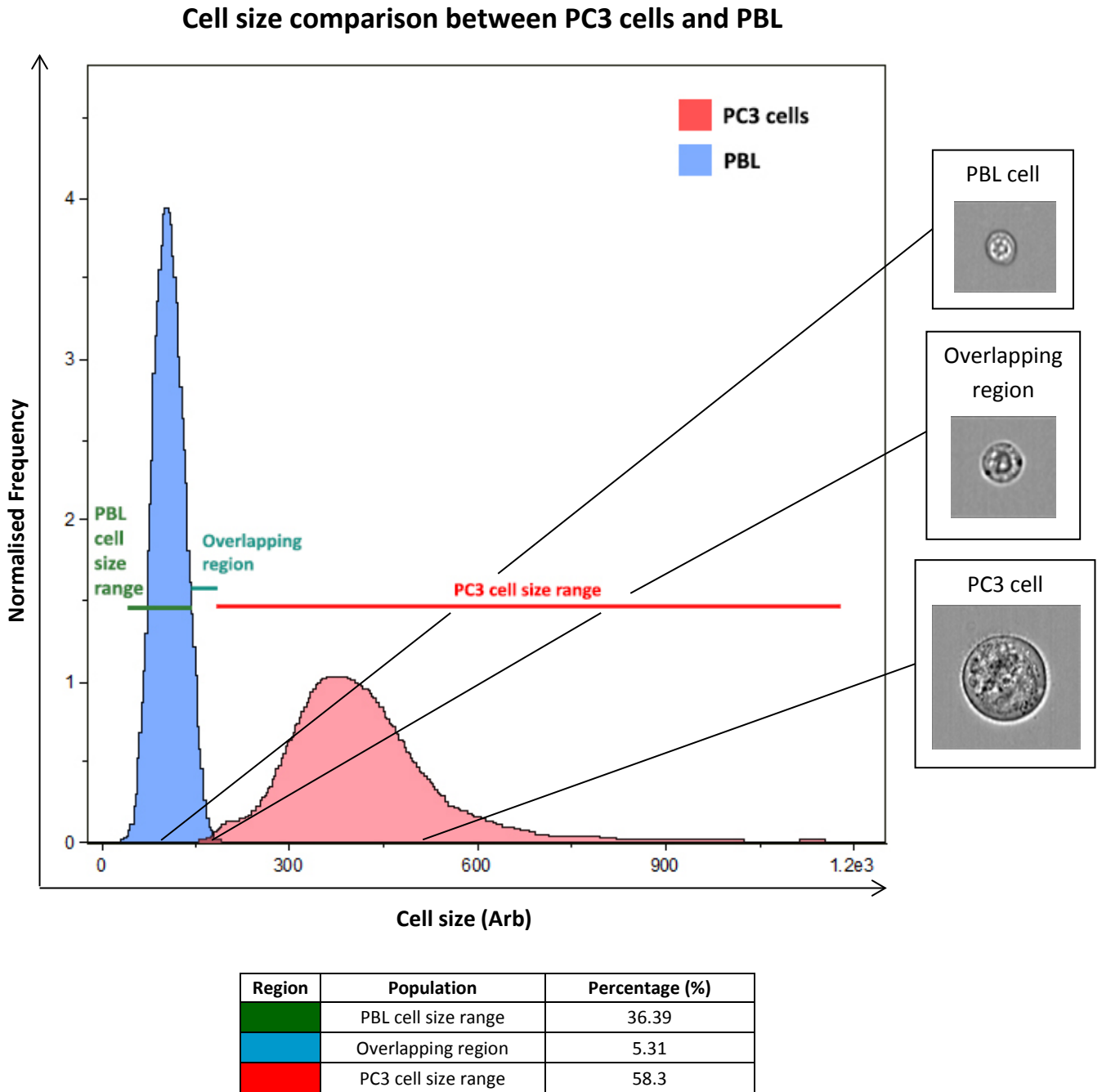
The figure above shows the cell size scale used in this study and demonstrates the difference between PC3, GMO0893 and PBL cells in terms of cell size. The PC3 cell size range is in red and can be seen not to overlap with that of the PBL (green). At the same time, a relatively large overlapping region occurs between the PC3 cell size range and the GMO0893 cell size range, expanding from 186.78Arb to 527.5Arb.

This test is similar to the ones that used immunological markers such as EpCAM and CD45 in that PC3 cells were spiked in dilutions with a large number of PBLs. The difference, however, is the absence of staining comparison. Instead, distinguishing the two cell-lines will be achieved based on their size and morphological features.

When observed within the same sample, PC3 and PBL cells were positioned separately, with the exception of a very minute number of cells that were located in an overlapping region on the graph (Figure 6.9). The reason behind obtaining cells (from both cell-lines) within that region remains unclear; however, individual examination of each one of these cells proved useful in identifying PC3 cells based on cellular morphology, such as nuclear localisation. Throughout numerous experiments, PC3 cells were characterised with having a clear, distinct cell structure and morphology. The DRAQ5 nuclear staining of PC3 cell nuclei also helped in the identification of nuclear localisation within these cells. Whereas PBL cells were commonly observed stained with DRAQ5 covering most of the cell.

Interestingly, the structure and morphology of both cell-lines remained as intact as when they were tested separately. Spiking PBL samples with PC3 cells did not seem to cause a major change in the physiological/structural appearance of either cell-line. This may be an indication that cells with a poor morphology captured in immunological experiments might have been obtained such properties as a result of the extensive sample preparation steps. Using the live cell analysis and the exclusion of cell fixation, blocking and the multiple staining and washing steps meant that both cell-lines were likely to retain optimal cell morphology and structure.

Figure 6.9: Distribution of PC3 and PBL cells based on their cell size



The figure above shows the distribution of PC3 and PBL cells from the same sample. The original number of cells within that test tube was 3×10^6 for each of the two cell-lines. The X axis represents the cell size (Arb), while the Y axis represents the normalised frequency for both cell-lines. Different cell size ranges are categorised on three different sections with the small overlapping region between the two cell-lines highlighted in a dark red colour. On the right side of the graph, brightfield images are shown as examples of cells that would be found within each region. The table below the graph shows exact percentages for cells, categorised based on their cell size. Images shown in this figure are captured at 60x plus EDF image acquisition.

The retention percentages of PC3 cells were fluctuating between different samples; however, samples with very low numbers of PC3 cells were showing higher retention percentages than samples with high PC3 numbers. Generally, live PC3 retention numbers were noticeably higher than immunological methods.

Table 6.1. Approximate retrieval numbers of live PC3 cells

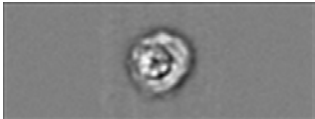
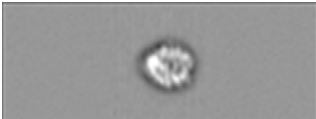
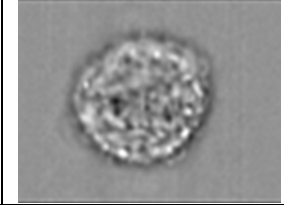
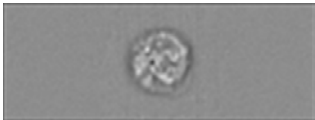
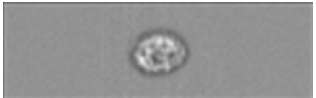
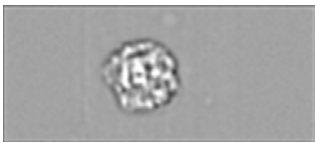
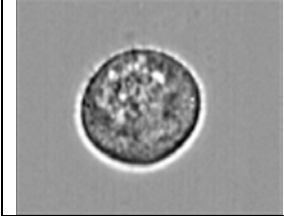
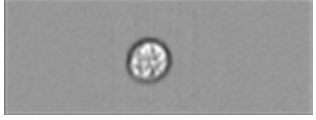
Total PC3 cells spiked into 1mL	Approximate retrieval of Live PC3 cells (Cell size)
3,000,000	7.46% (223,813)
300,000	2.29% (6,864)
30,000	6.48% (1,945)
3000	53.43% (1,603)
300	19.33% (58)
30	60% (18)

The left column of the table above shows the numbers of PC3 cells counted and spiked in each of the test tubes while the right column shows number of PC3 cells retrieved following examination with the ImageStream^x. The percentage of cells acquired varied from one tube to another, but the number of cells was in constant decline. Some of the numbers given in the right column, particularly for the last two samples, were different from the ones provided by the analysis software. The number of PC3 cells spiked in these two samples was very low, warranting a manual examination of each large object captured to confirm the identity of some of any PC3 cell that might be present.

6.4.5 Cellular morphology and structure comparison

The morphology and structural integrity of cells has been a subject of a consistent comparison in this study. Different cell structures and morphologies are demonstrated in Table 6.2 below for each of the cell-lines used and for different CTC-identification approaches. The aim of this research was to achieve an accurate identification of CTCs (PC3 cells) and to successfully isolate them, including when very minute PC3 numbers are used. When relying on immunological methods, there was the challenge of obtaining false positive and false negative cells.

Table 6.2: Comparison of cell morphology obtained from the four CTC identification methods used

	PC3	GMO0893	PBL
EpCAM			
CD45			
ZO-1 TJ			
Live cells			

The table above provides a comparison of cell clarity and structural integrity through examples of cells obtained in various CTC identification approaches. The first column on the left mentions the type of experiment undertaken, while the three other columns give brightfield images as examples of the three cell-lines used in each of the four types of experiments.

Non-specific staining was observed despite the use of a blocking buffer, which reduces the non-specific binding between antibodies and cells. As a result, a hypothesis emerged that perhaps antibody non-specificity was occurring due to the rigorous sample-preparation process, which results in the exhaustion of cells and loss of structural integrity in which cells become very porous/permeabilised. This permeabilisation might have in turn allowed for antibodies to be detected within cells that would otherwise not bind to cell antigens. This observation was noticeable for both PC3 and PBL cells when they were prepared for staining with EpCAM, CD45 and ZO-1 TJ antibodies. When live PC3 and PBL cells were used, the morphology of most cells was clear and the structure was intact (Table 6.2).

On the other hand, the GMO0893 cell-line was not only observed to show high levels of nonspecific staining, but it was also presenting a consistently suboptimal morphology and a flawed structure. This meant that it was difficult to discriminate between GMO0893 cells and PC3 cells based on immunological methods and/or physical properties. As a result, the GMO0893 cell-line was deemed un-useful and was discontinued from future experiments, including the proof of principle experiment where samples were spiked with dilutions of PC3 cells.

From the graphs that previously documented the existence of overlapping immunostaining intensities of PC3 and PBL cells (Figure 3.10, Figure 4.9 and Figure 5.10), the advantage of using the live cell analysis approach over immunological methods can be seen. Figure 6.9 clearly demonstrated that the cell size comparison approach provided a greater specificity in distinguishing between PC3 and PBL cells and therefore potentially identifying CTCs in a blood sample. The existence of a minute overlap between the two cell-lines can be dealt with in a relatively short period of time upon manual examination of cells included in that overlapping region.

6.4.6 Cell retrieval comparison

As well as possessing a high specificity, the sensitivity of the test has to also be ideal in order to consider using the test in detecting CTCs in cancer patients' samples. The sensitivity is measured by the retrieval numbers of PC3 cells from samples in which they were mixed with PBL cells. The higher the number of retrieved PC3 cells, the more sensitive and accurate the approach is.

Table 6.3 below shows the approximate retrieval numbers and percentages for the approaches undertaken in this study to isolate PC3 cells. The immunological approaches previously conducted proved to have fluctuating rates of cell retrieval. The experiment which was based on the use of ZO-1 TJ antibody to positively select PC3 cells in a mixed sample had the highest number of PC3 cells retrieved in the most diluted sample (20 out of 30 cells).

Table 6.3: Approximate CTC retrieval number from the four methods examined

Total PC3 cells spiked into 1mL	Approximate retrieval of EpCAM positive cells	Approximate retrieval of CD45 negative cells	Approximate retrieval of ZO-1 TJ positive cells	Approximate retrieval of Live PC3 cells (Cell size)
3,000,000	24.98% (749,540)	5.8% (174,107)	20.68% (620,503)	7.46% (223,813)
300,000	0.66% (1973)	2.19% (6579)	3.4% (10,202)	2.29% (6,864)
30,000	2.27% (680)	7.01% (2105)	4.22% (1267)	6.48% (1945)
3000	15.97% (479)	1.8% (54)	11.9% (357)	53.43% (1603)
300	7% (21)	8.76% (26)	13% (39)	19.33% (58)
30	16% (5)	33.33% (10)	66.67% (20)	60% (18)

The table above shows approximate retrieval numbers and percentages of the EpCAM, ZO-1 TJ, CD45 and the live cell analysis approaches.

The number of PC3 obtained from staining with EpCAM, ZO-1 TJ or CD45 antibodies, however, might not be accurate, as these numbers are based on cells that were EpCAM- and ZO-1 TJ positive or CD45-negative and is not always representative of the true PC3 population. As demonstrated in previous chapters of this research, antibody staining was very often nonspecific; meaning that some of the cells that were identified as PC3 cells could be PBL cells. In fact, careful examination of EpCAM and ZO-1 TJ stained cells in diluted samples revealed that cells that were identified by the analysis software as PC3 cells were false positive PBLs.

The same applies to CD45-negative cells, as images (Figure 4.2) provided in chapter 4 demonstrated how a portion of PC3 cells showed high intensity levels for the leukocyte-specific marker. Some of these cells were also excluded from the total PC3 cell count by the analysis software and replaced by PBL cells that showed little or no CD45 staining. With large overlapping regions such as the one shown in chapters 3, 4 and 5, it would take a relatively long period of time to manually examine all cells and distinguish PC3 cells from others. Hence why, the attainment of a relatively small overlapping region when PC3 and PBL sizes are compared may prove to be the ideal choice in identifying PC3 cells in imaging flow cytometry and ultimately for the identification and enumeration of CTCs in prostate cancer patients.

6.5 Discussion

With immunological approaches lacking specificity in distinguishing between PC3 cells and PBL and GMO0893 cells, a different and more fundamental approach was considered. The analysis of cellular features such as the morphology and cell size did not only provide a new opportunity for a detailed comparison of the cell-lines in question, but it also presented an alternative to the method that has so far yielded cells with poor cell morphology as a result of immunological sample preparation steps/procedure.

To begin with, the size range for each cell-line was established prior to comparing different cells and conducting the mixing experiment. This was done to eliminate the use of cell-lines that have similar size ranges as the method would become user-subjective and biased. The PC3 cells were found to have a cell size range that overlaps greatly with that of the GMO0893 cells. Having said that, the GMO0893 cells were repeatedly sighted in previous experiment to have poor morphology and unbalanced structure in which cells were seen to be expanded in size and have an irregular shape. On the other hand, PC3 cells and PBL cells did not overlap in size when examined separately, indeed there were approximately 40Arb separating the smallest PC3 cell from the largest PBL. As a result, the use of GMO0893 cells was discontinued; instead the reliance solely on PBL cells spiked with PC3 cells became the standard of the proof of principle live cell analysis experiments.

When the mixing experiment was constructed, the PC3 and PBL populations maintained separate size ranges with the exception of few cells. Approximately 5.31% of the cells in an evenly balanced sample (50% PC3 and 50% PBL) were found to be a mixture of PC3 and PBL cells that shared similar size. These cells kept a preserved shape and did not appear to have been enlarged due to the way the samples were prepared. Close examination of this region revealed that both types of cells indeed existed in that region; nonetheless, they were easily distinguishable as they morphology of these cells was optimal and clear, making for easy cell type categorisation.

The number of cells retrieved using this method far exceeded what has been previously obtained with immunological approaches. In the presence of low PC3 numbers, such as in the most diluted tube where as little as 30 PC3 cells were spiked (Table 6.3), 60% of these cells were successfully retrieved and verified. The preservation of cellular features and structure meant that an easy and accurate examination of cells can take place. Furthermore, with much less cell processing steps than when staining methods were used, fewer cells were lost during the sample preparation steps. Careful examination of cells in each sample also revealed that the numbers of retrieved cells using the live cell analysis approach were a more accurate representation of the true numbers of each population than methods used in previous chapters.

As the morphology of antibody staining experiments was compared to that of live cell analysis, it became clear that a simplified approach may perhaps provide more accurate results in clinical utility. It was also found that live cells retained more prototypical cell shape and structure, as well as preserving normal nuclear integrity as determined by DRAQ5 staining. The GMO0893 cells are excluded from these statements as they showed sustained characteristics of irregular shape and size, ultimately rendering the use of this cell-line unsuitable for the purposes of evaluating the live cell analysis as a method for CTC identification.

The use of biomarkers such as EpCAM and ZO-1 TJ antibodies was originally deemed to be essential for marking PC3 cells and isolating them from other cells. As various experiments and tests were conducted, it became apparent, that exposing such a large number of cells in suspension to numerous sample preparation steps would lead to the acquisition of misleading data in the form of false positive and false negative cells. Obtaining similar data when dealing with real cancer patients would not be ideal; instead a concise and accurate approach is certainly essential. Hence why, the preparation of cells in as few steps as possible might be the optimal choice for ImageStream^x examination.

Chapter 7

Identification of Circulating Tumour Cell in Prostate Cancer Patients

7. Identification of Circulating Tumour Cells in Prostate Cancer Patients

7.1 Introduction

This research explored a number of methods to detect and enumerate CTCs in metastatic prostate cancer using cultured prostate cancer (PC3) cells. The methods used utilised the use of immunological detection of CTCs, either via the positive selection of stained cells (with EpCAM or ZO1 TJ staining) or the negative selection of cells (CD45-negative cells). The lack of specificity of antibody staining and the poor morphology in some of the cells obtained prompted an investigation into an alternative approach to provide a higher sensitivity of CTC detection with improved cellular morphology. As a result, the physical characteristics of PC3 cells were compared to other cell types such as GMO0893 and PBL cells. Not only were PC3 cells found to be bigger in size than the PBL cells but also the examination of physical cellular features did not require a prolonged sample preparation procedure. This live cell analysis method helped preserve both, the number of cells in a sample as well as cell morphology and structure.

Clinical validation was then required in order to assess the efficacy of the live cell analysis in detecting CTCs and to evaluate its advantages over immunostaining techniques. Whole blood samples from advanced-stage CRPC patients were obtained from Mount Vernon Cancer Centre with informed consent and NHS ethical approval. The samples were processed to lyse RBCs (as described in the clinical samples preparation section in Chapter 2 on page 98) and the presence of CTCs was then observed using the live cell analysis technique as well as the positive selection of EpCAM-stained cells. The use of clinical samples in this research is essential as the sole reliance on cultured prostate cancer cells may provide misleading data and subsequently inaccurate conclusions. With regards to the research I am conducting, differences in the morphology of cells has previously been

reported in cells captured from cultured prostate cancer cell-lines (including PC3) and cells from prostate cancer patients (Park et al., 2014).

Differences such as the size of tumour cells, cell shape and nuclear cytoplasmic (N/C) ratio were examined in the study by Park *et al* and it was found that CRPC patient tumour cells were smaller in size than their cultured counterparts. The study relied on the use of the CellSearch® system which it claimed contributed to cell shrinkage (Approximately 6% cell diameter decrease) resulting from the prolonged storage of samples in CellSave® tubes, a factor that might have caused an alteration to in cell size. Additionally, patients' CTCs were found to have a more elongated shape and a greater nuclear to cytoplasm ratio than cultured cancer cells.

It is conceivable to assume that relying on the comparison of physical features between cultured cell-lines might lead to an inaccurate overestimation of the platform's (in this case, the ImageStream^x) ability to capture and identify CTCs. The reason for this hypothesis is that in spite of the established knowledge of epithelial cancer cells being relatively larger in size than leukocytes (Fehm et al., 2005), the heterogeneity of CTCs may cause a significant overlap in the physical properties of some CTCs with that of other cell types, such as WBCs (Peeters et al., 2011, Hyun et al., 2013, Jin et al., 2014). Crucially, the combination of leukocyte-like physical characteristics in some CTCs and the general rarity of circulating cancer cells in patients suggest that the detection of these cells may not be a simple task. Hence why the sole reliance on cultured CTCs (such as PC3 cells) as models for patients' CTCs may be misleading as these cultured cancer cells are far more different (physically) to leukocytes than patient CTCs are.

In order to avoid false estimations of the ImageStream^x capability in identifying and enumerating CTCs, as well as to validate the advantages of the live cell analysis method over immunostaining techniques with regards to detection accuracy and sensitivity, the use of CRPC patient samples was considered an indispensable requirement in this study.

7.2 Aim

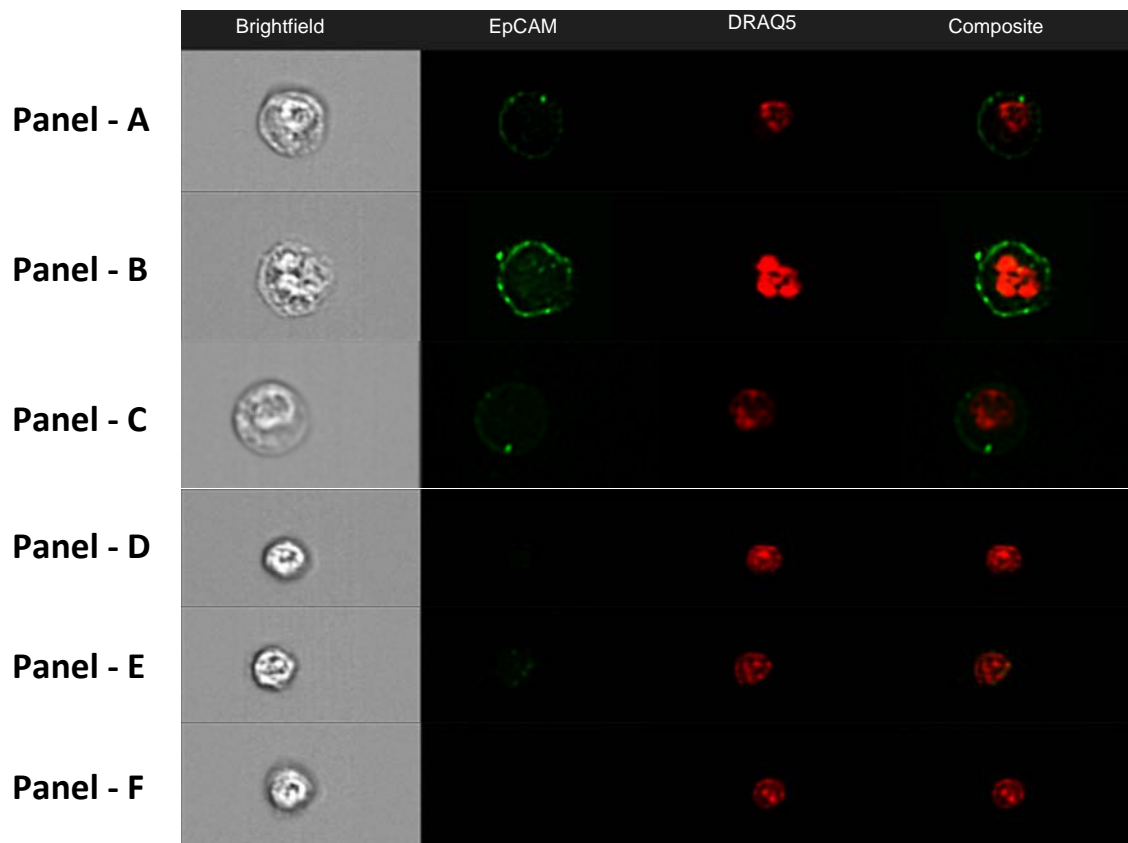
- To identify and enumerate Circulating Tumour Cells (CTCs) from two CRPC patients using the live cell analysis approach
- To identify and enumerate CTCs from the same patients using EpCAM staining
- To evaluate the specificity of EpCAM antibody in staining CTCs in CRPC patients
- To compare the sensitivity of the live cell analysis approach with that of EpCAM staining for the identification of CTCs from CRPC patients

7.3 Results

7.3.1 Identification of circulating tumour cells using EpCAM staining

Both patients' samples were depleted of RBCs and stained with the EpCAM antibody as previously explained. EpCAM is an epithelial-specific marker and was used to target potential CTCs present in these samples. The figure below gives account to images of CTCs and WBCs captured from patient 1 (Pt1) and patient 2 (Pt2).

Figure 7.1: EpCAM staining of CTCs and WBCs in prostate cancer patients

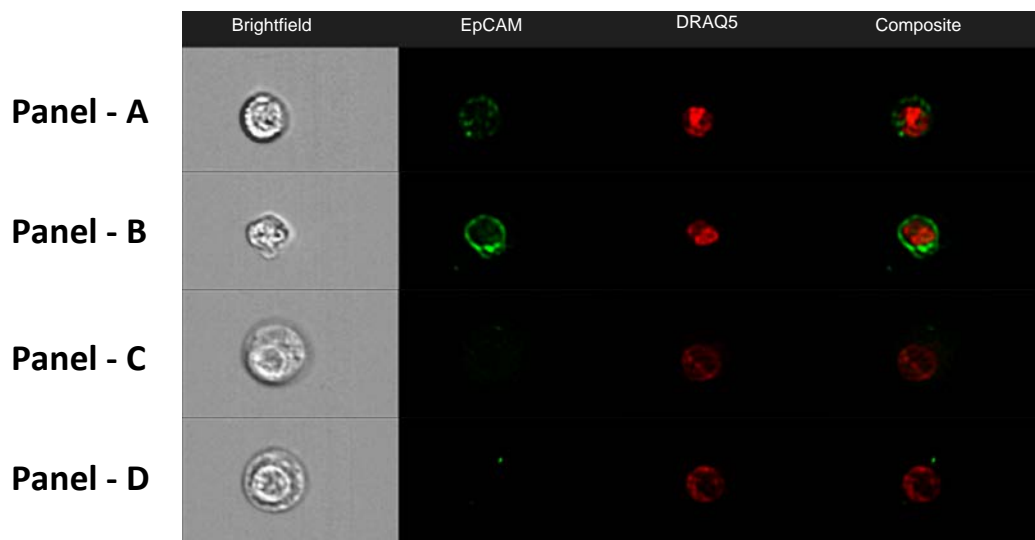


Samples shown in the figure above demonstrate different patterns of staining of CTCs with the EpCAM antibody. The first column, titled brightfield shows brightfield images of cells on Ch01. The second column shows EpCAM antibody staining in green on Ch02. DRAQ5 nuclear staining is displayed in red in the third column and captured on Ch05. At the far right, the fourth column shows a composite of EpCAM and DRAQ5, underlining the morphology within these cells. Panels A, B and C represent images of CTCs captured from both patients, while Panels D, E and F are examples of WBCs from the same samples. Images shown in this figure are captured at 60x plus EDF image acquisition.

Other than the cells shown in the figure above, many cells (CTCs and WBCs) were found to exhibit an irregular staining outline of the EpCAM antibody. EpCAM was found in high intensity in the

cytoplasmic region of cells and without confinement to the membrane. More importantly, several WBCs were found to be EpCAM-positive with a complete peripheral staining. Additionally, there were also several large CTCs that showed little or no EpCAM staining. This lack of specificity of EpCAM staining was evident in cultured CTCs (PC3 cells) and remains evident in patient clinical samples as demonstrated in the figure below.

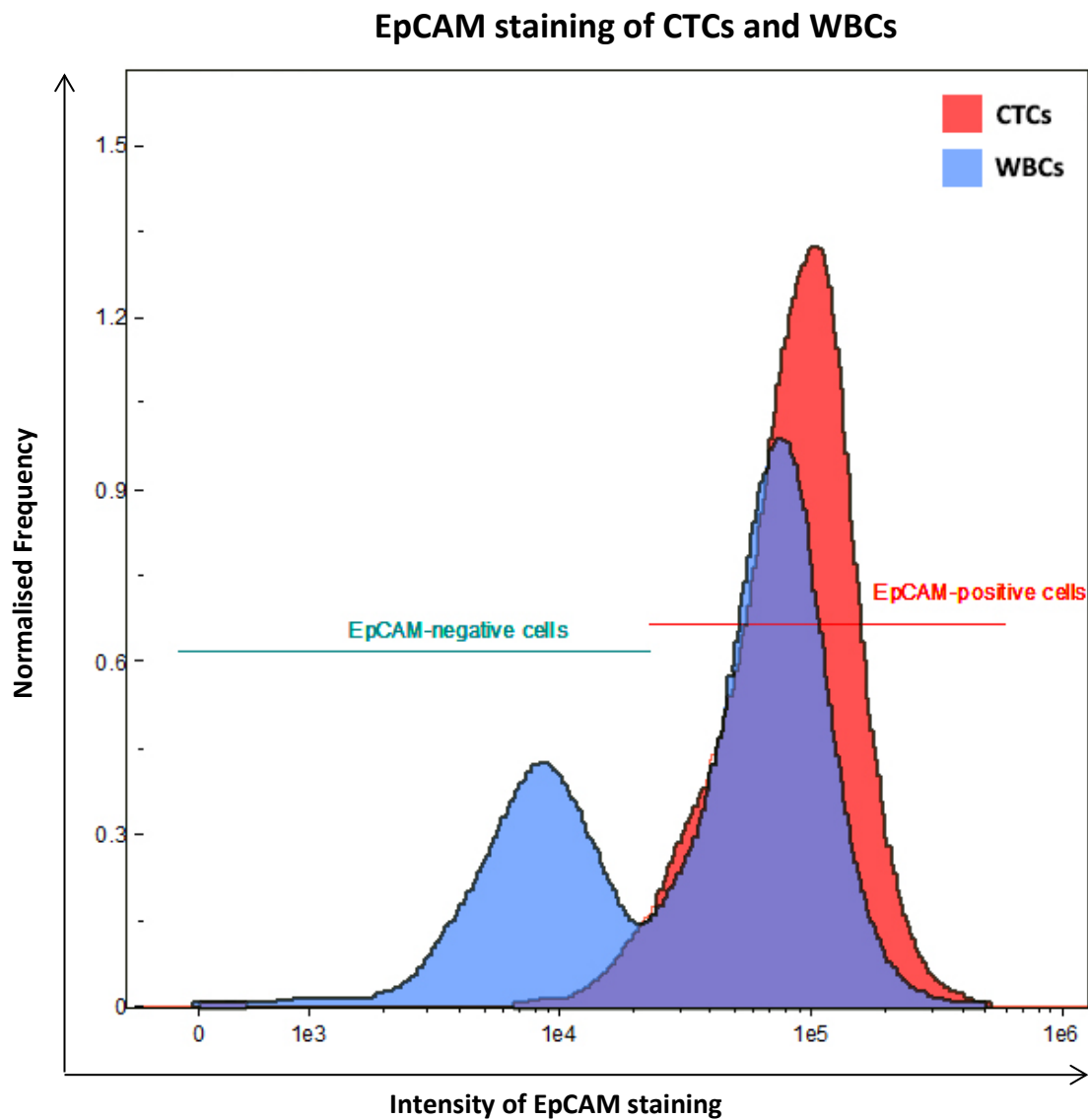
Figure 7.2: Lack of EpCAM staining specificity in WBCs and CTCs



Samples shown in the figure above demonstrate different patterns of staining of CTCs with the EpCAM antibody. The first column, titled brightfield shows brightfield images of cells on Ch01. The second column shows EpCAM antibody staining in green on Ch02. DRAQ5 nuclear staining is displayed in red in the third column and captured on Ch05. Finally, the fourth column shows a composite of EpCAM and DRAQ5, underlining the morphology within these cells. Panels-A and B represent images of WBCs captured from both patients showing an EpCAM staining similar to that of EpCAM positive CTCs (False positives). Panels-C and D on the other hand are examples of CTCs where there was an absence of EpCAM staining (False negatives). Images shown in this figure are captured at 60x plus EDF image acquisition.

The intensity of EpCAM staining for CTCs and WBCs is represented in Figure 7.3 for Pt1 and Figure 7.4 for Pt2. The two figures highlight the weakness of EpCAM as a specific marker for CTCs, an observation that is backed by evidence of lower EpCAM expression in CTCs when compared to cultured prostate cancer cell-lines (Lazar et al., 2012). Upon careful examination of the CTC populations in these samples, cells that were observed to retain a complete periphery staining with the EpCAM antibody (Figure 7.1, panel A) were counted and the percentage of CTCs in the sample was given in the table below each graph.

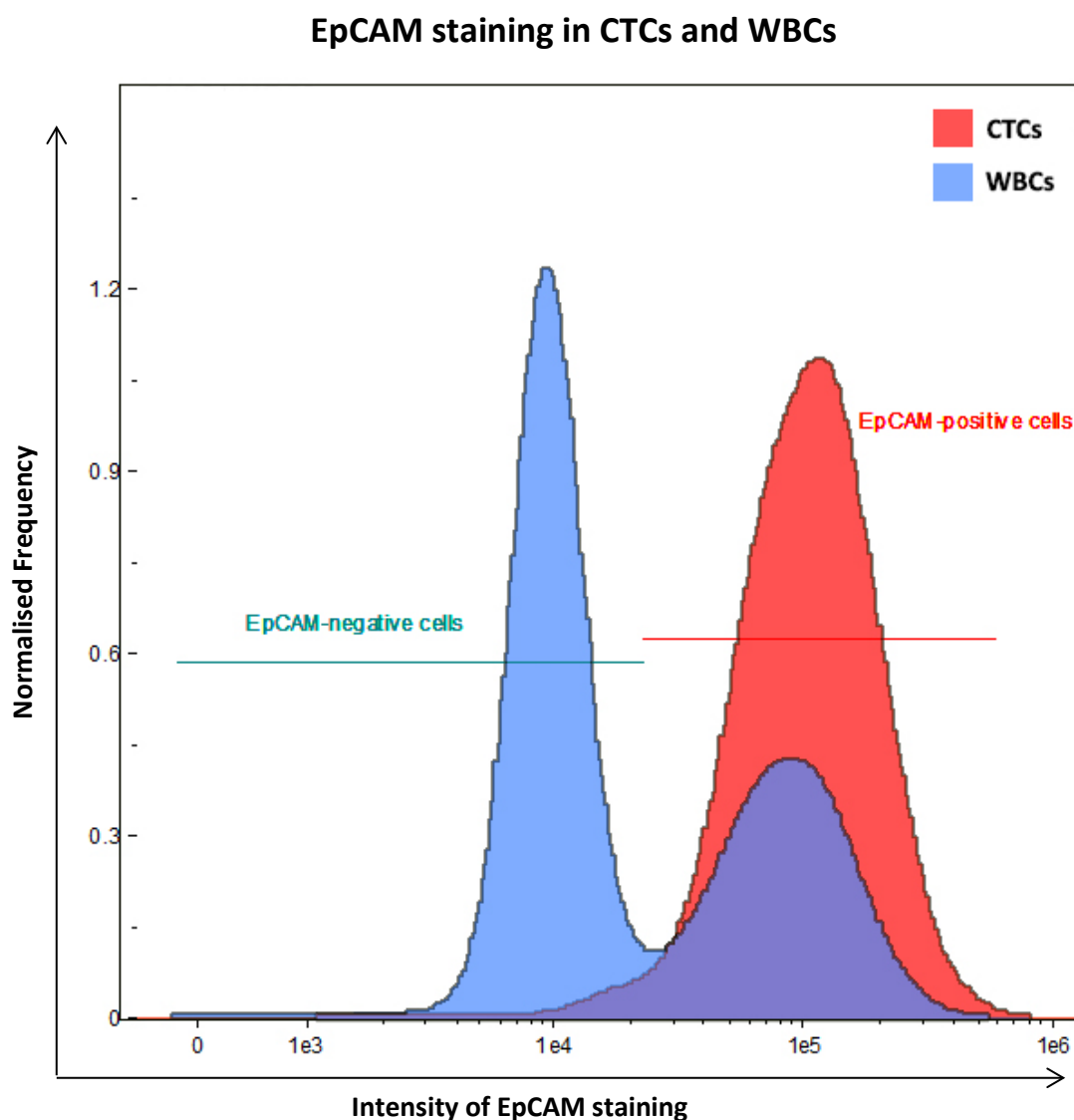
Figure 7.3: Distribution of CTCs and WBCs from Pt1 based on their EpCAM staining intensity



Examined volume (µl)	1.9657
Confirmed CTCs (size/staining)	48
Total sample volume (µl)	50.4
Approx. CTCs (in 7.5mL)	2461
Percentage of CTCs in sample	0.58%

The figure above shows the distribution of CTC and WBC populations based on their EpCAM staining intensity in Pt1. The X axis represents the intensity of EpCAM antibody staining, while the Y axis represents the normalised frequency of cells. The population of CTCs (highlighted in red) represents a large group of cells where CTCs might be present. While the blue region of the graph represents where most of the WBCs in the sample are located. Some cells from both populations overlap in their staining intensity, and these cells fall within the purple region on the graph. The table below the graph represents a count of CTCs within the sample, where only cells with a complete EpCAM staining in their periphery (e.g. Figure 7.1, panels A, B and C) were counted as CTCs.

Figure 7.4: Distribution of CTCs and WBCs from Pt2 based on their EpCAM staining intensity



Examined volume (μl)	2.6209
Confirmed CTCs (size/staining)	6
Total sample volume (μl)	45.3
Approx. CTCs (in 7.5mL)	207
Percentage of CTCs in sample	0.07%

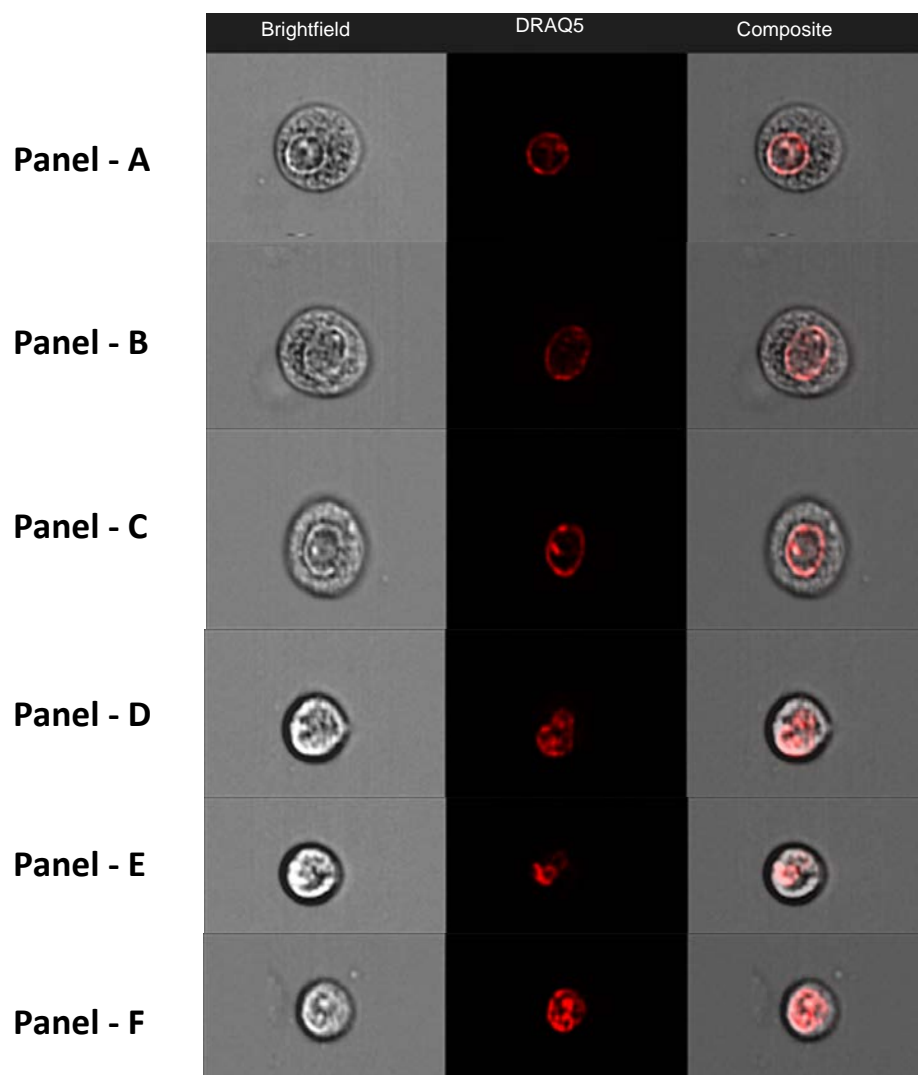
The figure above shows the distribution of CTC and WBC populations based on their EpCAM staining intensity in Pt2. The X axis represents the intensity of EpCAM antibody staining, while the Y axis represents the normalised frequency of cells. The population of CTCs (highlighted in red) represents a large group of cells where CTCs might be present. While the blue region of the graph represents where most of the WBCs in the sample are located. Some cells from both populations overlap in their staining intensity, and these cells fall within the purple region on the graph. The table below the graph represents a count of CTCs within the sample, where only cells with a complete EpCAM staining in their periphery (e.g. Figure 7.1, panels-A, B and C) were counted as CTCs.

7.3.2 Identification of circulating tumour cells using live cell analysis

Samples from the same two patients were also examined using the live cell analysis approach.

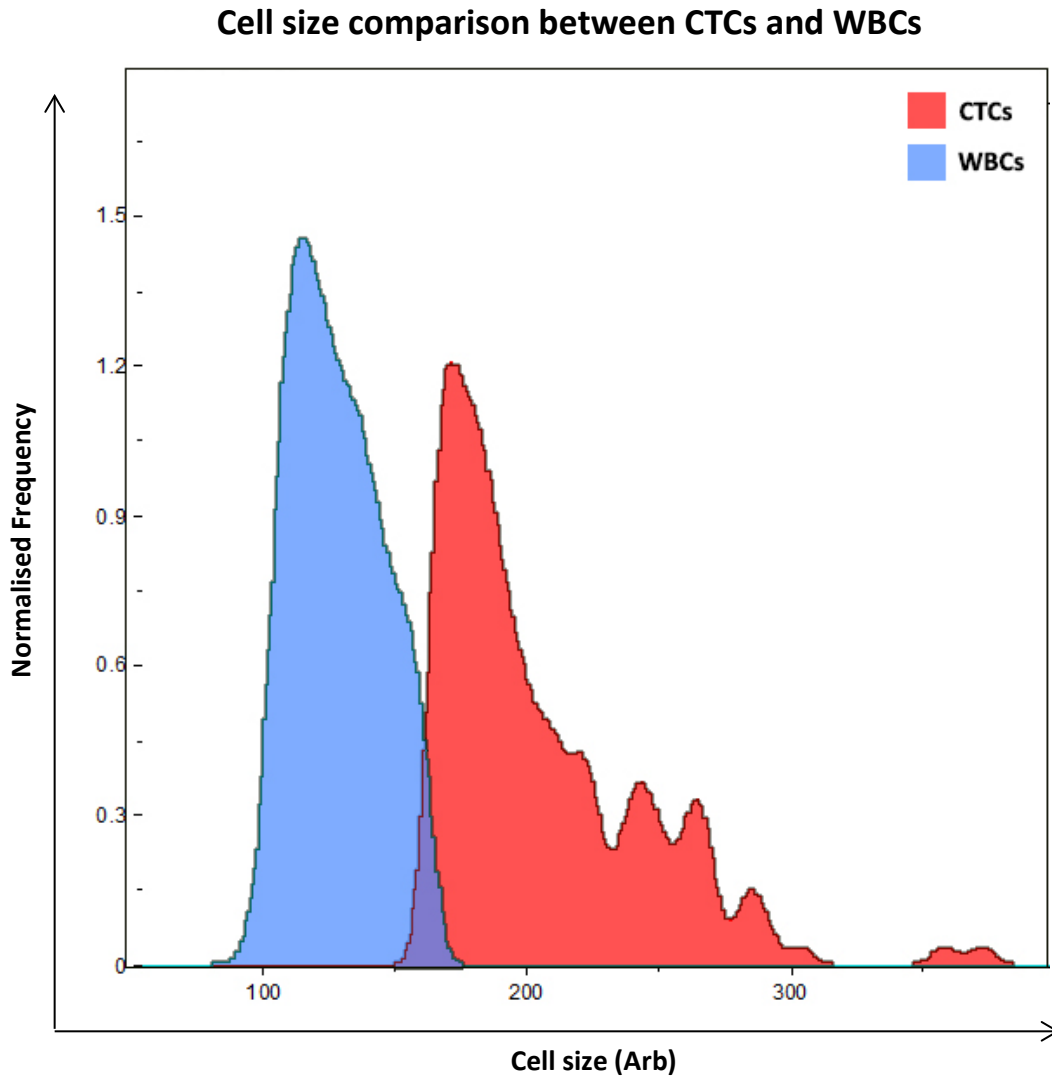
Whole blood samples were prepared in an identical way to the EpCAM-labelled samples but were not fixed, blocked or stained with any biomarker. The preparation of these samples for analysis took approximately 40-60 minutes from the moment they were collected from the patients and until they were examined with the ImageStream^X. The results of the live cell analysis are as follows:

Figure 7.5: Live cell images of CTCs and WBCs in prostate cancer samples



The figure above shows a gallery of images taken of live cells from CRPC patients' samples. The first column on the left, titled Brightfield, shows brightfield images of CTCs and WBCs. The middle column shows DRAQ5 nuclear stain in red, an indication that the captured object is a cell. The column on the right shows a composite of the brightfield images and the localisation of DRAQ5 nuclear stain, giving an account to the morphology in these cells. Panels-A, B and C represent CTCs in the two prostate cancer patients, while panels-D, E and F are images of WBCs from the same patients. Images shown in this figure are captured at 60x plus EDF image acquisition.

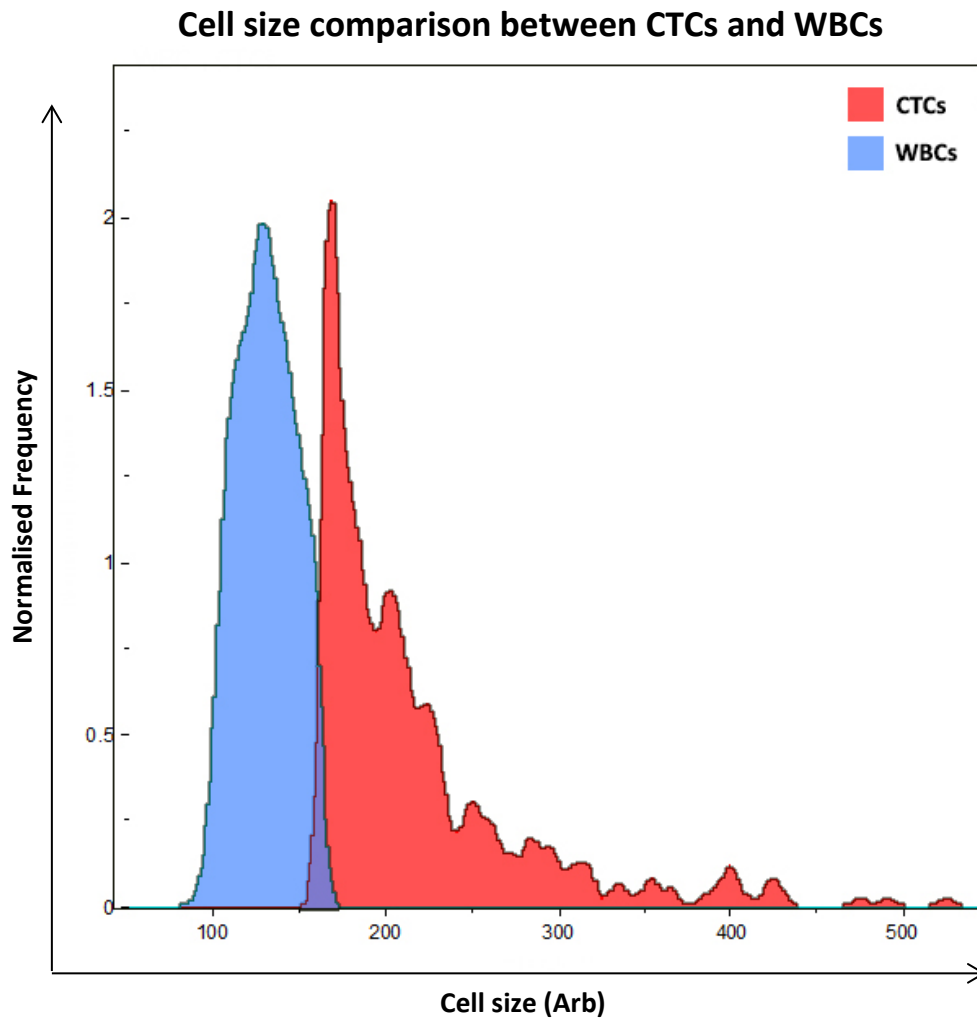
Figure 7.6: Distribution of CTCs and WBCs from Pt1 based on cell size



Examined volume (μl)	7.7873
Confirmed CTCs (size/staining)	123
Total sample volume (μl)	98.8
Approx. CTCs (in 7.5mL)	3121
Percentage of CTCs in sample	1.47%

The figure above shows the distribution of CTCs and WBCs based on their cell size as obtained from Pt1. The X axis represents the cell size (Arb), while the Y axis represents the normalised frequency of cells. The population of CTCs (highlighted in red) represents a large group of cells where CTCs might be present. While the blue region of the graph represents where most of the WBCs in the sample are located on the graph. The CTC population (red) was explored carefully and an accurate count of CTCs (e.g. Figure 7.5, panels A, B and C) in that sample was given in the table below the graph along with the percentage of CTCs in that sample.

Figure 7.7: Distribution of CTCs and WBCs from Pt2 based on cell size



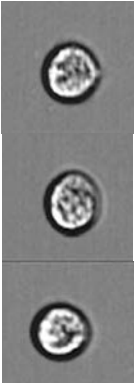
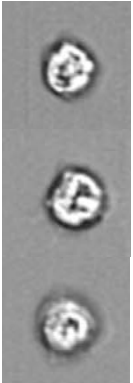
Examined volume (μl)	3.7567
Confirmed CTCs (size/staining)	144
Total sample volume (μl)	32.3
Approx. CTCs (in 7.5mL)	2476
Percentage of CTCs in sample	1.9%

The figure above shows the distribution of CTCs and WBCs based on their cell size as obtained from Pt2. The X axis represents the cell size (Arb), while the Y axis represents the normalised frequency of cells. The population of CTCs (highlighted in red) represents a large group of cells where CTCs might be present. While the blue region of the graph represents where most of the WBCs in the sample are located on the graph. The CTC population (red) was explored carefully and an accurate count of CTCs (e.g. Figure 7.5, panels-A, B and C) in that sample was given in the table below the graph along with the percentage of CTCs in that sample.

7.3.3 Cellular morphology and structure comparison

Differences in the morphology between cells captured using the live cell analysis approach and those that are EpCAM positive was clear. Images of CTCs and WBCs captured using both methods are shown in the figure below.

Table 7.1: Examples of CTCs and WBCs captured using live cell analysis and EpCAM staining

	Live cell analysis	EpCAM staining
CTCs		
WBCs		

The figure above shows brightfield images of CTCs and WBCs captured at 60× with EDF image acquisition. The middle column shows images of cells captured using the live cell analysis method, while the column on the right contains images of cells captured using the EpCAM staining method.

The previous table provides similar observations to the ones obtained in Table 6.2 when the morphology and structure of cultured cell lines were examined and compared. There appears to be a clear advantage in using live cell analysis approach over the use of immunological techniques indicated by the preservation of cellular morphology and structure. CTCs captured using the live cell analysis method retained a clearer membrane, perhaps due to not undergoing the permeabilisation procedure that the EpCAM stained cells had undergone. Moreover, the outline of the nucleus in live cells is far clearer than the EpCAM stained cells, allowing for a more accurate identification through the morphological and structural features within these cells.

Live WBCs on the other hand showed an optimal cellular integrity and appeared visibly clearer than the EpCAM stained WBCs. With a clear morphology as demonstrated in Table 7.1, discriminating leukocytes from CTCs was an easier task. The clear morphology of live CTCs and WBCs allowed for an accurate localisation of nuclear staining within these cells, which further helped in categorising each cell type.

7.3.4 Cell retrieval comparison

The high sensitivity of a CTC detection method is essential for its success and the sensitivity of the live cell analysis approach was compared to that of EpCAM staining in both patients. The table below contains the calculated average number of confirmed CTCs in both patients. This number is then multiplied to give an approximate account for the number of CTCs in the whole sample (7.5mL). The percentage of the average number of confirmed CTCs is also presented, showing a clear advantage in using live cell analysis method over the EpCAM immunostaining approach.

Table 7.2: Comparison between cell retrieval from live cell analysis and EpCAM staining

	Live cell analysis	EpCAM staining
Average number of confirmed CTCs	133	27
Average approximate number of CTCs in whole sample (7.5mL)	2798	1334
Average CTCs percentage in sample	1.69%	0.33%

The table above shows a comparison in CTCs numbers and percentages in Pt1 and Pt2 between the live cell analysis approach and the EpCAM staining method.

Several factors must be accounted for in the calculations above, such as the stage of cancer in these two patients, the treatment that they have undergone – which may cause a decline in CTC numbers – the age and more. However, there is a clear indication of higher cell retention using the live cell analysis, which is likely to be attributed to the simplicity of this sample preparation procedure.

7.4 Discussion

In this chapter, earlier observations of CTC targeting using EpCAM as well as the utilisation of CTC kinetical characteristics were validated using metastatic CRPC patient samples. 7.5mL whole blood samples were collected from two patients, with informed consent and full NHS ethical approval. Both sets of samples were processed to lyse RBCs in an identical procedure prior to analysing one set of the samples using the live cell analysis method (without fixing, blocking or staining) and analysing the other using EpCAM antibody staining.

Careful examination of approximately 17,000 images from both patients captured using the EpCAM staining method revealed the presence of 48 and 6 EpCAM-positive CTCs in Pt1 and Pt2 respectively. On the other hand, live cell analysis demonstrated the presence of 123 CTCs in Pt1 sample and 144 CTCs in Pt2 sample. The higher number of detected CTCs in the live cell analysis may have resulted from the simplicity of the sample preparation procedure prior to ImageStream^x examination. The EpCAM staining method was conducted over a time period of three consecutive days in which the primary EpCAM antibody was used to label CTCs in these samples. The EpCAM staining observed in patient samples showed small number of CTCs with a full and clear EpCAM staining on their membrane – a crucial requirement by pathologists to confirm the identity of a cell as a CTC.

Examining a large number of cells from each sample revealed the presence of many CTCs which lacked EpCAM staining as demonstrated in Figure 7.2. Likewise, EpCAM was found to be non-specific in targeting leukocytes as shown in the same figure. The lack of EpCAM specificity was a key weakness that undermined the use of this marker as a reliable identification tool for CTC detection in cultured cancer cells (PC3) and remains a challenging aspect in the identification of CTCs obtained from metastatic CRPC patients. It is also important to consider that most of the cells categorised by the analysis software (IDEAS[®]) as EpCAM-positive had expressed high staining intensity within the cells rather than on their periphery, providing a false estimation of the CTCs and WBCs populations

within these samples. This was best demonstrated by Figure 7.3Figure 7.4 which highlighted the significant overlap (purple region) in the staining properties of CTCs and WBCs.

Not only did the live cell analysis provide a higher count of CTCs from the same patient samples, but it also presented images of CTCs and WBCs that were significantly clearer than those obtained using EpCAM staining. The reduced number of sample preparation steps in the live cell analysis method meant that these cells were exposed to less morphologically altering factors such as fixation and permeabilising reagents which could have contributed to an improved cellular integrity and structure. This argument was backed by images of CTCs and WBCs obtained from both techniques in Table 7.1, outlining the clear superiority of the live cell analysis in the preservation of cellular morphology and structure.

The clear morphology of CTCs captured using the live cell analysis method allowed for a clear localisation of DRAQ5 nuclear staining. CTCs were characterised by a clearly defined nuclear membrane that was confined in a restricted region within cells as demonstrated in Figure 7.5. WBCs on the other hand displayed DRAQ5 nuclear staining covering a large area within these cells, outlining the difference in the nuclear cytoplasmic (N/C) ratio between CTCs and WBCs. This proved useful in providing an accurate discrimination of CTCs from leukocyte-rich samples based on the N/C ratio observation of cells.

Overall, the evidence provided in this chapter of improved cellular morphology and the increased CTCs detection when using the live cell analysis approach over immunological techniques (such as EpCAM staining), provided stronger evidence to back earlier notions about the advantages of this simple approach. Further testing in the clinical utility of this method, perhaps on a larger cohort, is worthy of investigation.

Chapter 7

General Discussion

8. General discussion

8.1 Inclusive analysis of results

8.1.1 Identification of PC3 cells using Immunostaining methods

The aim of this project was to develop a specific and sensitive detection method that is reliable in identifying CTCs in blood samples using Amnis ImageStream^X Mark II. To reconstruct the scenario where CTCs are found in the blood of metastatic prostate cancer patients, the PC3 human prostatic carcinoma cell-line were spiked in samples containing PBL cells. A number of approaches were undertaken and compared to determine the most effective and accurate means of detecting and enumerating CTCs (PC3 cells). Some of these approaches were immunological methods that relied on the use of biomarkers such as:

- Anti-EpCAM antibody
- Anti-CD45 antibody
- Anti-ZO-1 TJ antibody.

The EpCAM and ZO-1 TJ antibodies were epithelial biomarkers that were used to target PC3 cells and immunologically label them to help distinguish them from non-epithelial cells (PBLs) via positive-selection. The CD45 antibody was used to target non-epithelial cells such as PBL and GMO0893 cells, subsequently identifying PC3 cells via negative selection. For each of the three immunostaining methods used, different cell-lines were stained separately with the antibodies before the proof of principal experiment was conducted to determine the antibody specificity and binding efficiency.

A different approach, which filters different types of cells based on their physical and morphological properties, was also examined. Cellular properties such as the size of cells and the aspect ratio were

considered in order to distinguish different types of cells that may be found in the blood of a metastatic prostate cancer patient.

The EpCAM antibody displayed promiscuity in staining PC3 cells when initially used to test its specificity in a sample containing PC3 cells. More than 86% of the cells were found to be EpCAM-positive (Figure 3.4). Crucially, however, 2.21% of the PC3 cells were found to be EpCAM negative. The major limitation of using EpCAM was the lack of specificity of the antibody. When EpCAM was used in samples containing GMO0893 (B-lymphocytes) or PBL cells, it was found that 30.3% of the GMO0893 cells and 17.3% of the PBLs were EpCAM positive. The identification of these false-positive non-epithelial cells that were targeted by EpCAM, an epithelial-specific marker, raised early doubts about its usefulness as an accurate cancer biomarker.

The ambiguity over EpCAM staining specificity increased when the PC3 cells were spiked in PBL samples to mimic the presence of CTCs in prostate cancer patients. Although more than 94% of PC3 cells were fully stained with the antibody, there were some PC3 cells that showed weak or no EpCAM staining and therefore were not categorised as cancer cells by the analysis software. Additionally, the EpCAM staining patterns in PC3 cells varied; some cells showed expected peripheral (membrane) staining, while in some PC3 cells EpCAM was located in the cytoplasm (Panel-B in Figure 3.9). On the other hand, 95.1% of PBL cells showed little or no EpCAM staining, leaving approximately 4.9% of the PBL population positively staining for EpCAM and located in the overlapping region of EpCAM-positive PC3 cells (Figure 3.10). The presence of this overlapping region in which both PC3s and PBLs had a similar EpCAM staining intensity, presented a difficulty in identifying some PC3 cells with the EpCAM approach.

The promiscuity of EpCAM staining led to the investigation of another biomarker, the CD45 antibody, which targeted blood cells such as PBLs. It was hypothesised that as PC3 cells are epithelial in nature, they were not expected to stain with the CD45 antibody, enabling the negative-selection of these cells to help enumerate them within a sample. The CD45 antibody was initially tested on

PC3 cells alone to confirm staining specificity of this biomarker in epithelial cells. Despite most (69.9%) PC3 cells showing no CD45 staining, there was a percentage (6.8%) of these cells that were CD45-positive. Some PC3 cells showed weak, yet visible CD45 staining; and while some of the staining patterns observed in PC3 cells were weak and confined to small regions within cells, there were cells with full peripheral staining, similar to that expected of a PBL (Panel-E, Figure 4.2).

When the specificity and sensitivity of the CD45 antibody was examined by mixing PBL and PC3 cells, elevated levels of CD45-positive PC3 cells were obtained (up to 10% increase). Moreover, the number of CD45-positive PBL cells was reduced from 75.5% of the total population (when stained separately) to 62.27%, creating a large overlap of cells with similar CD45 staining intensity between the PC3 and PBL cells. Therefore, relying solely on the CD45 antibody as an exclusive marker for haematopoietic cells to isolate CD45-negative cells (CTCs) was not accurate nor reliable in this investigation. The presence of non-haematopoietic cells stained with the CD45 antibody has been previously reported in literature and will be discussed in the next section of this chapter (Stott et al., 2010a).

The ZO-1 TJ antibody is similar to the EpCAM antibody, being an epithelial cell-surface marker. This antibody targets the tight junction molecules located on the membrane of epithelial PC3 cells. When tested on PC3 cells, 95.76% of the cells were found to be ZO-1 TJ positive. On the other hand, the ZO-1 TJ antibody was detected at variable levels in more than 95% of the GMO0893 (B-lymphoblastoid) cells (Figure 5.6), rendering the use of these cells as unsuitable when testing the sensitivity of this antibody. PBL cells, however, proved to be a far more successful option to use as just over 4% of these cells showed any level of ZO-1 TJ staining (Figure 5.8). When PBL samples were spiked with PC3 cells to recreate the CTCs presence in prostate cancer patients, the PC3 cells maintained a high level of ZO-1 TJ staining but many PBL cells also expressed variable levels of ZO-1 TJ staining. With more than 46% of the PBL population identified as ZO-1 TJ positive, it was difficult to distinguish PC3 from PBL cells using this approach (Figure 5.10).

Various repeat experiments showing images collected of PC3, GMO0893 and PBL cells stained with the three biomarkers investigated in this research persistently highlighted the major weakness that arises from using immunological approaches, that is the lack of staining specificity. The graphs created with the analysis software, IDEAS[®], provided evidence for the presence of epithelial PC3 cells that exhibit immunostaining properties similar to that of haematopoietic (PBL) cells.

8.1.2 Identification of PC3 cells using live cell analysis

The lack of staining specificity and the reduced structural integrity of cells in immunological methods made it difficult to discriminate between PC3 and PBL cells. Therefore, I decided to compare cells based on physical parameters such as cell size and aspect ratio in a short, simplified test. After establishing a separate cell size range for each cell-line (PC3, GMO0893 and PBL cells) I was then able to compare the size parameters of each type of cells to confirm whether PC3 and PBL cells were the optimal choice for testing the sensitivity of this approach.

The results provided by this approach were robust in distinguishing PC3 cells from PBLs on the basis of cell size. The procedure in which the samples were prepared was relatively short and simple, meaning that the numerous sample preparation steps that were undertaken in immunological approaches were no longer required. This also preserved the structure and morphology of both PC3 and PBL cells and increased cell retention of diluted PC3 cells spiked in PBL samples. For the most diluted sample, 18 out of the 30 PC3 spiked into a PBL sample were identified based on their size. Providing a rapid and accurate enumeration of PC3 cells that otherwise would not be possible using immunostaining methods such as EpCAM, ZO-1 TJ and CD45 staining. There was, however, a relatively small overlap in the cell size of PC3 and PBL cells. The small margins of this overlap meant that the examination of cells within this region could be carried out in minutes to confirm the identity of cells in that region.

8.1.3 Clinical validation of CTC identification methods

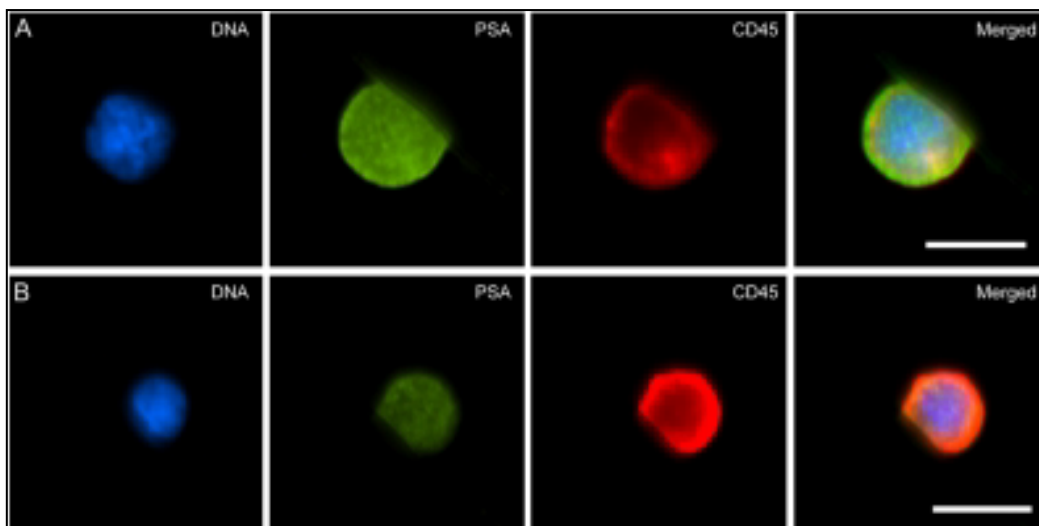
Identification of CTCs using EpCAM and cell morphology parameters (such as cell size and aspect ratio) was compared using clinical blood sample obtained from two metastatic CRPC patients. In Pt1, the number of confirmed CTCs using the live cell analysis was found to be 123 cells – a 256.25% increase on the number of enumerated EpCAM-positive CTCs (48). This significant increase in the detection of CTCs was even higher in Pt2 with 144 CTCs observed using the live cell analysis, compared to merely 6 EpCAM-positive CTCs (2400% increase).

Few factors may contribute the difference in CTC detection between the two patients such as the stage of cancer, age and treatment undertaken, but the enhancement of CTC detection and cellular morphology of captured cells is unquestionable. Furthermore, histograms (such as Figure 7.3 and Figure 7.6) comparing the immunostaining and physical properties of CTCs and WBCs, clearly demonstrated the benefit of using the live cell analysis instead of immunostaining in the identification and separation of CTCs from leukocytes in clinical samples.

8.2 Non-specific staining

The ability of some cells to be identified with both, epithelial (e.g. EpCAM, ZO-1 TJ) and hematopoietic (e.g. CD45) markers, has been previously outlined as a critical challenge in CTC isolation techniques (Stott et al., 2010a). Cells with similar immunostaining nature were referred to as “double positive” cells (Figure 8.1) and while many CTC isolation methods often disregard these cells when enumerating CTCs from metastatic cancer patients, the origin and nature of these cells remains unclear. Some groups claimed that overlooking these cells when isolating CTCs is justified by the fact that most of them possess similar morphology to that of leukocytes (Stott et al., 2010a). Others argue that the existence of these cells is due to a fusion of hematopoietic cells and CTCs and that CD45 staining in these cells might be caused by the non-specific binding of antibodies to these cells (Lustberg et al., 2012). Empirical evidence is required, however, to support these assertions.

Figure 8.1: Micrographs of isolated “double positive” cells from prostate cancer patients using the HB-Chip



A and B display micrographs of cells isolated from metastatic prostate cancer patients using the herringbone-chip device (HB-Chip). These cells were stained with PSA (epithelial marker, in green) and CD45 (hematopoietic marker, red) and were found to be more predominantly present than CTCs in these cancer patients. Additionally, their numbers were found to be significantly lower in healthy individuals than metastatic patients (Stott et al., 2010a).

In addition to obtaining false-positive staining in all three cell-lines used, the cell structure and morphology of the cells captured often appeared suboptimal. The troubleshooting of this issue led

to an investigation into whether the sample preparation steps, which were undertaken when cells were stained, were responsible for poor cell morphology and the non-specific staining observed. Therefore, a series of experiments were conducted in which the various steps of sample preparation such as fixing, blocking and staining cells, as well as the numerous washes with PBS between these steps, were removed. The result was a quick, more efficient method of imaging cells using the ImageStream^x with an enhanced cell morphology and structure.

Thorough analysis of results obtained using the live cell analysis method provided accurate morphological features of the PC3 and PBL cells, where different populations of these cells rarely shared similar properties (e.g. cell size, aspect ratio of cells). As a result, a simplified approach capable of preserving cellular integrity began to gather momentum in these investigations. The analysis software, IDEAS[®], was now capable of producing histograms that separated PC3 cells from PBLs with less error than before. Such graphs relied solely on the comparison of the cell size and aspect ratio of these cells and omitted the use any staining other than nuclear staining using the DRAQ5 antibody. The reason for continuing to use DRAQ5 in the live cell analysis experiments was to confirm the capture of single cells and exclude debris and other objects that may be captured. This simplified approach not only surpassed its predecessors in accuracy and cell retrieval, but also meant that CTC isolation may now be carried out in few hours rather than three days.

PC3 cells retrieval numbers were one of the key comparison criteria when the four methods were discussed. The ability to retrieve the highest possible number of PC3 cells with great accuracy would mean the method used could be a sensitive tool in the detection of CTCs in the blood of prostate cancer patients. Table 6.3, which compared the number of positively- or negatively-stained cells retrieved and the number of confirmed live PC3 cells, showed that the highest numbers of stained cells retrieved were achieved using the ZO-1 TJ antibody. The numbers in the ZO-1 TJ staining experiments were closely matched by the cell size experiment numbers, especially in the most

diluted samples. However, the accuracy of the three immunostaining techniques in identifying clear PC3 cells was much lower than that of the alternative physical analysis of cells.

For example, in the most diluted sample where 30 PC3 cells were spiked in PBL samples, the ZO-1 TJ staining experiment identified 20 cells as ZO-1 TJ-positive, categorising them as PC3 cells. These cells cannot, however, be certainly confirmed as PC3 cells as they appeared to exhibit a poor morphology, accompanied with a loss of membrane integrity, possibly allowing for the expansion of these cells into a larger size and permitting antibody presence and detection within them. This analysis was supported by images on Ch02 where ZO-1 TJ antibody staining was seen to be distributed throughout the cell rather than confining to cell periphery. In contrast, the cell size experiment provided images of cells with improved morphology and retention. The identity of the 18 cells that were identified as PC3 cells (when 30 PC3 cells were used) was confirmed upon manual examination of images of these cells, demonstrating that the numbers of confirmed PC3 cells obtained using this method (live cell analysis) could be a far more accurate representation of the actual number of PC3 cells than the immunological methods.

The CTC detection accuracy of live cell analysis and EpCAM immunostaining in clinical utility was also validated using the samples obtained from the CRPC patients. The number of CTCs detected using positive selection of EpCAM stained cells was relatively low in Pt1 and significantly inferior in Pt2 when compared to the numbers of CTCs captured using the live cell analysis approach. These CTC numbers provide strong evidence that the enumeration of EpCAM-positive CTCs may indeed present a misleading underestimation of the actual number of CTCs present in a sample.

8.3 Weaknesses and future work

This study explored the use of the live cell analysis approach using the ImageStream^X. The isolation of CTCs by size is a method that has been previously utilised through an ISET assay which allows for the isolation of tumour cells through size filtration (Vona et al., 2000). Nevertheless, little has been published using novel imaging flow cytometry in identifying circulating tumour cells based on their physical properties. The method provides a clear advantage over using immunological approaches by offering an enhanced cellular integrity and preserved cell structure and morphology. However, besides the accurate sorting of cells based on their physical properties (e.g. size, aspect ratio) and the examination of high quality brightfield images, this method provides little verification of the identity of cells captured. The exclusion of biomarkers use may lead to a user-bias judgement when confirming the presence of CTCs in a sample. For frequent ImageStream^X users, regular examination of the samples containing PC3 or PBL cells makes for an accurate classification of cells based on their type (cancerous or haematopoietic), but the same cannot be said for end users who are not used to observing CTCs images regularly.

EpCAM, ZO-1 TJ and CD45 antibodies are the three biomarkers that were examined in this study to verify the identity of PC3 cells using imaging flow cytometry. Other studies have used other techniques such as enrichment of CTCs via the expression of CKs along with the absence of CD45 staining. CKs that are expressed by CTCs include CK 4,5,6,8, 10, 13, 18, and 19 (Allard et al., 2004). Exploiting the expression of CK as a biomarker for CTCs identification could have been investigated using imaging flow cytometry as other studies have confirmed success in using it for CTC identification (Weissenstein et al., 2012, Dent et al., 2016).

The reason I deemed investigating CK expression in PC3 cells using the ImageStream^X as unurgent is the same reason why I chose to rely on live cell size analysis over immunological techniques. Lack of CTC targeting specificity is a common weakness for many biomarkers and cytokeratins are no exception. This was supported by other groups reporting susceptibility to error in CTC detection

when using a CK- (and EpCAM-) dependant methods compared to ISET (Mikolajczyk et al., 2011, Chinen et al., 2013). The study by Chinen *et al* particularly presented important findings as it examined CTC detection in clinical follow up (after treatment). The lack of EpCAM and CK staining in CTCs from lung cancer patients is attributed to the heterogeneous nature of CTCs. The presence of circulating tumour cells with epithelial, mesenchymal or even with both markers present (CTCs undergoing EMT) proved too difficult to target with immunocytochemical techniques only. It was concluded that relying on biomarker-dependant methods such as CK positive selection may prove misleading in evaluating patient's response to treatment.

To address the low EpCAM presence as well as the absence of other epithelial markers in some CTCs, it was suggested that a range of different antibodies to be used simultaneously to enhance the enrichment of CTCs and capture them more accurately (Schneck et al., 2015). My stance on using prolonged sample preparation protocols to detect CTCs remains firm in that it would cause a higher loss of CTCs during the various sample preparation steps than it would increase CTCs capture (detection sensitivity). Nonetheless, CK staining in PC3 cells (and CTCs) using imaging flow cytometry remains a future goal, chiefly to confirm early conclusions about the non-specificity of immunostaining techniques in identifying CTCs.

In addition to testing other biomarkers, further protocol optimisation to improve cell retention would have been useful. As seen in Table 6.3, cell retention numbers for the four methods examined varied and many cells were lost in the process of sample preparation. Some CTC detection studies utilised the use of immunomagnetic cell separation technologies to isolate CTCs with CK expression and the lack of CD45 expression (Wit et al., 2015, Dent et al., 2016). An example of such technology involves the use of EasySep™, a magnetic-particle based method which can help in the positive or negative selection of a desired type of cells (STEMCELL, 2016). The use of EasySep™ could have proved efficient in depleting samples of PBLs/WBCs prior to examination with the ImageStream^x, having previously been exploited for the depletion and isolation of blood cells (Le Dieu et al., 2009,

McQueen et al., 2016). In turn, this could have helped in reducing the sample running time as well as restricting the cell capture to the desired type of cells (PC3/CTCs).

The validation of the live cell analysis method utility in CTC capture and its advantages over the use of immunological techniques was essential in this study. Samples obtained from two CRPC patients provided data that supported early findings in cultured cancer cells about the benefits of relying on a rapid, simple technique for CTC detection and identification. If more resources were available, then perhaps the clinical utility of the live cell analysis could be further investigated. The use of more clinical samples from a variety of patients with different stages of the disease would provide an excellent verification of the method's capabilities and weaknesses. Samples from cancer patients before and after treatment would have provided the much-needed evaluation of the possibility of using live cell analysis in imaging flow cytometry as a point-of-care system in prostate cancer. Future studies could perhaps test the possibility of using a similar method in imaging flow cytometry for the detection of CTCs in other types of cancers, such as ovarian and colorectal cancers.

Bibliography

- ABCAM. 2016. *Anti-CD45 antibody [EP322Y] (ab40763)* [Online]. Available: http://www.abcam.com/cd45-antibody-ep322y-ab40763.html#description_images_2 2016].
- ACS. 2015. *What is prostate cancer?* [Online]. American Cancer Society Available: <http://www.cancer.org/cancer/prostatecancer/overviewguide/prostate-cancer-overview-what-is-prostate-cancer> [Accessed 07/02/2015].
- ADHYAM, M. & GUPTA, A. K. 2012. A Review on the Clinical Utility of PSA in Cancer Prostate. *Indian Journal of Surgical Oncology*, 3, 120-129.
- AGILENT. 2016. *Mycoplasma Assay Kits* [Online]. Available: <http://www.genomics.agilent.com/en/Mycoplasma-Detection/Mycoplasma-Assay-Kits/?cid=AG-PT-153&tabId=AG-PR-1130>.
- AL-MEHDI, A. B., TOZAWA, K., FISHER, A. B., SHIENTAG, L., LEE, A. & MUSCHEL, R. J. 2000. Intravascular origin of metastasis from the proliferation of endothelium-attached tumor cells: a new model for metastasis. *Nat Med*, 6, 100-2.
- ALIBHAI, S. M., GOGOV, S. & ALLIBHAI, Z. 2006. Long-term side effects of androgen deprivation therapy in men with non-metastatic prostate cancer: a systematic literature review. *Crit Rev Oncol Hematol*, 60, 201-15.
- ALIX-PANABIERES, C., BROUILLET, J. P., FABBRO, M., YSSEL, H., ROUSSET, T., MAUDELONDE, T., CHOQUET-KASTYLEVSKY, G. & VENDRELL, J. P. 2005. Characterization and enumeration of cells secreting tumor markers in the peripheral blood of breast cancer patients. *J Immunol Methods*, 299, 177-88.
- ALIX-PANABIÈRES, C., RIETHDORF, S. & PANTEL, K. 2008. Circulating Tumor Cells and Bone Marrow Micrometastasis. *Clinical Cancer Research*, 14, 5013-5021.
- ALLARD, W. J., MATERA, J., MILLER, M. C., REPOLLET, M., CONNELLY, M. C., RAO, C., TIBBE, A. G., UHR, J. W. & TERSTAPPEN, L. W. 2004. Tumor cells circulate in the peripheral blood of all major carcinomas but not in healthy subjects or patients with nonmalignant diseases. *Clin Cancer Res*, 10, 6897-904.
- ALTIN, J. G. & SLOAN, E. K. 1997. The role of CD45 and CD45-associated molecules in T cell activation. *Immunol Cell Biol*, 75, 430-45.
- ANAND, P., KUNNUMAKARA, A. B., SUNDARAM, C., HARIKUMAR, K. B., THARAKAN, S. T., LAI, O. S., SUNG, B. & AGGARWAL, B. B. 2008. Cancer is a Preventable Disease that Requires Major Lifestyle Changes. *Pharmaceutical Research*, 25, 2097-2116.
- ARMAKOLAS, A., PANTELEAKOU, Z., NEZOS, A., TSOUMA, A., SKONDRA, M., LEMBESSIS, P., PISSIMISSIS, N. & KOUTSILIERIS, M. 2010. Detection of the Circulating Tumor Cells in Cancer Patients. *Future Oncology*, 6, 1849-1856.
- ASHWORTH, T. 1869. A case of cancer in which cells similar to those in the tumours were seen in the blood after death. *Aust Med J*, 14, 146-149.
- ATTARD, G., SWENNENHUIS, J. F., OLMOS, D., REID, A. H., VICKERS, E., A'HERN, R., LEVINK, R., COUMANS, F., MOREIRA, J., RIISNAES, R., OOMMEN, N. B., HAWCHE, G., JAMESON, C.,

- THOMPSON, E., SIPKEMA, R., CARDEN, C. P., PARKER, C., DEARNALEY, D., KAYE, S. B., COOPER, C. S., MOLINA, A., COX, M. E., TERSTAPPEN, L. W. & DE BONO, J. S. 2009. Characterization of ERG, AR and PTEN gene status in circulating tumor cells from patients with castration-resistant prostate cancer. *Cancer Res*, 69, 2912-8.
- BABAIAN, R. J., DONNELLY, B., BAHN, D., BAUST, J. G., DINEEN, M., ELLIS, D., KATZ, A., PISTERS, L., RUKSTALIS, D., SHINOHARA, K. & THRASHER, J. B. 2008. Best Practice Statement on Cryosurgery for the Treatment of Localized Prostate Cancer. *The Journal of Urology*, 180, 1993-2004.
- BACKMAN, S. A., STAMBOLIC, V. & MAK, T. W. 2002. PTEN function in mammalian cell size regulation. *Current Opinion in Neurobiology*, 12, 516-522.
- BALDA, M. S., GARRETT, M. D. & MATTER, K. 2003. The ZO-1-associated Y-box factor ZONAB regulates epithelial cell proliferation and cell density. *J Cell Biol*, 160, 423-32.
- BALDA, M. S. & MATTER, K. 2016. Tight junctions as regulators of tissue remodelling. *Current Opinion in Cell Biology*, 42, 94-101.
- BARAN, J., PITUCH-NOWOROLSKA, A., KRZESZOWIAK, A., WIECKIEWICZ, J., STACHURA, J., PRYJMA, J., POPIELA, T., SZCZEPANIK, A. & ZEMBALA, M. 1998. Detection of cancer cells in the blood by FACS sorting of CD45- cells. *Int J Mol Med*, 1, 573-8.
- BARH, D. 2014. *Omics Approaches in Breast Cancer*.
- BARRIERE, G., FICI, P., GALLERANI, G., FABBRI, F. & RIGAUD, M. 2015. Epithelial Mesenchymal Transition: a double-edged sword. *Clinical and Translational Medicine*, 4, 1-6.
- BARTENEVA, N. S., FASLER-KAN, E. & VOROBEV, I. A. 2012. Imaging Flow Cytometry: Coping with Heterogeneity in Biological Systems. *Journal of Histochemistry and Cytochemistry*, 60, 723-733.
- BASIJI, D. A., ORTYN, W. E., LIANG, L., VENKATACHALAM, V. & MORRISSEY, P. 2007. Cellular Image Analysis and Imaging by Flow Cytometry. *Clinics in laboratory medicine*, 27, 653-viii.
- BAUER, H., ZWEIMUELLER-MAYER, J., STEINBACHER, P., LAMETSCHWANDTNER, A. & BAUER, H. C. 2010. The Dual Role of Zonula Occludens (ZO) Proteins. *Journal of Biomedicine and Biotechnology*, 2010.
- BECKMANCOULTER. 2015. *History of Flow Cytometry* [Online]. Beckman Coulter. Available: https://www.beckmancoulter.com/wsrportal/wsrportal.portal?_nfpb=true&_windowLabel=UCM_RENDERER&_urlType=render&wlpUCM_RENDERER_path=%2Fwsr%2Fresearch-and-discovery%2Fproducts-and-services%2Fflow-cytometry%2Fhistory-of-flow-cytometry%2Findex.htm [Accessed 22/02 2015].
- BERGMAN, R. A., AFIFI, A. K. & HEIDGER, P. M. 2016. *Atlas of Microscopic Anatomy: Section 4 - Blood* [Online]. Anatomy Atlases Available: <http://www.anatomyatlases.org/MicroscopicAnatomy/Section04/Plate0453.shtml> 2016].
- BJORK, T., PIIRONEN, T., PETTERSSON, K., LOVGREN, T., STENMAN, U. H., OESTERLING, J. E., ABRAHAMSSON, P. A. & LILJA, H. 1996. Comparison of analysis of the different prostate-specific antigen forms in serum for detection of clinically localized prostate cancer. *Urology*, 48, 882-8.

- BOURTON, E. C., PLOWMAN, P. N., ZAHIR, S. A., SENGULOGLU, G. U., SERRAI, H., BOTTLEY, G. & PARRIS, C. N. 2012. Multispectral imaging flow cytometry reveals distinct frequencies of γ -H2AX foci induction in DNA double strand break repair defective human cell lines. *Cytometry*, 81A, 130-137.
- BRACARDA, S., DE COBELLI, O., GRECO, C., PRAYER-GALETTI, T., VALDAGNI, R., GATTA, G., DE BRAUD, F. & BARTSCH, G. 2005. Cancer of the prostate. *Critical Reviews in Oncology/Hematology*, 56, 379-396.
- BROWN, D. M. & RUOSLAHTI, E. Metadherin, a cell surface protein in breast tumors that mediates lung metastasis. *Cancer Cell*, 5, 365-374.
- BRUNER, D. W., MOORE, D., PARLANTI, A., DORGAN, J. & ENGSTROM, P. 2003. Relative risk of prostate cancer for men with affected relatives: systematic review and meta-analysis. *Int J Cancer*, 107, 797-803.
- BURFORD, D., M, K. & J., A. 2009. *Prostate Cancer Risk Management Programme information for primary care; PSA testing in asymptomatic men* [Online]. NHS Cancer Screening Programmes: NHS. Available: <https://www.gov.uk/government/publications/prostate-cancer-risk-management-programme-psa-test-benefits-and-risks>.
- CAVALLARO, U., SCHAFFHAUSER, B. & CHRISTOFORI, G. 2002. Cadherins and the tumour progression: is it all in a switch? *Cancer Letters*, 176, 123-128.
- CHAMBERS, A. F., GROOM, A. C. & MACDONALD, I. C. 2002. Dissemination and growth of cancer cells in metastatic sites. *Nat Rev Cancer*, 2, 563-72.
- CHEN, Y. Y., CHENG, B. R., HE, Z. B., WANG, S. Y., WANG, Z. M., SUN, M., SONG, H. B., FANG, Y., CHEN, F. F. & XIONG, B. 2016. Capture and Identification of Heterogeneous Circulating Tumor Cells Using Transparent Nanomaterials and Quantum Dots-Based Multiplexed Imaging. *J Cancer*, 7, 69-79.
- CHINEN, L. T. D., DE CARVALHO, F. M., ROCHA, B. M. M., AGUIAR, C. M., ABDALLAH, E. A., CAMPANHA, D., MINGUES, N. B., DE OLIVEIRA, T. B., MACIEL, M. S., CERVANTES, G. M., DETTINO, A. L. A., SOARES, F. A., PATERLINI-BRÉCHOT, P. & FANELLI, M. F. 2013. Cytokeratin-based CTC counting unrelated to clinical follow up. *Journal of Thoracic Disease*, 5, 593-599.
- CONLON, I. & RAFF, M. 1999. Size control in animal development. *Cell*, 96, 235-44.
- COUZIN-FRANKEL, J. 2015. Backlash greets 'bad luck' cancer study and coverage. *Science*, 347, 224-224.
- CRAENE, B. D. & BERX, G. 2013. Regulatory networks defining EMT during cancer initiation and progression. *Nat Rev Cancer*, 13, 97-110.
- CRONIER, L., CRESPIAN, S., STRALE, P. O., DEFAMIE, N. & MESNIL, M. 2009. Gap junctions and cancer: new functions for an old story. *Antioxid Redox Signal*, 11, 323-38.
- CRUK 2012. World Cancer Factsheet Cancer Research UK
- CRUK. 2014a. *Cancer incidence for common cancers* [Online]. UK: Cancer Research UK. Available: <http://www.cancerresearchuk.org/cancer-info/cancerstats/incidence/commoncancers/uk-cancer-incidence-statistics-for-common-cancers#source1> [Accessed 02/06/2015 2015].

- CRUK. 2014b. *Cancer survival statistics* [Online]. UK: Cancer Research UK. Available: <http://www.cancerresearchuk.org/cancer-info/cancerstats/survival/england-and-wales-cancer-survival-statistics> [Accessed 06/02 2015].
- CRUK. 2014c. *Factors in deciding treatment for prostate cancer* [Online]. UK: Cancer Research UK. Available: <http://www.cancerresearchuk.org/about-cancer/type/prostate-cancer/treatment/types/factors-in-deciding-treatment-for-prostate-cancer> [Accessed 07/02 2015].
- DANILA, D. C., FLEISHER, M. & SCHER, H. I. 2011. Circulating tumor cells as biomarkers in prostate cancer. *Clinical cancer research : an official journal of the American Association for Cancer Research*, 17, 3903-3912.
- DAVDA, R., HUGHES, S., JONES, R., CRABB, S. J., TROUP, J. & PAYNE, H. 2016. Chemotherapy at First Diagnosis of Advanced Prostate Cancer – Revolution or Evolution? Findings from a British Uro-oncology Group UK Survey to Evaluate Oncologists' Views on First-line Docetaxel in Combination with Androgen Deprivation Therapy in Castrate-sensitive Metastatic and High-risk/Locally Advanced Prostate Cancer. *Clinical Oncology*, 28, 376-385.
- DAVIDSON, B., HOLTH, A., HELLESYLT, E., TAN, T. Z., HUANG, R. Y.-J., TROPÉ, C., NESLAND, J. M. & THIERY, J. P. 2015. The clinical role of epithelial-mesenchymal transition and stem cell markers in advanced-stage ovarian serous carcinoma effusions. *Human Pathology*, 46, 1-8.
- DE BONO, J. S., SCHER, H. I., MONTGOMERY, R. B., PARKER, C., MILLER, M. C., TISSING, H., DOYLE, G. V., TERSTAPPEN, L. W., PIENTA, K. J. & RAGHAVAN, D. 2008. Circulating tumor cells predict survival benefit from treatment in metastatic castration-resistant prostate cancer. *Clin Cancer Res*, 14, 6302-9.
- DE MARTEL, C., FERLAY, J., FRANCESCHI, S., VIGNAT, J., BRAY, F., FORMAN, D. & PLUMMER, M. 2012. Global burden of cancers attributable to infections in 2008: a review and synthetic analysis. *The Lancet Oncology*, 13, 607-615.
- DENG, G., HERRLER, M., BURGESS, D., MANNA, E., KRAG, D. & BURKE, J. F. 2008. Enrichment with anti-cytokeratin alone or combined with anti-EpCAM antibodies significantly increases the sensitivity for circulating tumor cell detection in metastatic breast cancer patients. *Breast Cancer Research : BCR*, 10, R69-R69.
- DENMEADE, S. R. & ISAACS, J. T. 2002. A history of prostate cancer treatment. *Nature reviews. Cancer*, 2, 389-396.
- DENT, B. M., OGLE, L. F., O'DONNELL, R. L., HAYES, N., MALIK, U., CURTIN, N. J., BODDY, A. V., PLUMMER, E. R., EDMONDSON, R. J., REEVES, H. L., MAY, F. E. B. & JAMIESON, D. 2016. High-resolution imaging for the detection and characterisation of circulating tumour cells from patients with oesophageal, hepatocellular, thyroid and ovarian cancers. *International Journal of Cancer*, 138, 206-216.
- DEOCAMPO, N. D., HUANG, H. & TINDALL, D. J. 2003. The role of PTEN in the progression and survival of prostate cancer. *Minerva Endocrinol*, 28, 145-53.
- DESGROSELLIER, J. S. & CHERESH, D. A. 2010. Integrins in cancer: biological implications and therapeutic opportunities. *Nat Rev Cancer*, 10, 9-22.
- DOMINGUEZ, R. & HOLMES, K. C. 2011. Actin structure and function. *Annu Rev Biophys*, 40, 169-86.
- EDGAR, B. A. 2006. How flies get their size: genetics meets physiology. *Nat Rev Genet*, 7, 907-916.

- EROL, B., GULPINAR, M. T., BOZDOGAN, G., OZKANLI, S., ONEM, K., MUNGAN, G., BEKTAS, S., TOKGOZ, H., AKDUMAN, B. & MUNGAN, A. 2014. The cutoff level of free/total prostate specific antigen (f/t PSA) ratios in the diagnosis of prostate cancer: a validation study on a Turkish patient population in different age categories. *Kaohsiung J Med Sci*, 30, 545-50.
- ETZIONI, R. D. 2013. Review of evidence concerning PSA screening for prostate cancer has limitations as basis for policy development. *Evidence Based Medicine*, 18, 75-76.
- FALL, K., FANG, F., MUCCI, L. A., YE, W., ANDRÉN, O., JOHANSSON, J.-E., ANDERSSON, S.-O., SPARÉN, P., KLEIN, G., STAMPFER, M., ADAMI, H.-O. & VALDIMARSDÓTTIR, U. 2009. Immediate Risk for Cardiovascular Events and Suicide Following a Prostate Cancer Diagnosis: Prospective Cohort Study. *PLoS Medicine*, 6, e1000197.
- FANNING, A. S., JAMESON, B. J., JESAITIS, L. A. & ANDERSON, J. M. 1998. The tight junction protein ZO-1 establishes a link between the transmembrane protein occludin and the actin cytoskeleton. *J Biol Chem*, 273, 29745-53.
- FEHM, T., SOLOMAYER, E. F., MENG, S., TUCKER, T., LANE, N., WANG, J. & GEBAUER, G. 2005. Methods for isolating circulating epithelial cells and criteria for their classification as carcinoma cells. *Cytotherapy*, 7, 171-85.
- FIDLER, I. J. 2003. The pathogenesis of cancer metastasis: the 'seed and soil' hypothesis revisited. *Nat Rev Cancer*, 3, 453-8.
- FOKAS, E., ENGENHART-CABILLIC, R., DANIILIDIS, K., ROSE, F. & AN, H. X. 2007. Metastasis: the seed and soil theory gains identity. *Cancer Metastasis Rev*, 26, 705-15.
- FRANKEN, B., DE GROOT, M. R., MASTBOOM, W. J., VERMES, I., VAN DER PALEN, J., TIBBE, A. G. & TERSTAPPEN, L. W. 2012. Circulating tumor cells, disease recurrence and survival in newly diagnosed breast cancer. *Breast Cancer Research*, 14, 1-8.
- FRIEDLANDER, T. W. & FONG, L. 2014. The end of the beginning: circulating tumor cells as a biomarker in castration-resistant prostate cancer. *J Clin Oncol*, 32, 1104-6.
- GADALLA, S.-E., ÖJEMALM, K., VASQUEZ, P. L., NILSSON, I., ERICSSON, C., ZHAO, J. & NISTÉR, M. 2013. EpCAM associates with endoplasmic reticulum aminopeptidase 2 (ERAP2) in breast cancer cells. *Biochemical and Biophysical Research Communications*, 439, 203-208.
- GILES, R. H., VAN ES, J. H. & CLEVERS, H. 2003. Caught up in a Wnt storm: Wnt signaling in cancer. *Biochimica et Biophysica Acta (BBA) - Reviews on Cancer*, 1653, 1-24.
- GILMORE, A. P. 2005. Anoikis. *Cell Death Differ*, 12, 1473-1477.
- GINZBERG, M. B., KAFRI, R. & KIRSCHNER, M. 2015. On being the right (cell) size. *Science (New York, N.Y.)*, 348, 1245075-1245075.
- GOFRIT, O. N., KATZ, R., SHAPIRO, A., YUTKIN, V., PIZOV, G., ZORN, K. C., DUVDEVANI, M., LANDAU, E. H. & PODE, D. 2013. Gross Hematuria in Patients with Prostate Cancer: Etiology and Management. *ISRN Surgery*, 2013, 4.
- GOLDKORN, A., ELY, B., QUINN, D. I., TANGEN, C. M., FINK, L. M., XU, T., TWARDOWSKI, P., VAN VELDHUIZEN, P. J., AGARWAL, N., CARDUCCI, M. A., MONK, J. P., 3RD, DATAR, R. H., GARZOTTO, M., MACK, P. C., LARA, P., JR., HIGANO, C. S., HUSSAIN, M., THOMPSON, I. M., JR., COTE, R. J. & VOGELZANG, N. J. 2014. Circulating tumor cell counts are prognostic of

- overall survival in SWOG S0421: a phase III trial of docetaxel with or without atrasentan for metastatic castration-resistant prostate cancer. *J Clin Oncol*, 32, 1136-42.
- GOLDSTEIN, A. S., HUANG, J., GUO, C., GARRAWAY, I. P. & WITTE, O. N. 2010. Identification of a cell of origin for human prostate cancer. *Science*, 329, 568-71.
- GONZÁLEZ-MARISCAL, L., BETANZOS, A., NAVA, P. & JARAMILLO, B. E. 2003. Tight junction proteins. *Progress in Biophysics and Molecular Biology*, 81, 1-44.
- GREENLEE, R. T., HILL-HARMON, M. B., MURRAY, T. & THUN, M. 2001. Cancer statistics, 2001. *CA Cancer J Clin*, 51, 15-36.
- GRIMWADE, L. F., FULLER, K. A. & ERBER, W. N. 2017. Applications of imaging flow cytometry in the diagnostic assessment of acute leukaemia. *Methods*.
- GULLEY, J. L. & MADAN, R. A. 2016. Developing immunotherapy strategies in the treatment of prostate cancer. *Asian Journal of Urology*, 3, 278-285.
- GUPTA, G. P. & MASSAGUÉ, J. Cancer Metastasis: Building a Framework. *Cell*, 127, 679-695.
- HANAHAN, D. & WEINBERG, R. A. 2000. The Hallmarks of Cancer. *Cell*, 100, 57-70.
- HANAHAN, D. & WEINBERG, ROBERT A. 2011. Hallmarks of Cancer: The Next Generation. *Cell*, 144, 646-674.
- HART, I. R. & FIDLER, I. J. 1980. Role of organ selectivity in the determination of metastatic patterns of B16 melanoma. *Cancer Res*, 40, 2281-7.
- HAYES, J. H. & BARRY, M. J. 2014. Screening for prostate cancer with the prostate-specific antigen test: a review of current evidence. *Jama*, 311, 1143-9.
- HEADLAND, S. E., JONES, H. R., D'SA, A. S. V., PERRETTI, M. & NORLING, L. V. 2014. Cutting-Edge Analysis of Extracellular Microparticles using ImageStreamX Imaging Flow Cytometry. *Sci. Rep.*, 4.
- HEIDENREICH, A., BASTIAN, P. J., BELLMUNT, J., BOLLA, M., JONIAU, S., VAN DER KWAST, T., MASON, M., MATVEEV, V., WIEGEL, T., ZATTONI, F. & MOTTET, N. 2014a. EAU guidelines on prostate cancer. part 1: screening, diagnosis, and local treatment with curative intent-update 2013. *Eur Urol*, 65, 124-37.
- HEIDENREICH, A., BASTIAN, P. J., BELLMUNT, J., BOLLA, M., JONIAU, S., VAN DER KWAST, T., MASON, M., MATVEEV, V., WIEGEL, T., ZATTONI, F. & MOTTET, N. 2014b. EAU Guidelines on Prostate Cancer. Part 1: Screening, Diagnosis, and Local Treatment with Curative Intent—Update 2013. *European Urology*, 65, 124-137.
- HEITZER, E., AUER, M., GASCH, C., PICHLER, M., ULZ, P., HOFFMANN, E. M., LAX, S., WALDISPUEHL-GEIGL, J., MAUERMANN, O., LACKNER, C., HÖFLER, G., EISNER, F., SILL, H., SAMONIGG, H., PANTEL, K., RIETHDORF, S., BAUERNHOFER, T., GEIGL, J. B. & SPEICHER, M. R. 2013. Complex Tumor Genomes Inferred from Single Circulating Tumor Cells by Array-CGH and Next-Generation Sequencing. *Cancer Research*, 73, 2965-2975.
- HELO, P., CRONIN, A. M., DANILA, D. C., WENSKE, S., GONZALEZ-ESPINOZA, R., ANAND, A., KOSCUISZKA, M., VAANANEN, R. M., PETTERSSON, K., CHUN, F. K., STEUBER, T., HULAND, H., GUILLONNEAU, B. D., EASTHAM, J. A., SCARDINO, P. T., FLEISHER, M., SCHER, H. I. & LILJA, H. 2009. Circulating prostate tumor cells detected by reverse transcription-PCR in men with

- localized or castration-refractory prostate cancer: concordance with CellSearch assay and association with bone metastases and with survival. *Clin Chem*, 55, 765-73.
- HERLYN, M., STEPLEWSKI, Z., HERLYN, D. & KOPROWSKI, H. 1979. Colorectal carcinoma-specific antigen: Detection by means of monoclonal antibodies. *Proceedings of the National Academy of Sciences of the United States of America*, 76, 1438-1442.
- HERNÁNDEZ, J. & THOMPSON, I. M. 2004. Prostate-specific antigen: A review of the validation of the most commonly used cancer biomarker. *Cancer*, 101, 894-904.
- HERVÉ, J.-C., DERANGEON, M., SARROUILHE, D. & BOURMEYSTER, N. 2014. Influence of the scaffolding protein Zonula Occludens (ZOs) on membrane channels. *Biochimica et Biophysica Acta (BBA) - Biomembranes*, 1838, 595-604.
- HOLLSTEIN, M., SIDRANSKY, D., VOGELSTEIN, B. & HARRIS, C. C. 1991. p53 mutations in human cancers. *Science*, 253, 49-53.
- HOLMES, N. 2006. CD45: all is not yet crystal clear. *Immunology*, 117, 145-155.
- HOU, H. W., WARKIANI, M. E., KHOO, B. L., LI, Z. R., SOO, R. A., TAN, D. S.-W., LIM, W.-T., HAN, J., BHAGAT, A. A. S. & LIM, C. T. 2013. Isolation and retrieval of circulating tumor cells using centrifugal forces. *Sci. Rep.*, 3.
- HUANG, B., LU, M., JOLLY, M. K., TSARFATY, I., ONUCHIC, J. & BEN-JACOB, E. 2014. The three-way switch operation of Rac1/RhoA GTPase-based circuit controlling amoeboid-hybrid-mesenchymal transition. *Sci Rep*, 4, 6449.
- HUGGINS, C. & HODGES, C. V. 2002. Studies on prostatic cancer: I. The effect of castration, of estrogen and of androgen injection on serum phosphatases in metastatic carcinoma of the prostate. 1941. *J Urol*, 168, 9-12.
- HUI, Y. Y., SU, L.-J., CHEN, O. Y., CHEN, Y.-T., LIU, T.-M. & CHANG, H.-C. 2014. Wide-field imaging and flow cytometric analysis of cancer cells in blood by fluorescent nanodiamond labeling and time gating. *Sci. Rep.*, 4.
- HYUN, K. A., GOO, K. B., HAN, H., SOHN, J., CHOI, W., KIM, S. I., JUNG, H. I. & KIM, Y. S. 2016. Epithelial-to-mesenchymal transition leads to loss of EpCAM and different physical properties in circulating tumor cells from metastatic breast cancer. *Oncotarget*.
- HYUN, K. A., KWON, K., HAN, H., KIM, S. I. & JUNG, H. I. 2013. Microfluidic flow fractionation device for label-free isolation of circulating tumor cells (CTCs) from breast cancer patients. *Biosens Bioelectron*, 40, 206-12.
- IGNATIADIS, M., XENIDIS, N., PERRAKI, M., APOSTOLAKI, S., POLITAKI, E., KAFOUSI, M., STATHOPOULOS, E. N., STATHOPOULOU, A., LIANIDOU, E., CHLOUVERAKIS, G., SOTIRIOU, C., GEORGOULIAS, V. & MAVROUDIS, D. 2007. Different prognostic value of cytokeratin-19 mRNA positive circulating tumor cells according to estrogen receptor and HER2 status in early-stage breast cancer. *J Clin Oncol*, 25, 5194-202.
- JANETSCHKEK, G. 2008. Radioisotope-Guided Lymph Node Dissection for Prostate Cancer: Potential and Limitations. *European Urology*, 53, 16-18.
- JAVIER, R. T. 2008. Cell polarity proteins: common targets for tumorigenic human viruses. *Oncogene*, 27, 7031-46.

- JIANG, P., ENOMOTO, A. & TAKAHASHI, M. 2009. Cell biology of the movement of breast cancer cells: Intracellular signalling and the actin cytoskeleton. *Cancer Letters*, 284, 122-130.
- JIN, C., MCFAUL, S. M., DUFFY, S. P., DENG, X., TAVASSOLI, P., BLACK, P. C. & MA, H. 2014. Technologies for label-free separation of circulating tumor cells: from historical foundations to recent developments. *Lab on a Chip*, 14, 32-44.
- JOLLY, M. K., BOARETO, M., HUANG, B., JIA, D., LU, M., BEN-JACOB, E., ONUCHIC, J. N. & LEVINE, H. 2015. Implications of the Hybrid Epithelial/Mesenchymal Phenotype in Metastasis. *Frontiers in Oncology*, 5, 155.
- JOO, Y.-E., REW, J.-S., PARK, C.-S. & KIM, S.-J. 2002. Expression of E-cadherin, alpha-and beta-catenins in patients with pancreatic adenocarcinoma. *Pancreatology*, 2, 129-137.
- KALLURI, R. & WEINBERG, R. A. The basics of epithelial-mesenchymal transition. *The Journal of Clinical Investigation*, 119, 1420-1428.
- KANTOFF, P. W., HIGANO, C. S., SHORE, N. D., BERGER, E. R., SMALL, E. J., PENSON, D. F., REDFERN, C. H., FERRARI, A. C., DREICER, R., SIMS, R. B., XU, Y., FROHLICH, M. W. & SCHELLHAMMER, P. F. 2010. Sipuleucel-T Immunotherapy for Castration-Resistant Prostate Cancer. *New England Journal of Medicine*, 363, 411-422.
- KELLER, E. T. & BROWN, J. 2004. Prostate cancer bone metastases promote both osteolytic and osteoblastic activity. *J Cell Biochem*, 91, 718-29.
- KIESSLICH, T., PICHLER, M., & NEUREITER, D. 2013. Epigenetic control of epithelial-mesenchymal-transition in human cancer (Review). *Molecular and Clinical Oncology*, 1, 3-11.
- KLEIN, C. A. 2008. The Metastasis Cascade. *Science*, 321, 1785-1787.
- KOIVUSALO, M., KAPUS, A. & GRINSTEIN, S. 2009. Sensors, Transducers, and Effectors That Regulate Cell Size and Shape. *Journal of Biological Chemistry*, 284, 6595-6599.
- KOKKINOPOULOS, I., SHAHABI, G., COLMAN, A. & JEFFERY, G. 2011. Mature Peripheral RPE Cells Have an Intrinsic Capacity to Proliferate; A Potential Regulatory Mechanism for Age-Related Cell Loss. *PLoS ONE*, 6, e18921.
- KREBS, M. G., HOU, J.-M., WARD, T. H., BLACKHALL, F. H. & DIVE, C. 2010. Circulating tumour cells: their utility in cancer management and predicting outcomes. *Therapeutic Advances in Medical Oncology*, 2, 351-365.
- KREBS, M. G., METCALF, R. L., CARTER, L., BRADY, G., BLACKHALL, F. H. & DIVE, C. 2014. Molecular analysis of circulating tumour cells[mdash]biology and biomarkers. *Nat Rev Clin Oncol*, 11, 129-144.
- KUPHAL, S., BAUER, R. & BOSSERHOFF, A.-K. 2005. Integrin signaling in malignant melanoma. *Cancer and Metastasis Reviews*, 24, 195-222.
- LAZAR, D. C., CHO, E. H., LUTTGEN, M. S., METZNER, T. J., USON, M. L., TORREY, M., GROSS, M. E. & KUHN, P. 2012. Cytometric comparisons between circulating tumor cells from prostate cancer patients and the prostate tumor derived LNCaP cell line. *Physical Biology*, 9, 016002-016002.

- LE DIEU, R., TAUSSIG, D., LISTER, T. A. & GRIBBEN, J. G. 2009. Negative immunomagnetic selection of T cells from peripheral blood of presentation AML specimens. *Journal of Immunological Methods*, 348, 95-100.
- LEBER, M. F. & EFFERTH, T. 2009. Molecular principles of cancer invasion and metastasis (review). *Int J Oncol*, 34, 881-95.
- LEDBETTER, J. A., DEANS, J. P., ARUFFO, A., GROSMARE, L. S., KANNER, S. B., BOLEN, J. B. & SCHIEVEN, G. L. 1993. CD4, CD8 and the role of CD45 in T-cell activation. *Current Opinion in Immunology*, 5, 334-340.
- LENZ, M., ROUMANS, N. J. T., VINK, R. G., VAN BAAK, M. A., MARIMAN, E. C. M., ARTS, I. C. W., DE KOK, T. M. & ERTAYLAN, G. 2016. Estimating real cell size distribution from cross-section microscopy imaging. *Bioinformatics*, 32, i396-i404.
- LEUNG, C., SHAHEEN, F., BERNATCHEZ, P. & HACKETT, T. L. 2012. Expression of myoferlin in human airway epithelium and its role in cell adhesion and zonula occludens-1 expression. *PLoS One*, 7, e40478.
- LILJA, H., ULMERT, D. & VICKERS, A. J. 2008. Prostate-specific antigen and prostate cancer: prediction, detection and monitoring. *Nat Rev Cancer*, 8, 268-278.
- LITVINOV, S., VELDERS, M., BAKKER, H., FLEUREN, G. J. & WARNAAR, S. O. 1994. Ep-CAM: a human epithelial antigen is a homophilic cell-cell adhesion molecule. *The Journal of Cell Biology*, 125, 437-446.
- LLOYD, ALISON C. 2013. The Regulation of Cell Size. *Cell*, 154, 1194-1205.
- LODISH H, B. A., ZIPURSKY SL, ET AL. 2000. *Molecular Cell Biology* [Online]. New York: W. H. Freeman. Available: <http://www.ncbi.nlm.nih.gov/books/NBK21493/>.
- LOEB, S., BERGLUND, A. & STATTIN, P. 2013. Population Based Study of Use and Determinants of Active Surveillance and Watchful Waiting for Low and Intermediate Risk Prostate Cancer. *The Journal of Urology*, 190, 1742-1749.
- LOGAN, C. Y. & NUSSE, R. 2004. The Wnt signaling pathway in development and disease. *Annu Rev Cell Dev Biol*, 20, 781-810.
- LOPEZ-RIQUELME, N., MINGUELA, A., VILLAR-PERMUY, F., CIPRIAN, D., CASTILLEJO, A., ALVAREZ-LOPEZ, M. R. & SOTO, J. L. 2013. Imaging cytometry for counting circulating tumor cells: comparative analysis of the CellSearch vs ImageStream systems. *Apmis*, 121, 1139-43.
- LOU, X.-L., SUN, J., GONG, S.-Q., YU, X.-F., GONG, R. & DENG, H. 2015. Interaction between circulating cancer cells and platelets: clinical implication. *Chinese Journal of Cancer Research*, 27, 450-460.
- LUSTBERG, M., JATANA, K. R., ZBOROWSKI, M. & CHALMERS, J. J. 2012. Emerging Technologies for CTC Detection Based on Depletion of Normal Cells. *Recent results in cancer research. Fortschritte der Krebsforschung. Progres dans les recherches sur le cancer*, 195, 97-110.
- MAKOWSKA, KATARZYNA A., HUGHES, RUTH E., WHITE, KATHRYN J., WELLS, CLAIRE M. & PECKHAM, M. Specific Myosins Control Actin Organization, Cell Morphology, and Migration in Prostate Cancer Cells. *Cell Reports*, 13, 2118-2125.

- MALISSEN, B. & SCHMITT-VERHULST, A. M. 1993. Transmembrane signalling through the T-cell-receptor-CD3 complex. *Curr Opin Immunol*, 5, 324-33.
- MANI, S. A., GUO, W., LIAO, M. J., EATON, E. N., AYYANAN, A., ZHOU, A. Y., BROOKS, M., REINHARD, F., ZHANG, C. C., SHIPITSIN, M., CAMPBELL, L. L., POLYAK, K., BRISKEN, C., YANG, J. & WEINBERG, R. A. 2008. The epithelial-mesenchymal transition generates cells with properties of stem cells. *Cell*, 133, 704-15.
- MARTIN, T. A. 2014. The role of tight junctions in cancer metastasis. *Seminars in Cell & Developmental Biology*, 36, 224-231.
- MASSONER, P., THOMM, T., MACK, B., UNTERGASSER, G., MARTOWICZ, A., BOBOWSKI, K., KLOCKER, H., GIRES, O. & PUHR, M. 2014. EpCAM is overexpressed in local and metastatic prostate cancer, suppressed by chemotherapy and modulated by MET-associated miRNA-200c/205. *British Journal of Cancer*, 111, 955-964.
- MCCABE, N. P., DE, S., VASANJI, A., BRAINARD, J. & BYZOVA, T. V. 2007. Prostate cancer specific integrin alphavbeta3 modulates bone metastatic growth and tissue remodeling. *Oncogene*, 26, 6238-43.
- MCQUEEN, K. L., DIXON, J. W., LEE, T. N., PETERS, C. E., EAVES, A. C. & THOMAS, T. E. 2016. P122 Rapid isolation of CD15 positively selected cells from blood following use of the new EasySep™ RBC Depletion Reagent. *Human Immunology*, 77, Supplement, 127.
- MIDDLESEXHOSPITAL.ORG. 2016. *Comprehensive Prostate Program* [Online]. Middlesex Hospital. Available: <https://middlesexhospital.org/our-services/hospital-services/cancer-center/cancer-programs-and-services/comprehensive-prostate-program/stage-and-grade-2016>].
- MIKOLAJCZYK, S. D., MILLAR, L. S., TSINBERG, P., COUTTS, S. M., ZOMORRODI, M., PHAM, T., BISCHOFF, F. Z. & PIRCHER, T. J. 2011. Detection of EpCAM-Negative and Cytokeratin-Negative Circulating Tumor Cells in Peripheral Blood. *Journal of Oncology*, 2011.
- MILLER, M. C., DOYLE, G. V. & TERSTAPPEN, L. W. M. M. 2010. Significance of Circulating Tumor Cells Detected by the CellSearch System in Patients with Metastatic Breast Colorectal and Prostate Cancer. *Journal of Oncology*, 2010.
- MILLIPORE. 2016. *ImageStreamX Mark II Imaging Flow Cytometer - Extended Depth of Field* [Online]. Available: <https://www.merckmillipore.com/GB/en/life-science-research/cell-analysis/amnis-imaging-flow-cytometers/imagestreamx-Mark-ii-imaging-flow-cytometer/extended-depth-of-field/UZCb.qB.KZkAAAFM4o40ix6F,nav>.
- MILLNER, L. M., LINDER, M. W. & VALDES, R. 2013. Circulating Tumor Cells: A Review of Present Methods and the Need to Identify Heterogeneous Phenotypes. *Annals of Clinical & Laboratory Science*, 43, 295-304.
- MIYAMOTO, D. T., SEQUIST, L. V. & LEE, R. J. 2014. Circulating tumour cells[mdash]monitoring treatment response in prostate cancer. *Nat Rev Clin Oncol*, 11, 401-412.
- MOHAMMADI, H., MOHAMMADNEJAD, J. & YAVARI, K. 2014. Human Peripheral Blood Derived Hematopoietic Stem Cell: History, the Isolation Methods and Investigation of Different Parameters Effects on Their Differentiation to the Body Cells. *International Journal of Stem Cell Research and Transplantation (IJST)*, 02, 59-62.

- MOUW, J. K., YUI, Y., DAMIANO, L., BAINER, R. O., LAKINS, J. N., ACERBI, I., OU, G., WIJEKON, A. C., LEVENTAL, K. R., GILBERT, P. M., HWANG, E. S., CHEN, Y.-Y. & WEAVER, V. M. 2014. Tissue mechanics modulate microRNA-dependent PTEN expression to regulate malignant progression. *Nat Med*, 20, 360-367.
- MPBIOMEDICALS. 2016. *LSM™-LYMPHOCYTE SEPARATION MEDIUM* [Online]. Available: <http://www.mpbio.com/product.php?pid=0850494>.
- NADAL, R., LORENTE, J. A., ROSELL, R. & SERRANO, M. J. 2013. Relevance of Molecular Characterization of Circulating Tumor Cells in Breast Cancer in the Era of Targeted Therapies. *Expert Rev Mol Diagn*, 13, 295-307.
- NAGRATH, S., SEQUIST, L. V., MAHESWARAN, S., BELL, D. W., IRIMIA, D., ULKUS, L., SMITH, M. R., KWAK, E. L., DIGUMARTHY, S., MUZIKANSKY, A., RYAN, P., BALIS, U. J., TOMPKINS, R. G., HABER, D. A. & TONER, M. 2007a. Isolation of rare circulating tumour cells in cancer patients by microchip technology. *Nature*, 450, 1235-9.
- NAGRATH, S., SEQUIST, L. V., MAHESWARAN, S., BELL, D. W., IRIMIA, D., ULKUS, L., SMITH, M. R., KWAK, E. L., DIGUMARTHY, S., MUZIKANSKY, A., RYAN, P., BALIS, U. J., TOMPKINS, R. G., HABER, D. A. & TONER, M. 2007b. Isolation of rare circulating tumour cells in cancer patients by microchip technology. *Nature*, 450, 1235-1239.
- NAKANO, A., HARADA, T., MORIKAWA, S. & KATO, Y. 1990. Expression of Leukocyte Common Antigen (CD45) on Various Human Leukemia/Lymphoma Cell Lines. *Pathology International*, 40, 107-115.
- NAM, H.-J., POY, F., SAITO, H. & FREDERICK, C. A. 2005. Structural basis for the function and regulation of the receptor protein tyrosine phosphatase CD45. *The Journal of Experimental Medicine*, 201, 441-452.
- NANOENTEK. 2015. *Automatic cell counter* [Online]. Available: <http://www.nanoentek.com/product.php?id=15>.
- NCI. 2014. *Treatment Option Overview for Prostate Cancer* [Online]. Available: <http://www.cancer.gov/cancertopics/pdq/treatment/prostate/HealthProfessional/page3> [Accessed 07/02 2015].
- NGUYEN, T. M. & PASTUSZAK, A. W. 2016. Testosterone Therapy Among Prostate Cancer Survivors. *Sexual Medicine Reviews*, 4, 376-388.
- NHS. 2015a. *Prostate cancer* [Online]. UK: NHS. Available: <http://www.nhs.uk/conditions/cancer-of-the-prostate/Pages/Introduction.aspx> [Accessed 07/02/2015 2015].
- NHS. 2015b. *Prostate cancer - Symptoms* [Online]. UK: NHS. Available: <http://www.nhs.uk/Conditions/Cancer-of-the-prostate/Pages/Symptoms.aspx> [Accessed 07/02 2015].
- NI, J., COZZI, P., HAO, J., BERETOV, J., CHANG, L., DUAN, W., SHIGDAR, S., DELPRADO, W., GRAHAM, P., BUCCI, J., KEARSLEY, J. & LI, Y. 2013a. Epithelial cell adhesion molecule (EpCAM) is associated with prostate cancer metastasis and chemo/radioresistance via the PI3K/Akt/mTOR signaling pathway. *Int J Biochem Cell Biol*, 45, 2736-48.
- NI, S., XU, L., HUANG, J., FENG, J., ZHU, H., WANG, G. & WANG, X. 2013b. Increased ZO-1 expression predicts valuable prognosis in non-small cell lung cancer. *Int J Clin Exp Pathol*, 6, 2887-95.

- NIERODZIK, M. L., KLEPFISH, A. & KARPATKIN, S. 1995. Role of platelets, thrombin, integrin IIb-IIIa, fibronectin and von Willebrand factor on tumor adhesion in vitro and metastasis in vivo. *Thromb Haemost*, 74, 282-90.
- NING, N., ZHAN, T., ZHANG, Y., CHEN, Q., FENG, F., YANG, Z., LIU, Z., XU, D., WANG, F., GUO, Y., XING, J., GUAN, Y. & CUI, W. 2014. Improvement of specific detection of circulating tumor cells using combined CD45 staining and fluorescence in situ hybridization. *Clinica Chimica Acta*, 433, 69-75.
- NISWANDER, L. M., MCGRATH, K. E., KENNEDY, J. C. & PALIS, J. 2014a. Improved Quantitative Analysis of Primary Bone Marrow Megakaryocytes Utilizing Imaging Flow Cytometry. *Cytometry. Part A : the journal of the International Society for Analytical Cytology*, 85, 302-312.
- NISWANDER, L. M., MCGRATH, K. E., KENNEDY, J. C. & PALIS, J. 2014b. Improved quantitative analysis of primary bone marrow megakaryocytes utilizing imaging flow cytometry. *Cytometry A*, 85, 302-12.
- NTOUROUPI, T. G., ASHRAF, S. Q., MCGREGOR, S. B., TURNEY, B. W., SEPPO, A., KIM, Y., WANG, X., KILPATRICK, M. W., TSIPOURAS, P., TAFAS, T. & BODMER, W. F. 2008. Detection of circulating tumour cells in peripheral blood with an automated scanning fluorescence microscope. *Br J Cancer*, 99, 789-795.
- OUYANG, L., SHI, Z., ZHAO, S., WANG, F. T., ZHOU, T. T., LIU, B. & BAO, J. K. 2012. Programmed cell death pathways in cancer: a review of apoptosis, autophagy and programmed necrosis. *Cell Prolif*, 45, 487-98.
- PAOLI, P., GIANNONI, E. & CHIARUGI, P. 2013. Anoikis molecular pathways and its role in cancer progression. *Biochimica et Biophysica Acta (BBA) - Molecular Cell Research*, 1833, 3481-3498.
- PARK, J. W., LEE, J. K., PHILLIPS, J. W., HUANG, P., CHENG, D., HUANG, J. & WITTE, O. N. 2016. Prostate epithelial cell of origin determines cancer differentiation state in an organoid transformation assay. *Proc Natl Acad Sci U S A*, 113, 4482-7.
- PARK, S., ANG, R. R., DUFFY, S. P., BAZOV, J., CHI, K. N., BLACK, P. C. & MA, H. 2014. Morphological Differences between Circulating Tumor Cells from Prostate Cancer Patients and Cultured Prostate Cancer Cells. *PLOS ONE*, 9, e85264.
- PARRIS, C. N., ADAM ZAHIR, S., AL-ALI, H., BOURTON, E. C., PLOWMAN, C. & PLOWMAN, P. N. 2015a. Enhanced gamma-H2AX DNA damage foci detection using multimagnification and extended depth of field in imaging flow cytometry. *Cytometry A*, 87, 717-23.
- PARRIS, C. N., ADAM ZAHIR, S., AL-ALI, H., BOURTON, E. C., PLOWMAN, C. & PLOWMAN, P. N. 2015b. Enhanced γ -H2AX DNA damage foci detection using multimagnification and extended depth of field in imaging flow cytometry. *Cytometry*, 87, 717-723.
- PATERLINI-BRECHOT, P. & BENALI, N. L. 2007. Circulating tumor cells (CTC) detection: clinical impact and future directions. *Cancer Lett*, 253, 180-204.
- PAWELEK, J. M. & CHAKRABORTY, A. K. 2008. The cancer cell-leukocyte fusion theory of metastasis. *Adv Cancer Res*, 101, 397-444.
- PECKHAM, M. 2003. *White Blood Cells* [Online]. The Histology Guide University of Leeds Available: http://www.histology.leeds.ac.uk/blood/blood_wbc.php 2016].

- PECORINO, L. 2012. *Molecular Biology of Cancer*, Oxford, UK, Oxford University Press.
- PEETERS, D. J. E., VAN DEN EYNDEN, G. G., VAN DAM, P. J., PROVÉ, A., BENOY, I. H., VAN DAM, P. A., VERMEULEN, P. B., PAUWELS, P., PEETERS, M., VAN LAERE, S. J. & DIRIX, L. Y. 2011. Circulating tumour cells in the central and the peripheral venous compartment in patients with metastatic breast cancer. *British Journal of Cancer*, 104, 1472-1477.
- PERLMUTTER, R. M., LEVIN, S. D., APPLEBY, M. W., ANDERSON, S. J. & ALBEROLA-ILA, J. 1993. Regulation of lymphocyte function by protein phosphorylation. *Annu Rev Immunol*, 11, 451-99.
- PETRYLAK, D. P., TANGEN, C. M., HUSSAIN, M. H., LARA, P. N., JR., JONES, J. A., TAPLIN, M. E., BURCH, P. A., BERRY, D., MOINPOUR, C., KOHLI, M., BENSON, M. C., SMALL, E. J., RAGHAVAN, D. & CRAWFORD, E. D. 2004. Docetaxel and estramustine compared with mitoxantrone and prednisone for advanced refractory prostate cancer. *N Engl J Med*, 351, 1513-20.
- POLASCIOK, T. J., OESTERLING, J. E. & PARTIN, A. W. 1999. Prostate specific antigen: a decade of discovery--what we have learned and where we are going. *J Urol*, 162, 293-306.
- PSAILA, B. & LYDEN, D. 2009. The metastatic niche: adapting the foreign soil. *Nat Rev Cancer*, 9, 285-93.
- PULUKURI, S. M., GONDI, C. S., LAKKA, S. S., JUTLA, A., ESTES, N., GUJRATI, M. & RAO, J. S. 2005. RNA Interference-directed Knockdown of Urokinase Plasminogen Activator and Urokinase Plasminogen Activator Receptor Inhibits Prostate Cancer Cell Invasion, Survival, and Tumorigenicity in Vivo. *Journal of Biological Chemistry*, 280, 36529-36540.
- PUNNOOSE, E. A., ATWAL, S. K., SPOERKE, J. M., SAVAGE, H., PANDITA, A., YEH, R. F., PIRZKALL, A., FINE, B. M., AMLER, L. C., CHEN, D. S. & LACKNER, M. R. 2010. Molecular biomarker analyses using circulating tumor cells. *PLoS One*, 5, e12517.
- QIAN, C.-N. & TEH, B. 2012. "Seed and Soil" Theory of Metastasis. In: SCHWAB, M. (ed.) *Encyclopedia of Cancer*. Springer Berlin Heidelberg.
- RAMBURAN, A. & GOVENDER, D. 2002. Cadherins and catenins in pathology. *Current Diagnostic Pathology*, 8, 305-317.
- RASSWEILER, J., TEBER, D., KUNTZ, R. & HOFMANN, R. 2006. Complications of Transurethral Resection of the Prostate (TURP)—Incidence, Management, and Prevention. *European Urology*, 50, 969-980.
- REYMOND, N., D'AGUA, B. B. & RIDLEY, A. J. 2013. Crossing the endothelial barrier during metastasis. *Nat Rev Cancer*, 13, 858-870.
- RIBATTI, D., MANGIALARDI, G. & VACCA, A. 2006. Stephen Paget and the 'seed and soil' theory of metastatic dissemination. *Clinical and Experimental Medicine*, 6, 145-149.
- RIETHDORF, S. A. P., K. 2010. Advancing personalized cancer therapy by detection and characterization of circulating carcinoma cells. *Annals of the New York Academy of Sciences*, 1210, 66-77.
- RUSCETTI, M., QUACH, B., DADASHIAN, E. L., MULHOLLAND, D. J. & WU, H. 2015. Tracking and Functional Characterization of Epithelial-Mesenchymal Transition and Mesenchymal Tumor Cells during Prostate Cancer Metastasis. *Cancer Res*, 75, 2749-59.

- SAMSEL, L. & MCCOY JR, J. P. 2015. Imaging flow cytometry for the study of erythroid cell biology and pathology. *Journal of Immunological Methods*, 423, 52-59.
- SANSOM, O. J., REED, K. R., HAYES, A. J., IRELAND, H., BRINKMANN, H., NEWTON, I. P., BATLLE, E., SIMON-ASSMANN, P., CLEVERS, H., NATHKE, I. S., CLARKE, A. R. & WINTON, D. J. 2004. Loss of Apc in vivo immediately perturbs Wnt signaling, differentiation, and migration. *Genes & Development*, 18, 1385-1390.
- SAYLOR, P. J., LEE, R. J. & SMITH, M. R. 2011. Emerging Therapies to Prevent Skeletal Morbidity in Men With Prostate Cancer. *Journal of Clinical Oncology*, 29, 3705-3714.
- SCHISCHMANOV, N. 2013. NEW HYPOTHESIS ON THE ORIGIN OF METASTASES. *Nagoya Journal of Medical Science*, 75, 153-159.
- SCHNECK, H., GIERKE, B., UPPENKAMP, F., BEHRENS, B., NIEDERACHER, D., STOECKLEIN, N. H., TEMPLIN, M. F., PAWLAK, M., FEHM, T., NEUBAUER, H. & DISSEMINATED CANCER CELL NETWORK, D. 2015. EpCAM-Independent Enrichment of Circulating Tumor Cells in Metastatic Breast Cancer. *PLOS ONE*, 10, e0144535.
- SCHNELL, U., CIRULLI, V. & GIEPMANS, B. N. G. 2013. EpCAM: Structure and function in health and disease. *Biochimica et Biophysica Acta (BBA) - Biomembranes*, 1828, 1989-2001.
- SEGUIN, L., DESGROSELLIER, J. S., WEIS, S. M. & CHERESH, D. A. 2015. Integrins and cancer: regulators of cancer stemness, metastasis, and drug resistance. *Trends in Cell Biology*.
- STEMCELL. 2016. *EasySep™* [Online]. STEMCELL Technologies. Available: <https://www.stemcell.com/products/brands/easysep.html> 2016].
- STEVENSON, R. P., VELTMAN, D. & MACHESKY, L. M. 2012. Actin-bundling proteins in cancer progression at a glance. *Journal of Cell Science*, 125, 1073-1079.
- STORKUS, W. J. & DAWSON, J. R. 1991. Target structures involved in natural killing (NK): characteristics, distribution, and candidate molecules. *Crit Rev Immunol*, 10, 393-416.
- STOTT, S. L., HSU, C.-H., TSUKROV, D. I., YU, M., MIYAMOTO, D. T., WALTMAN, B. A., ROTHENBERG, S. M., SHAH, A. M., SMAS, M. E., KORIR, G. K., FLOYD, F. P., GILMAN, A. J., LORD, J. B., WINOKUR, D., SPRINGER, S., IRIMIA, D., NAGRATH, S., SEQUIST, L. V., LEE, R. J., ISSELBACHER, K. J., MAHESWARAN, S., HABER, D. A. & TONER, M. 2010a. Isolation of circulating tumor cells using a microvortex-generating herringbone-chip. *Proceedings of the National Academy of Sciences of the United States of America*, 107, 18392-18397.
- STOTT, S. L., LEE, R. J., NAGRATH, S., YU, M., MIYAMOTO, D. T., ULKUS, L., INSERRA, E. J., ULMAN, M., SPRINGER, S., NAKAMURA, Z., MOORE, A. L., TSUKROV, D. I., KEMPNER, M. E., DAHL, D. M., WU, C.-L., IAFRATE, A. J., SMITH, M. R., TOMPKINS, R. G., SEQUIST, L. V., TONER, M., HABER, D. A. & MAHESWARAN, S. 2010b. Isolation and Characterization of Circulating Tumor Cells from Patients with Localized and Metastatic Prostate Cancer. *Science translational medicine*, 2, 25ra23-25ra23.
- STRAUSS, R., SOVA, P., LIU, Y., LI, Z. Y., TUVE, S., PRITCHARD, D., BRINKKOETTER, P., MOLLER, T., WILDNER, O., PESONEN, S., HEMMINKI, A., URBAN, N., DRESCHER, C. & LIEBER, A. 2009. Epithelial phenotype confers resistance of ovarian cancer cells to oncolytic adenoviruses. *Cancer Res*, 69, 5115-25.
- TAI, S., SUN, Y., SQUIRES, J. M., ZHANG, H., OH, W. K., LIANG, C.-Z. & HUANG, J. 2011. PC3 Is a Cell Line Characteristic of Prostatic Small Cell Carcinoma. *The Prostate*, 71, 1668-1679.

- TAKEICHI, M. 1993. Cadherins in cancer: implications for invasion and metastasis. *Current Opinion in Cell Biology*, 5, 806-811.
- TANNOCK, I. F., DE WIT, R., BERRY, W. R., HORTI, J., PLUZANSKA, A., CHI, K. N., OUDARD, S., THÉODORE, C., JAMES, N. D., TURESSON, I., ROSENTHAL, M. A. & EISENBERGER, M. A. 2004. Docetaxel plus Prednisone or Mitoxantrone plus Prednisone for Advanced Prostate Cancer. *New England Journal of Medicine*, 351, 1502-1512.
- THALGOTT, M., RACK, B., MAURER, T., SOUVATZOGLOU, M., EIBER, M., KREB, V., HECK, M., ANDERGASSEN, U., NAWROTH, R., GSCHWEND, J. & RETZ, M. 2013. Detection of circulating tumor cells in different stages of prostate cancer. *Journal of Cancer Research and Clinical Oncology*, 139, 755-763.
- THARA, E., DORFF, T. B., PINSKI, J. K. & QUINN, D. I. 2011. Vaccine therapy with sipuleucel-T (Provenge) for prostate cancer. *Maturitas*, 69, 296-303.
- THOMPSON, I. M., PAULER, D. K., GOODMAN, P. J., TANGEN, C. M. & DR.P.H., M. S. L., M.D., HOWARD L. PARNES, M.D., LORI M. MINASIAN, M.D., LESLIE G. FORD, M.D., SCOTT M. LIPPMAN, M.D., E. DAVID CRAWFORD, M.D., JOHN J. CROWLEY, PH.D., AND CHARLES A. COLTMAN, JR., M.D 2004. Prevalence of Prostate Cancer among Men with a Prostate-Specific Antigen Level ≤ 4.0 ng per Milliliter. *The New England Journal of Medicine*, 350, 2239-2246.
- TOMASETTI, C. & VOGELSTEIN, B. 2015. Variation in cancer risk among tissues can be explained by the number of stem cell divisions. *Science*, 347, 78-81.
- TOMITA, K., VAN BOKHOVEN, A., VAN LEENDERS, G. J., RUIJTER, E. T., JANSEN, C. F., BUSSEMAKERS, M. J. & SCHALKEN, J. A. 2000. Cadherin switching in human prostate cancer progression. *Cancer Res*, 60, 3650-4.
- TRAN, S.-L., PUHAR, A., NGO-CAMUS, M. & RAMARAO, N. 2011. Trypan Blue Dye Enters Viable Cells Incubated with the Pore-Forming Toxin HlyII of *Bacillus cereus*. *PLoS ONE*, 6, e22876.
- TROSKO, J. E. 2009. Review Paper: Cancer Stem Cells and Cancer Nonstem Cells: From Adult Stem Cells or from Reprogramming of Differentiated Somatic Cells. *Veterinary Pathology Online*, 46, 176-193.
- TRZPIS, M., MCLAUGHLIN, P. M. J., DE LEIJ, L. M. F. H. & HARMSSEN, M. C. 2007. Epithelial Cell Adhesion Molecule: More than a Carcinoma Marker and Adhesion Molecule. *The American Journal of Pathology*, 171, 386-395.
- VALASTYAN, S. & WEINBERG, ROBERT A. Tumor Metastasis: Molecular Insights and Evolving Paradigms. *Cell*, 147, 275-292.
- VAN BEERS, E. J., SAMSEL, L., MENDELSON, L., SAIYED, R., FERTRIN, K. Y., BRANTNER, C. A., DANIELS, M. P., NICHOLS, J., MCCOY, J. P. & KATO, G. J. 2014. Imaging flow cytometry for automated detection of hypoxia-induced erythrocyte shape change in sickle cell disease. *Am J Hematol*, 89, 598-603.
- VILEN, S. T., SUOJANEN, J., SALAS, F., RISTELI, J., YLIPALOSAARI, M., ITKONEN, O., KOISTINEN, H., BAUMANN, M., STENMAN, U. H., SORSA, T., SALO, T. & NYBERG, P. 2012. Trypsin-2 enhances carcinoma invasion by processing tight junctions and activating ProMT1-MMP. *Cancer Invest*, 30, 583-92.

- VONA, G., SABILE, A., LOUHA, M., SITRUK, V., ROMANA, S., SCHUTZE, K., CAPRON, F., FRANCO, D., PAZZAGLI, M., VEKEMANS, M., LACOUR, B., BRECHOT, C. & PATERLINI-BRECHOT, P. 2000. Isolation by size of epithelial tumor cells : a new method for the immunomorphological and molecular characterization of circulating tumor cells. *Am J Pathol*, 156, 57-63.
- WEISSENSTEIN, U., SCHUMANN, A., REIF, M., LINK, S., TOFFOL-SCHMIDT, U. D. & HEUSSER, P. 2012. Detection of circulating tumor cells in blood of metastatic breast cancer patients using a combination of cytokeratin and EpCAM antibodies. *BMC Cancer*, 12, 206.
- WENT, P., VASEI, M., BUBENDORF, L., TERRACCIANO, L., TORNILLO, L., RIEDE, U., KONONEN, J., SIMON, R., SAUTER, G. & BAEUERLE, P. A. 2006. Frequent high-level expression of the immunotherapeutic target Ep-CAM in colon, stomach, prostate and lung cancers. *British Journal of Cancer*, 94, 128-135.
- WHO. 2014. *Cancer* [Online]. <http://www.who.int/>: WHO Available: <http://www.who.int/mediacentre/factsheets/fs297/en/> [Accessed 20 January 2015].
- WILSON, E. B. 1925. *The cell in development and heredity*, The Macmillan company; New York.
- WIT, S. D., DALUM, G. V., LENFERINK, A. T. M., TIBBE, A. G. J., HILTERMANN, T. J. N., GROEN, H. J. M., VAN RIJN, C. J. M. & TERSTAPPEN, L. W. M. M. 2015. The detection of EpCAM+ and EpCAM– circulating tumor cells. *Scientific Reports*, 5, 12270.
- WU, L., GONZALEZ, S., SHAH, S., KYUPELYAN, L., PETRIGLIANO, F. A., MCALLISTER, D. R., ADAMS, J. S., KARPERIEN, M., TUAN, T. L., BENYA, P. D. & EVSEENKO, D. 2014. Extracellular matrix domain formation as an indicator of chondrocyte dedifferentiation and hypertrophy. *Tissue Eng Part C Methods*, 20, 160-8.
- ZAHABI, A., SHAHBAZI, E., AHMADIEH, H., HASSANI, S. N., TOTONCHI, M., TAEI, A., MASOUDI, N., EBRAHIMI, M., AGHDAMI, N., SEIFINEJAD, A., MEHRNEJAD, F., DAFTARIAN, N., SALEKDEH, G. H. & BAHARVAND, H. 2012. A new efficient protocol for directed differentiation of retinal pigmented epithelial cells from normal and retinal disease induced pluripotent stem cells. *Stem Cells Dev*, 21, 2262-72.
- ZIHNI, C., BALDA, M. S. & MATTER, K. 2014. Signalling at tight junctions during epithelial differentiation and microbial pathogenesis. *Journal of Cell Science*, 127, 3401-3413.
- ZORN, K. C. 2016. *PSA Test (Prostate Specific Antigen)* [Online]. Medicinenet. Available: http://www.medicinenet.com/prostate_specific_antigen/page2.htm.